

NASA

CR 112179

TR-3720295

(NASA-CR-112179) BALLOON LAUNCHED
DECELERATOR TEST PROGRAM, POST-TEST TEST
REPORT, BLT VEHICLE AV-4 D.
DICKINSON, et al (Martin Marietta Corp.)
20 Oct. 1972 207 p
CSCL 012

53/02
Unclass
50284

N73-13024

Viking'75 Project

BALLOON LAUNCHED DECELERATOR TEST PROGRAM
POST - FLIGHT TEST REPORT
BLDT VEHICLE AV- 4



MARTIN MARIETTA

NAS1-9000

ABSTRACT

Four BLDT flights were conducted during the summer of 1972 over the White Sands Missile Range. The purpose of these tests was to qualify the Viking DGB parachute system behind a full-scale simulator of the Viking Entry Vehicle over the maximum range of entry conditions anticipated in the Viking '75 soft landing on Mars. Test concerns centered on the ability of a minimum weight parachute system to operate without structural damage in the turbulent wake of the blunt-body entry vehicle (140° cone 11.5' diameter). This is the first known instance of successful parachute operation at supersonic speeds in the wake of such a large blunt body. The flight tests utilized the largest successful balloon-payload weight combination known to get to high altitudes in the earth's atmosphere where rocket engines were employed to boost the test vehicle to supersonic speeds and dynamic pressures simulating the range of conditions on Mars.

This report presents the results of the third test, a repeat of the first, in the series where the test conditions at parachute deployment were the most severe expected at Mars; Mach number of approximately 2.0 and dynamic pressure of approximately 10.0 psf. The report also contains appendices describing the test vehicle, parachute postflight inspection report, parachute dimensional description, and descriptions of the BLDT mission and computer software. The parachute sustained no flight damage. Detailed parachute performance data obtained from tensiometers, cameras, accelerometers, and radar are presented and analyzed. Aeroshell separation dynamics and vehicle motions as influenced by the parachute opening process and performance obtained from the above instruments and rate gyros are also presented and analyzed.

TR-3720295

20 October 1972

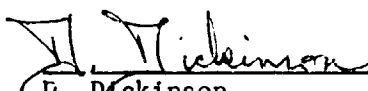
DRL Line Item No.: N3-T040

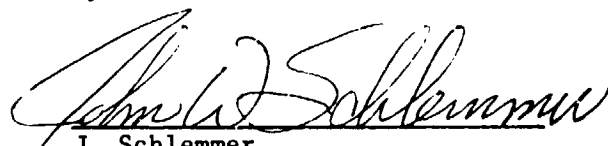
BALLOON LAUNCHED DECELERATOR
TEST PROGRAM
POST-TEST TEST REPORT

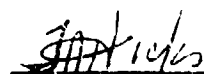
(45 day)

BLDT VEHICLE AV-4

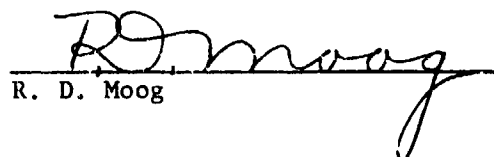
prepared by:


D. Dickinson


J. Schlemmer


F. Hicks


F. Michel


R. D. Moog

PREPARED UNDER CONTACT NAS1-9000 by
MARTIN MARIETTA CORPORATION
DENVER DIVISION
P. O. Box 179
Denver, Colorado 80201

APPROVAL SHEET

R. J. Polutchko
 Robert J. Polutchko
 Project Engineer
 Viking Vehicle Engineering

10/16/72
 Date

P. Donohue
 P. Donohue
 Program Manager
 BLDT Program

10/23/72
 Date

TABLE OF CONTENTS

	<u>PAGE</u>
APPROVAL SHEET	ii
TABLE OF CONTENTS	iii
I. PURPOSE OF REPORT	I-1
II. MISSION OBJECTIVES	II-1
III. DECELERATOR QUALIFICATION SUMMARY	III-1
A. Operations Summary	III-1
B. Vehicle Performance	III-2
C. Decelerator System Summary	III-2
IV. MISSION OPERATIONS	IV-1
A. Flight Readiness Test and Launch	IV-1
B. Ascent and Float	IV-1
C. Vehicle Flight	IV-3
D. Recovery Operations	IV-4
V. DECELERATOR SYSTEM ANALYSIS	V-1
A. System Description	V-1
B. Mortar Fire Conditions	V-1
C. Mortar Performance	V-2
D. Decelerator Inflation Sequence	V-4
E. Opening Load	V-6
F. Vehicle Stability	V-7
G. Parachute Drag Performance	V-9
H. Aeroshell Separation	V-13
I. Parachute Recovery Assessment	V-15

TABLE OF CONTENTS (CONTINUED)

	<u>PAGE</u>
VI. VEHICLE PERFORMANCE ANALYSIS	VI-1
A. Flight Dynamics	VI-1
B. Capsule Aerodynamic Characteristics	VI-11
C. Thermal Control Subsystem	VI-12
D. Propulsion, Azimuth Pointing and Ordnance Subsystem	VI-14
E. Structural Subsystem	VI-16
F. Electrical Subsystem	VI-17
G. Instrumentation Subsystem	VI-18
H. RF Subsystem	VI-19
I. TSE/OSE	VI-19
J. Mass Properties	VI-19
VII. CONCLUSIONS	VII-1
VIII. REFERENCES AND OTHER DATA SOURCES	VIII-1
A. References	VIII-1
B. Abbreviations	VIII-2
APPENDIX A - Description of Balloon Launched Decelerator Test Vehicle	A-1
APPENDIX B - Description of BLDT System Mission	B-1
APPENDIX C - GAC Post-Test Inspection	C-1
APPENDIX D - Parachute Dimensions	D-1
APPENDIX E - BLDT Computer Software	F-1

LIST OF ILLUSTRATIONS

<u>FIGURE</u>	<u>TITLE</u>	<u>PAGE</u>
II-1	BLDT AV-1 Test Conditions	II-3
IV-1	Mission Ground Track - AV-4	IV-7
IV-2	Balloon Altitude Profile	IV-8
IV-3	System Porpoising Profile	IV-9
IV-4	Mortar Fire Command System Operation	IV-10
V-1	Viking Decelerator System	V-18
V-2	Ejected Weight Distribution	V-19
V-3	On-board Camera Photographs	V-20
V-4	Angle of Attack Line Bowing Effect	V-24
V-5	Canopy Growth Parameter	V-25
V-6	Canopy Area Oscillations	V-26
V-7	Parachute Fillint Time from Line Stretch	V-27
V-8	Parachute Opening Load, 0-10 Seconds	V-28
V-9	Parachute Opening Load 0-50 Seconds	V-29
V-10	Tensiometer Reading, Bridle Leg No. 1	V-30
V-11	Tensiometer Reading, Bridle Leg No. 2	V-31
V-12	Tensiometer Reading, Bridle Leg No. 3	V-32
V-13	Parachute Pull Angle, Pitch Plane	V-33
V-14	Parachute Pull Angle, Yaw Plane	V-34
V-15	Total Parachute Pull Angle	V-35
V-16	Longitudinal Acceleration	V-36
V-17	Transverse Acceleration	V-37
V-18	Normal Acceleration	V-38
V-19	Vehicle Pitch Rate	V-39
V-20	Vehicle Roll Rate	V-40
V-21	Vehicle Yaw Rate	V-41
V-22	Parachute Lift During Descent	V-42
V-23	Parachute Axial Force Coefficient (Accelerometer Data vs. Mach)	V-43
V-24	Parachute Axial Force Coefficient (Tensiometer Data vs. Mach)	V-44

<u>FIGURE</u>	<u>TITLE</u>	<u>PAGE</u>
V-25	Parachute Axial Force Coefficient (Accelerometer Data vs Time)	V-45
V-26	Parachute Axial Force Coefficient (Tensiometer Data vs Time)	V-46
V-27	Dynamic Pressure Time - History	V-47
V-28	Mach Number Time - History	V-48
V-29	Flight Path Angle Time History	V-49
V-30	Aeroshell Separation Distance, 0-3 seconds	V-50
V-31	Extensiometer Separation Distance	V-51
V-32	Extensiometer and Guide Rail Location	V-52
V-33	Relative Angular Motion between Aeroshell and Lander	V-53
VI-1	BLDT AV-4 Test Condition	VI-25
VI-2	WSMR Map Showing TM and Radar Sites	VI-26
VI-3	Gyro Data Prior to Drop	VI-27
VI-4	Accelerometer Data Prior to Drop	VI-28
VI-5	Gyro Data During Powered Flight	VI-29
VI-6	Accelerometer Data During Powered Flight	VI-30
VI-7	Comparison between Radar Data (R122 to R128)	VI-31
VI-8	Comparison between Radar Data (R123 to R128)	VI-32
VI-9	Comparison between Radar Data (R122 to R123)	VI-33
VI-10	Radar (R123) Velocity vs. Flight Time	VI-34
VI-11	Radar (R123) Flight Path Angle vs. Flight Time	VI-35
VI-12	Radar (R123) Altitude (MSL) vs. Flight Time	VI-36
VI-13	STEP Trajectory Reconstruction of Altitude and Velocity	VI-37
VI-14	STEP Trajectory Reconstruction of Mach Number and Dynamic Pressure	VI-38
VI-15	STEP Trajectory Reconstruction of Vehicle Attitude and Flight Path Angle	VI-39
VI-16	STEP Trajectory Reconstruction of Body Heading and Velocity Heading	VI-40
VI-17	STEP Trajectory Reconstruction of Angle of Attack and Sideslip	VI-41

<u>FIGURE</u>	<u>TITLE</u>	<u>PAGE</u>
VI-18	STEP Trajectory Reconstruction of Total Angle of Attack	VI-42
VI-19	Vehicle Aerodynamic Characteristics	VI-43
VI-20	Angles of Attack and Sideslip at Parachute Deployment	VI-44
VI-21	Mission Ascent Profiles	VI-45
VI-22	Rocket Motor Support Structure Temperature-History	VI-46
VI-23	Aeroshell Temperature History	VI-47
VI-24	S-Band Transmitter Temperature History	VI-48
VI-25	Base Cover Temperature History	VI-49
VI-26	BLDT AV-4 Vehicle Azimuth Heading	VI-50
VI-27	BLDT AV-4 Torsional Stiffness	VI-51

LIST OF TABLES

<u>TABLE NO.</u>	<u>TITLE</u>	<u>PAGE</u>
IV-1	AV-1 Vehicle Flight Sequence of Events	IV-5
IV-2	Summary of Flight Parameters	IV-6
V-1	Parachute Geometric Properties	V-17
VI-1	BLDT AV-4 Atmospheric Properties	VI-21
VI-2	State Vector Data	VI-22
VI-3	Battery Performance Data	VI-23
VI-4	Final BLDT Mass Properties	VI-24

I. PURPOSE OF REPORT

The purpose of this report is to document the pertinent events concerned with the launch, float and flight of Balloon Launched Decelerator Test Vehicle AV-4 and the performance of the Decelerator System installed therein. The report will describe and provide data pertinent to the flight trajectory and decelerator test points at the time of decelerator deployment as well as a description of the time history of vehicle events and anomalies encountered during the mission.

The final test reports for BLDT Vehicles AV-1, AV-2 and AV-3 are contained in the following MMC documents:

AV-1 - Document number TR-3720289

AV-2 - Document number TR-3720291

AV-3 - Document number TR-3720293

II. MISSION OBJECTIVES

The mission objective for the BLDT program is to subject the Viking Decelerator System to qualification test requirements at simulated Mars entry conditions and in the wake of a full scale blunt body which simulates the Viking Lander Capsule. The program test requirements provide for parachute qualification at simulated Mars atmospheric conditions which are consistent with parachute deployment at supersonic, transonic and subsonic conditions.

The flight of Vehicle AV-4 provide for deployment of the decelerator under the simulated Mars atmospheric conditions equivalent to a supersonic case. The Mach number and dynamic pressure resulting from this simulated entry condition is shown on Figure II-1. The total vehicle requirements described in Paragraph 3.3 of "Parachute Test Objectives and Requirements Document for BLDT Program" (RD-3720247) are:

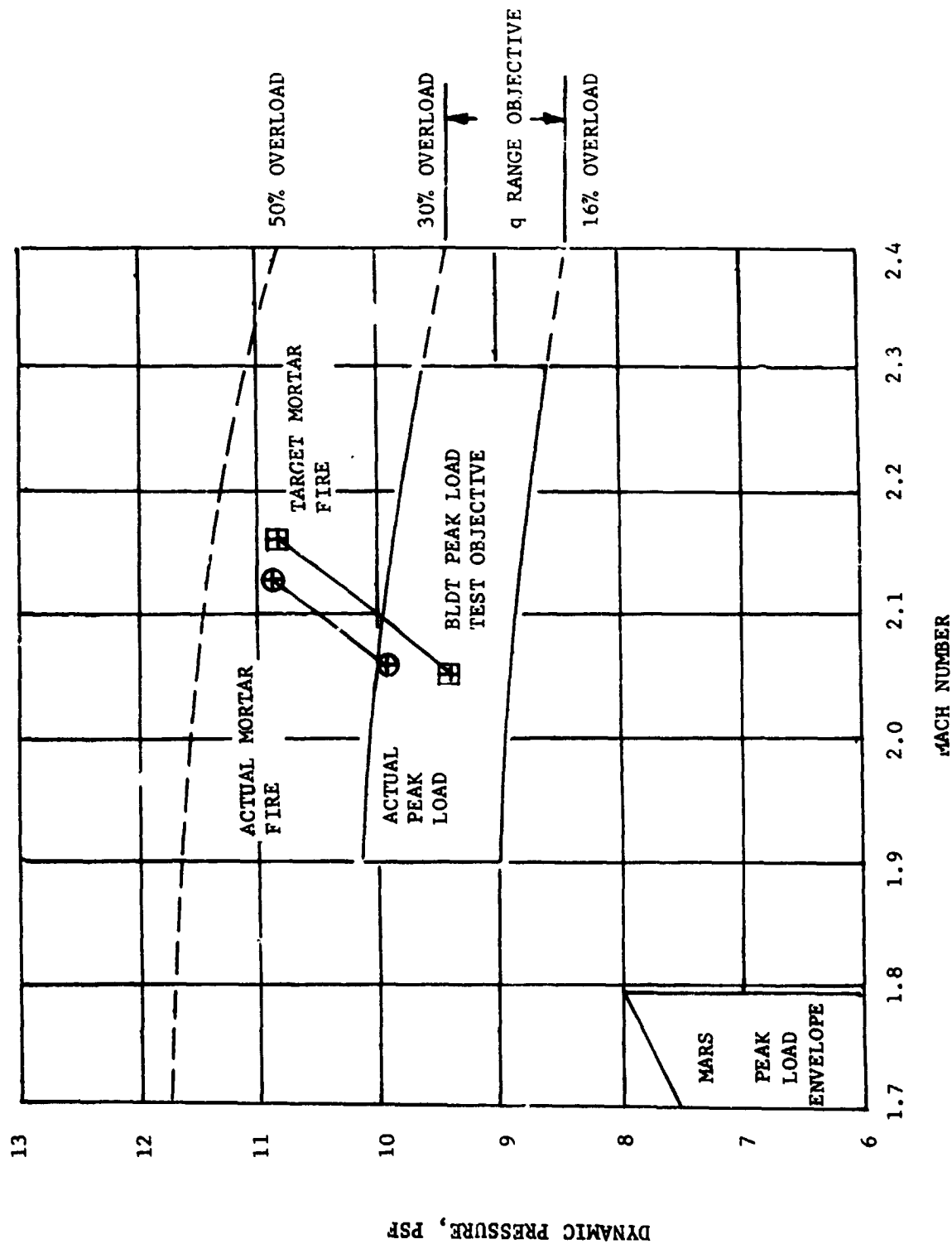
Angle of Attack at Mortar Fire	$\leq 17^{\circ}$
Residual Spin Rate	$\leq 100^{\circ}/\text{second}$
Parachute Temperature at Mortar Fire	$\leq 80^{\circ}\text{F}$
Simulated Mach Number/"q" conditions	See Figure II-1

It is noted that the flight of vehicle AV-4 was required due to the fact that vehicle AV-1, Case 1 supersonic test (see Appendix B) was declared a decelerator qualification "no test". The no test resulted from the imposition of overtest dynamic pressure conditions at decelerator mortar fire and at peak load with subsequent damage to the parachute, (see BLDT Vehicle AV-1 Post-Flight Test Report - TR-3720289).

In order to provide the velocity/atmospheric density equivalent to a supersonic Mars entry, the BLDT vehicle was lifted to high altitude (120,000 feet) beneath a balloon system. Once at the correct altitude and over the White Sands Missile Range, the flight vehicle was released from the balloon load bar and under control of airborne programming, the vehicle was boosted by solid rocket motors to the altitude (density)/velocity equivalent of the supersonic test condition.

It was also a goal of this mission to separate the vehicle aeroshell following decelerator deployment in order to obtain a time (distance history of the separation function).

A description of the BLDT vehicle, which served as the qualification test bed, is included in Appendix A of this report. A description of the BLDT mission is provided in Appendix B.



BLDT AV-4 TEST CONDITIONS

FIGURE II-1

III. DECELERATOR QUALIFICATION SUMMARY

The following is a summary of program events, pertinent to the decelerator system, occurring from the time of decelerator system installation in the BLDT vehicle through the recovery of the decelerator system at the point of payload impact.

A. Operations Summary

The decelerator system was installed in the base cover of vehicle AV-4 prior to final vehicle assembly for Flight Readiness Test. The system was Martin Marietta Corporation Serial Number 0000075 (GAC System S/N 16) with a system weight of 127.08# and an ejected pack weight of 90.1#.

During vehicle stand time while awaiting satisfactory meteorological conditions for launch, conditioned air was applied to the vehicle in order to maintain the vehicle interior, including the decelerator cannister, at a temperature below 80°F.

The decelerator system was subject to cooling during the ascent and float phases of the mission with pertinent decelerator temperatures just prior to release from the load bar as follows:

<u>Sensor Location</u>	<u>Spec. Req'd (°F)</u>	<u>Actual Temp (°F)</u>
*Bridle #1	+210 to -90	+34
*Bridle #2	+210 to -90	+35
*Bridle #3	+210 to -90	+37
Mortar Cannister #1	+80 (No Min)	+44
Mortar Cannister #2	+80 (No Min)	+46
Mortar Breach	+75 to +25	+49 (Automatic heater controlled)
Mortar Breach Flange	+75 to +25	+48

*Temperature measured on the base cover interior beneath the bridle leg.

B. Vehicle Performance

The AV-4 vehicle performed normally and all anticipated functions occurred. Mortar fire was commanded from the ground at the proper flight conditions for the decelerator test. The mortar fire conditions were:

	<u>TARGET</u>	<u>ACTUAL</u>
Mach Number	2.17	2.126
Dynamic Pressure (PSF)	10.84	10.9
Residual Spin Rate (Deg/Sec)	± 100	-30
Total Angle of Attack (Deg)	<17	5.2

There was no vehicle induced damage to the decelerator system.

During the flight of AV-4, it was anticipated that the solid rocket motors would create a heating condition on the base cover and bridle legs requiring thermal control. The base cover and bridle legs were protected with passive thermal control materials similar to vehicle AV-1. The recovered base cover of AV-4 provided no evidence of base heating which would have been detrimental to the bridle legs.

C. Decelerator System Summary

Mortar fire conditions were within the desired limits to produce opening load conditions that fell within the test objective Mach number and dynamic pressure envelope of Figure II-1. Mortar velocity of 114.2 fps was slightly higher than nominal but within the expected tolerance. Bag strip and inflation were normal with little unsymmetrical loading in evidence.

The maximum parachute opening load of 16,196 pounds occurred shortly after first full inflation. After a short period of area oscillations, the canopy reached stable inflation and showed good stability for the remainder of flight. No major damage was sustained by the parachute. Several black

smudges and small holes in the canopy appear to have resulted from exhaust residue from either the mortar or the BLDT propulsion units.

Parachute drag exceeded expectations in the supersonic regime and was near nominal below Mach 0.6. There was evidence of a drag reduction near Mach 1.0 as predicted by wind tunnel testing.

The parachute opening transient induced vehicle attitude rates as high as 111 degrees/second initially, which damped to less than 50 degrees/second in 10 seconds. The damping characteristics of the parachute, however, are not as good as expected.

Aeroshell separation was successfully demonstrated at a dynamic pressure of 3.18 psf and a Mach number of 1.18. The separation distance of 206 feet in 3 seconds more than adequately fulfills the minimum system requirement of 50 feet in 3 seconds.

IV MISSION OPERATIONS

The following is a description of the program events occurring from the time of vehicle AV-4 Flight Readiness Test through Recovery Operations.

A. Flight Readiness Test and Launch

BLDT Vehicle AV-4 completed Flight Readiness Test on August 3, 1972 with data review being completed on August 4, 1972. The airborne battery activation was completed on August 3, and installed prior to FRT.

A launch attempt was initiated on the evening of August 7 for a launch on August 8. This launch attempt was aborted due to thunderstorms in the Roswell launch area. Due to lack of range availability, no launch attempts were scheduled until the evening of August 12, at which time a launch operation was initiated for a launch on August 13. This launch attempt resulted in the launch of vehicle AV-4 at 1340 hours Z on August 13.

Balloon winch up and system launch were smooth and without incident with launch winds (surface to 1000 ft.) of approximately 4 to 6 mph.

During the prelaunch vehicle checkout, there were no BLDT system anomalies.

B. Ascent and Float

The balloon ground track during ascent and float was as shown in Figure IV-1. The float track to range, range intersect point, float heading at range intersect and range intersect time were in general agreement with the preflight predictions for these parameters.

Figure IV-2 presents the ascent profile of altitude versus time of day. It can be seen that the preflight predicted profile of 1000 feet/minute was not maintained with the result that float altitude was reached 24 minutes prior to vehicle release from the load bar rather than a possible 47 minutes.

Unlike vehicle AV-1, where the porpoising motion continued into the vehicle drop time phase, Vehicle AV-4 float altitude was nearly stable at the time of vehicle drop. Figure IV-3 presents an expanded view of the float motions for the final 29 minutes prior to vehicle release from the load bar.

During the ascent phase, the vehicle was acquired by range telemetry stations at approximately 13:52 hours Z and a balloon altitude of approximately 13 K feet. The vehicle command system was captured at approximately 14:01 hours Z at an altitude of 18.6 K feet. At approximately 14:09 hours Z (27 K feet), a vehicle command system check was performed by transmitting commands which did not change vehicle status (i.e., safe, safe backup) and verifying receipt of the commands at the vehicle via the vehicle to ground TM link.

Vehicle azimuth pointing operations during the float phase just prior to vehicle drop are covered in Section VI - Vehicle Performance Analysis.

During the ascent phase, at approximately 15:29 hours Z (97 K feet) azimuth point ground commands were transmitted to operate the airborne azimuth pointing system. Receipt of the commands and response of the vehicle was verified by TM data which provided a revised azimuth turning rate at the control center plot boards.

The azimuth pointing system installation and operation was required as a range safety constraint in order to assure that the vehicle azimuth at drop would maximize the probability of vehicle impact on range in the event of a complete failure of the decelerator system.

C. Vehicle Flight

All airborne and ground functions occurred as planned during the vehicle flight portion of the mission. The real time mortar fire command was issued by the WSMR ground computer based on radar tracking and T-24 hour meteorological data. The computer software used is described in Appendix E. The real time computed dynamic pressure is compared to the actual (T-1 hour meteorological data and reconstructed post flight trajectory) and also to the reference dynamic pressure (software reference) in Figure IV-4. The difference in the real time computed and reference dynamic pressure was used to predict the time when the desired dynamic pressure (10.84 PSF) would be obtained. When the real time prediction matched this value, the computer fired the mortar through the command system. The variation in this predicted mortar fire time just prior to mortar fire is also shown in Figure IV-4. The low noise level in the computer dynamic pressure allowed mortar fire to occur at a predicted dynamic pressure 2% above the target, at an overload of 1.26. The programmed sequence of flight events and actual event times for the vehicle flight are provided in Table IV-1. Table IV-2 contains a summary of predicted and actual flight parameters.

During this phase of the mission, the decelerator was deployed as planned. The analysis of the decelerator performance is provided in Section V.

It was a requirement during this phase of the mission to separate the aeroshell from the BLDT test bed in order to obtain a separation time-distance history. The analysis of the flight film, covered in Section V of this report, reveals that the actual separation rate exceeded the minimum requirement of 50 feet in 3 seconds.

Inspection of the recovered vehicle indicated -

1. All ordnance functions occurred with no damage to the vehicle due to separation processes or vehicle ordnance functions.
2. Base recirculation of SRM exhaust products during the boost phase was minimal since there was no evidence of high temperature effect on the base cover ablator.

D. Recovery Operations

The vehicle flight path was such that the payload impacted approximately 23 miles southwest of the vehicle drop point. (See Figure IV-1). The point of impact in the range was in sandy terrain and close to a major range road which minimized vehicle impact damage and provided easy access for recovering the expended vehicle and decelerator. All recovery operations were completed on the launch day.

Discussion of the condition of the recovered hardware is covered in later appropriate paragraphs.

TABLE IV-1

AV-4 VEHICLE FLIGHT SEQUENCE OF EVENTS

	Programmed Time (Seconds)	Actual Time (Seconds)	Source
1. Drop from Load Bar/ Initiate A/B Programmer	0	0	Ground Command
2. Ignite Spin Motors/ Enable Boost Motors	+1	1.02	A/B Programmer
3. Ignite Boost Motors	+2	2.04	A/B Programmer
4. Ignite Despin Motors/ Release Camera Lens Covers/ Start Aft Milliken Camera	+33	33.09	A/B Programmer
5. Initiate Mortar Fire/ Start Aft Photosonics Camera/ Start Forward Milliken Camera	33.5 to 42.0	40.43	Ground Command
6. Initiate Mortar Fire Backup/ Start Aft Photosonics Camera B/U/ Start Forward Milliken Camera B/U	+41	41.08	A/B Programmer
7. Separate Aeroshell	+48	48.08	A/B Programmer

TABLE IV-2
SUMMARY OF FLIGHT PARAMETERS

	<u>PREDICTED</u>	<u>ACTUAL</u>
A. Drop Time, GMT	--	16:24:30.75
B. Drop Conditions		
1. Longitude (DEG)	--	106.232
2. Latitude (DEG)	--	23.287
3. Altitude, Geometric (FT)	121,200	120,543
4. Drop Azimuth (DEG)	--	222.8
C. Spin/Despin		
1. Spin-up Rate (DEG/SEC)	194	203
2. Spin Rate at Despin (DEG/SEC)	140	110
3. Residual Spin Rate (DEG/SEC)	9	-30
D. Maximum Flight Conditions		
1. Maximum Q/V		
a. Time from Drop (SEC)	28.0	26.9
b. Max. Q (PSF)	22.1	24.8
c. Velocity (FPS)	2710	2844
2. Maximum Acceleration		
a. Time from Drop (SEC)	14.0	14.0
b. Max. Longitudinal Acceleration (g's)	4.52	4.77
E. Mortar Fire Conditions		
1. Mach Number	2.178	2.126
2. Dynamic Pressure (PSF)	10.84	10.9
3. Velocity (FPS)	2324	2290
4. Axial Acceleration (g's)	-0.94	-0.92
5. Altitude (FEET)	143,625	147,186
6. Angle of Attack (DEG)	-9.0	-4.1
7. Angle of Yaw (DEG)	0.0	-3.1
F. Aeroshell Separation Conditions		
1. Mach Number	1.10	1.18
2. Dynamic Pressure (PSF)	2.43	3.18
3. Time for 1 Foot (SEC)	0.18	0.16
4. Time for 50 Feet (SEC)	3.0	1.40
5. Distance at 3 seconds (FEET)	50.0	206

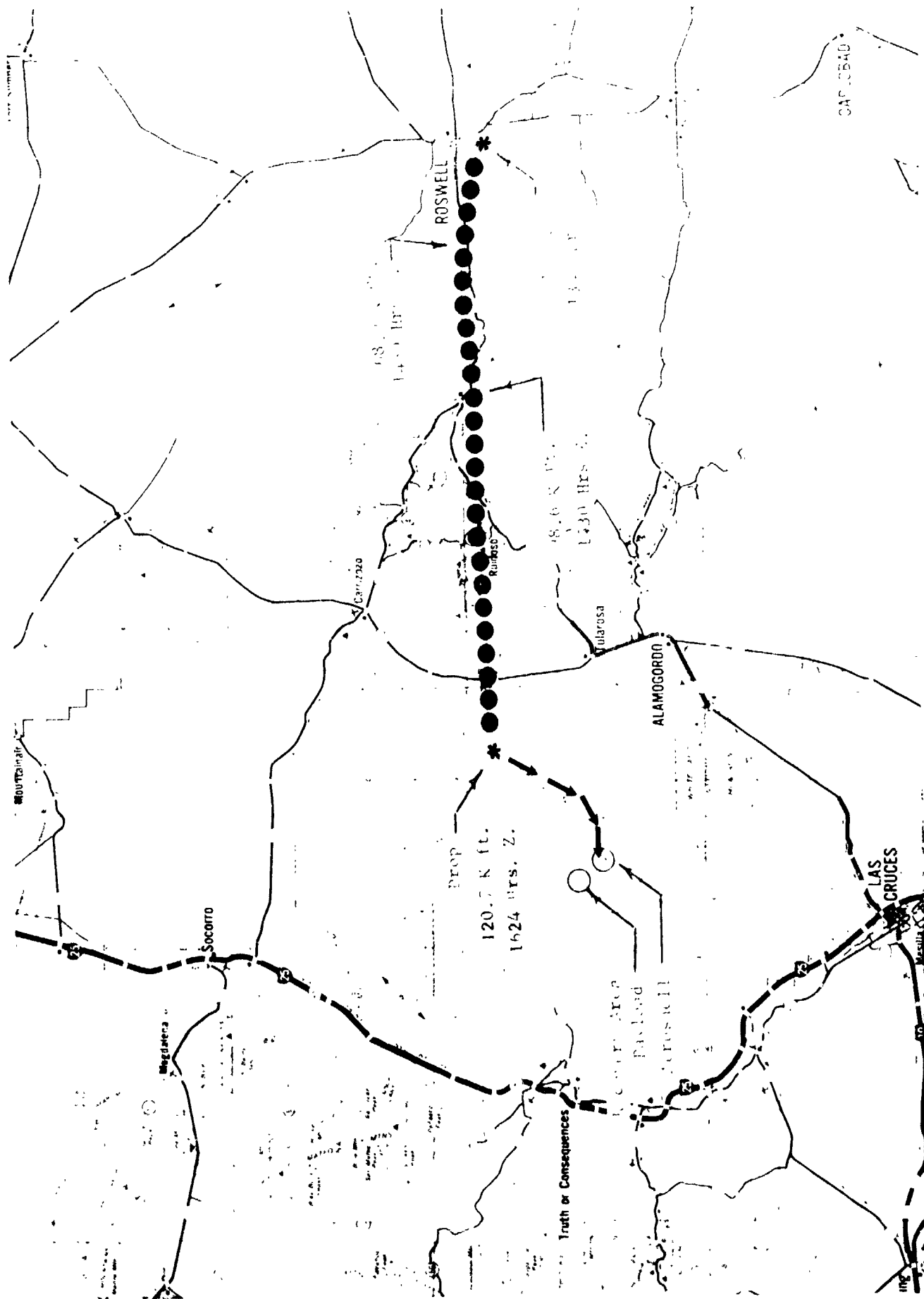


FIGURE IV-1
MISSION GROUND TRACK AN4

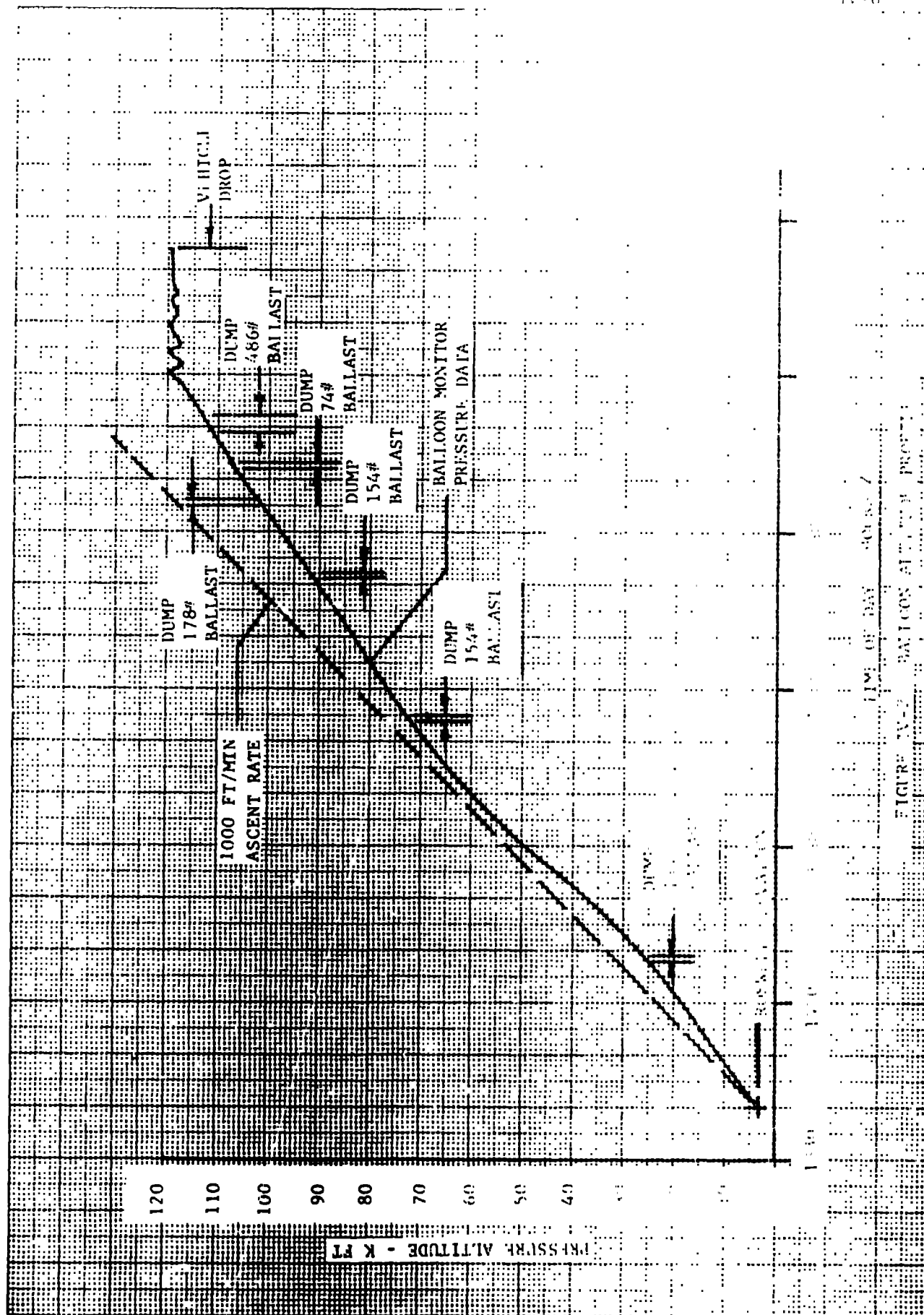
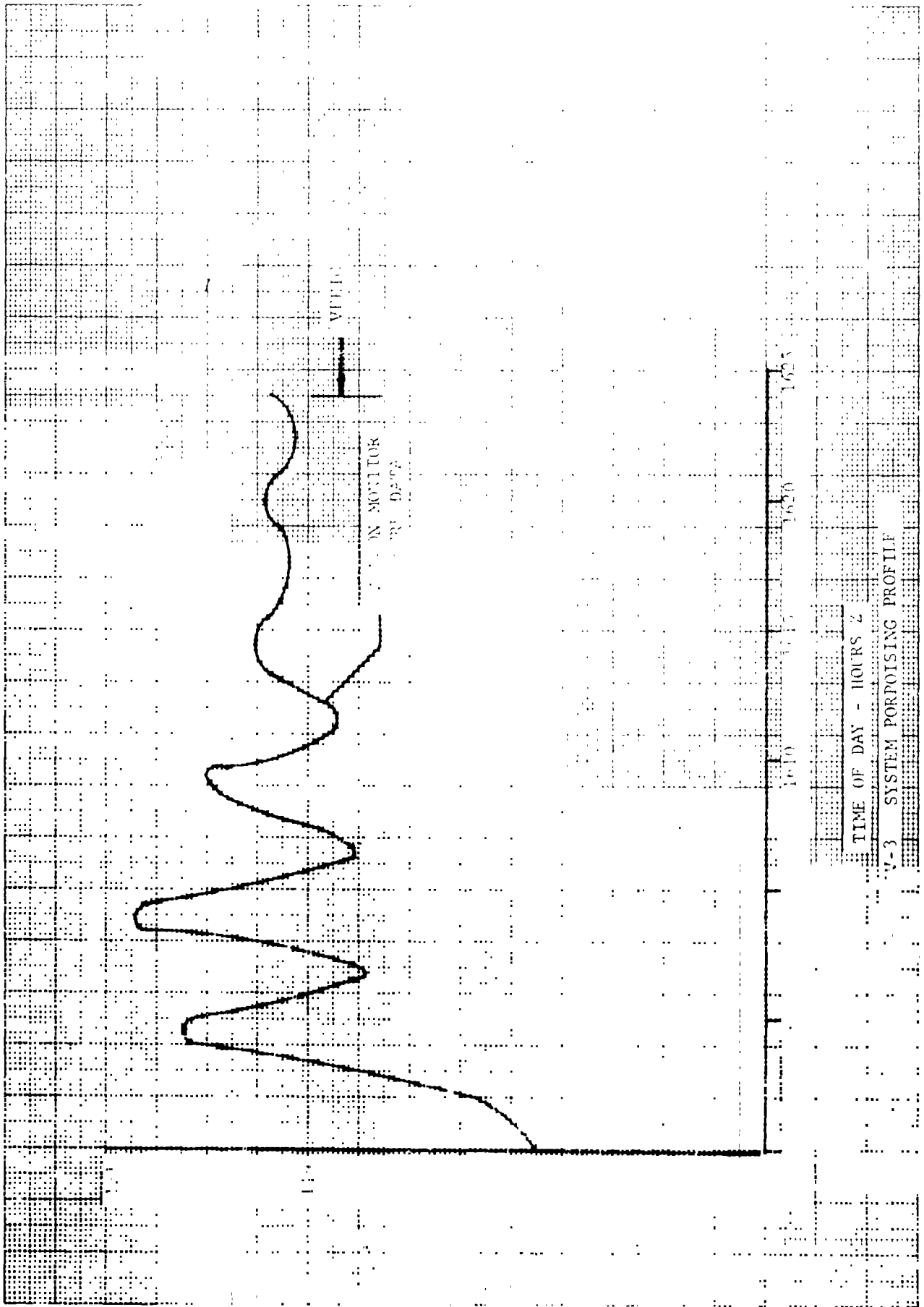


FIGURE IV-2 BALLOON ALTITUDE PROFILE



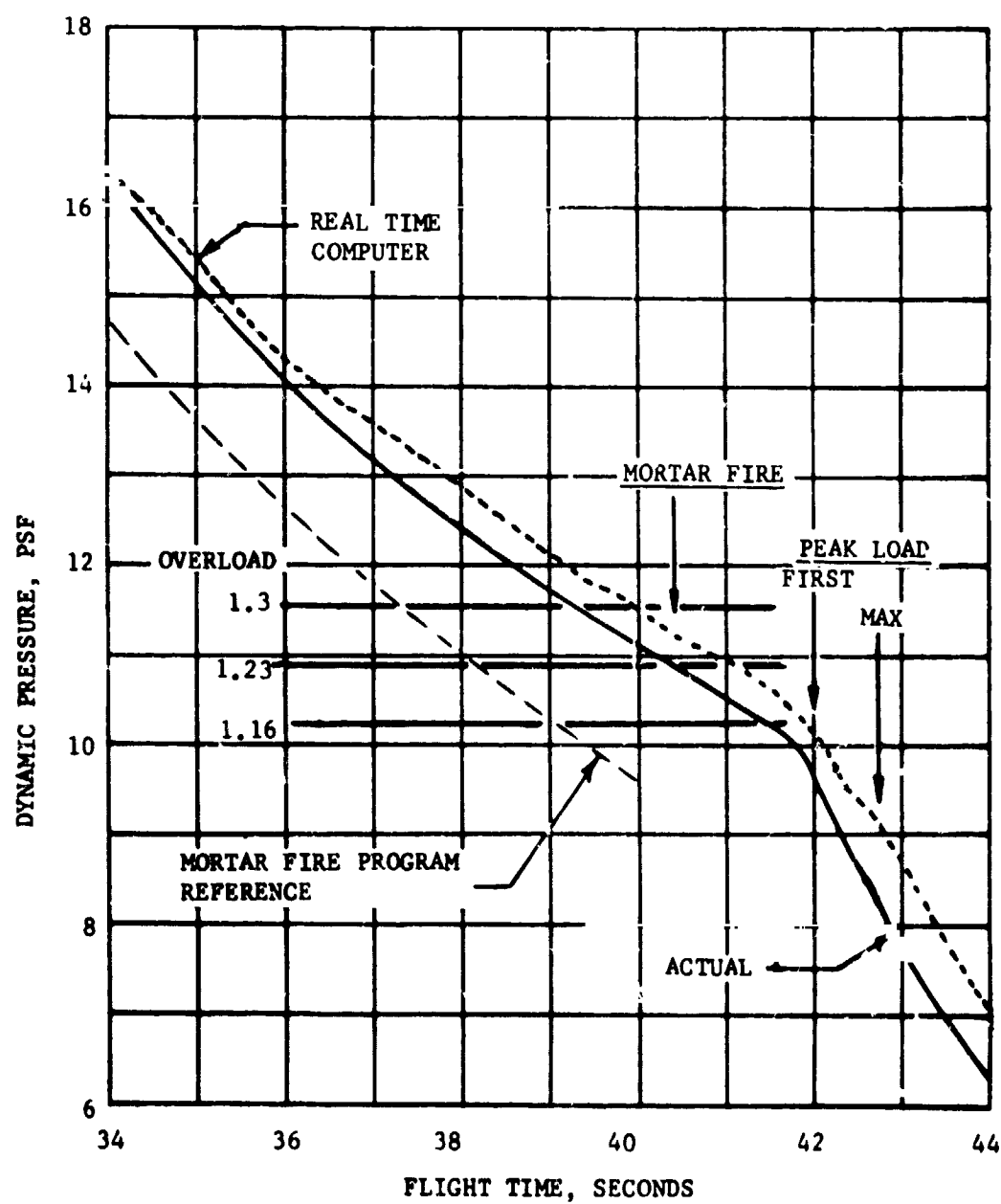
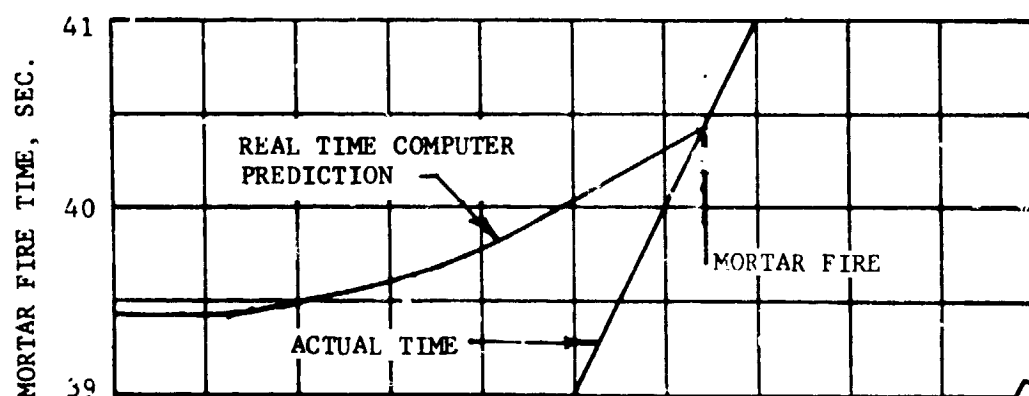


FIGURE IV-4 MORTAR FIRE COMMAND SYSTEM OPERATION

V. DECELERATOR SYSTEM ANALYSIS

A. System Description

Testing of the Viking decelerator system is the primary objective of this flight test. The Viking decelerator is a 53-foot nominal diameter Disk-Gap-Band (DGB) parachute with dimensions and general arrangement shown in Figure V-1. The parachute is fabricated entirely from Dacron type 52 except for the three-legged bridle which uses a special Goodyear proprietary fiber. The band cloth material is a 1.53 oz/sq. yd. rip-stop material having a minimum specified strength of 60 lbs/in. The disk cloth is a 2.12 oz/sq. yd. rip-stop material having a minimum specified strength of 90 lbs/in. The minimum strengths of the radial tapes, circumferential tapes and suspension lines are 900 pounds, 900 pounds and 880 pounds respectively.

The parachute is packed in a deployment bag to a density of 43 lbs/ft³ and stored in a mortar can aboard the BLDT vehicle in much the same manner as the Viking system. The BLDT vehicle itself is practically identical in shape and size to the Viking Lander Capsule. At mortar fire, the deployment bag is ejected straight back by a mortar whose reaction force is nominally oriented through the vehicle c.g. A breakdown of the ejected weight is seen in Figure V-2 to total 97 lbs. The relative velocity imparted to the deployment bag is expected from ground mortar test experience to be 112 ± 3 FPS.

Additional geometric data on the parachute are tabulated in Table V-1.

B. Mortar Fire Conditions

At mortar fire, the vehicle had a residual roll rate of -30 degrees per second and was coning about the velocity vector with a 5-6 degree angle. Plots of angle of attack and sideslip in Figure VI-20, Section VI, show

the mortar fire values to be -4.1 and -3.1 degrees respectively. Observation of the mortar smoke puff in the airborne film data 0.2 seconds after mortar fire shows an angle of attack of -5.5 degrees with sideslip angle near zero. The vehicle was therefore very near aerodynamic trim but was moving away from the trim at 14 deg/sec as indicated in Figure VI-19, Section VI.

A summary of the important mortar fire conditions compared with expected nominal values are tabulated below:

<u>MORTAR FIRE CONDITIONS</u>	<u>NOMINAL</u>	<u>FLIGHT</u>
Mach Number	2.178	2.126
Dynamic Pressure, psf	10.84	10.90
Velocity, fps	2324	2290
Axial Acceleration, g's	.94	.93
Altitude, ft	143625	147186
Angle of Attack	-8.4	-4.1
Angle of Sideslip	0	-3.1
Total Angle of Attack	8.4	5.2
Parachute Temperature	80°F	46°F

The mortar fire conditions for this flight produced dynamic pressure and Mach number at first peak load which fell within the desired envelope of test conditions as shown in Section II, Figure II-1.

C. Mortar Performance

The mortar performance is evaluated by observing the bag stripping process from the on-board camera. The time at which the canopy first starts emerging from the bag can be clearly seen to be .985 seconds from mortar fire. The actual distance the deployment bag must travel for the suspension lines to be pulled from the bag is defined by the length of the lines themselves. By simulating the mortar firing process with complete aerodynamic forces on the forebody and the deployment bag, the mortar velocity can be established.

The AV-4 flight conditions of Mach number, dynamic pressure and flight path angle at mortar fire are used. Assumptions were used as follows where flight data are not available:

1. Deployment bag $C_D S = 1.6$
2. Dynamic pressure gradient behind blunt body (Reference 3)
3. Forebody aerodynamic coefficients (Reference 4)
4. Line and canopy stripping forces of 2 and 6 lbs. respectively (Reference 5).

Past experience, most notably on the flight of AV-1 (TR-3720289) has shown that suspension lines do not follow a straight line between forebody and the deployment bag but are bowed as a result of aerodynamic force on the lines in proportion to the angle of attack and dynamic pressure existing at mortar fire. This characteristic has to be considered in the simulation for estimating mortar velocity. On the flight of AV-4, however, the angle of attack at mortar fire is relatively low (5.2 degrees compared with 13 on AV-1). The extent of line bowing can be seen in the deployment picture sequence in Figure V-3 to be very minor especially in the final stages of bag strip. In fact, the lateral motion of the swivel sets up traveling waves on the suspension lines which mask out the small line bowing effect due to angle of attack. One of these waves may be seen nearing the bag in Figure V-3 at $t = .546$. The suspension line alignment to the relative wind is therefore very erratic as seen in Figure V-4.

The net result of the foregoing discussion is that the difference between assuming straight lines or bowed lines on the distance between bodies at line stretch is small and amounts to less than 1 FPS on the estimated mortar velocity. A small amount of line bowing commensurate with the small angle of attack at mortar fire was used in estimating the mortar velocity to be 114.2 FPS. This is near the high side of the expected tolerance on this variable.

Simulation of the bag stripping process using a mortar velocity of 114.2 FPS resulted in the following sequence:

	<u>TIME-SECONDS</u>		<u>RELATIVE VELOCITY-FPS</u>
	<u>SIMULATION/ACTUAL</u>		
Mortar Fire	0	0	114.2
Line Stretch	.99	.985	86.4
Lowest ΔV	1.23		79.6
Bag Strip	1.30	1.233	83.6

The relative velocity at bag strip is seen to be more than adequate to assure positive bag strip. The difference between the simulated and actual time to bag strip is not unusual. The actual instant of bag strip from film data is difficult to obtain because the event is obscured by the inflating canopy. The inflation of the canopy material already out of the bag also shortens the distance the bag must travel before complete stripout occurs. This effect, if simulated, would reduce the simulated time to bag strip.

D. Decelerator Inflation Sequence

The on-board Milliken and Photosonic camera films were examined in detail to establish event times and to document the character of the parachute inflation. In the sequence shown below, certain events such as first peak load and aeroshell separation were obtained from telemetry data: Good correlation of all three sources of data was achieved:

<u>SEQUENCE OF EVENTS</u>	<u>TIME-SECONDS</u>
Mortar Fire	0
Line Stretch	.985
Bag Strip	1.233
Bag Behind Canopy	1.265
First Full Open	1.545
First Peak Load	1.570
Aeroshell Separation	7.650

Selected frames from the Milliken aft viewing camera show in Figure V-3 some of the significant events during and shortly after the inflation phase. The growth of the canopy from line stretch was obtained by tracing the projected area images from the Milliken camera and integrating these images with a planimeter. A canopy growth parameter curve of normalized area versus time is then constructed in Figure V-5. The projected area at any time is divided by the projected area observed in the final seconds of film coverage. The time scale is normalized by the total filling time. Although the curve of Figure V-5 is fairly typical for a DGB parachute, it is seen to be considerably different than that experienced on the AV-1 damaged canopy inflation. On AV-4, bag strip is complete before any appreciable inflation has taken place. Once inflation begins, the growth rate is very rapid with very little round-off at the peak value.

A plot of the projected area ratio, $S_p/S_{p_{final}}$, versus time from line stretch is presented in Figure V-6. Two features of this curve deserve mention. First, the initial peak area exceeds the final steady state value, $S_{p_{final}}$, by about 12 percent. This would normally be interpreted as an indication of high canopy loading. Secondly, there are two significant dips in the area time-history at Mach numbers of 1.90 and 1.66. Past experience with the DGB parachute (Reference 6) has shown a tendency towards unstable canopy inflation above Mach 1.4. The second dip experienced on AV-4 is larger than experience would predict and occurs after a period of relatively stable inflation. An examination of the aft viewing camera data reveals that the parachute appears to move across the forebody wake at 1.0 and 3 seconds after line stretch. These times suggest a possible cause and effect relationship between inflation stability and wake interference. This

is considered a transient situation which becomes less significant at lower Mach numbers.

No correction has been applied to the projected area ratio in Figure V-6 to correct for variation in the canopy image plane under changing load conditions.

Parachute inflation was smooth and uniform. The time from line stretch to first full inflation is seen in Figure V-6 to be .56 seconds. This value is plotted in Figure V-7 along with similar data from PEPP and LADT flight tests. The filling time for AV-4 agrees very closely with AV-1, falling near the lower edge of the expected uncertainty in this parameter. The nominal and expected dispersion envelope shown will be re-established as a result of the total BLDT experience.

E. Opening Load

Figures V-8 and V-9 show the time-history of the total longitudinal parachute load recorded by the bridle attach point tensiometers for 10 and 50 seconds after mortar fire. The first peak load is seen to be 13,253 lbs. and occurs 1.57 seconds after mortar fire (.025 seconds after first full open). The actual maximum load of 16,196 lbs. occurring at 2.30 seconds is reasonably close to the opening load of 17,123 lbs. obtained by simulating AV-4 deployment conditions.

The individual tensiometer readings are recorded in Figures V-10, V-11 and V-12. By proper combination of the three tensiometer readings, the equivalent parachute load pull angles in pitch and yaw are obtained and plotted in Figures V-13 and V-14. These angles are the projections in the pitch and yaw planes of the total angle between the parachute load and the forebody vehicle centerline. The total pull angle is shown in Figure

V-15. The large pull angles prior to load build-up (0 to 1.5 seconds from mortar fire) are influenced by line and swivel dynamics and do not reflect significant load conditions. The structurally significant pull-off angle occurring at peak load ($t = 2.3$ seconds) is 3.2 degrees. This value is within 0.2 degree of the AV-1 peak load pull-off angle and agrees quite well with analytical predictions in Reference 8.

Accelerometer readings in the X, Y and Z axis directions during the 10 and 50 second time periods are shown in Figures V-16, V-17 and V-18. The peak longitudinal acceleration of -9.728 g's occurs at 2.29 seconds after mortar fire and reflects a parachute opening load of 16050 lbs. This is based on subtracting out the aeroshell drag component using C_D of 1.6, a dynamic pressure of 8.5 PSF, and a payload mass of 55.8 slugs. The longitudinal accelerometer, therefore, confirms the opening load recorded by the tensiometers almost exactly. Mortar fire at $t = 0$ and aeroshell separation at $t = 7.65$ seconds are clearly visible on the accelerometer plots. Noise spikes on the accelerometer traces at $t = 33$, 35 and 42.5 seconds should be ignored.

F. Vehicle Stability

The BLDT vehicle was coning about the velocity vector with an angle of 5-6 degrees and had a residual spin rate of 30 degrees per second. Although the vehicle was very near aerodynamic trim at mortar fire, it had an attitude rate of -14 degrees/second and was moving to a higher angle of attack. The motion of the vehicle after mortar fire aggravates the initial alignment between the inflating parachute and the vehicle centerline and is a measure of the severity of the attitude rate transient to the vehicle. The attitude rate transient on AV-4, therefore, should represent near worst

case conditions. The vehicle attitude rate time-histories in Figure V-19, V-20 and V-21 confirm a significant attitude perturbation at parachute opening shock. Peak rates of 111 degrees/second in pitch and 81 degrees/second in yaw occur 2.97 seconds after mortar fire or shortly after peak load. The damping characteristics of the parachute in reducing the magnitude of this oscillation are not as good as was predicted in Reference 2. It takes 22 seconds before the pitch and yaw rates fall below 30 degrees/second. The rates out beyond 50 seconds are significantly lower than the AV-1 experience mostly because the long period oscillation attributed to canopy damage was not in evidence on AV-4. It is noted that pitch and yaw rates do not exceed 17 degrees/second beyond 77 seconds from mortar fire. The roll rate in Figure V-20 is seen to gradually reduce from 30 degrees/second at mortar fire to near zero at 150 seconds.

The rotation rate data generated on this flight is probably more typical of what to expect on Mars than the data produced by the flight of AV-1 with its damaged canopy. Nevertheless, these flight results will have to be extrapolated to Mars before being applied as requirements to Viking hardware.

The tendency of the DGB parachute to oscillate or cone about the velocity vector has been observed on this flight. During the high altitude phase of parachute flight, radar ground track and trajectory reconstruction efforts indicate a coning parachute motion. Film coverage of the parachute motion just prior to ground impact, seems to indicate more of an oscillatory motion with an amplitude of ± 8.5 degrees and a period of 10 seconds per cycle. This characteristic motion will require further evaluation and comparison with other BLDT flights.

G. Parachute Drag Performance

The evaluation of the drag of the parachute was conducted in two overlapping phases. The first used the reconstructed vehicle trajectory parameters at mortar fire and integrated the axial accelerometer data as a drag acceleration to obtain the subsequent trajectory. This zero lift trajectory deviated grossly from the tracking data. The deviations indicated a force normal to the velocity vector was present. The radar data was then re-examined to evaluate this acceleration vector converted to an L/D (lift-to-drag ratio). When this lift time history was included in the analysis, the integrated trajectory conformed to the radar measurements and was used to obtain the dynamic pressure for non-dimensionalizing the tensiometer and accelerometer data into a force coefficient. The conversion to an incremental parachute force coefficient was then made to the tensiometer data by adding to it the force necessary to maintain the relative velocity between the parachute and vehicle equal to zero; i.e., the acceleration force on the parachute mass.

The telemetered accelerometer data was used for this correction in the equation.

$$C_{FT} = (F_T - A_x * W_p) / Q S_p$$

where:

C_{FT} = Parachute Force Coefficient

F_T = Sumation of Tensiometer data, lb.

A_x = Vehicle Axial Acceleration, g's

W_p = Weight of the parachute, 95 lb.

Q = Dynamic pressure

S_p = 2206 ft

The axial acceleration of the vehicle was converted to the incremental parachute force by removing the estimated drag of the aeroshell or base cover from Reference 4. The equation used is:

$$C_{FA} = A_x * W_T / (Q S_p) - C_{D_v} S_v / S_p$$

where:

C_{FA} = Parachute Force Coefficient

A_x = Vehicle Axial Acceleration, g's

Q = Dynamic Pressure, PSF

S_p = 2206 ft²

C_{D_v} = Forebody drag coefficient

S_v = Forebody reference area, 103.8 ft²

W_T = Total system weight, 1897 lbs. before Aeroshell Separation
1541 lbs. after Aeroshell Separation

It should be noted that the coefficient derived using these equations has been labeled a force coefficient since the loads have not been resolved relative to the velocity vector. In order to separate the lift component more information concerning the angle of attack of the vehicle and angle of attack of the parachute would be required. The relative loads in the 3 bridles give some information as to their relative attitude and show this angle is small, however the overall attitudes will require further evaluation. This evaluation phase was conducted until 50 seconds after parachute deployment.

The second phase was begun using trajectory data from radar just after aeroshell separation and evaluated the drag coefficient necessary to obtain the radar altitude at various subsequent times. In both phases the best estimates of the meteorological data was used. During this evaluation, the parachute lift again produced irregularities in the

tracking data which could not be matched with a zero lift trajectory. A more detailed examination of the tracking data showed sinusoidal oscillations in the North-South and East-West velocities after vertical descent should have been attained (80 seconds after deployment). The mean value of the oscillation was in agreement with the prevailing wind data but deviated alternately in a North, West, South, East repetitive fashion. The acceleration necessary to cause such a velocity change to the descending parachute was interpreted as a lift vector which was coning counter clockwise about the descent velocity. Figure V-22 presents the magnitude and rotation rate of this coning angle as well as the L/D used in Phase 1. Since the quasi-steady state drag is time averaged, the lift was not included in the drag evaluation which is based only on the descent rate.

Parachute axial force coefficients derived from accelerometer data and tensiometer data are plotted versus Mach number in Figures V-23 and V-24 respectively. The two plots are almost identical to one another, showing dips at Mach 1.66 and 1.90 where the canopy collapses partially (See Figure V-6) and at aeroshell separation (Mach 1.18). The expected dispersion of parachute drag from wind tunnel results, (Reference 7), is superimposed over the flight test results in the two figures. Both plots show a dramatic drop in magnitude near Mach 1.0 as predicted by the wind tunnel results. The supersonic drag performance is near the high side of the expected dispersion of this parameter.

When near steady state descent conditions are achieved, the tensiometer and accelerometer data become poor sources of drag performance. The vehicle is so near equilibrium that noise on the traces becomes larger than variation in the parameter of interest. The quasi-steady state drag performance is determined by iterating on drag coefficient until the altitude

change over a time increment matches the tracking data. The drag coefficient estimates derived in this manner are plotted in Figure V-23 and average at 0.63, slightly above the wind tunnel nominal value of 0.61. A trend toward an increase in C_D at low Mach number below 40,000 feet altitude is indicated.

Plots of parachute axial force coefficient versus time in Figures V-25 and V-26 are included for convenience in correlating this data with time. The trajectory parameters of dynamic pressure, Mach number and flight path angle which were used in post mortar fire trajectory reconstruction are presented in Figures V-27, V-28 and V-29 respectively.

H. Aeroshell Separation

Aeroshell separation on this flight was intended to demonstrate satisfactory system operation at a Mach number of 1.1 and dynamic pressure of 2.43 psf. Actual AV-4 separation took place 7.65 seconds after mortar fire at which time the Mach number was 1.18 and the dynamic pressure was 3.18 psf. The vehicle was pitching at 56 degrees per second at the instant of aeroshell separation. This is almost twice as high as the specification rate of 30 degrees/second which is a design criteria for the separation guide rail system but is significantly lower than the 69 degrees/second experienced on AV-1.

The objectives of the separation demonstration are:

- (1) To determine that there are no unpredictable aerodynamic disturbances at separation that would compromise the Viking mission,
- (2) To exercise the separation hardware and concept to insure that analytical evaluations of separation dynamics are valid, and
- (3) To determine that parachute drag is adequate to produce a minimum of 50 feet of separation between aeroshell and lander in 3 seconds.

Photographic evaluation of aeroshell separation on AV-4 reveals a well behaved, predictable performance. Separation distance versus time is obtained from the Milliken camera film by knowing the diameter of the aeroshell to be 11.5 feet, the horizontal field of view of the camera to be 54.9 degrees and the frame rate to be 32 frames/second. The separation distance may then be calculated by measuring the aeroshell image size on a specific horizontal field of view and correlating with the number of frames since separation.

$$\text{Separation Distance} = \frac{11.5 \times \text{H.F.V.}}{.958 \times \text{Image Diameter}}$$

The separation distance versus time plot in Figure V-30 shows 206 feet of separation in 3 seconds. Simulation of this separation using actual AV-4 flight conditions including parachute drag shows excellent agreement with the flight results. It should be noted that a slight dip in parachute drag shortly after aeroshell separation (7.65 seconds after mortar fire) as seen in Figure V-25 had to be simulated to get good agreement in the simulation. This drag reduction occurs in the transonic region where wind tunnel tests predicted a reduction in drag coefficient. No significant change in the parachute projected area was observed during aeroshell separation that would account for the changing drag (see Figure V-3 at $t = 7.72$). The fact that separation took place at a dynamic pressure 31 percent higher than planned would have the effect of increasing the separation distance in 3 seconds by almost the same percentage.

The first 12 inches of aeroshell separation distance versus time is obtained from extensometer data and plotted in Figure V-31. The AV-4 separation motion is slightly faster than simulation would predict. The fact that all three extensometer readings do not agree is an indication of relative angular rotation between bodies as the aeroshell separates. In order to compute the extent of angular rotation, the guide rail and extensometer locations must be defined as in Figure V-32. The guide rail system involves 3 rails and guides which provide moment constraint for the first 6 inches of separation and shear constraint for the final 6 inches of travel. The relative rotation angle between aeroshell and lander is plotted in Figure V-33. The maximum angle at the point where total moment constraint is lost is seen to be 1.7 degrees. This compares with a 1.53 degree relative angle recorded in a ground test of the system subjected to a bending moment of 560 ft-lbs ($.87 \times$ design moment). The AV-4 guide rail system therefore

appears to have been subjected to near design bending moment on this flight and functioned satisfactorily without any apparent damage. Also evident in Figure V-33 is the constraining influence of the rails after bottoming out approximately 0.7 degrees of system tolerance at .06 seconds. This tolerance agrees well with the expected tolerance of .5 to 1.0 degree between mating parts of the system.

I. Parachute Recovery Assessment

A detailed post-test examination of the parachute was conducted by MMC and GAC. A report of this inspection by the parachute contractor is presented in Appendix C. A graphic description of canopy anomalies is included as Figure C-1 therein. In general, the parachute suffered no significant damage and this test is therefore considered a successful qualification of the decelerator. There were black smudge marks noted that probably came from mortar or BLDT engine exhaust residue. The several small tears and holes found in the canopy seemed to show evidence of heat damage and would suggest hot engine exhaust particle impingement or bag stripping frictional damage.

Pre-flight and post-flight parachute dimensions are recorded in Appendix D. Between the time of pre-flight measurement and post-flight inspection, the packed parachute is exposed to a heat compatibility test. Experience has shown that suspension line lengths shrink approximately 2 percent during the heat cycle. Therefore we can assume suspension lines that are initially 90 feet long shrink to 88 feet prior to flight. The suspension line length increase, as a result of flight load, ranges from 2 feet 11 inches on radial 35 to 4 feet 8 inches on radial 6. The disk radial dimension increase varied uniformly between 1 inch and 2-3/8 inches.

Compared with AV-1, these changes indicate a fairly symmetric canopy inflation. The bridle leg length increases were $3/8$, $3/8$ and $1/2$ inch respectively. Other dimensional changes were minor.

TABLE V-1

PARACHUTE GEOMETRIC PROPERTIES

<u>Item</u>	<u>Relative Value</u>	<u>Value</u>
Nominal diameter	D_o	53 feet
Geometric porosity*	$0.125 S_o$	276 ft^2
Total area (S_o)**	$(\pi/4) D_o^2$	2206.2 ft^2
Disk area+	$0.53 S_o$	1169.3 ft^2
Disk diameter	$0.726 D_o$	38.5 ft
Disk circumference	$2.285 D_o$	121 ft
GAP area	$0.12 S_o$	264.7 ft^2
GAP width	$0.042 D_o$	2.2 ft.
Band area	$0.35 S_o$	772.2 ft^2
Band width	$0.121 D_o$	6.4 ft
Vent area	$0.005 S_o$	11.0 ft^2
Vent diameter	$0.07 D_o$	3.7 ft
Number of suspension lines	--	48
Length of suspension lines	$1.7 D_o$	90 ft

* Vent plus gap provide 12.5 percent geometric porosity

** Disk + gap + band

+ Includes vent

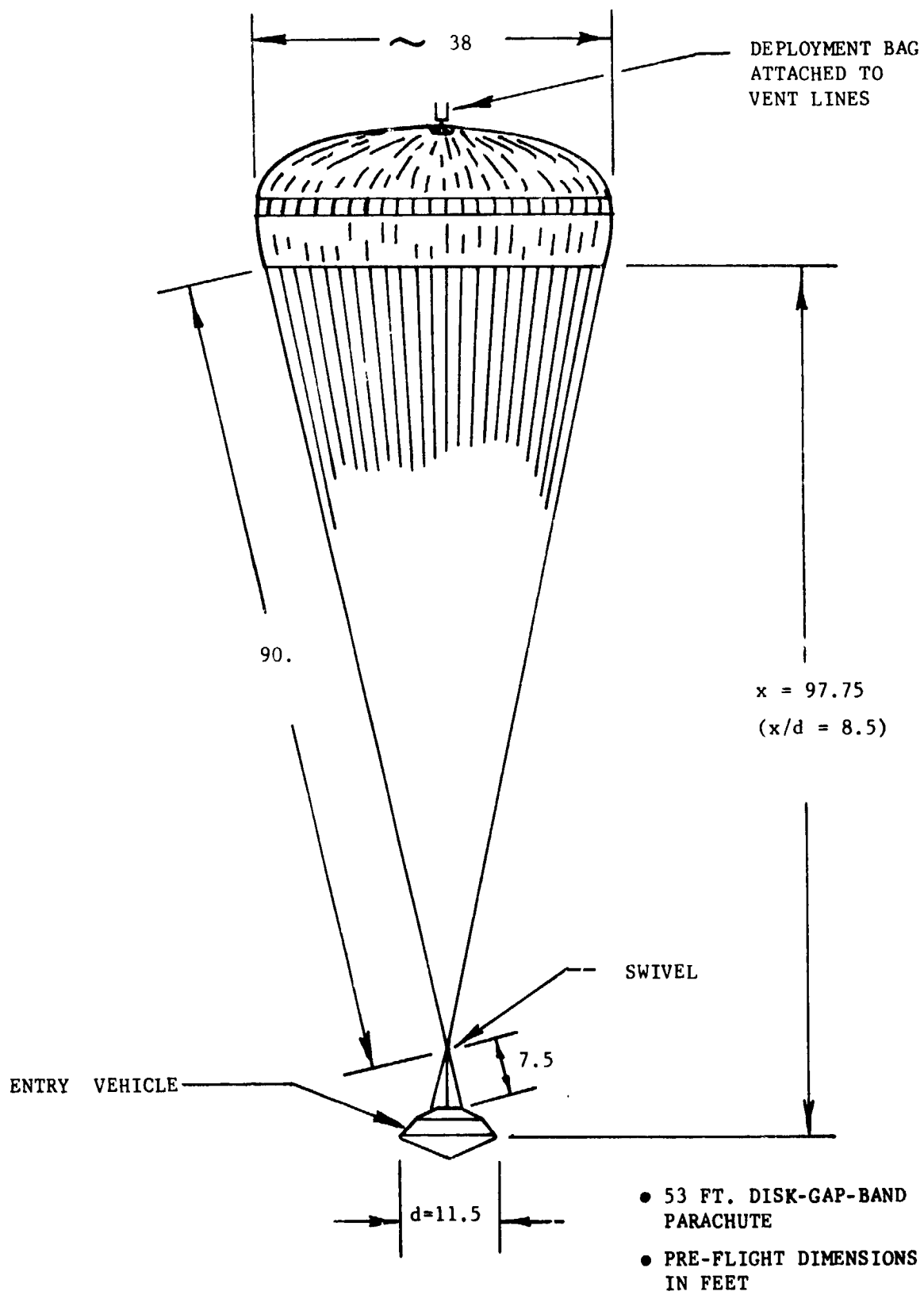


FIGURE V-1 VIKING DECELERATOR SYSTEM

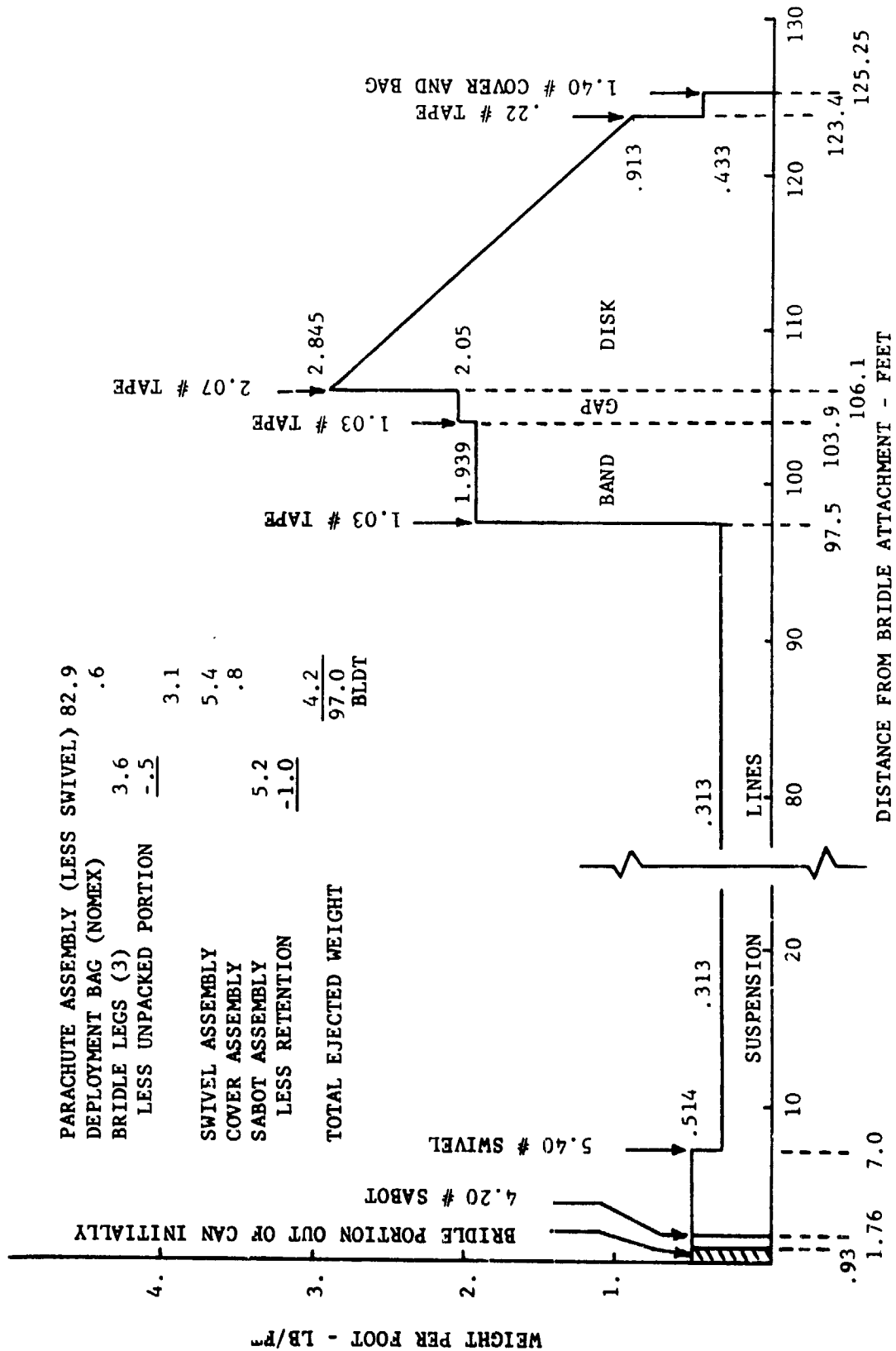


FIGURE V-2 EJECTED WEIGHT DISTRIBUTION



$t = .094$
BAG EMERGING



$t = .250$
STRAIGHT LINE



$t = .468$
LINE BOWING



$t = .556$
TRAVELING WAVE ON LINE

FIGURE V-3 ON-BOARD CAMERA PHOTOGRAPHS



$t = .985$
LINE STRETCH



$t = 1.233$
BAG STRIP



$t = 1.310$
INFLATION



$t = 1.390$
INFLATION



U = 1.00
1.00000



U = 1.00
1.00000



U = 1.00
PARTIAL COLLAPSE



U = 1.00
OVERSTRESS

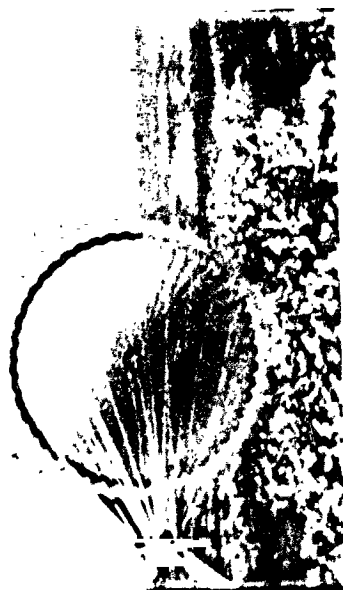
FIGURE V-7 OVERFORD CAMERA PHOTOGRAPHS OF (a) (b) (c) (d)



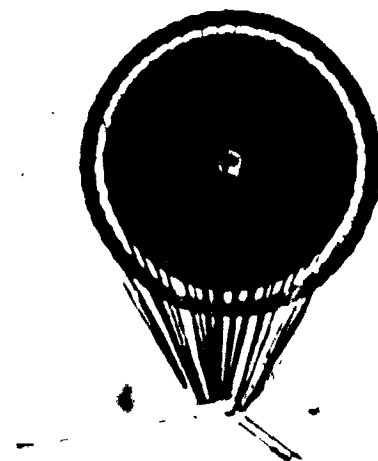
$t = 8.550$
PARTIAL COLLAPSE



$t = 9.000$
OPEN AGAIN



$t = 7.720$
AFTER AEROSHELL SEPARATION



$t = 12.200$
FINAL VIEW

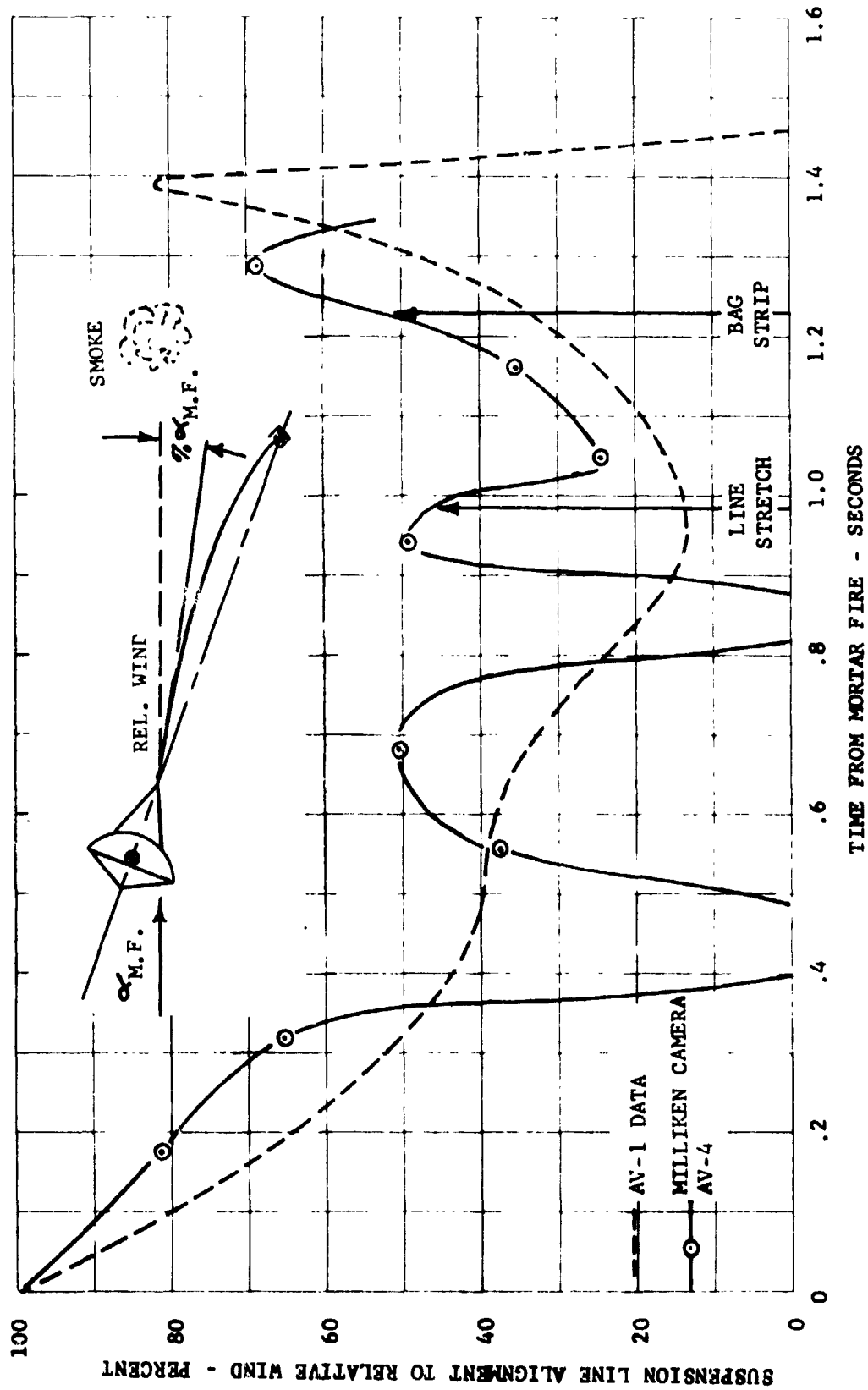


FIGURE V-4 ANGLE OF ATTACK LINE BOWING EFFECT

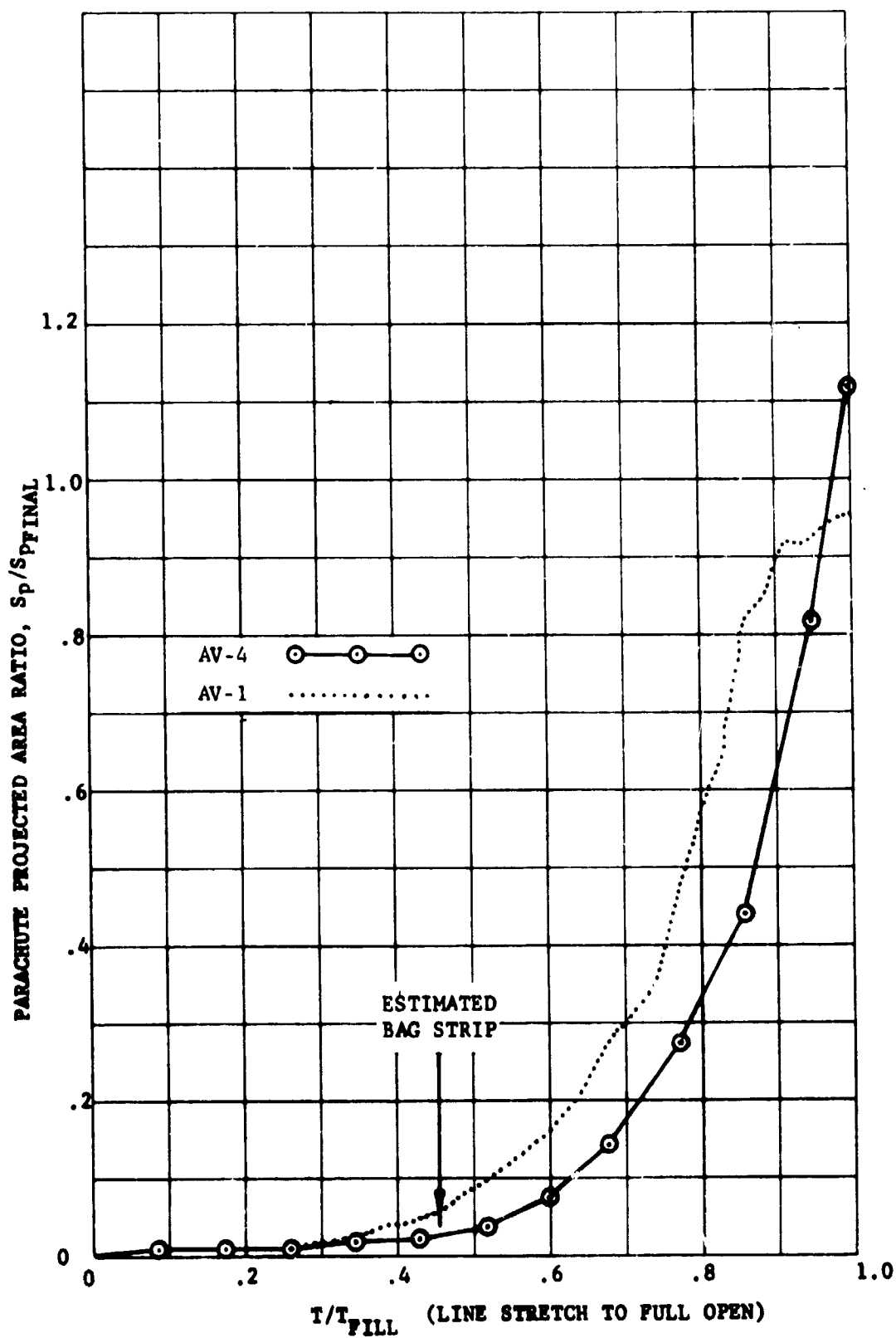


FIGURE V-5 CANOPY GROWTH PARAMETER

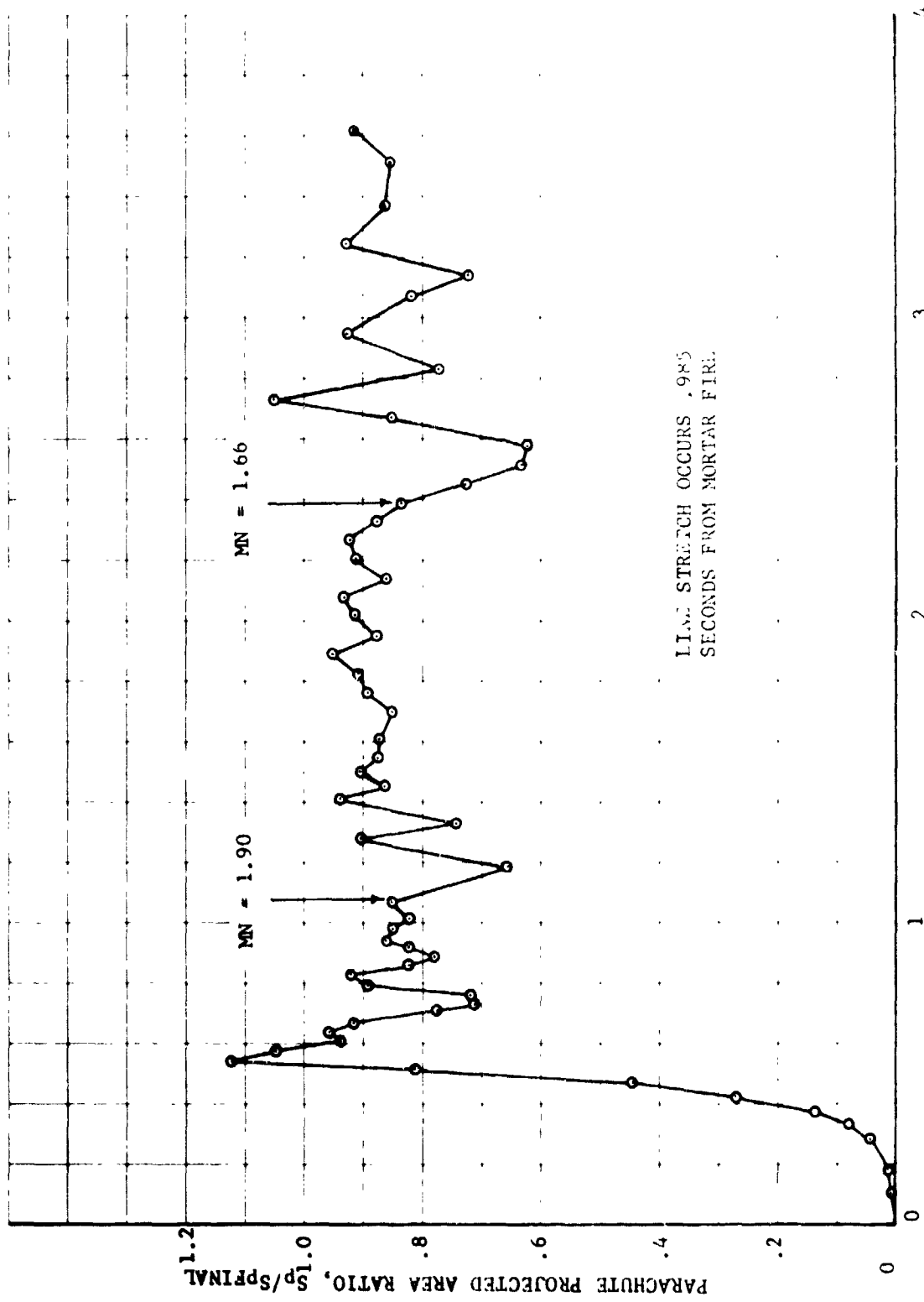


FIGURE V-6 CANOPY AREA OSCILLATIONS

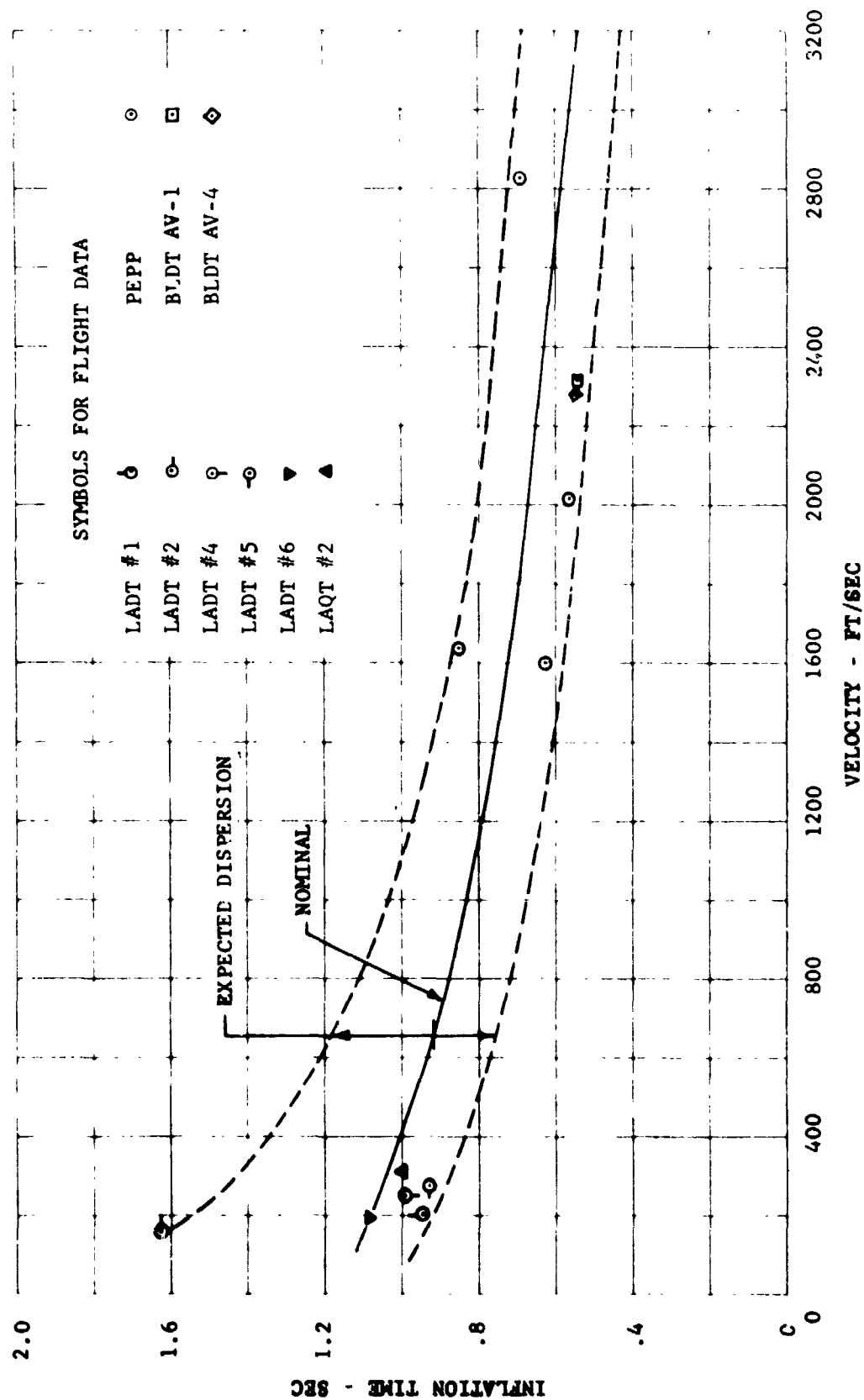


FIGURE V-7 PARACHUTE FILLING TIME FROM LINE STRETCH

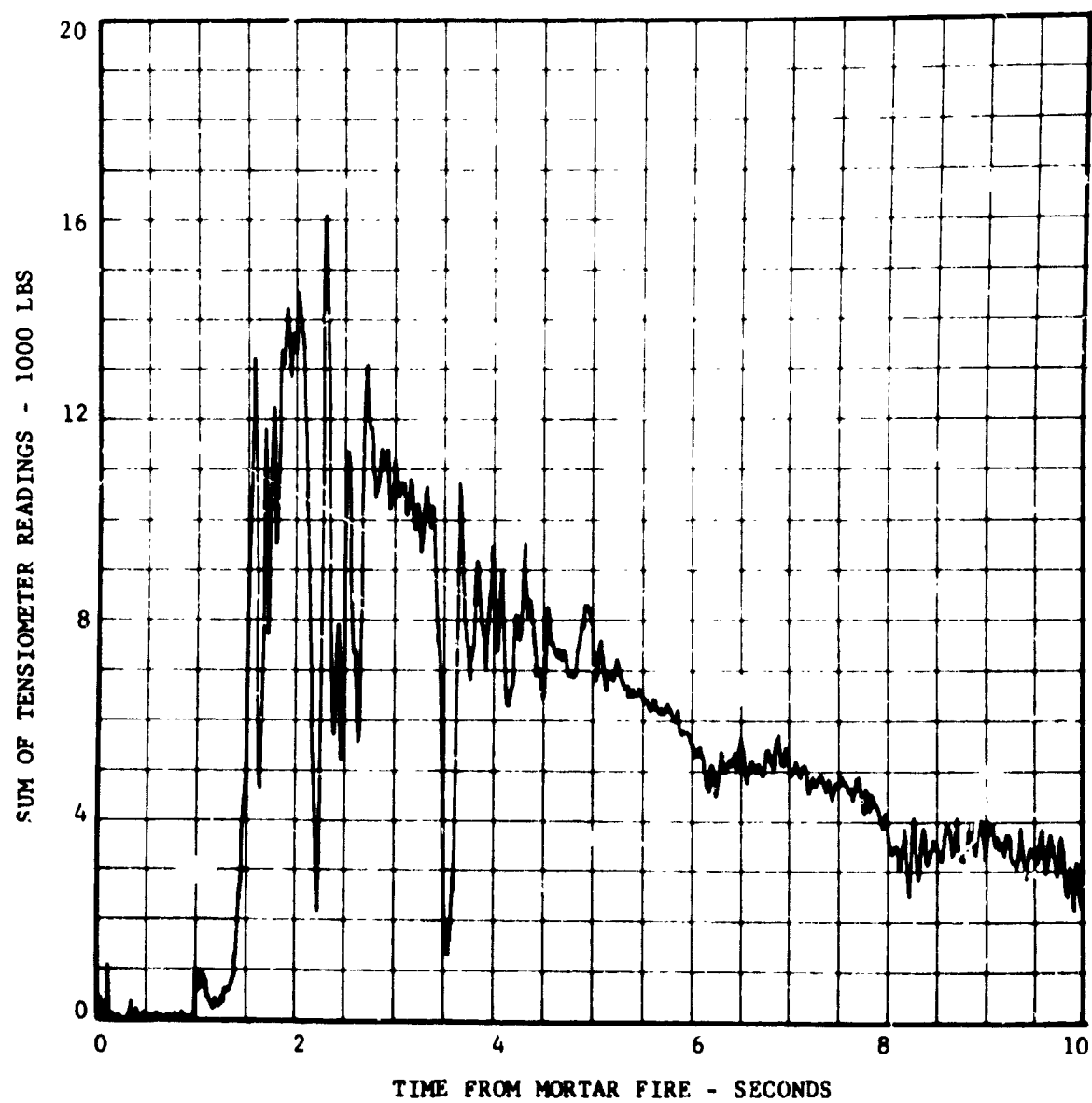


FIGURE V-8 PARACHUTE OPENING LOAD, 0-10 SECONDS

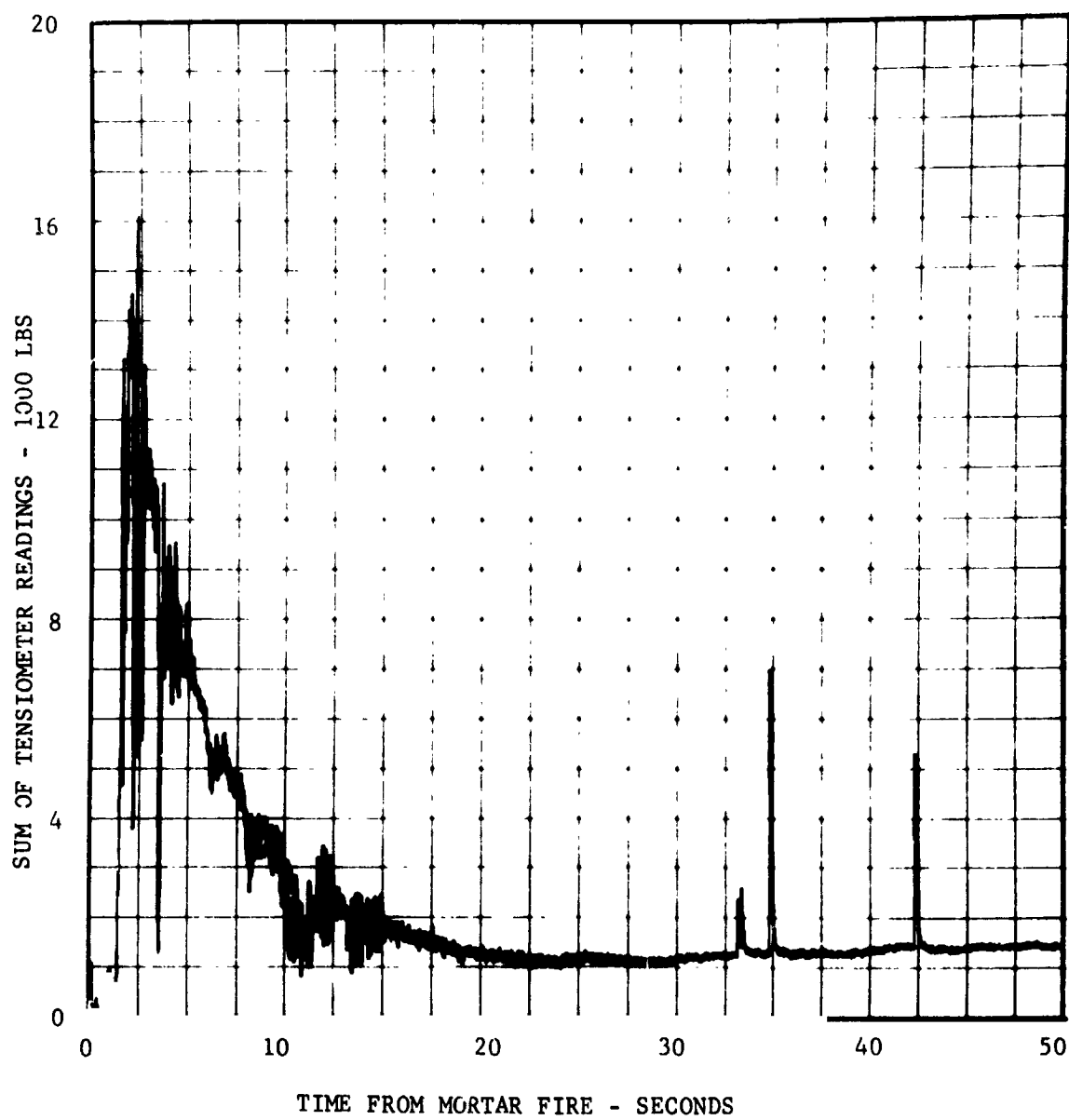


FIGURE V-9 PARACHUTE OPENING LOAD, 0-50 SECONDS

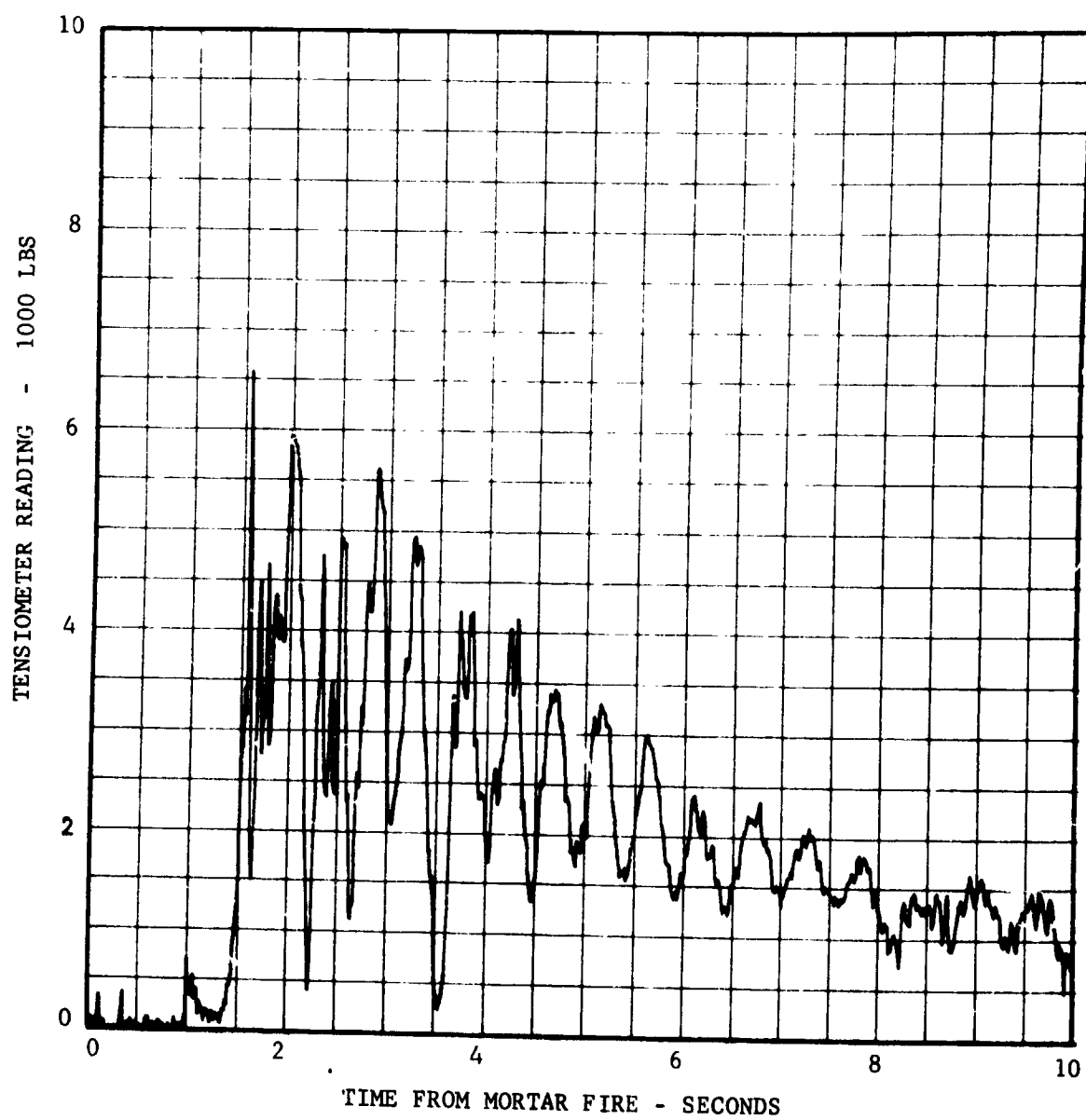


FIGURE V-10 TENSIO METER READING, BRIDLE LEG NO. 1

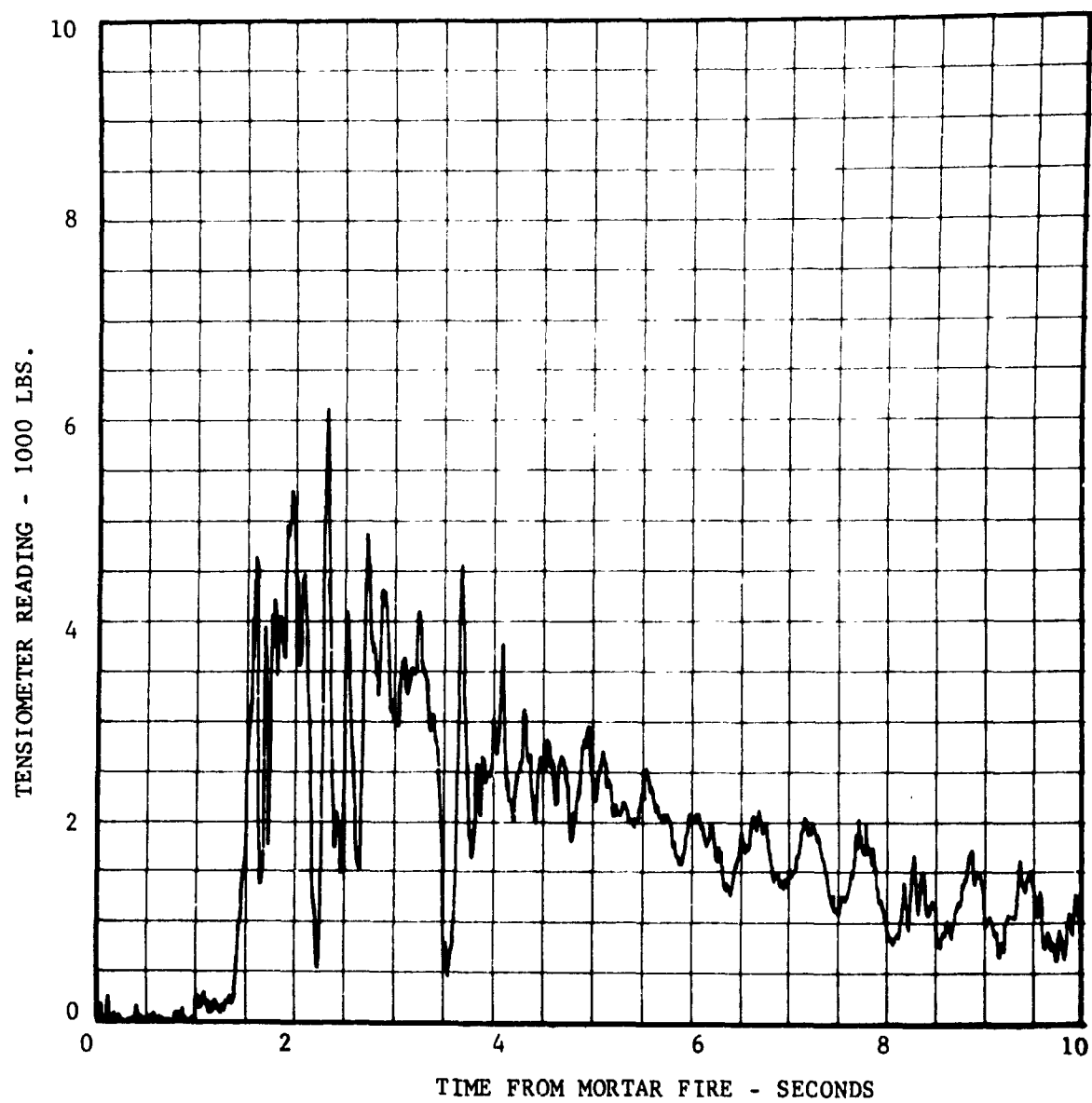


FIGURE V-11 TENSIO METER READING, BRIDLE LEG NO. 2

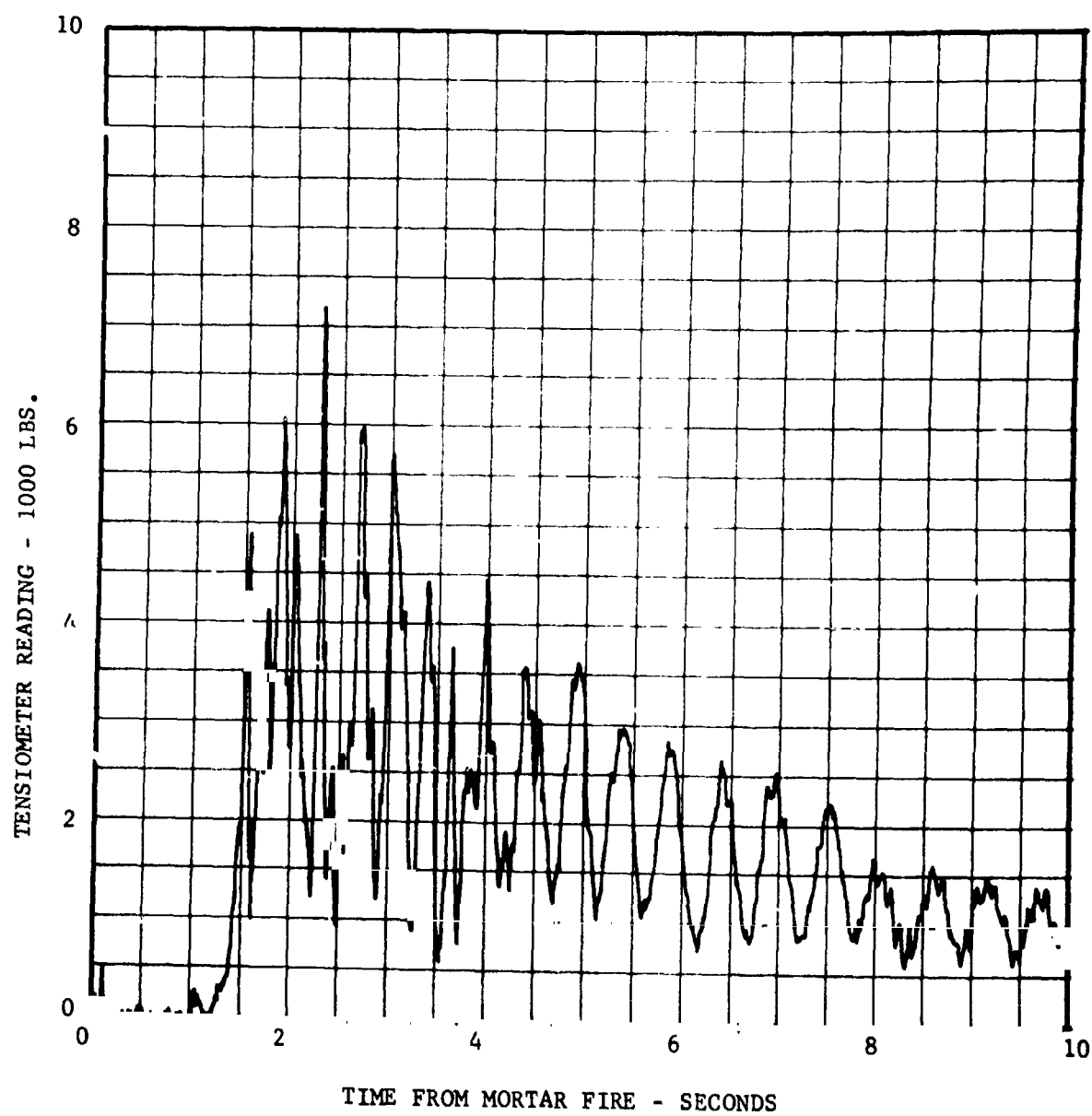


FIGURE V-12 TENSIO METER READING, BRIDLE LEG NO. 3

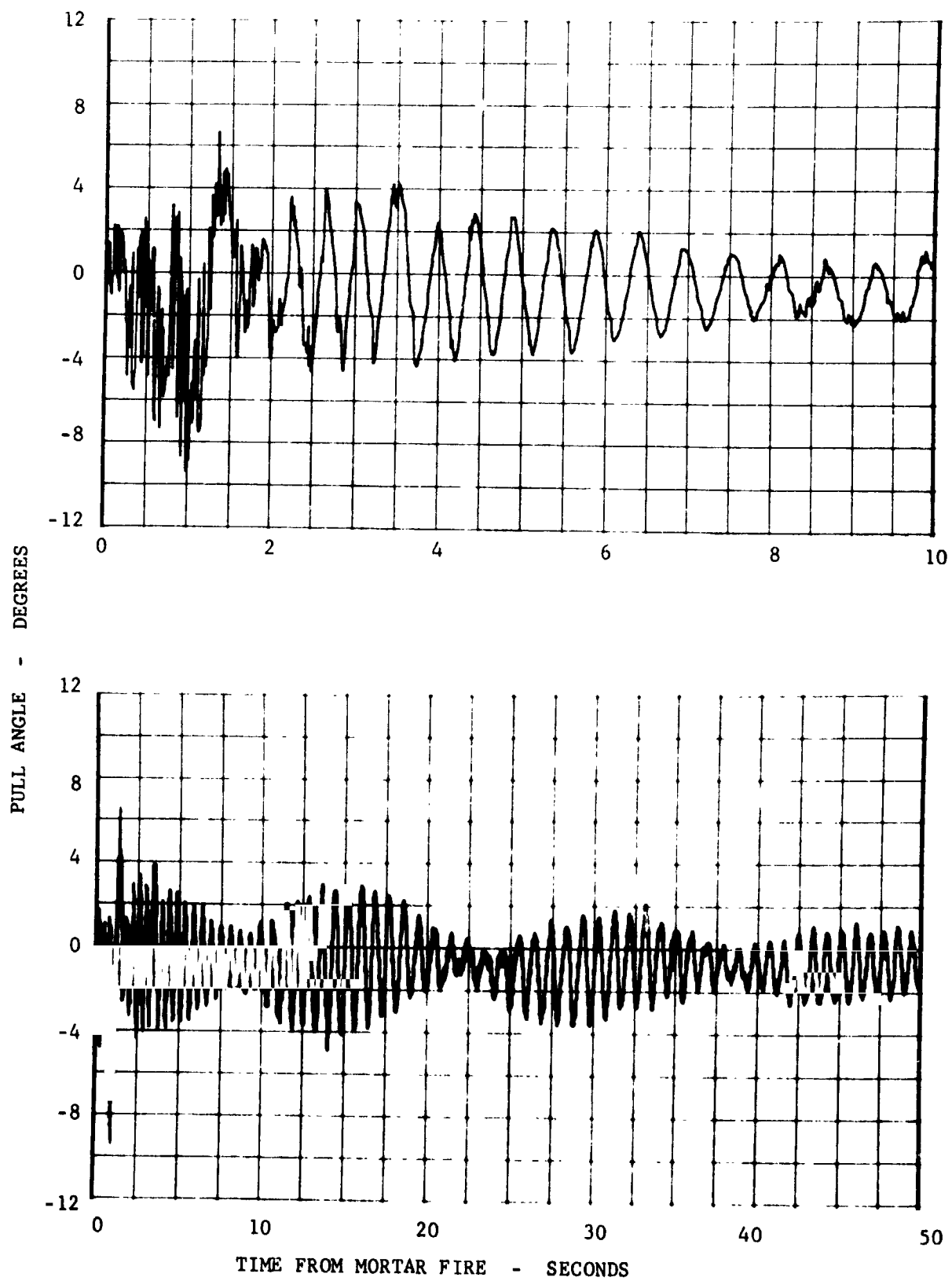


FIGURE V-13 PARACHUTE PULL ANGLE, PITCH PLANE

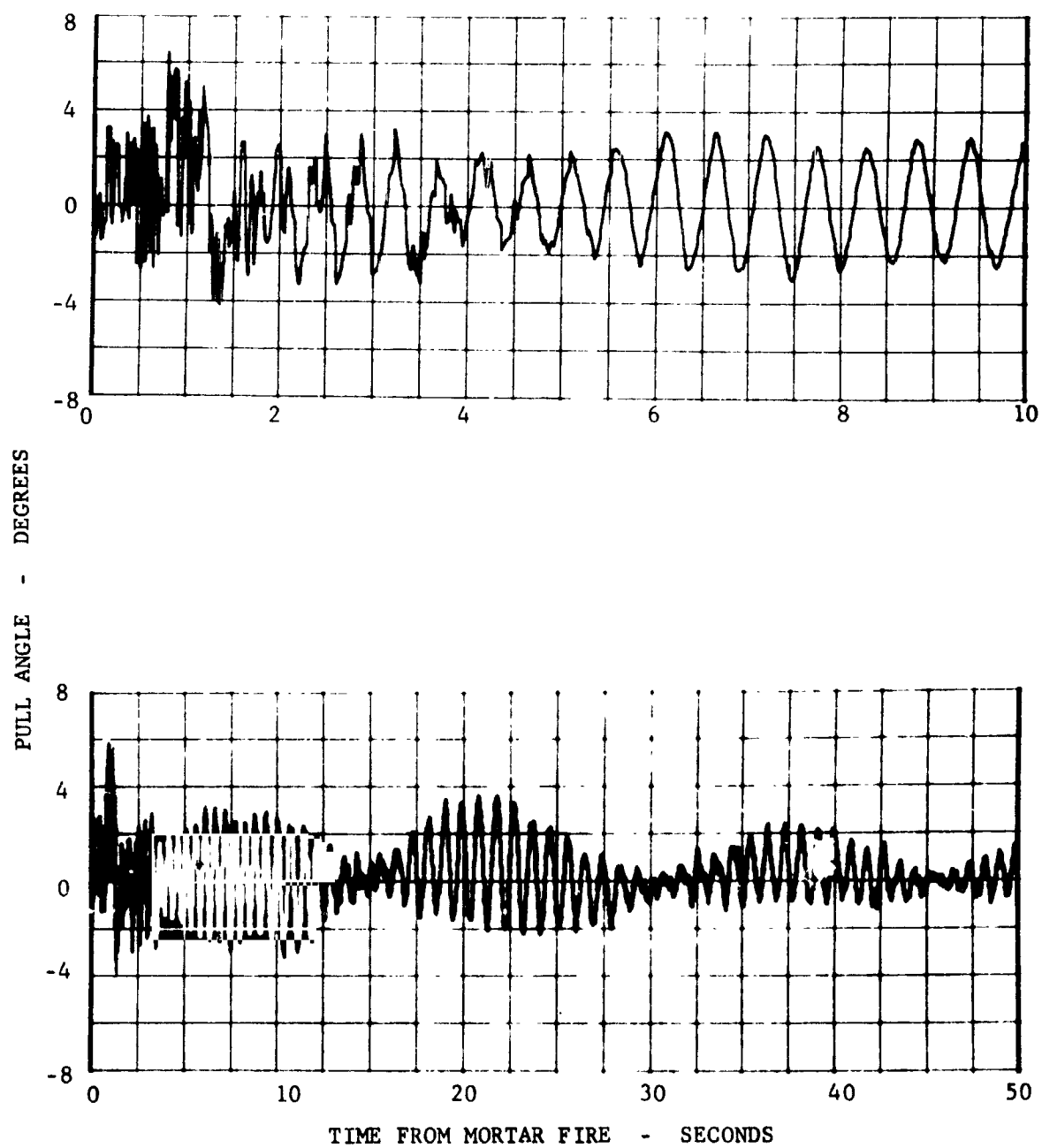


FIGURE V-14 PARACHUTE PULL ANGLE, YAW PLANE

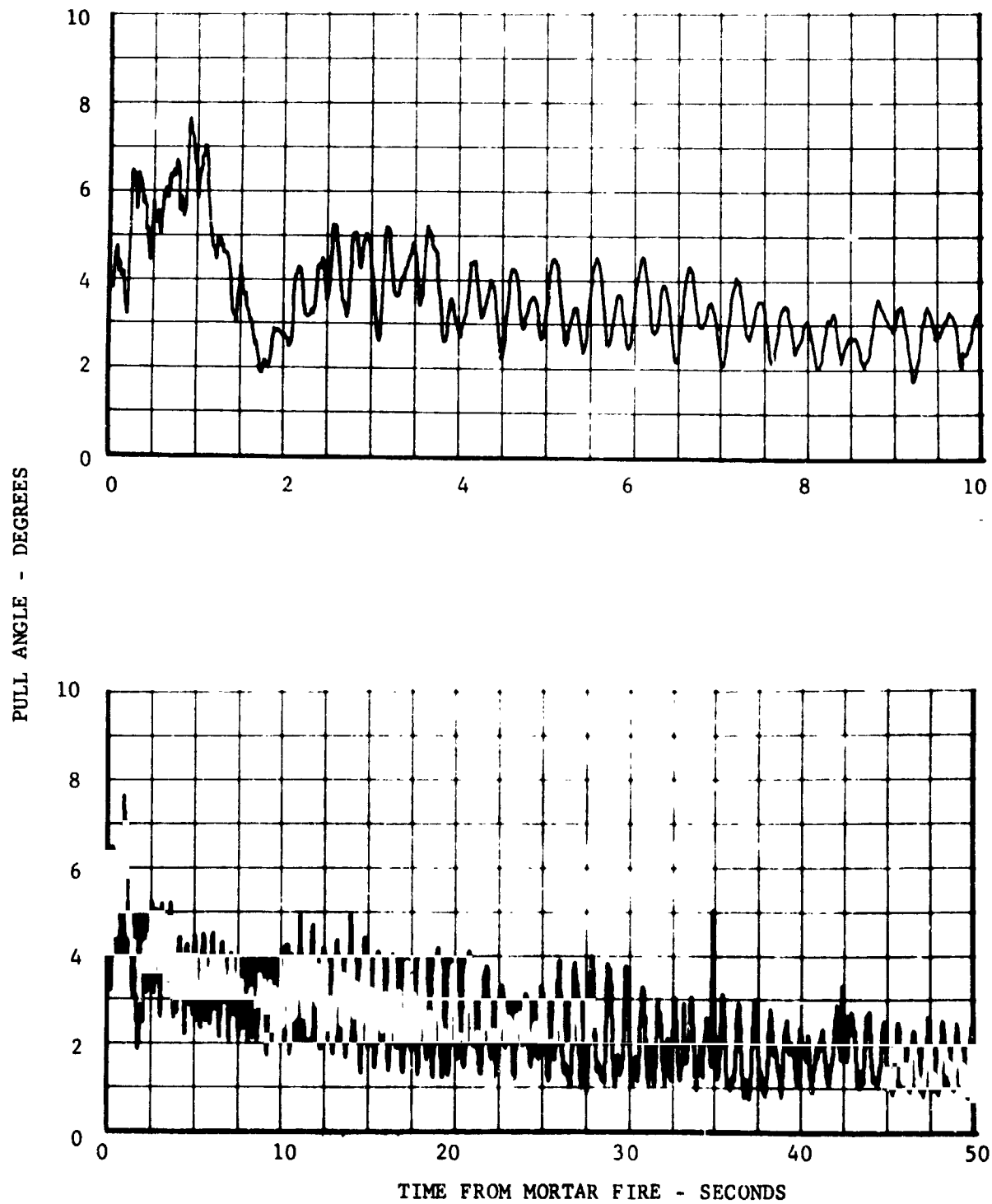


FIGURE V-15 PARACHUTE TOTAL PULL ANGLE (RSS)

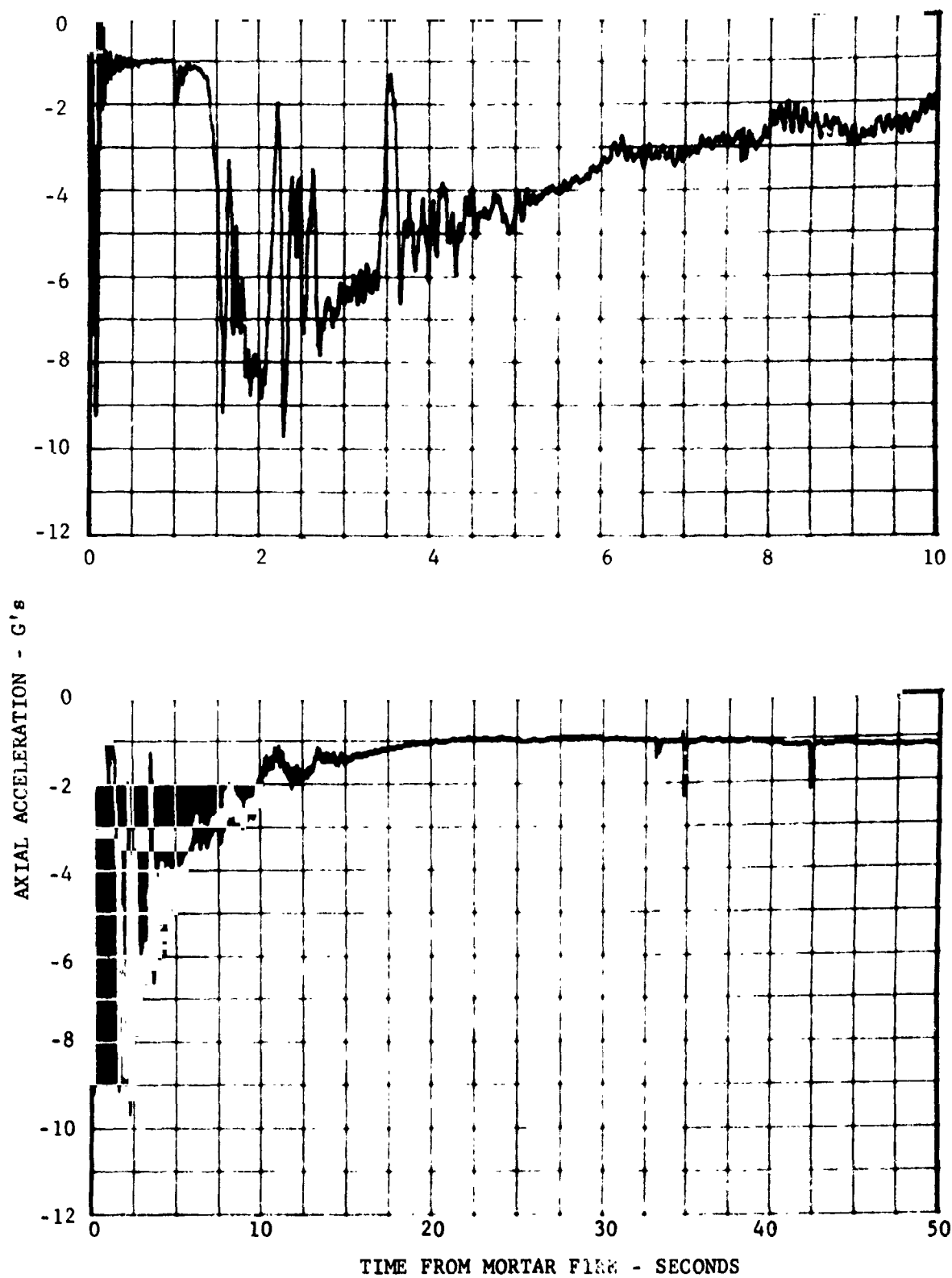


FIGURE V-16 LONGITUDINAL ACCELERATION

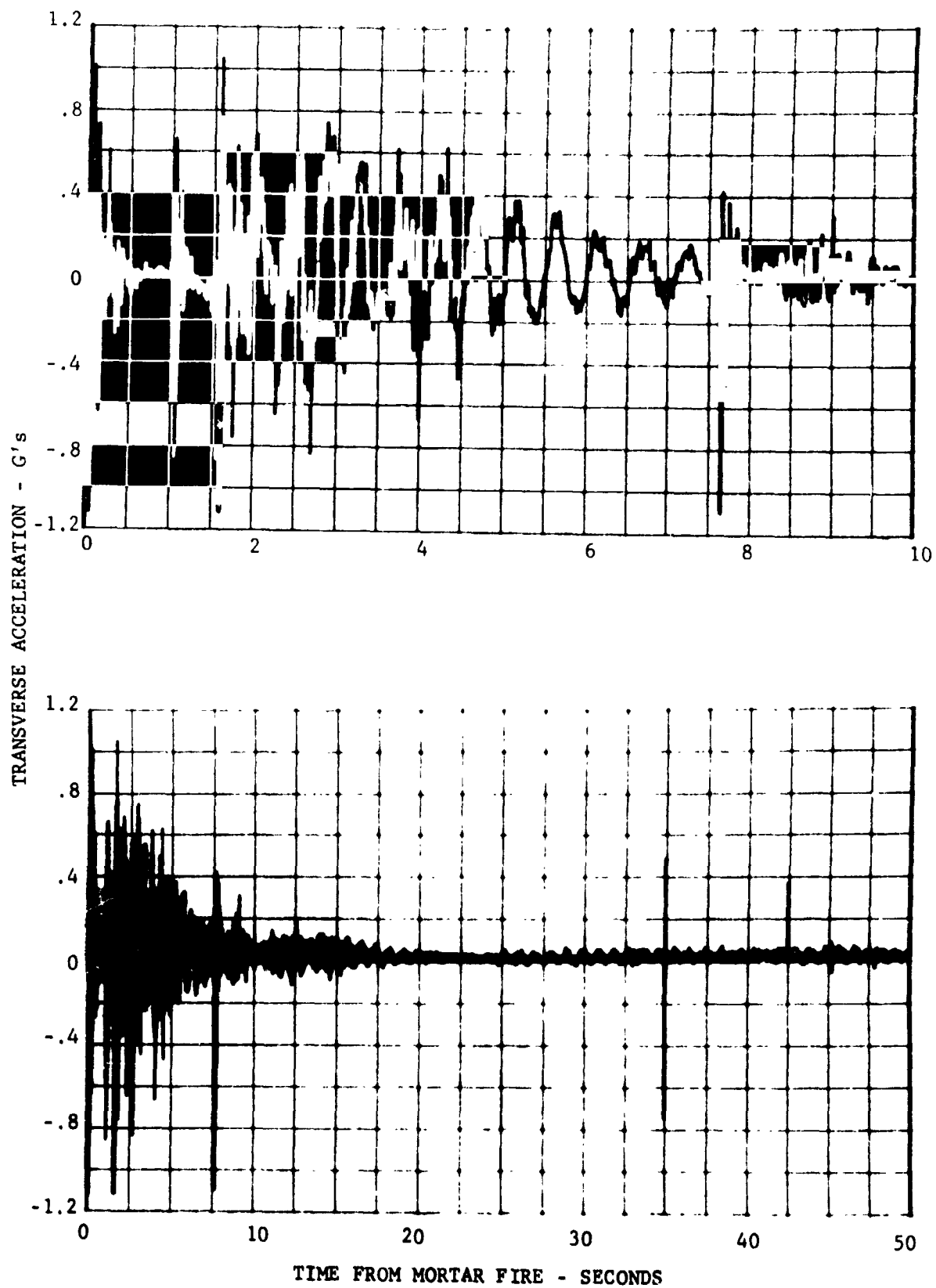


FIGURE V-17 TRANSVERSE ACCELERATION

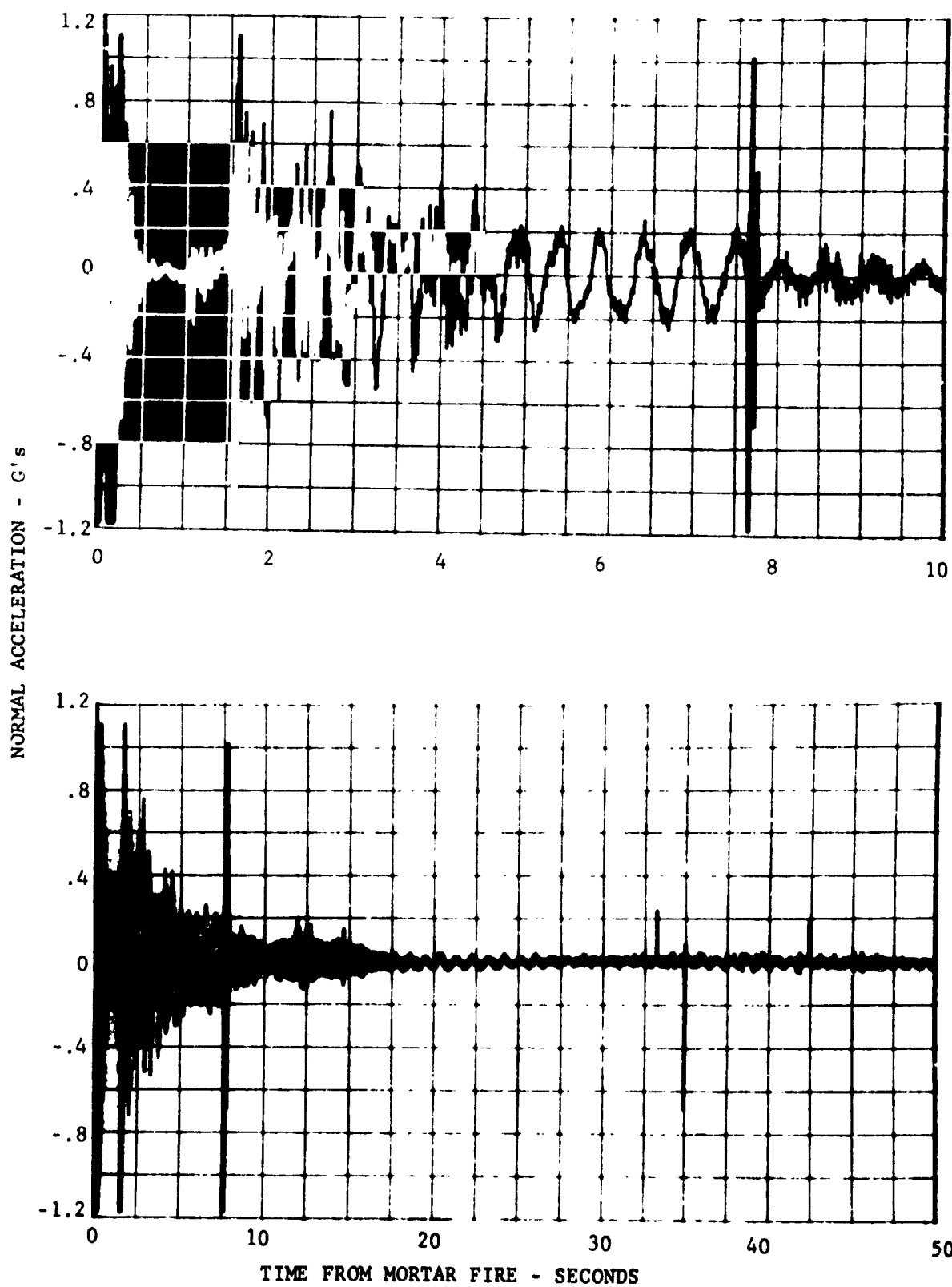


FIGURE V-18 NORMAL ACCELERATION

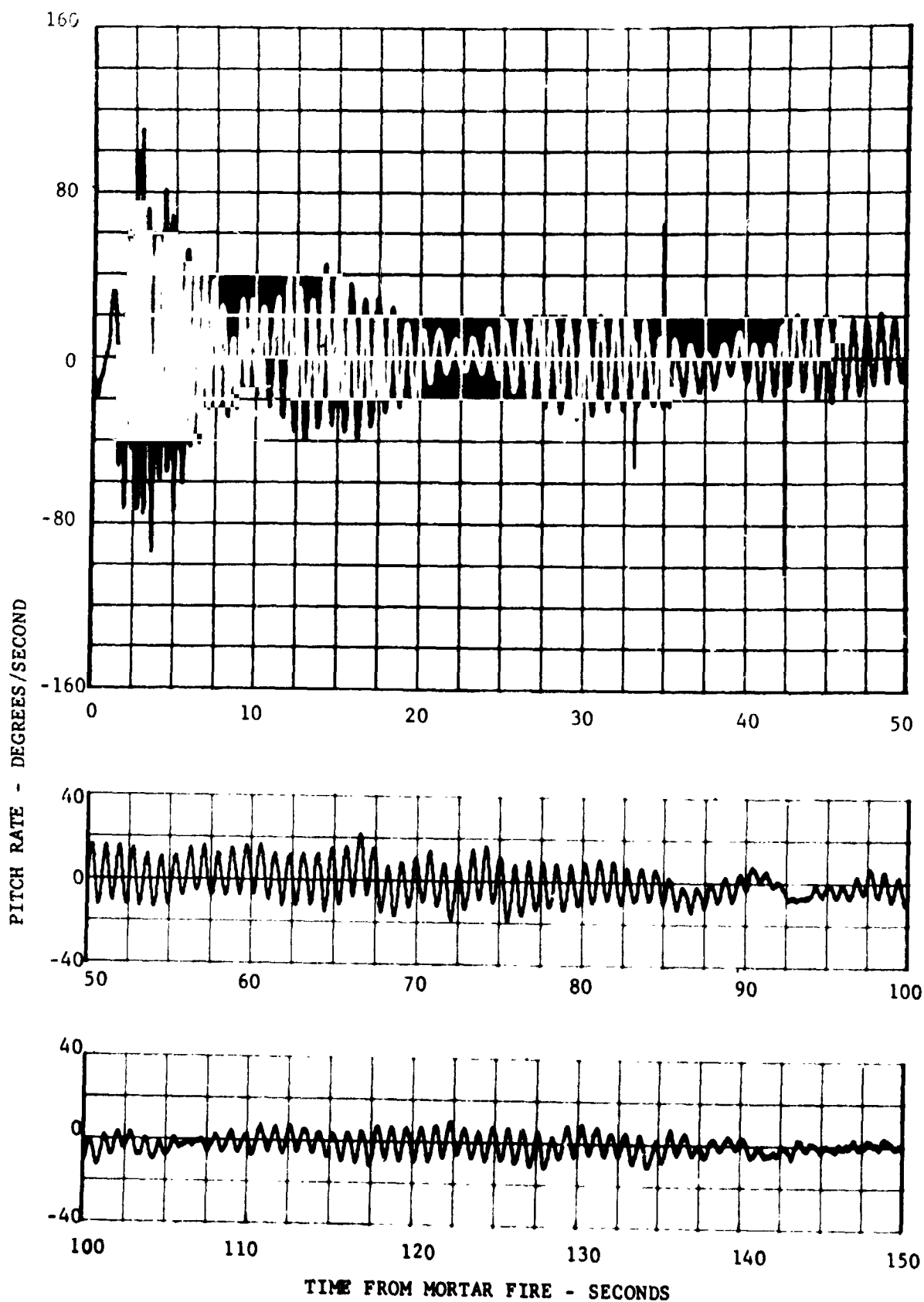


FIGURE V-19 VEHICLE PITCH RATE

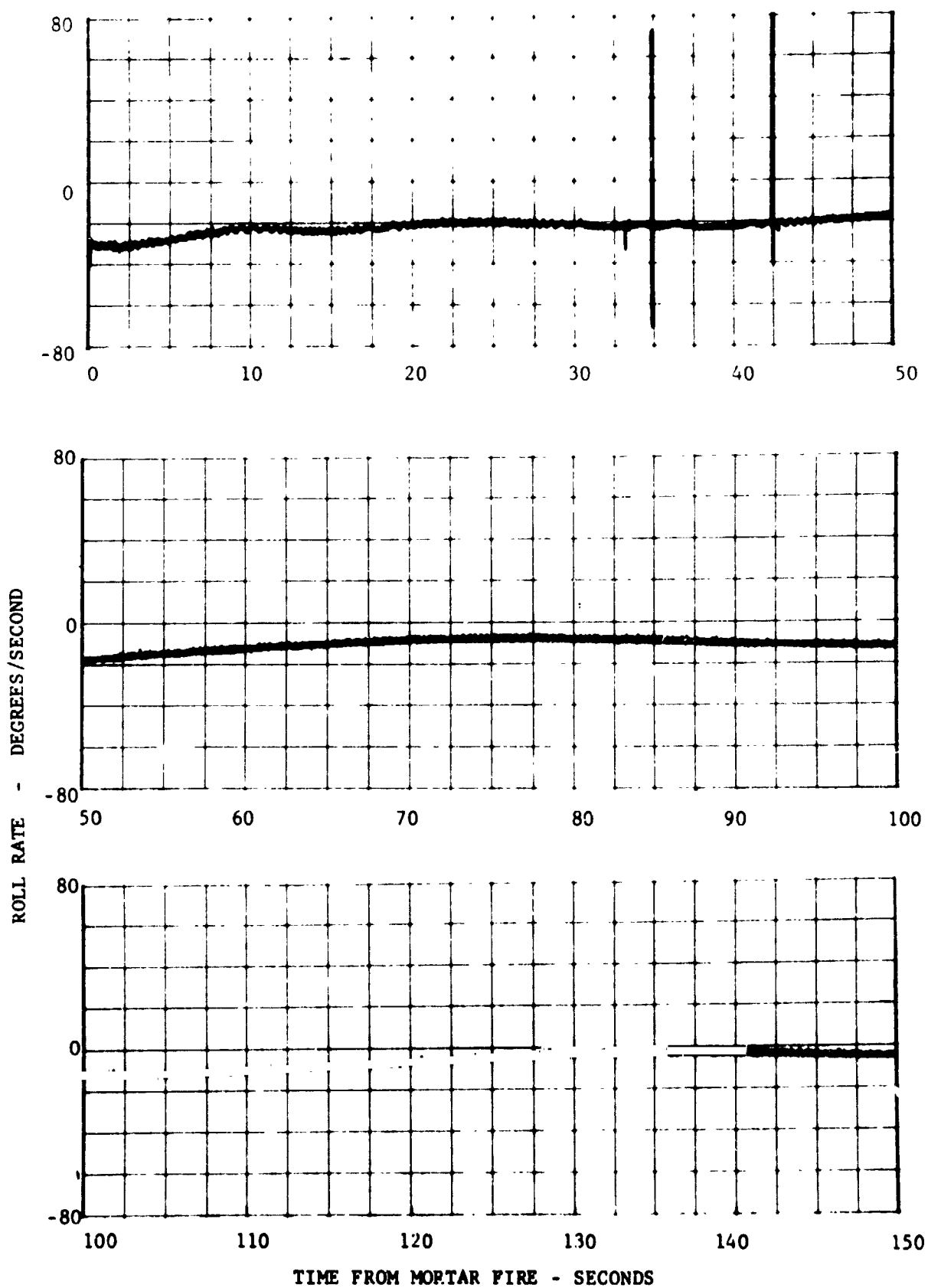
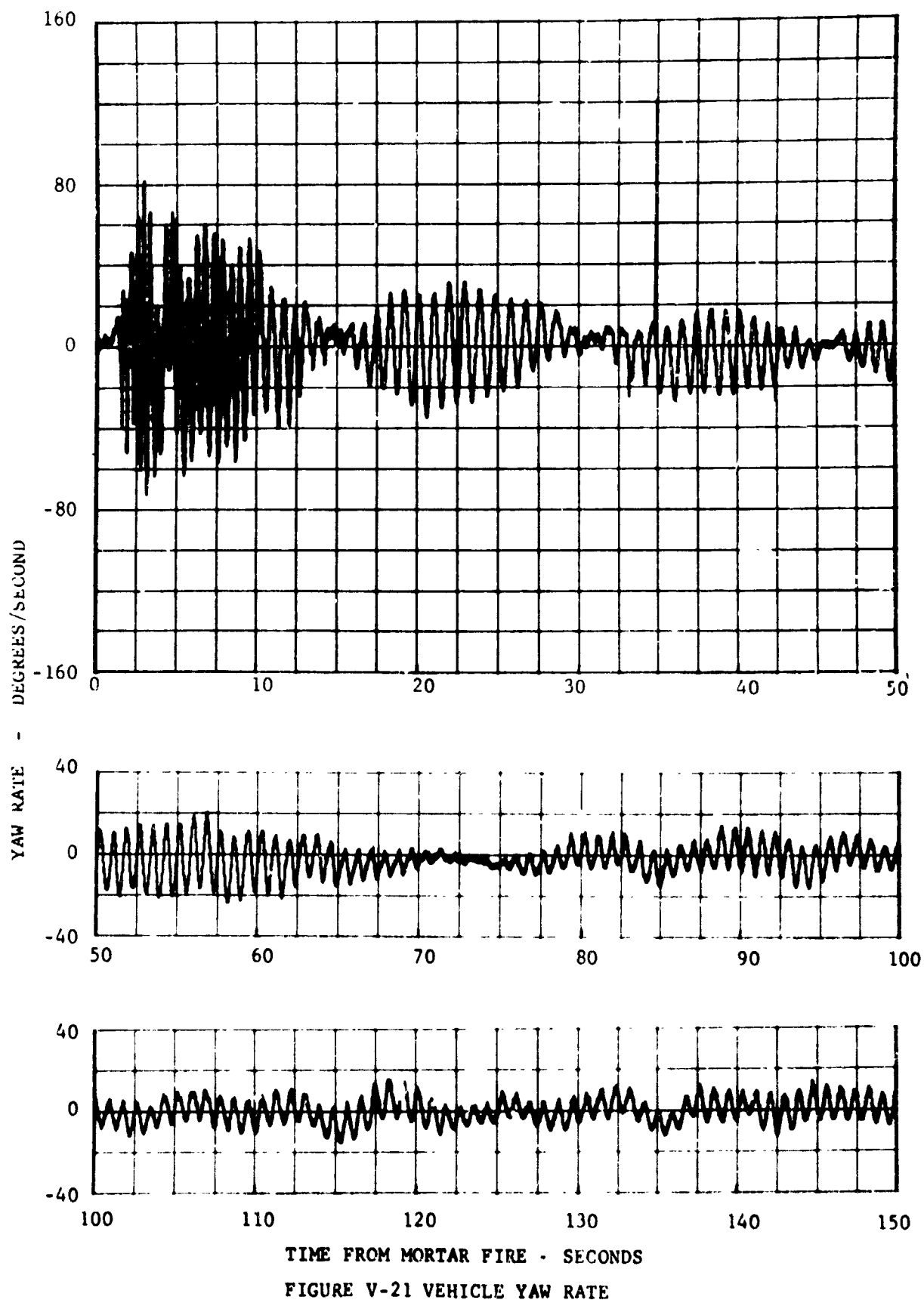
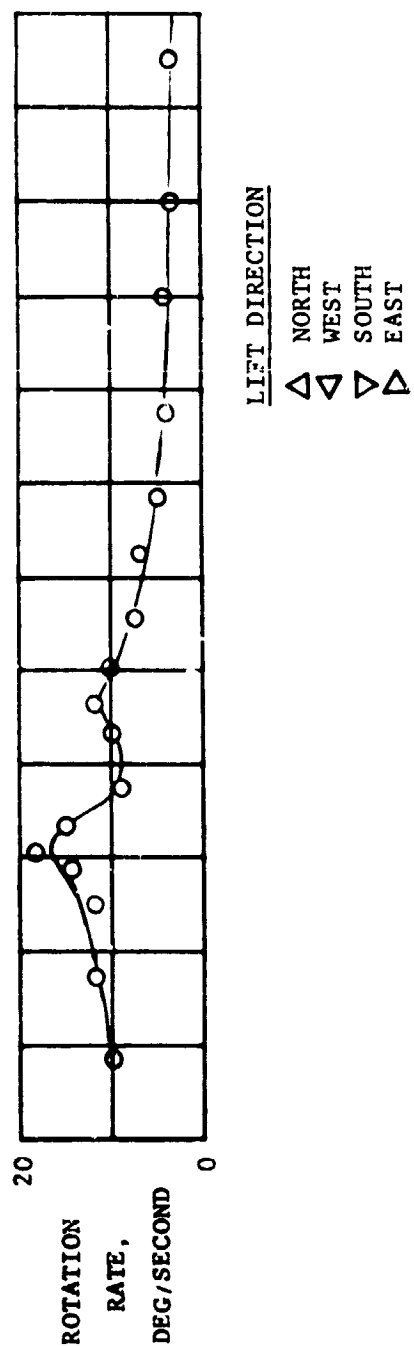


FIGURE V-20 VEHICLE ROLL RATE





LIFT DIRECTION

- △ NORTH
- ▽ WEST
- ▽ SOUTH
- ▷ EAST

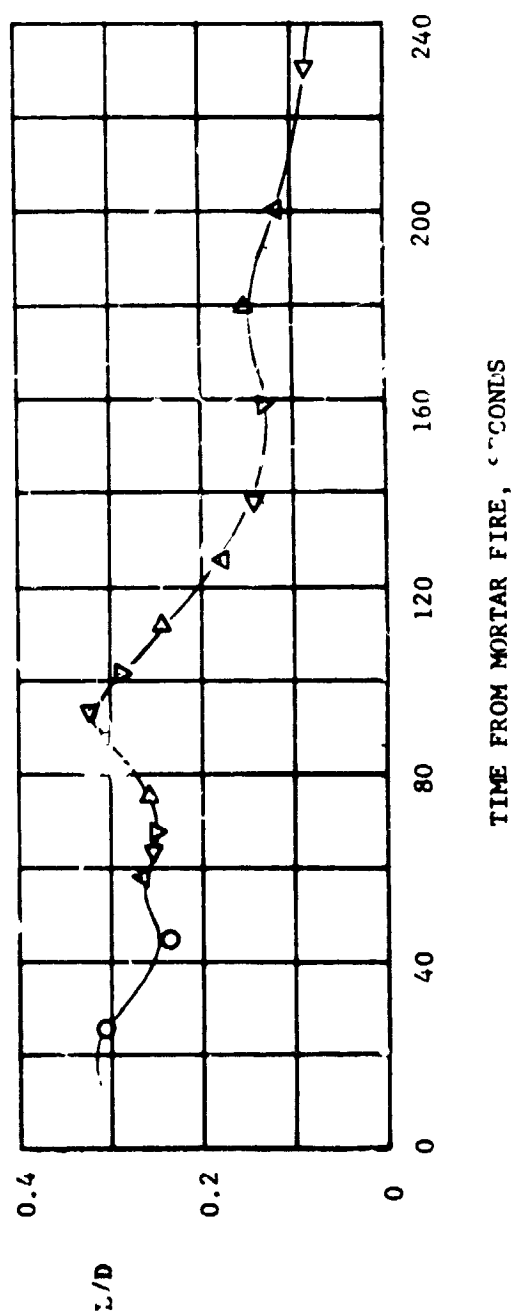


FIGURE V-22 PARACHUTE LIFT DURING DESCENT

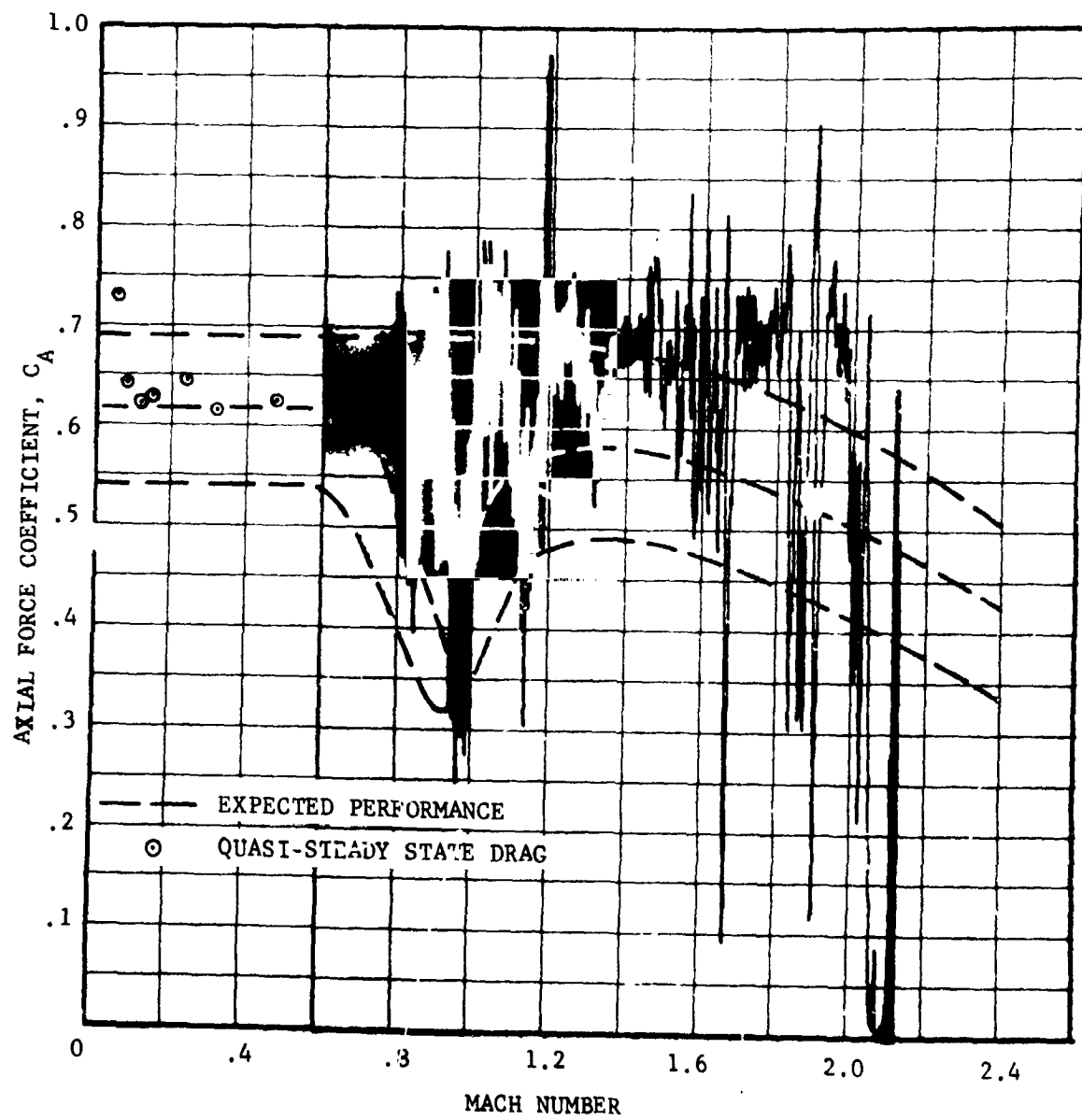


FIGURE V-23 PARACHUTE AXIAL FORCE COEFFICIENT (ACCELEROMETER DATA)

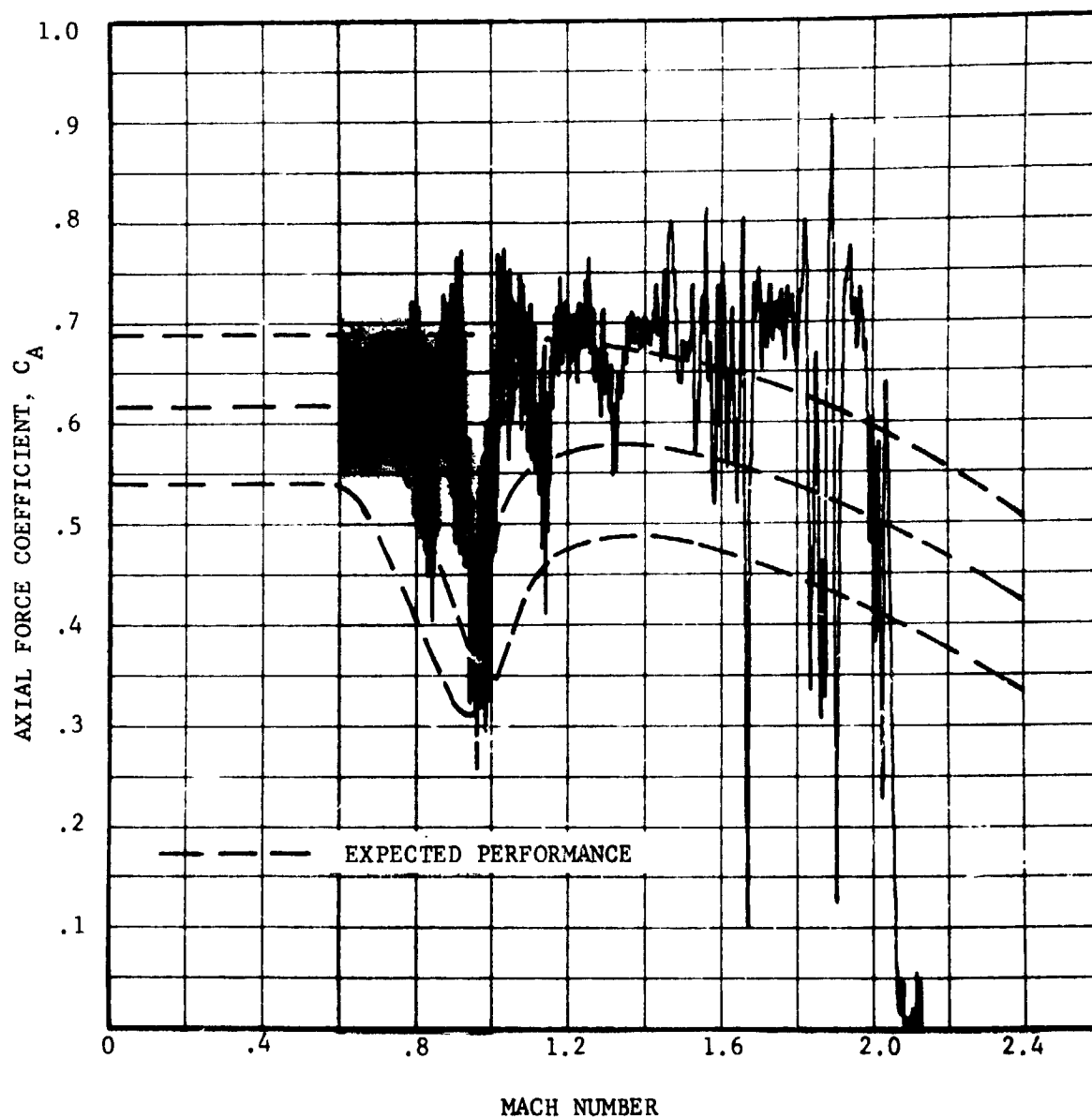


FIGURE V-24 PARACHUTE AXIAL FORCE COEFFICIENT (TENSIO METER DATA)

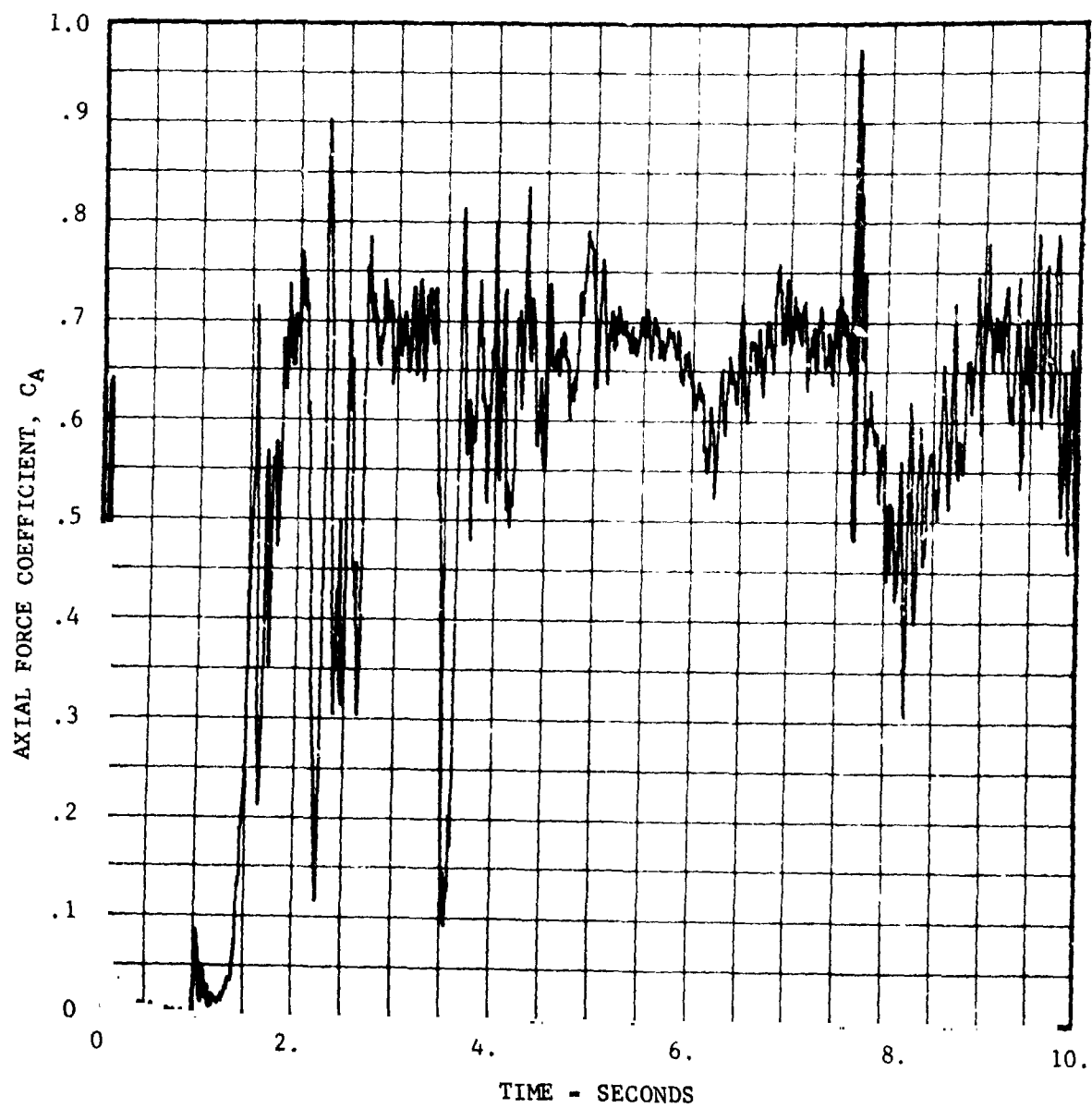


FIGURE V-25 PARACHUTE AXIAL FORCE COEFFICIENT (ACCELEROMETER DATA)

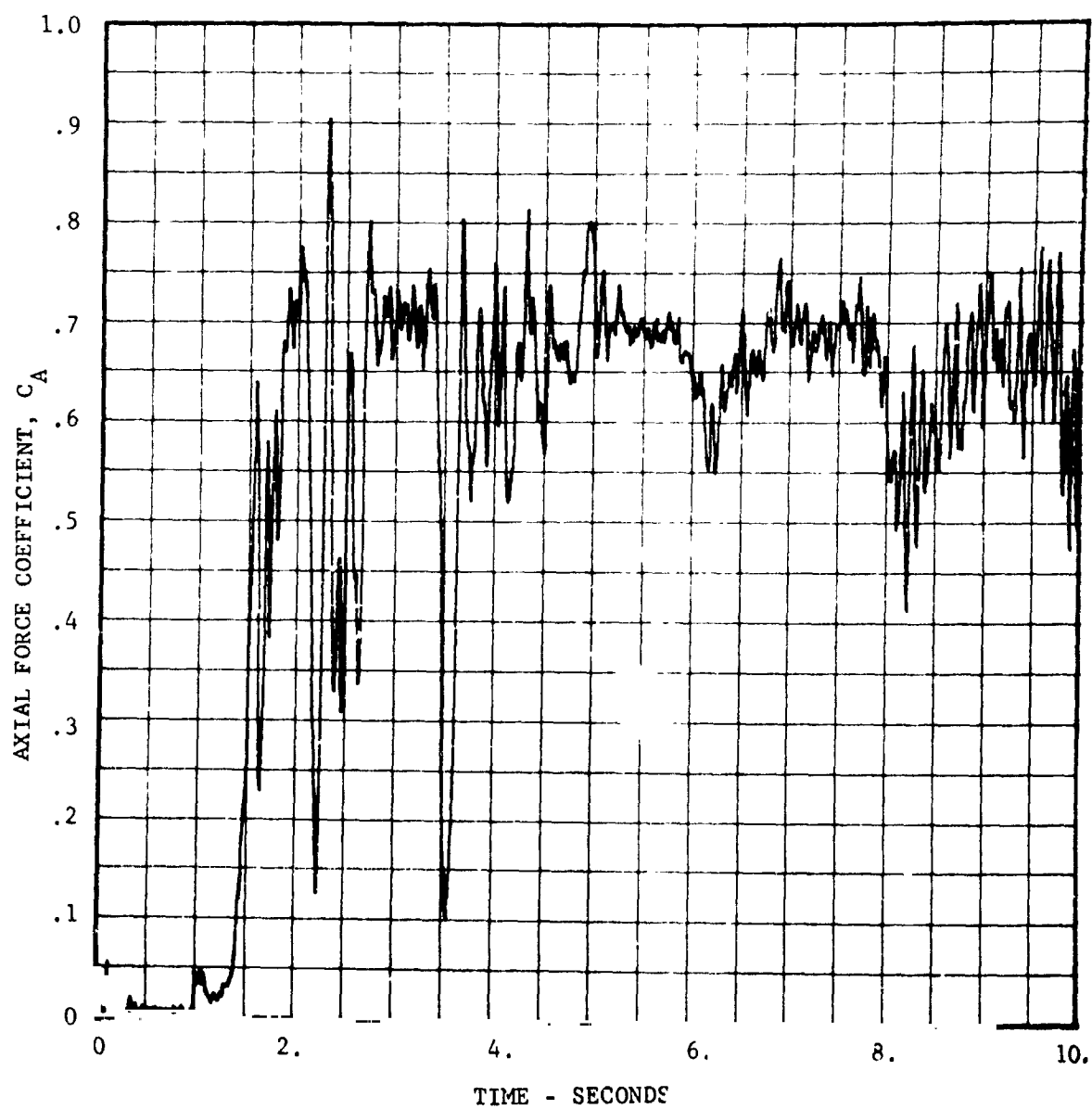


FIGURE V-26 PARACHUTE AXIAL FORCE COEFFICIENT (TENSIMETER DATA)

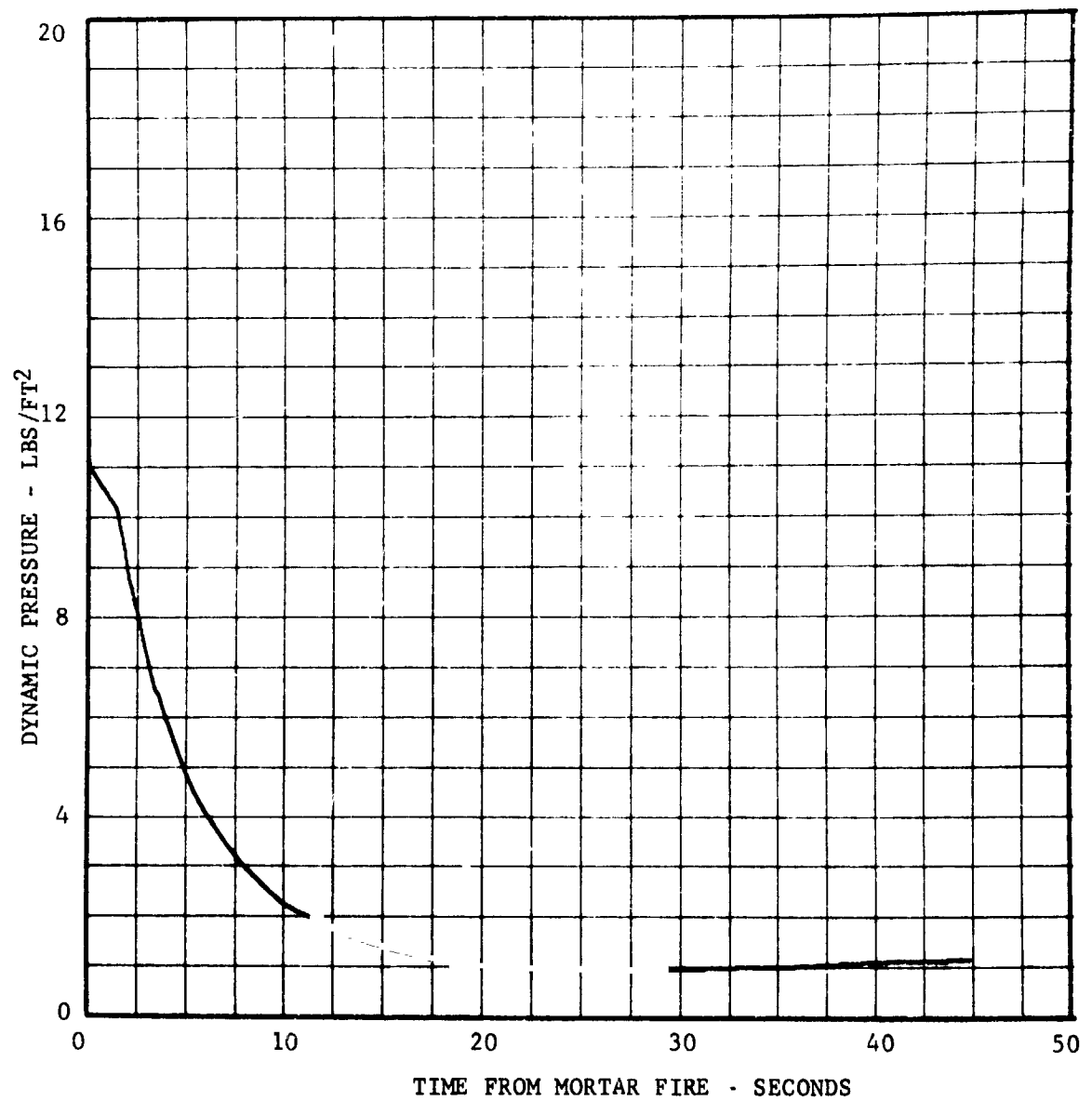


FIGURE V-27 DYNAMIC PRESSURE TIME-HISTORY

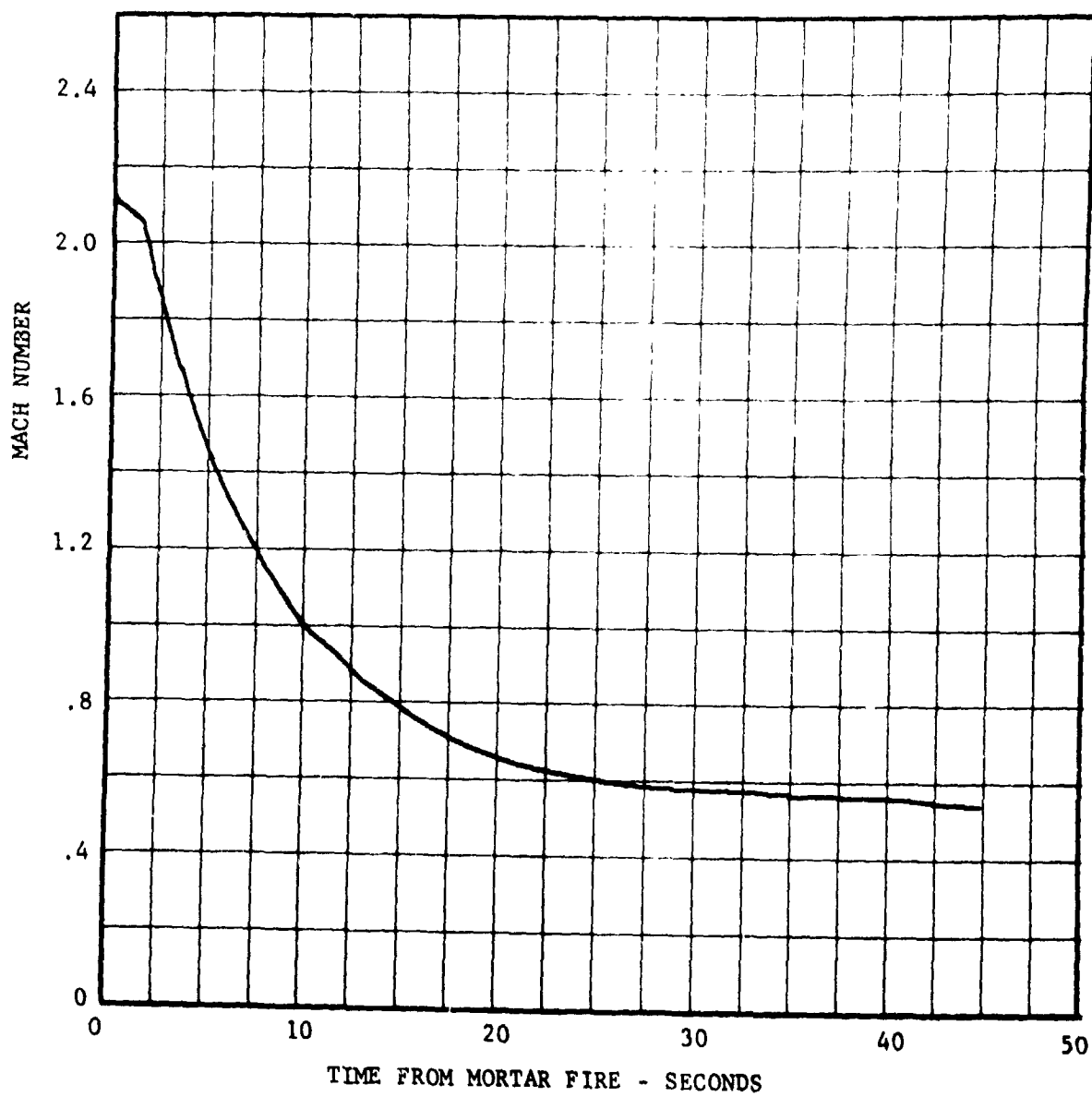


FIGURE V-28 MACH NUMBER TIME-HISTORY

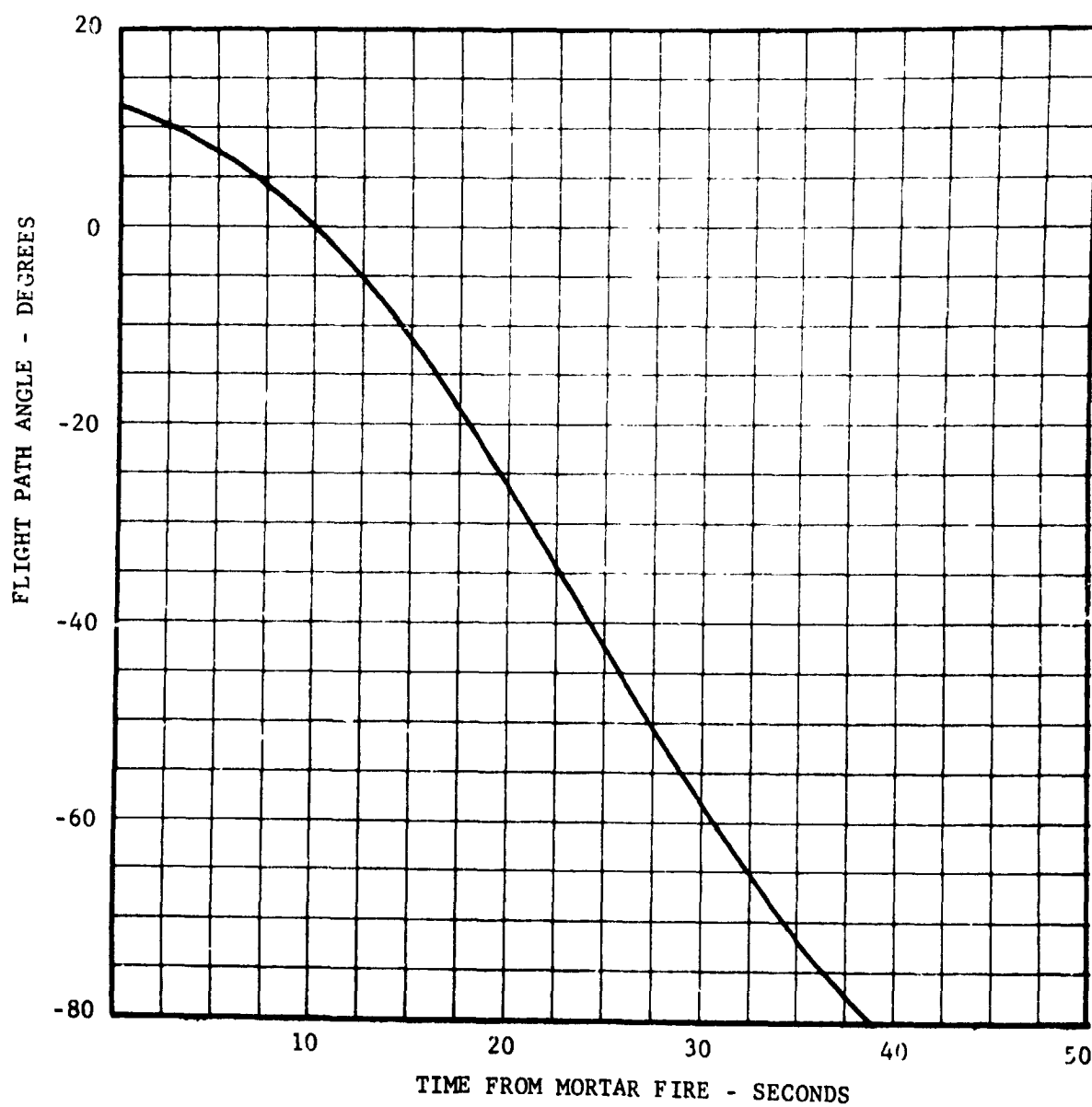


FIGURE V-29 FLIGHT PATH ANGLE

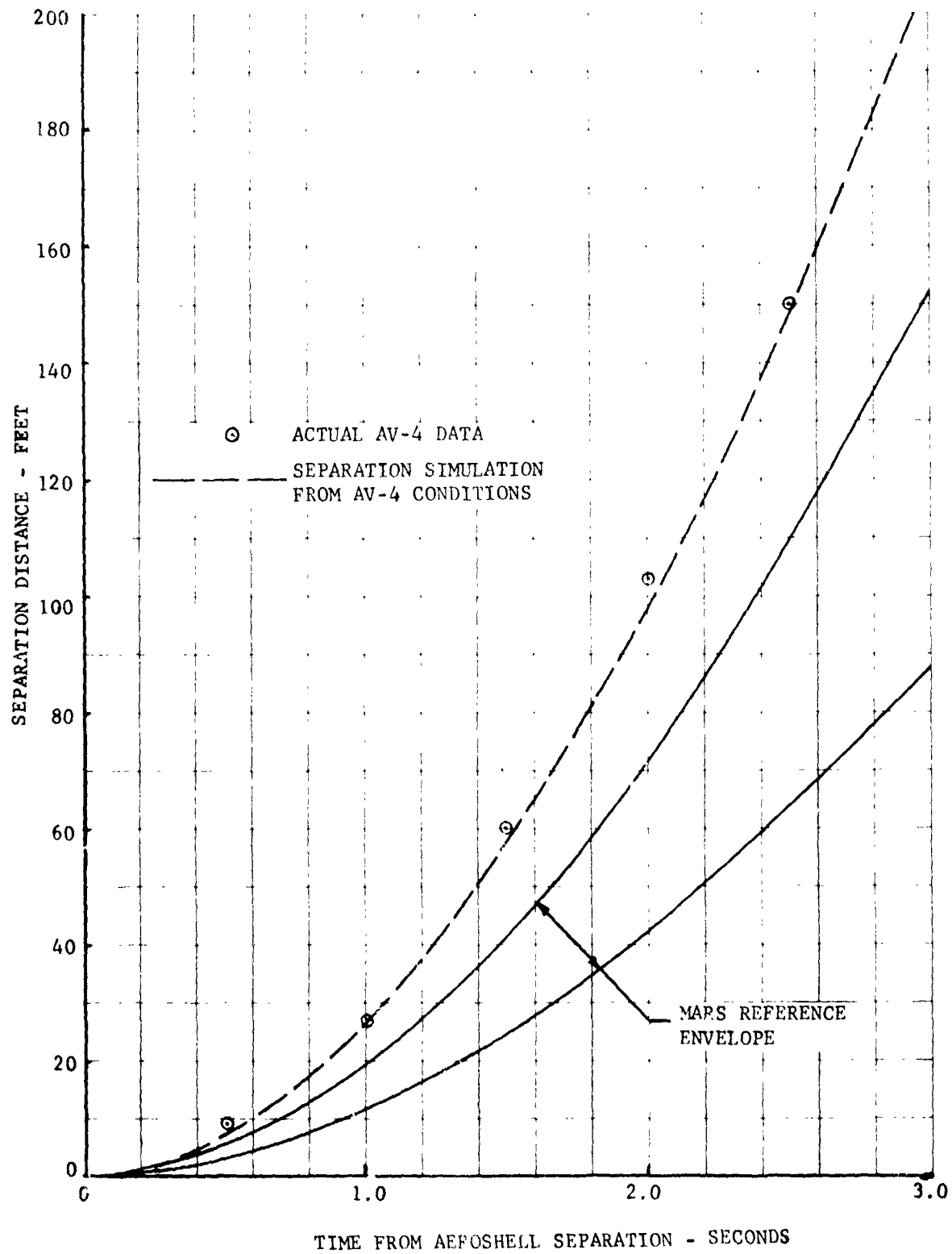


FIGURE V-30 AEROSHELL SEPARATION DISTANCE - 0-3 SECONDS

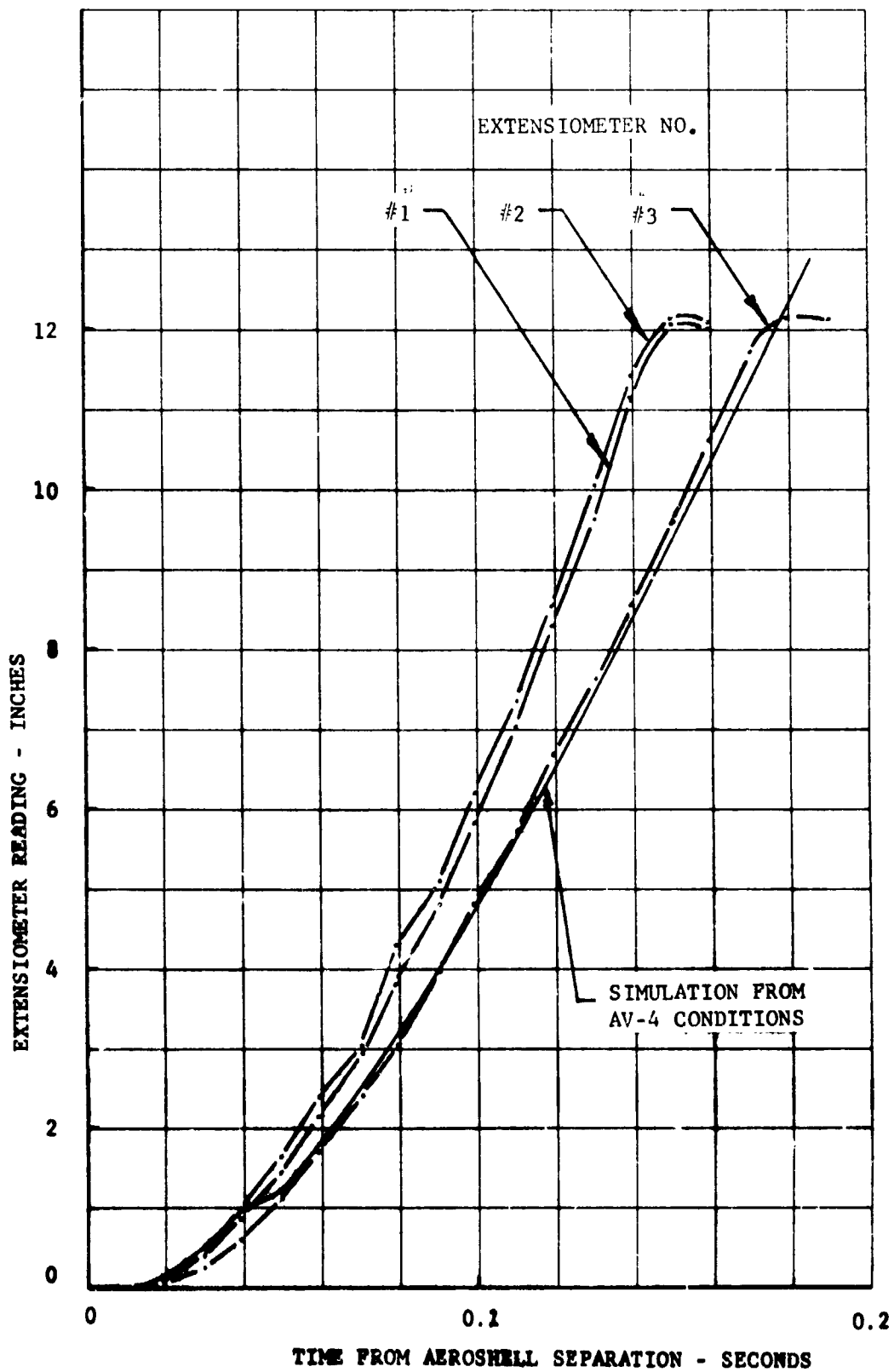


FIGURE V-31 EXTENSOMETER SEPARATION DISTANCE

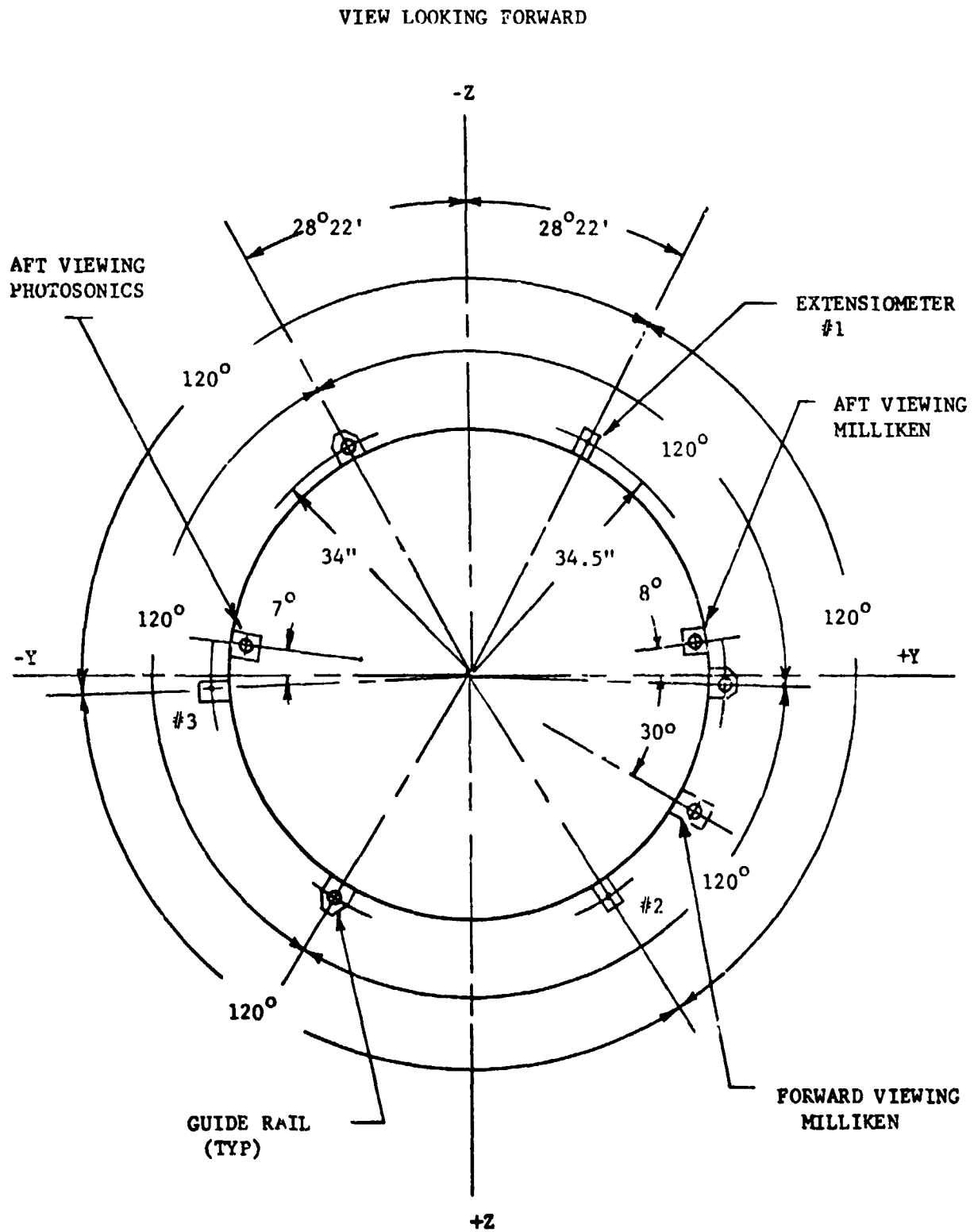
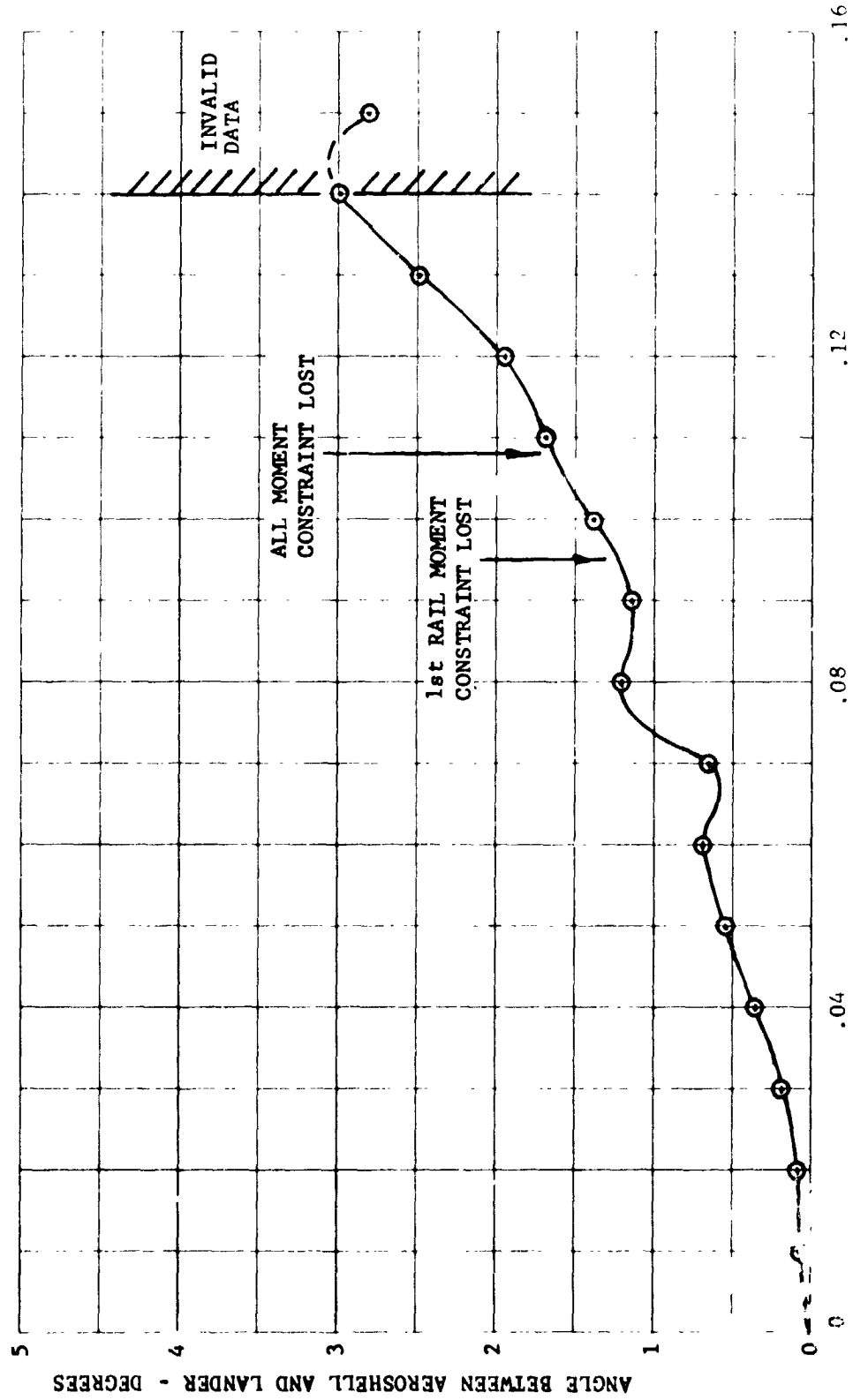


FIGURE V-32 EXTENSOMETER AND GUIDE RAIL LOCATION



TIME FROM AEROSHELL SEPARATION - SECONDS

FIGURE V-33 RELATIVE ANGULAR MOTION BETWEEN AEROSHELL AND LANDER

VI. VEHICLE PERFORMANCE ANALYSIS

The following is a summary assessment of the BLDT vehicle performance. The summary is presented by subsystem/discipline.

A. Flight Dynamics

The objective of the flight dynamics portion of the report is to establish the actual flight performance of the AV-4 vehicle from the command for vehicle release from the load bar through the command for decelerator mortar fire. It is noted that the flight of vehicle AV-4 was required due to the fact that vehicle AV-1, Case 1, supersonic test was declared a decelerator qualification "no test". The no test resulted from the imposition of overtest dynamic pressure conditions at decelerator mortar fire and at peak load with subsequent damage to the parachute (see TR-3720289).

Subsequent to the flight of vehicle AV-1, the Mach number/dynamic pressure test requirements for the supersonic test case were amended to reflect a new Mars atmospheric definition. (See Reference 1). A comparison of the AV-1 and AV-4 target mortar fire and peak load conditions are given below:

	<u>Mach Number</u>	<u>Dynamic Pressure (PSF)</u>
Mortar Fire AV-1	2.27	11.8
AV-4	2.17	10.84
Peak Load AV-1	2.17	10.66
AV-4	2.06	9.39

The vehicle performance requirements for the Case 2 supersonic test vehicle based on the revised Mars worst case environments and characteristics of the BLDT vehicle which will differ from the actual VLC are:

1. Resultant angle of attack at mortar fire ≤ 17 degrees
2. Residual spin rate at deployment ≤ 100 degrees/second
3. Mach number and dynamic pressure at peak load within the test envelope shown in Figure VI-1.

The peak load requirements box is established such that a 2σ dispersion ellipse of dynamic pressure, based on BLDT performance parameters tolerances, is tangent to the revised 30% overload limit of the decelerator and at a Mach number greater than 1.9.

Figure VI-1 also presents the actual mortar fire and peak load Mach number/dynamic pressure conditions for the flight of vehicle AV-4. The Mach number/dynamic pressure performance requirement box for vehicle AV-1, Case 1 supersonic flight is shown on Figure VI-1 for comparison purposes.

1. Data Sources

The intent of this section is to evaluate the flight performance of BLDT AV-4 by reconstructing its trajectory using flight data data. The reconstruction is primarily based on three sources of data:

- o Meteorological data (density, velocity of sound, and winds);
- o Telemetry data (accelerometers, gyros and magnetometers); and
- o Radar data (slant range, azimuth and elevation).

a. Meteorological Data - Meteorological data were obtained by standard WSMR radiosonde observation balloons (RAOB) and LOKI rocket probes. The RAOB probe produced pressure, wind direction and velocity and temperature at 5000 foot intervals from surface to approximately 110,000 feet. The LOKI rocket probe produced temperature and wind data at 5000 foot intervals from 80,000 feet to approximately 150,000 feet. The combination of the

RAOB and LOKI data defined the atmospheric parameters from surface to altitude. Three atmospheric profiles were obtained for the AV-4 flight as follows:

T-24 hr. data:

LOKI #160	Launched 12 August 1972
RAOB #550	Launched 12 August 1972

T-1 hr. data:

RAOB #136	Launched 13 August 1972
LOKI #162	Launched 13 August 1972

T+1 hr. data:

RAOB #225	Launched 13 August 1972
LOKI #162	Launched 13 August 1972

The T-24 hr. data were used by the real time computer* during the actual flight to predict impact and command mortar fire. A comparison of the density of the above 3 sets of data shows that the T-1 hr. data were close to the average. Therefore, the T-1 hr. data as shown in Table VI-1 were used for all flight performance analysis.

b. Telemetry Data - The flight vehicle telemetry (TM) data were transmitted via an S-band link to the WSMR receiving stations J-10 and J-67 where they were recorded and retransmitted via microwave links to the flight operations control station at building 300. These receiving stations are geographically located to provide continuous coverage of the real time mission. Their locations are shown in Figure VI-2. At building 300, the TM data were recorded for post-flight usage and also terminated a various displays for observation and control of the mission.

* The WSMR computer real time software is discussed in Appendix E.

The conditioned and smoothed TM accelerometer and rate gyro data, which were used for flight performance analysis, are shown in Figures VI-3 through VI-6. Figures VI-3 and VI-4 are gyro and accelerometer data respectively for the time period prior to the vehicle release from the load bar. The effect of pointing commands are reflected in the spin and yaw gyro data. Figures VI-5 and VI-6 are the same data during vehicle powered flight. It is noted that all of the accelerometer and gyro data were smoothed and conditioned except the accelerometer data prior to drop which was only conditioned. These data were filtered with a seventy (70) point standard least squares quadratic leading edge filter. The conditioning was based on a two sigma (2σ) dispersion limit of the filtered data with wild points replaced by the quadratic prediction.

The initial estimates of instrumentation bias, were obtained from these plots by integrating the gyro data during the float period (Figure VI-3) and adjusting the accelerometer data for zero setting during the free fall portion of flight immediately after release from the load bar (Figure VI-4). The TM instrumentation system is designed to provide a 5% end to end error tolerance limit but with the above biases it is judged that the instrumentation accuracies can be assumed to be 2%. This provides the following accuracies:

<u>FUNCTION</u>	<u>TOLERANCE</u>
Gyros	6 deg/sec
Lateral Accelerometers	0.02 g's
Longitudinal Accelerometer	0.10 g's

c. Radar Data - The BLDT vehicle was tracked by (4) WSMR FPS-16 radar sets, three (3) were beacon track and one was skin track. The beacon track radars (R122, R123 and R128) were used for continuous

track of the vehicle until loss of beacon (T + 400 sec) at which time they switched to skin track. The skin track radar was utilized to track other system components such as balloons, load bar and aeroshell. The stated accuracy of the FPS-16 radars is 0.1 to 0.3 mils in angles and 15 to 45 feet in range, which is approximately 50 feet of space position.

The radars provided slant range (R), azimuth (A) and elevation (E) data with respect to the radar site. Only the beacon track radars were considered for performance analysis. These radar locations are shown in Figure VI-2. Comparison of the data from the three beacon track radar sites show significant errors in all three parameters, therefore an analysis of the radar data was undertaken. This analysis consisted of transforming the (R), (A) and (E) from a given site to an (R), (A) and (E) of a second site where the derived (R), (A) and (E) were compared with the actual measured data for the second site. This analysis was completed for radar sites R122 vs. R128, R123 vs. R128 and R122 vs. R123 and the reverse of each. This analysis indicates the maximum systematic difference existing in the data are:

	RANGE (ft)	AZIMUTH (ft)	ELEVATION (°)
R122 vs. R128	125	350	180
R123 vs. R128	15	180	140
R122 vs. R123	15	350	200

The time plots of (R), (A) and (E) differences are presented in Figures VI-7, VI-8 and VI-9.

The analysis of the plots indicates that the data from site R128 was consistently noisier than the other two sites with high tracking error spikes in elevation on any comparative data where site R128 was involved. When site R122 was transformed to site R128, a large systematic range

error occurred while transformation of site R123 data to R128 did not produce a gross range error. This indicates that site R122 data contains errors in the azimuth and elevation parameters.

The conclusion of this analysis is that radar data from the flight of vehicle AV-4 does not meet the accuracy specification for the FPS-16 radars and that the site R123 data contains the least error, therefore site R123 data was selected as prime radar data for AV-4 data analysis.

For beacon track radar, range rate can be determined very accurately while azimuth and elevation cannot be determined with a high degree of accuracy. Since the flight direction of the AV-4 vehicle with respect to the beacon radar site locations (See Figure VI-2) are such that slant range is almost a constant (i.e. small range rate change), the vehicle radar positions are derived mainly from azimuth and elevation which are subject to slew rate errors. The type of errors seen in the radar comparative analysis are probably slew rate errors.

The radar data were post flight corrected by WSMR for systematic errors which were determined by pre-flight calibrations. Raw data of range azimuth and elevation were smoothed by standard WSMR filter techniques to produce velocity, altitude, flight path angle and azimuth. These velocity, flight path angle and altitude data are presented in Figures VI-10 through VI-12 for radar site R123. These data are earth reference measurements and are not ambient aerodynamic conditions.

2. STEP Trajectory Reconstruction

The Statistical Trajectory Estimation Program (STEP) (Reference 9) was used to determine the reconstructed trajectory. This program solves for the initial conditions (position, velocity, and attitude of the vehicle)

so that by integration of the gyros and accelerometers the trajectory matches the radar data (range, azimuth and elevation). Besides solving for initial condition it has the capability of determining the systematic errors (biases and scale factors) on the gyros and accelerometers. The program gives a minimum variance solution on the radar measurements (range, azimuth and elevation). The trajectory is considered to be the optimum when the radar data are randomly dispersed about the reconstructed trajectory and the variance of the range, azimuth and elevation is within the expected tracking accuracies of the radar.

STEP requires an estimate of the biases and scale factors on the gyros and the accelerometers. In order to obtain these biases on the gyros, the telemetry data were examined from T-45 seconds to T+0 (vehicle drop). These data are shown in Figure VI-3. At this time the vehicle had very small motions and the centers of the oscillatory motions were determined to be the biases on the gyros. These biases are:

Roll gyro (P)	-1.0 degrees/second
Pitch gyro (Q)	-.61 degrees/second
Yaw gyro (R)	-3.50 degrees/second

To determine the biases on the accelerometers, the data between T+0 and T+1 second were analyzed. These are shown in Figure VI-4. At this time the vehicle is in a near zero force field which permits establishing a zero setting. The average values of the accelerometer readings at this time were:

X-accelerometer	0.0 ft/sec ²
Y-accelerometer	-0.48 ft/sec ²
Z-accelerometer	-0.756 ft/sec ²

The scale factors on the gyros and accelerometers were initialized at unity.

The initial estimates of position and velocity at drop were obtained from smoothed radar data:

Latitude	33.2871 deg.
Longitude	-106.2322 deg.
Altitude	120,850 ft.
Velocity	100 ft/sec.
Flight Path Angle (gamma)	+1.4 deg.
Azimuth	-126 deg.

The initial estimates of the body Euler angles are required for body heading (PSI), pitch (THETA) and roll angle (PHI). The initial Euler angle estimates are:

PSI	-137°
THETA	55°
PHI	0°

The initial estimate for PSI was taken from the magnetometer reading at drop while THETA was estimated at 55° based on nominal value.

Given initial conditions and previously established biases and scale factors, STEP was not able to provide a comparative trajectory match to the radar data between T+0 and T+38 seconds due to systematic errors in the radar data and the necessity for scale factors on the TM data. By changing the scale factor on the gyros, STEP was able to improve the trajectory match. The most sensitive parameter was the scale factor on the roll gyro (P). A scale factor of .9815 gave the best fit to the radar data from site R123. As previously discussed under Radar Data (VI A,1,c) all beacon track radar data showed systematic errors with R123 data being selected as having the least error.

STEP reconstruction for vehicle AV-4 did not display radar random dispersion about the vehicle reconstruction trajectory which would have been considered optimum, but this result was anticipated since the radar comparative data (see Figures VI-7, VI-8 and VI-9) displayed systematic error rather than a random type of error. The STEP reconstruction trajectory differed from the radar track in a systematic manner and within the deviations established by the radar comparison analysis. It is felt that the trajectory reconstruction is optimized to the maximum extent possible using the existing radar data.

STEP was also programmed to compute the best estimate of the biases and scale factors on the gyros and accelerometers. The only revision resulting from this analysis was to change the roll gyro scale factor from 1.0 to 0.9815 and this is within the accuracy of the instrumentation system.

STEP reconstructed trajectory provides a very accurate measurement of altitude and velocity. Combining these values with the meteorology data, velocity relative to the wind, Mach number and dynamic pressure were computed. Time history of altitude, velocity, Mach Number and dynamic pressure are shown in Figures VI-13 and VI-14. Figures VI-15 and VI-16 show the body and velocity vector orientation versus time. The conditions established by STEP at mortar fire and peak load, provided in Table VI-2, show that the flight performance did meet the requirements for dynamic pressure as required in Figure VI-1.

The angle of attack, sideslip and total angle of attack are shown in Figures VI-17 and VI-18. The total angle of attack shown on Figure VI-18 never exceeds the value of 15° which is less than the required value of $\leq 17^{\circ}$.

In conclusion, the actual trajectory of BLDT AV-4 was predictable. All flight parameters were within 2σ statistical dispersions of nominal predicted values. The deployment Mach Number/dynamic pressure test conditions were within the designed 2σ ellipses shown in Figure VI-1. Below, the nominal flight conditions with respective statistical dispersions are compared with the actual flight conditions at mortar fire:

<u>Flight Parameter</u>	<u>Predicted Value</u>	<u>2σ Dispersion</u>	<u>Actual Value</u>
Dynamic Pressure (q) - lbs/ft ²	10.85	9.34 - 12.34	10.90
Mach Number (Mn)	2.178	2.074 - 2.282	2.126
Total Angle of Attack (N) - Deg.	10.7	5.0 - 16.4	5.2
Spin Rate (p) - Deg/sec	9.0	-21 - 39	30.0
Altitude (h) - ft	146,425.	143,791-149,059	147,186.
Velocity (V) - ft/sec	2324.	2204.- 2444.	2290.

The above flight parametric values at mortar fire and the statistical dispersions comprise the success criteria for the BLDT AV-4 performance. As shown above each flight parameter is within its 2σ predicted dispersion. This comparison is also shown in Figure VI-13 for velocity and altitude, and Figure VI-14 for Mach Number dynamic pressure and Figure VI-18 for total angle of attack.

The actual mortar fire test conditions are displayed in the upper portion of the 2σ ellipse shown in Figure VI-1. The deviation from nominal can be attributed to a combination of random deviations in the 111 independent parameters considered in the statistical analysis, which are impossible to isolate using flight data. However, two basic facts influence this condition;

- (1) The computer generated mortar fire command (Appendix E) was designed to adjust the dynamic pressure upward depending upon the noise level in the real time radar data.

- (2) The drop altitude, which was consistently low for all missions, caused a lower than nominal Mach Number at mortar fire because of an increased atmosphere density through which the vehicle flew. The sensitivity of Mach Number at mortar fire to drop altitude is approximately .06/1000 ft. The fact that the altitude was 700 feet low at drop of vehicle AV-4 provides a Mach Number shift of approximately 0.042 which is sufficient to account for the lower than nominal Mach number test condition at mortar fire.

B. Capsule Aerodynamic Characteristics

The aerodynamic characteristics of the vehicle are difficult to separate from the thrust misalignment effects and inertial cross coupling due to roll during the powered portions of flight. However, after despin and prior to mortar fire the vehicle motion was due to the aerodynamic forces and moments. The aerodynamic drag and the pitch and yaw moment coefficients were evaluated based on the acceleration and the gyro data using the equation:

$$C_D = \frac{A_D + WT}{qS}$$

$$C_m = \frac{\dot{Q} + IYY - P \cdot R (IZZ - IXX)}{qSL}$$

$$C_n = \frac{\dot{R} + IZZ - P \cdot Q (IXX - IYY)}{qSL}$$

where: A_D = T/M acceleration component along the velocity vector, g's

WT = weight, 1891 lb.

q = dynamic pressure, PSF

S = reference area, 103.8 ft²

L = reference length, 11.5 ft

IXX = roll moment of inertia, slug ft²

IYY = pitch moment of inertia, slug ft²

IZZ = yaw moment of inertia, slug ft²

P = roll rate, rad/sec

Q = pitch rate, rad/sec

R = yaw rate, rad/sec

\dot{Q} = pitch acceleration, rad/sec²

\dot{R} = yaw acceleration, rad/sec²

These data are shown in Figure VI-19 where the drag coefficient is compared to the predicted data from Reference 4 evaluated at the flight total angle of attack and Mach Number. The flight data are below the predictions probably due to residual thrust. The aerodynamic moment coefficient data were used in conjunction with the predicted moment data to estimate the angles of attack and sideslip. These data are compared to the Step Reconstruction of the angles of attack and sideslip in Figure VI-20. The difference is probably due to a slight roll attitude error in the STEP reconstruction.

C. Thermal Control Subsystem

The design requirements for the BLDT Thermal Control subsystem were based on maintaining previously qualified hardware within the maximum and minimum specified qualification temperatures. Except for several isolated electrical heaters, a passive thermal control system was utilized on the BLDT vehicle for ascent and float control. The passive system was based on vehicle attitude and vehicle ascent rate to float altitude with convection, solar radiation, reflected solar radiation and infrared radiation being the major heat transfer parameters being considered.

The design ascent profiles are shown in Figure VI-21 with the fast ascent rate, when integrated with the above mentioned parameters, producing the hot case and the slow ascent rate producing the cold case. Figures VI-22, VI-23, VI-24 and VI-25 show select hot and cold case predicted temperature profiles for

the base cover, rocket motor support structure, aeroshell and S-band transmitter respectively. Also shown in these figures are discrete point actual temperatures, expected from the TM data which were recorded at approximately half hour intervals. It is noted that the actual temperatures generally remain within the hot and cold case predictions and are generally closer to the hot case as would be expected due to the actual ascent rate.

Presented below is a table showing the temperatures measured by the "on-board" thermistors at the time of vehicle release from the load bar and at aeroshell separation compared with the specified requirement at vehicle drop.

<u>THERMISTOR NAME</u>	<u>SPECIFICATION REQUIREMENT (°F)</u>		<u>ACTUAL TEMPERATURE (°F)</u>	
	<u>MAX.</u>	<u>MIN.</u>	<u>DROP</u>	<u>A/S SEPARATION</u>
Rate Gyro	125	0	79	77
Boost Motor #1	165	-65	57	124
Equipment Ballast	165	0	82	80
S-Band Transmitter #1	165	0	100	99
Instrument Beams #1	125	0	63	63
Bridle #1	210	-90	34	35
Aeroshell #1	175	-115	42	48
Boost Motor #2	165	-65	54	130
Mortar Cannister #1	80	No Min	44	81
Mortar Breech	75	25	49	52
Instrument Beam #2	125	0	59	59
Bridle #2	210	-90	35	36
Aeroshell #2	173	-115	3	11
Rocket Motor Support Structure	(No Prediction)		44	45
Mortar Cannister #2	80	No Min	46	85
Mortar Breech Flange	72	25	48	68
Bridle #3	210	-90	37	38
* Main Battery	80	50	46	46

* The thermistor titled "main battery temperature" is misnamed, it really measures rocket motor support structure temperature.

D. Propulsion, Azimuth Pointing and Ordnance Subsystems

The main propulsive system on the AV-4 vehicle was the 4 Rocketdyne solid rocket motors. These motors have classified performance characteristics and therefore their specific performance parameters will not be given. Solid rockets were also used to affect spin and despin of the vehicle to minimize the effect of the main rocket motor thrust vector to center of gravity misalignment. In addition to the solid rockets, pyrotechnic ordnance was used to effect load bar separation, aeroshell separation, and camera lens cover opening. Cold gas thrusters located at the extremities of the AFCRL load bar were commanded from the ground through the command receivers on-board the vehicle. The flight performance of these subsystems will be discussed in this section.

1. Spin/Despin Motor Performance

The spin-up command generated by the onboard programmers 1.02 seconds after drop from the load bar, caused ignition of the 6 spin motors with no noticeable delay between motors. The spin rate generated was 203 degrees per second. This was 2.5% higher than predicted. The 4 despin rocket motors were ignited at 33.09 seconds and produced an incremental rate of 140 degrees/second. This was 6% higher than predicted. This higher performance is probably due to the plume over expanding and recirculating to produce a pressure force on the spin/despin motor bracket. The base cover near the spin motors showed some evidence of plume impingement on both the spinup and despin side.

2. Main Propulsion System

The four solid rocket motors were ignited 2.04 seconds after release from the load bar and showed no noticeable time delay between their thrust buildup. There was a slight thrust differential which produced a slight

lateral (Y) acceleration at ignition (see Figure VI-6) and also a slight misalignment between the thrust vector and the center of gravity.

The body rates at ignition, prior to developing element aerodynamic forces indicate a yaw moment which is in agreement with the lateral acceleration, however, the pitch moment indicates a 0.030 inch displacement of the thrust vector from center of gravity in the -Z direction. The subsequent variation in lateral accelerations appear to be the result of a relatively low burn rate on rocket motor No. 1 (+Y +Z).

There was no evidence of Rocket exhaust recirculation heating nor plume radiative heating of the base cover and parachute bridle or camera lens cover.

3. Azimuth Pointing Subsystem

The azimuth pointing system performed as predicted during flight. During ascent, the wind shears and main balloon inflating produced erratic torques to the load bar which resulted in rotational amplitudes up to 3 revolutions, peak-to-peak. The zero torque azimuth also varied (see Figure VI-26). Ballasting continued until 35 minutes prior to drop at which time all remaining ballast was released. The pointing system cold gas thrusters were checked out during this period of time by pulsing them at times which would reduce the oscillation amplitude. This aided the natural damping of the system such that when the float altitude was reached, the oscillation amplitude was 205 degrees peak-to-peak. The variation in the moment of inertia of the suspended system was the maximum possible since all ballast was dropped, however, the torsional stiffness of the recovery parachute system, based on the period of oscillation, agreed well with the torsional test measurements used for design, (see Figure VI-27). The oscillation amplitude decay at float exhibited damping ratio of 0.08 which was close to the predicted value of

of 0.1 used in design. The zero azimuth varied sinusoidally during float and while the azimuth was being maintained, passed through the required drop azimuth. This required the pointing operator to change from counter clockwise thrusting to clockwise during the last eight minutes prior to drop, however, no difficulty was encountered and the proper drop azimuth was maintained within ± 4 degrees. The thrusters exhibited 16 torque which was more than sufficient to counter the 2.3 ft-lb of torque which was generated by the 95 degrees of windup. The pointing pressure supply was consumed at a rate of 5.3 psi/sec of jet on time and the residual supply pressure was 1585 psi. The last command was terminated 7.7 seconds before drop with maximum rates less than 0.5 degrees/second. These effects of pointing commands on the roll and yaw gyros can be seen in the gyro data shown in Figure VI-3 and was taken into account when the biases were evaluated.

4. Ordnance Subsystem

All pyrotechnic and pyromechanical devices performed properly as programmed. Post-flight inspection revealed that all ordnance functions occurred with no damage to the flight vehicle.

E. Structural Subsystem

The structural subsystem provided adequate support and dynamic operation during all phases of the AV-4 mission. There was no evidence of any structural failure in the load carrying structure and the dynamic portions of the system including flip away lens covers and aeroshell separation system functioned as required. It is noted that the sponge seal which was installed between the mortar cannister and the mortar truss prevented the flow of mortar gases into the BLDT instrument compartment. Post flight inspection showed

that the late gyro section of the instrument compartment was relatively clean compared with the same section on Vehicle AV-1.

Inspection of the recovered hardware indicated the following conditions:

1. Aeroshell - nose cap poked out and inboard skins bent. All damage resulted from ground impact.

2. Rocket Motor Support Structure - The RMSS was undamaged except that the forward command antenna was poked from its installation with the two antenna structural brackets breaking. All damage was due to ground impact.

3. Base Cover - The base cover was recovered in an undamaged condition. It is noted that the ablative material which is bonded to the base cover remained intact during the flight and recovery operation.

4. Parachute Truss - no visual damage.

5. Equipment Beam - no visual damage.

6. Load Bar Support Structure - no visual damage.

F. Electrical Subsystem

The electrical power and sequencing systems operated satisfactorily during the complete mission. All battery voltages and timed events remained within predicted/required limits. The actual airborne programmers sequence times are provided in Table IV-1.

Flight batteries were activated on August 1, using previously established activation procedures. On August 2, following installation in the vehicle, main battery electrolyte leak established an electrical short between the battery "plus" stud and the battery case (ground) which resulted in a subsequent explosion which ripped open the battery cover. No personnel were injured or flight hardware damaged.

A second main battery was activated August 2 without incident and installed in the vehicle prior to FRT. Activation stand time prior to installing battery cell caps has been increased, for all remaining batteries, as an aid in assuring absorption of electrolyte in the individual cells. Battery voltages were above minimum at launch and as shown in Table VI-3 during the flight. Camera batteries, which were not instrumented, operated satisfactorily as evidenced by "on-board" camera operations during the flight sequence.

The vehicle command system operated as required following launch in response to the following commands:

- 14:09 HRS Z - Safe/Safe B/11 (Command System Check)
- 15:29 HRS Z - CCW (Verify Azimuth Pointing)
- 16:19 HRS Z - Arm Vehicle (Power Programmer on Next Pointing Command)
- 16:24 HRS Z - Azimuth Pointing and Hold
- 16:24:30.75 HRS Z - Vehicle Drop
- 16:25:11.18 HRS Z - Mortar Fire

G. Instrumentation Subsystem

The 53 commutated data channels and the 16 continuous data channels performed without malfunction and provided data for each phase of the mission. The quality of the data was improved by actions taken following the flight of Vehicle AV-1 (see report TR-3720289). The data provided during the mission were in accordance with the data list shown in Table A-3 of Appendix A.

H. RF Subsystem

The airborne S-band telemetry, C-band tracking and command control RF subsystems performed without malfunction throughout the flight. Signal acquisition for all frequencies occurred within 30 minutes after launch.

Command system ground station checkouts were performed at launch - 2 hours. All command transmitters were monitored at the J-67 site for center frequency, single tone deviation and triple tone execution of commands. All command system checkouts were satisfactory, however the north Oscars Peak transmitter "A" deviation was slightly of the nominal 30 KHZ value. Consequently, the Test Conductor requested that transmitter "B" at NOP be identified as the primary NOP transmitter for the mission.

Telemetry data was monitored throughout the flight at J-67 and appeared satisfactory in all respects.

I. TSE/OSE

The Test Support Equipment and Operational Support Equipment performed within the design requirements for this equipment.

J. Mass Properties

The BLDT vehicle mass properties at decelerator mortar fire, were established, based on the mass properties of the Viking Lander Capsule, to be as follows:

Vehicle Weight	1888 \pm 12#
Y Axis Cg Location	0 Offset
Z Axis Cg Location	-1.41 \pm 0.030 inches
* X Axis Cg Location	31.7 to 33.7 inches.

* Referenced to Aeroshell Theoretical Apex.

In order to fulfill the Y and Z axis Cg location requirements, the AV-4 vehicle was subject to a spin balance operation at Sandia Corporation Laboratories, Albuquerque, New Mexico. During this operation, lead balance weights were fastened to the vehicles to precisely locate the vehicle Cg with respect to the Y and Z axis.

The vehicle AV-4 mass properties are summarized in Table VI-4.

TABLE VI-1 BLDT AV-4 FLIGHT TEST ATMOSPHERIC PROPERTIES

ALTITUDE (5000 FT)	EAST- WEST WIND (FT/SEC)	NORTH- SOUTH WIND (FT/SEC)	SPEED OF SOUND (FT/SEC)	DENSITY (SLUGS/FT ²)
1.	-1.	-1.	1128.	.23067-02
2.	-8.	-1.	1105.	.16934-02
3.	-10.	-1.	1084.	.14611-02
4.	-5.	4.	1071.	.12368-02
5.	-4.	9.	1053.	.10501-02
6.	-9.	17.	1029.	.89393-03
7.	-7.	22.	1004.	.75578-03
8.	11.	23.	978.	.63315-03
9.	-10.	16.	961.	.51711-03
10.	-32.	18.	946.	.41621-03
11.	-39.	16.	940.	.32812-03
12.	-33.	0.	947.	.25109-03
13.	-43.	4.	956.	.19268-03
14.	-50.	14.	964.	.14863-03
15.	-42.	10.	968.	.11603-03
16.	-53.	-0.	981.	.89063-04
17.	-51.	2.	984.	.70282-04
18.	-63.	12.	990.	.55189-04
19.	-69.	-3.	992.	.43772-04
20.	-87.	-13.	999.	.34483-04
21.	-83.	12.	1013.	.26876-04
22.	-82.	16.	1016.	.21529-04
23.	-83.	5.	1021.	.17212-04
24.	-71.	-23.	1032.	.13636-04
25.	-99.	-18.	1031.	.11071-04
26.	-93.	28.	1033.	.89492-05
27.	-116.	14.	1044.	.71305-05
28.	-144.	-3.	1059.	.56704-05
29.	-150.	-0.	1073.	.45372-05
30.	-159.	-2.	1087.	.36531-05
31.	-132.	18.	1096.	.29855-05
32.	-107.	15.	1086.	.25222-05
33.	-101.	44.	1070.	.21466-05
34.	-102.	62.	1061.	.17977-05
35.	-143.	17.	1059.	.14813-05
36.	-243.	29.	1062.	.12101-05

TABLE VI-2 STATE VECTOR DATA - AV-4

	<u>DROP</u>	<u>MORTAR FIRE</u>	<u>FULL OPEN</u>
Time (t) - sec	00.	40.43	42.0
Altitude (h) - ft	120543.	147186.	147900.
Velocity (V) - ft/sec	--	2290.2	2223.7
Gamma (γ) - deg	--	12.3	11.24
PSI (ψ) - deg.	-135.12	-148.5	-145.52
Theta (θ) - deg.	56.03	+6.6	11.68
Mach No. (MN)	--	2.126	2.057
Dynamic Pressure (q) - lb/ft ²	--	10.9	9.95
Angle of Attack (α) - deg.	--	-4.1	.39
Sideslip (β) - deg.	--	-3.1	-2.15
Total Angle of Attack (η) - deg.	--	5.2	2.18
Spin (p) - deg/sec.	--	30.	30.

TABLE VI-3
BATTERY PERFORMANCE DATA

	<u>MAIN BATTERY</u>	<u>TRANS. BATTERY</u>	<u>PYRO A BATTERY</u>	<u>PYRO B BATTERY</u>	<u>CAMERA BATTERY POSITIVE</u>	<u>CAMERA BATTERY NEGATIVE</u>
1. Activation Voltage						
a. Open Circuit	34.92	32.97	36.79	36.75	16.55	-16.56
b. 5 Second Load*	29.0	26.5	29.0	29.0	13.1	-13.1
2. Prelaunch Voltage						
No Load	31.94	32.92	32.73	32.23	16.07	-16.17
3. Float Voltage						
Drop - 2 hours	29.2	27.8	38.5	33.5	NO TM	NO TM
Drop - 1 hour	29.3	27.6	33.3	32.7	DATA	DATA
Drop - 1 minute	29.2	27.7	30.8	30.8		
4. Flight Voltages						
T + 1 minute	29.2	27.6	30.6	30.5		
T + 6 minutes	29.2	27.7	30.4	30.4		
5. Main Battery Amps.	3-6 amps					

* 5 Second Load Levels - 30 amps for main battery
10 amps for all others.

TABLE VI-4

FINAL BLDT MASS PROPERTIES STATUS - AV-4

Condition	Weight (lb)	Center of Gravity (Vehicle Sta.)			Moment & Product of Inertia (Slug Ft ²)					
		X	Y	Z	I _{xx}	I _{yy}	I _{zz}	P _{xy}	P _{xz}	P _{yz}
On Load Bar	3593									
At Drop	3368	38.09	0	-1.41	577	493	407	.43	1.73	.25
At Mortar Fire	1897	37.16	0	-1.41	439	349	336	.43	1.73	.16
With Decelerator Deployed	1802	36.01	0	-1.41	437	335	322	.46	1.73	.16
With Decelerator Deployed and Aeroshell Dropped	1446	39.65	0	-1.76	262	227	214	.43	3.86	-.17
Aeroshell	356	21.23	+0.08	+1.10	178	91	91			

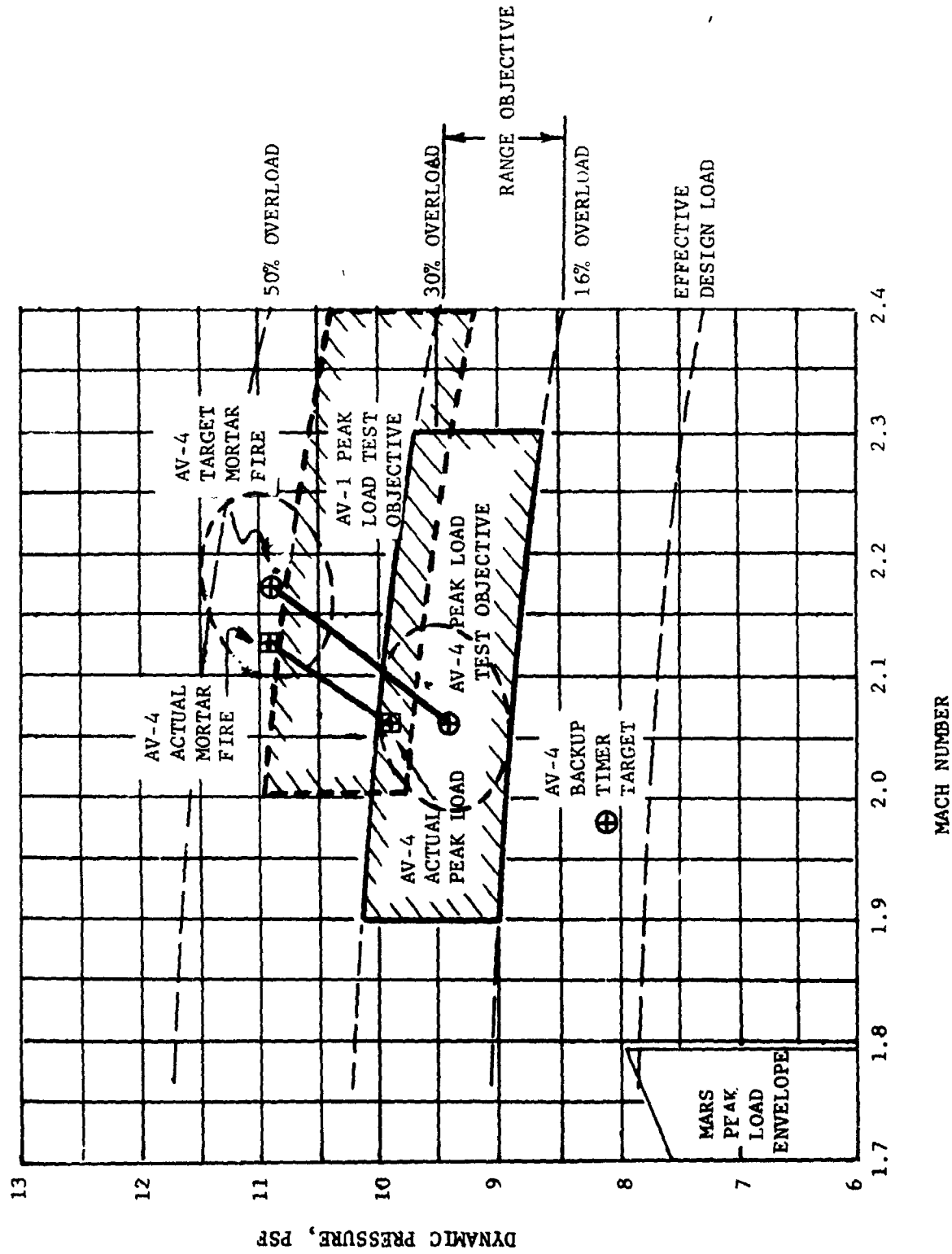
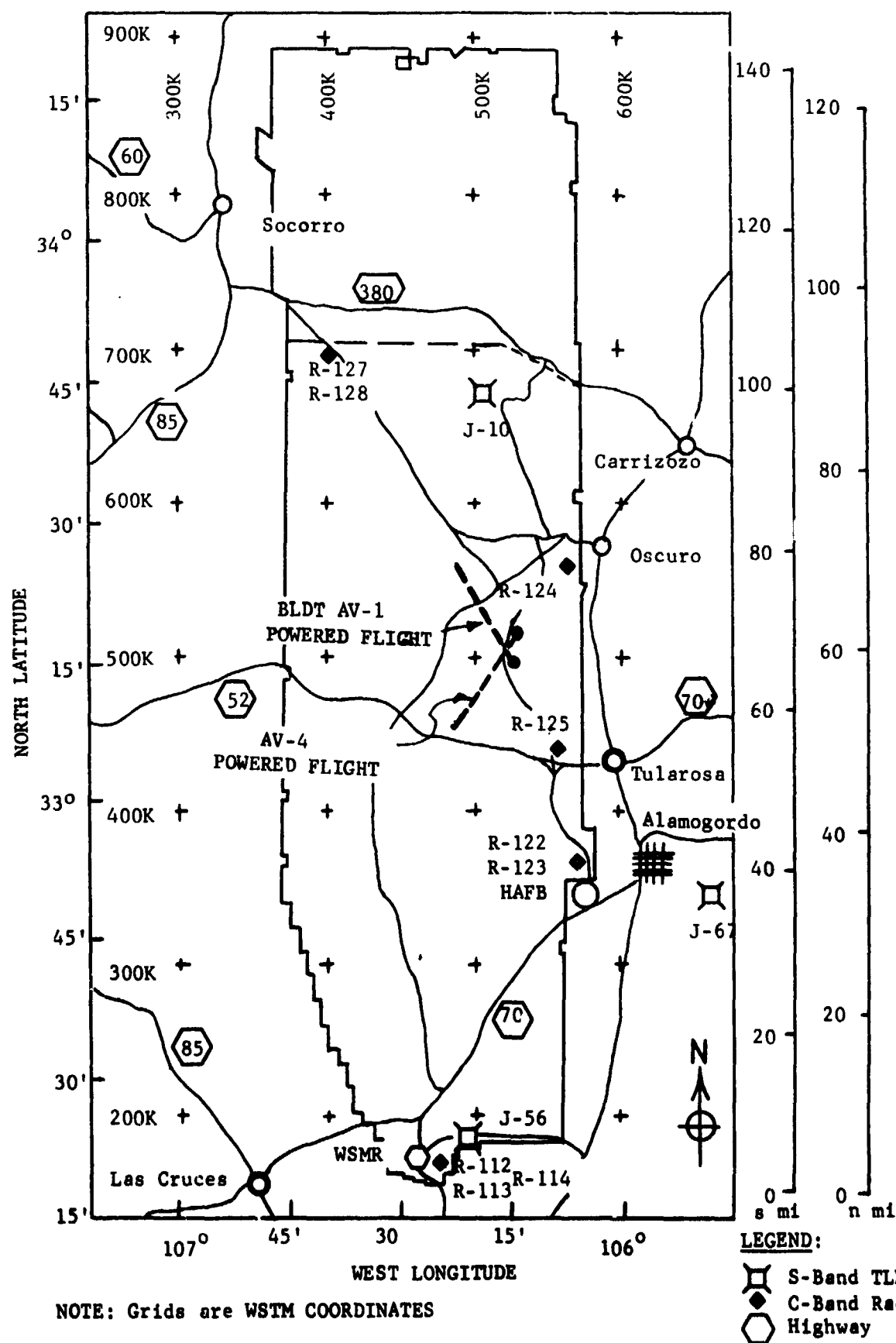


FIGURE VI-1 BLDT AV-4 TEST CONDITIONS



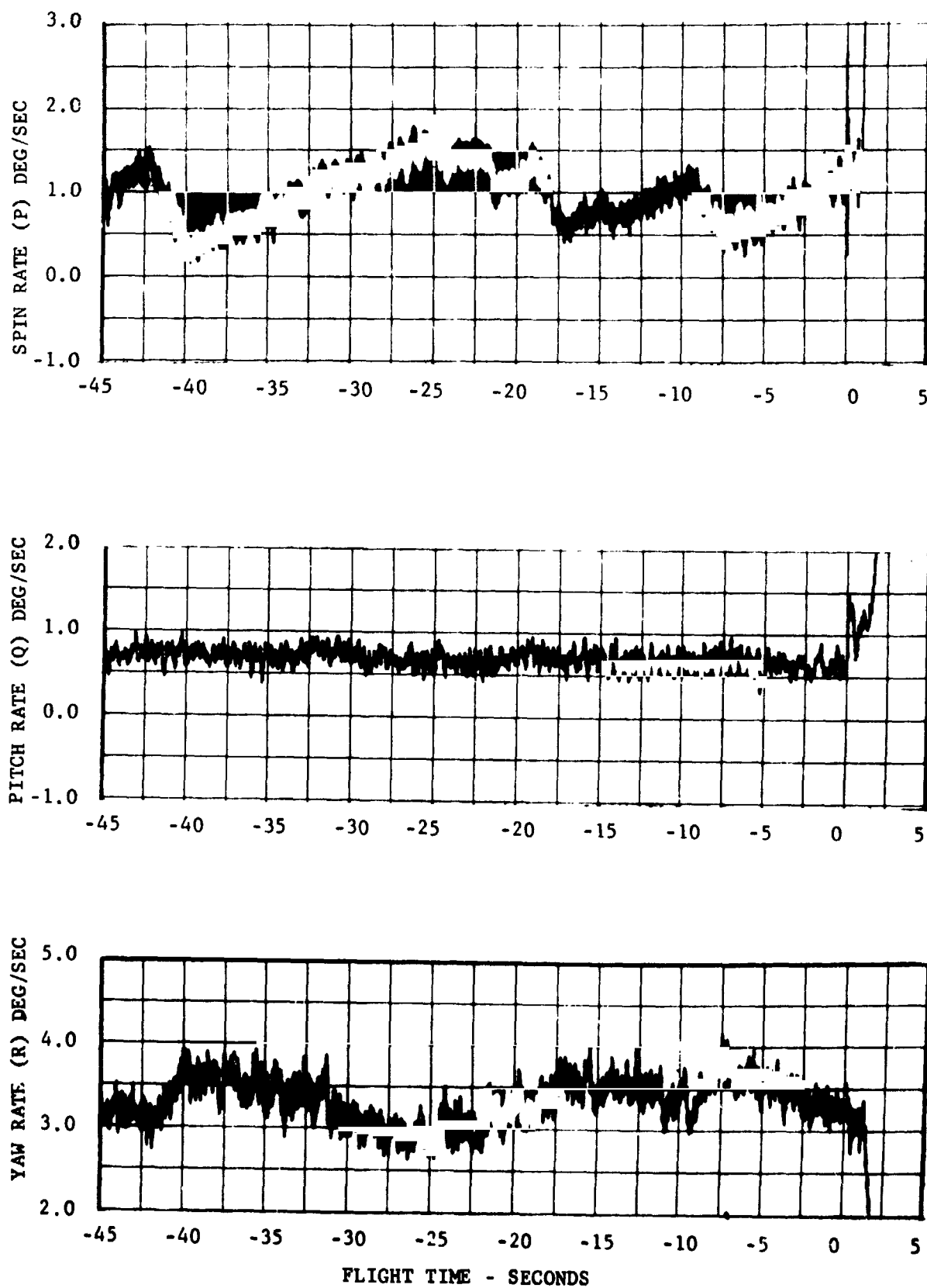


FIGURE VI-3 GYRO DATA PRIOR TO DROP

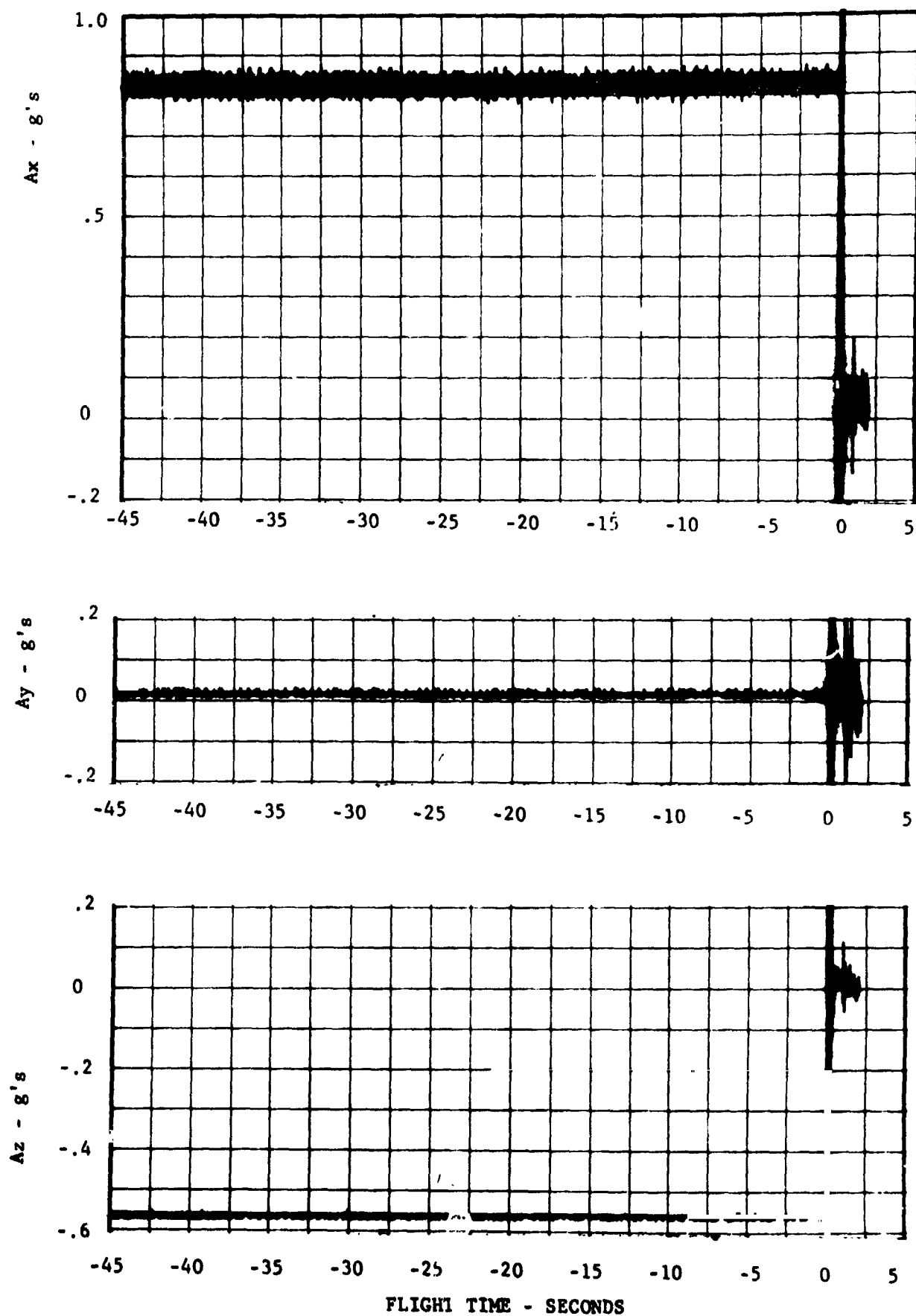


FIGURE VI-4 ACCELEROMETER DATA PRIOR TO DROP

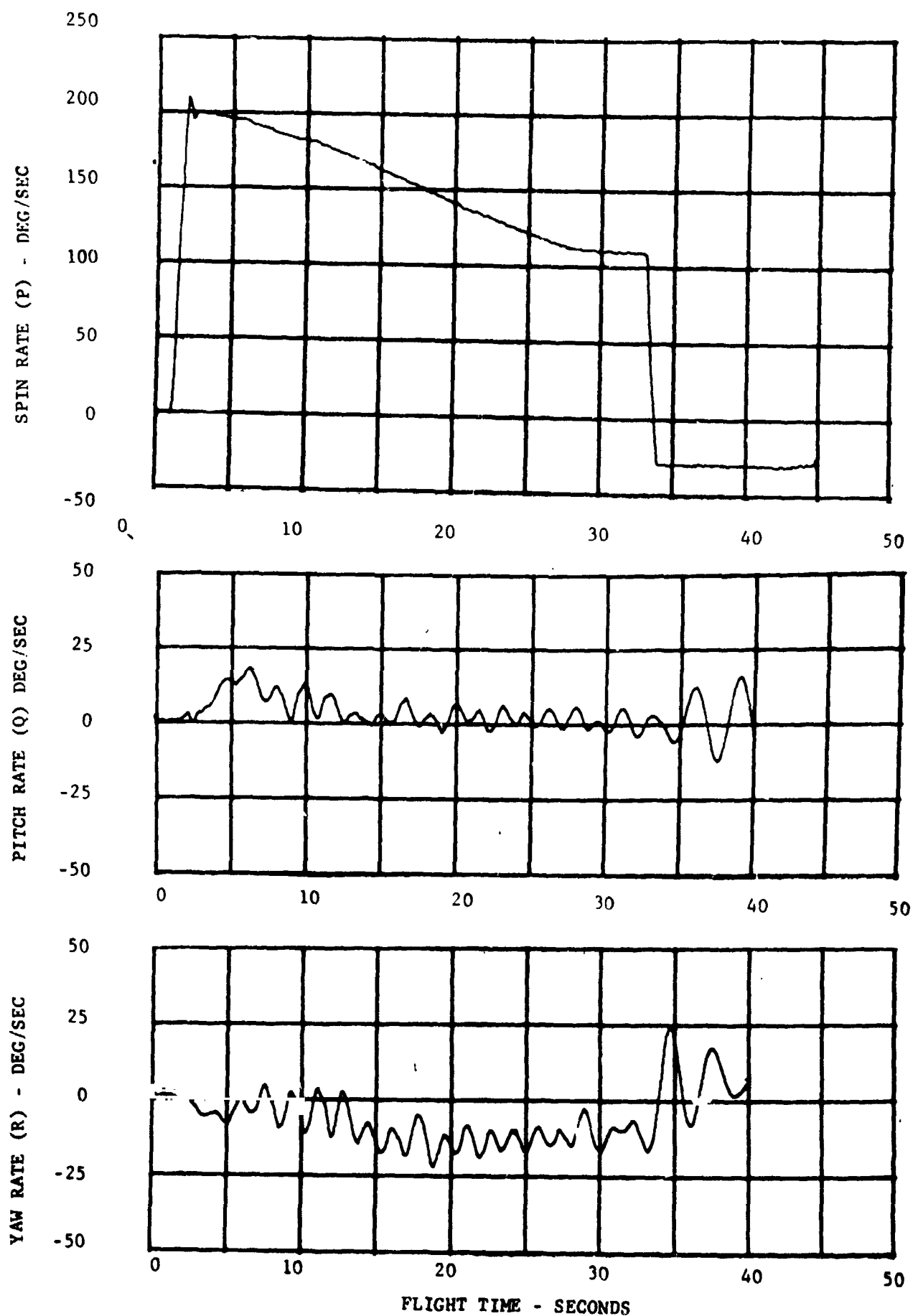
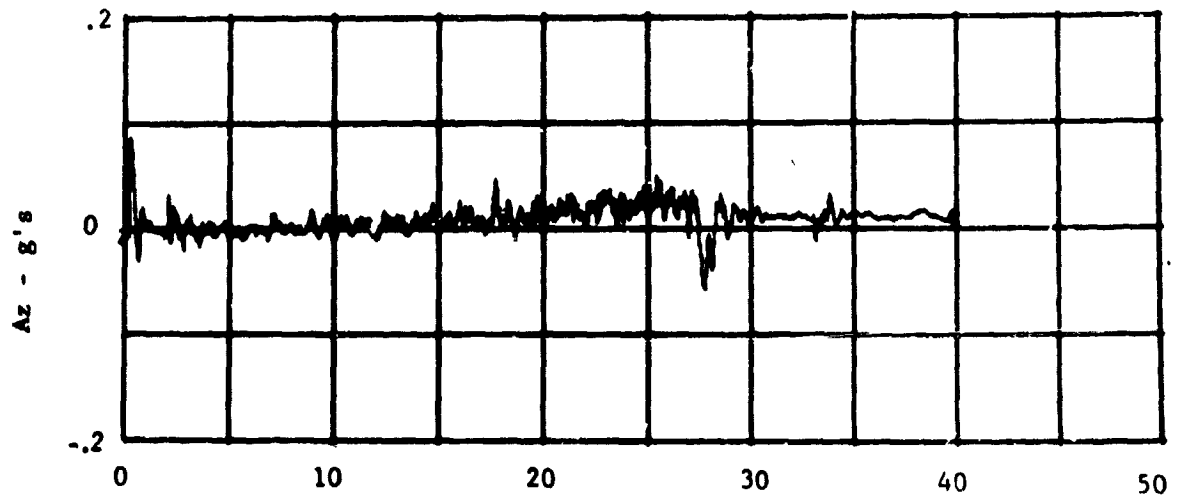
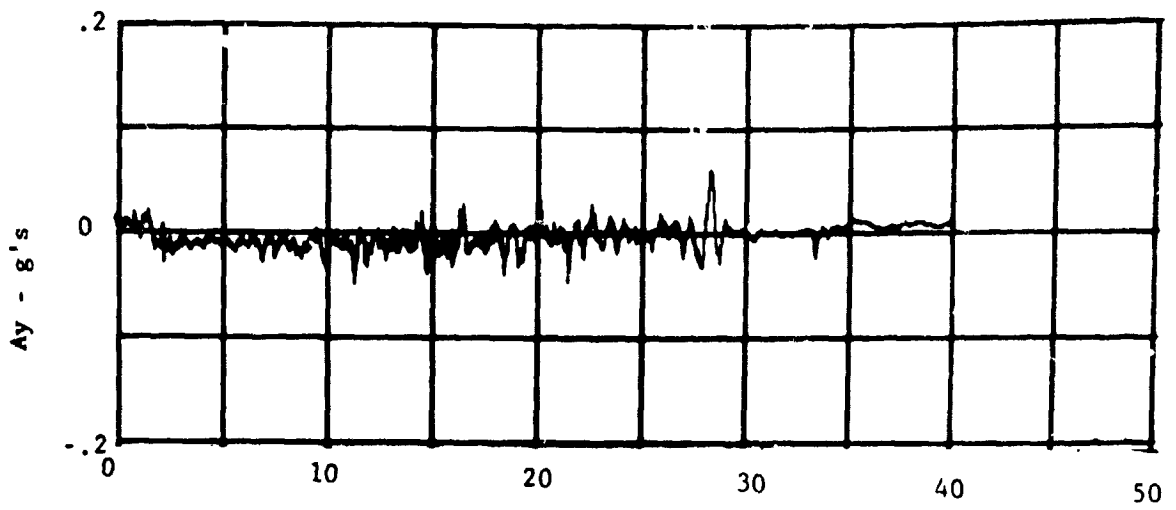
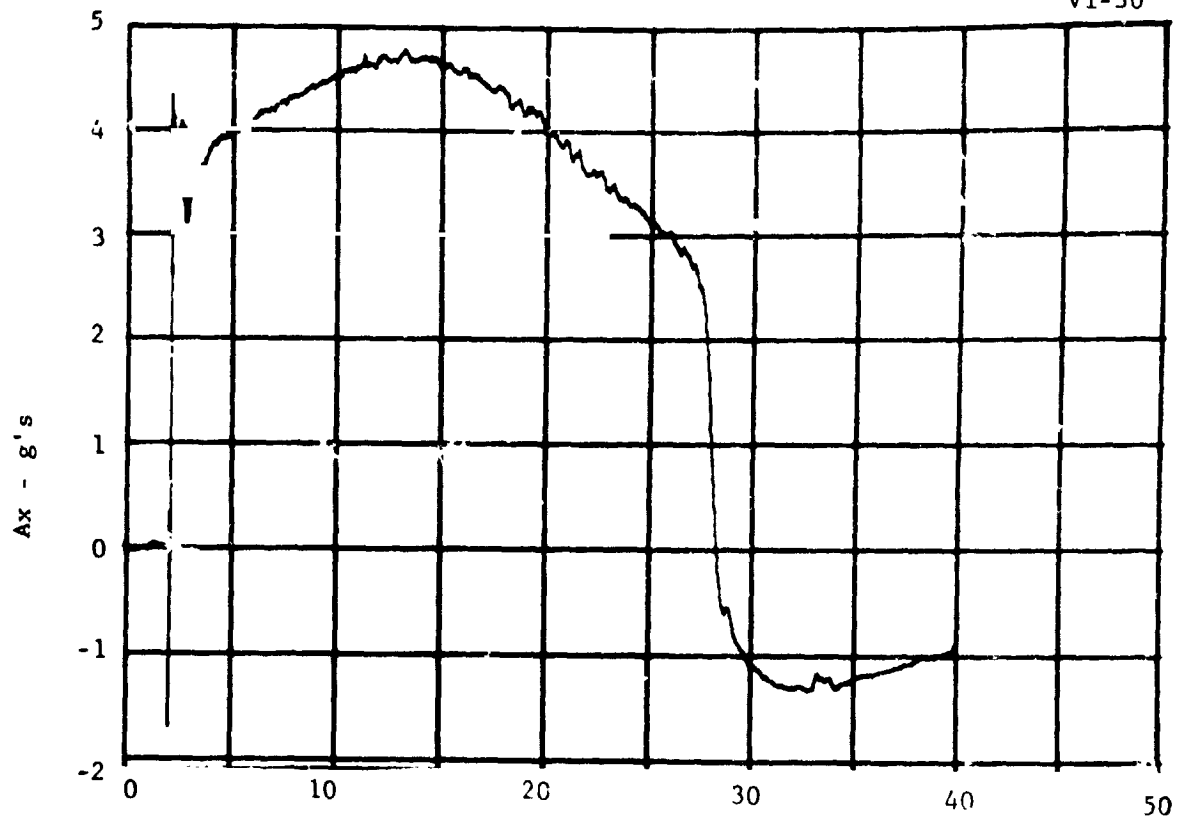


FIGURE VI-5 GYRO DATA DURING POWERED FLIGHT

VI-30



FLIGHT TIME - SECONDS

THE CASE OF TWO-ENGINE FLIGHT

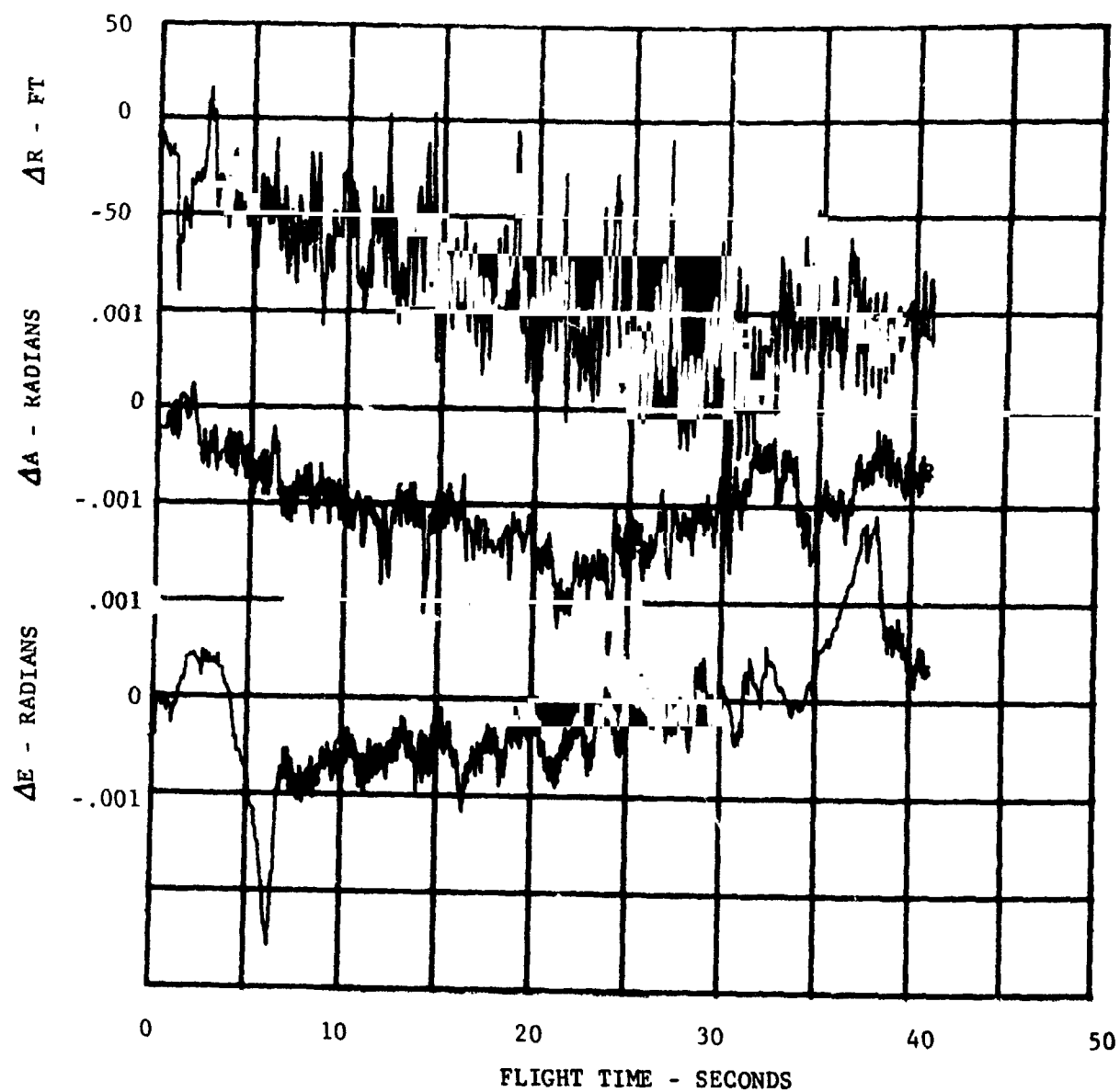


FIGURE VI-7 COMPARISON BETWEEN RADAR DATA (R122 TRANSFORMED TO R128)

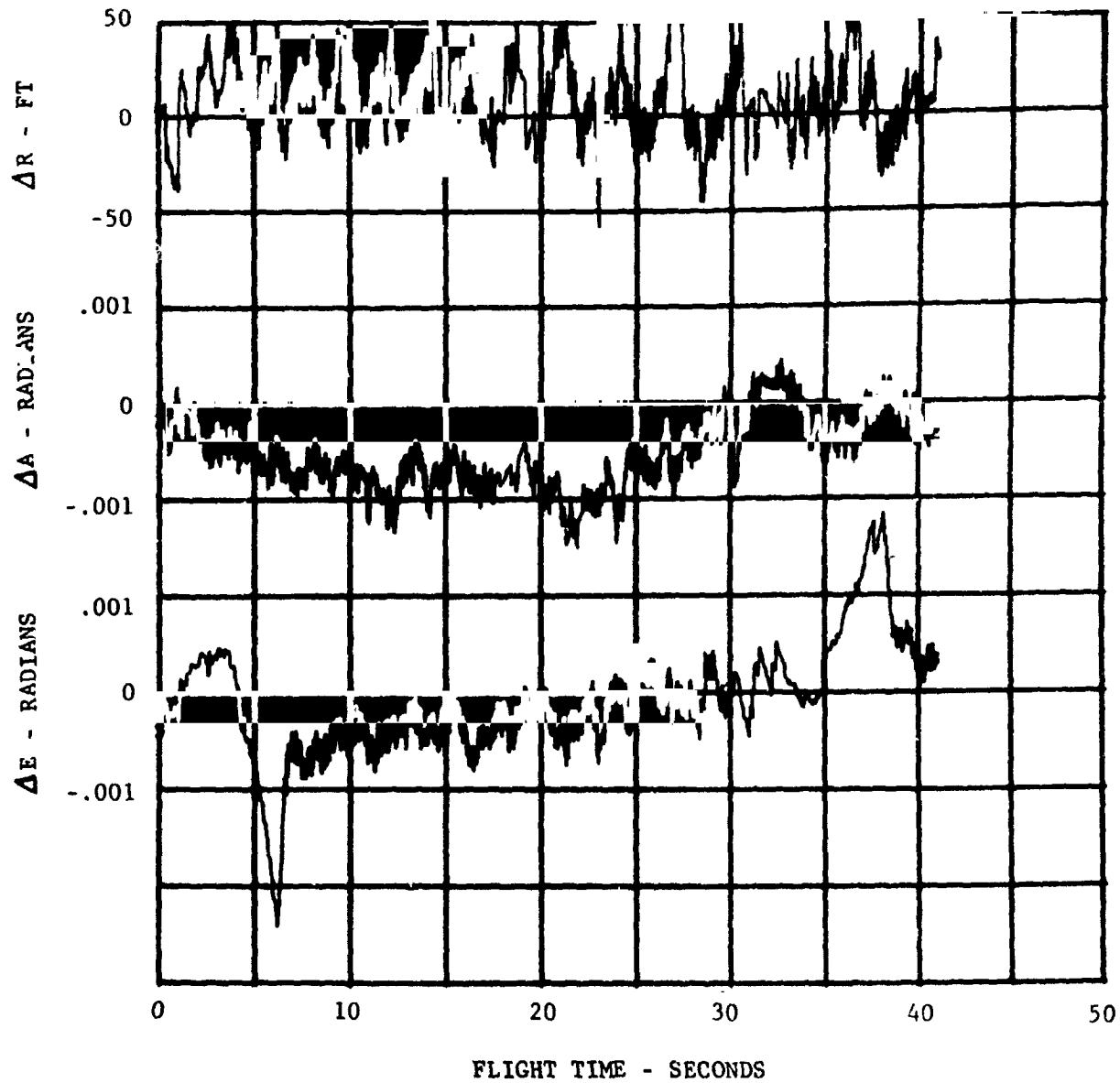


FIGURE VI-8 COMPARISON BETWEEN RADAR DATA (R123 TRANSFORMED TO R128)

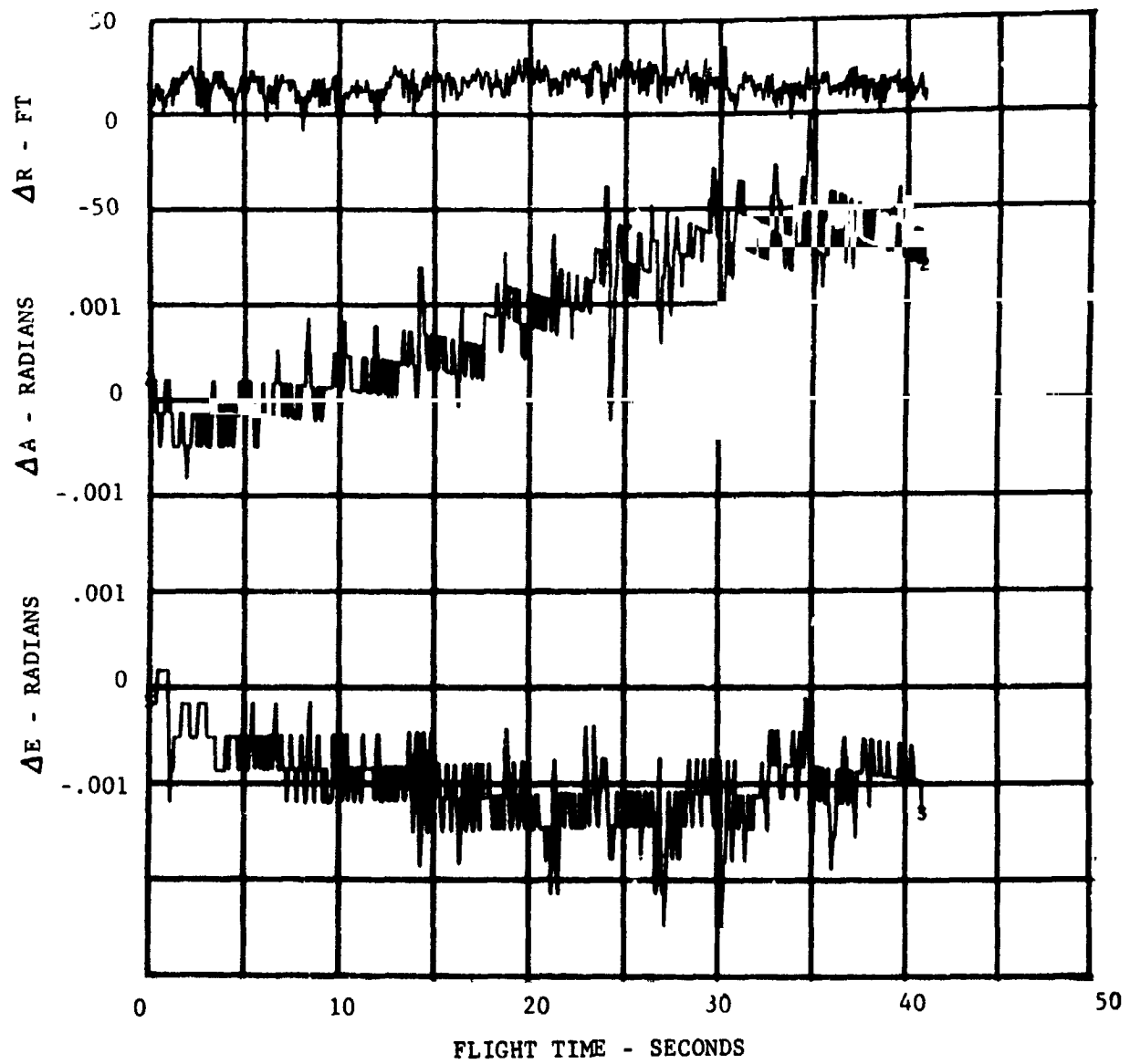


FIGURE VI-9 COMPARISON BETWEEN RADAR DATA (R122 TRANSFORMED TO R123)

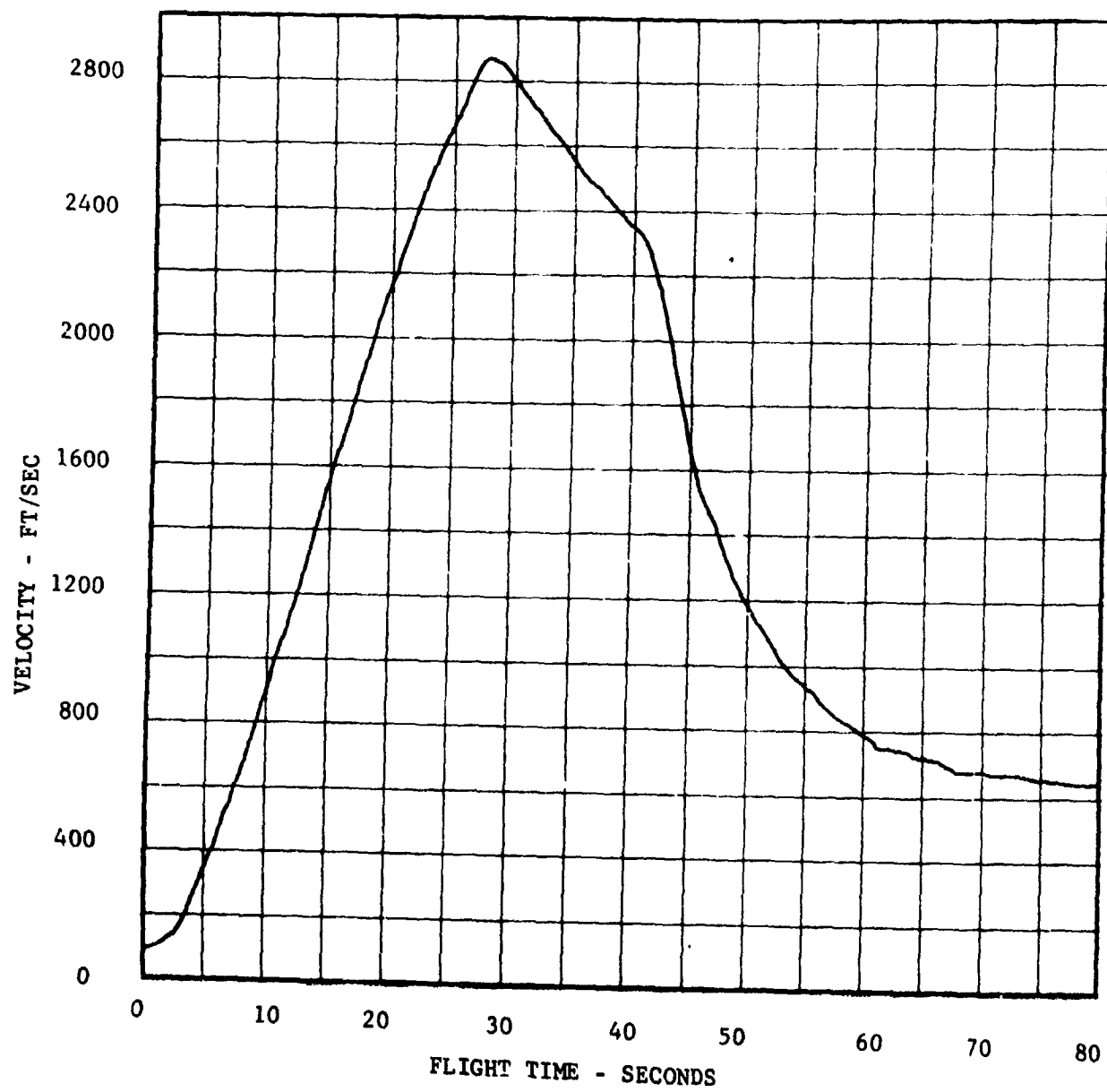


FIGURE VI-10 RADAR (R123) VELOCITY VS. FLIGHT TIME

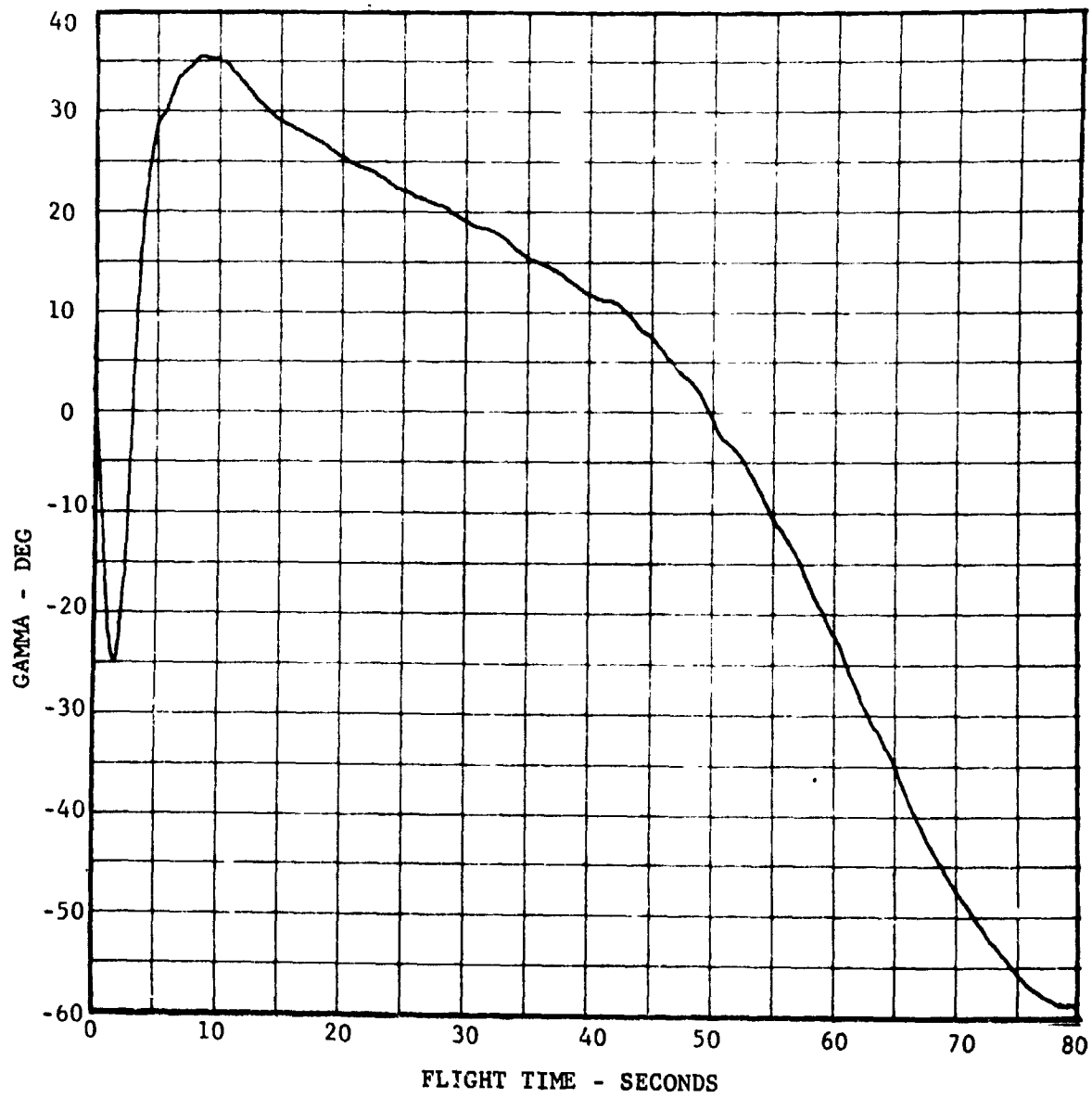


FIGURE VI-11 RADAR (R123) FLIGHT PATH ANGLE VS. FLIGHT TIME

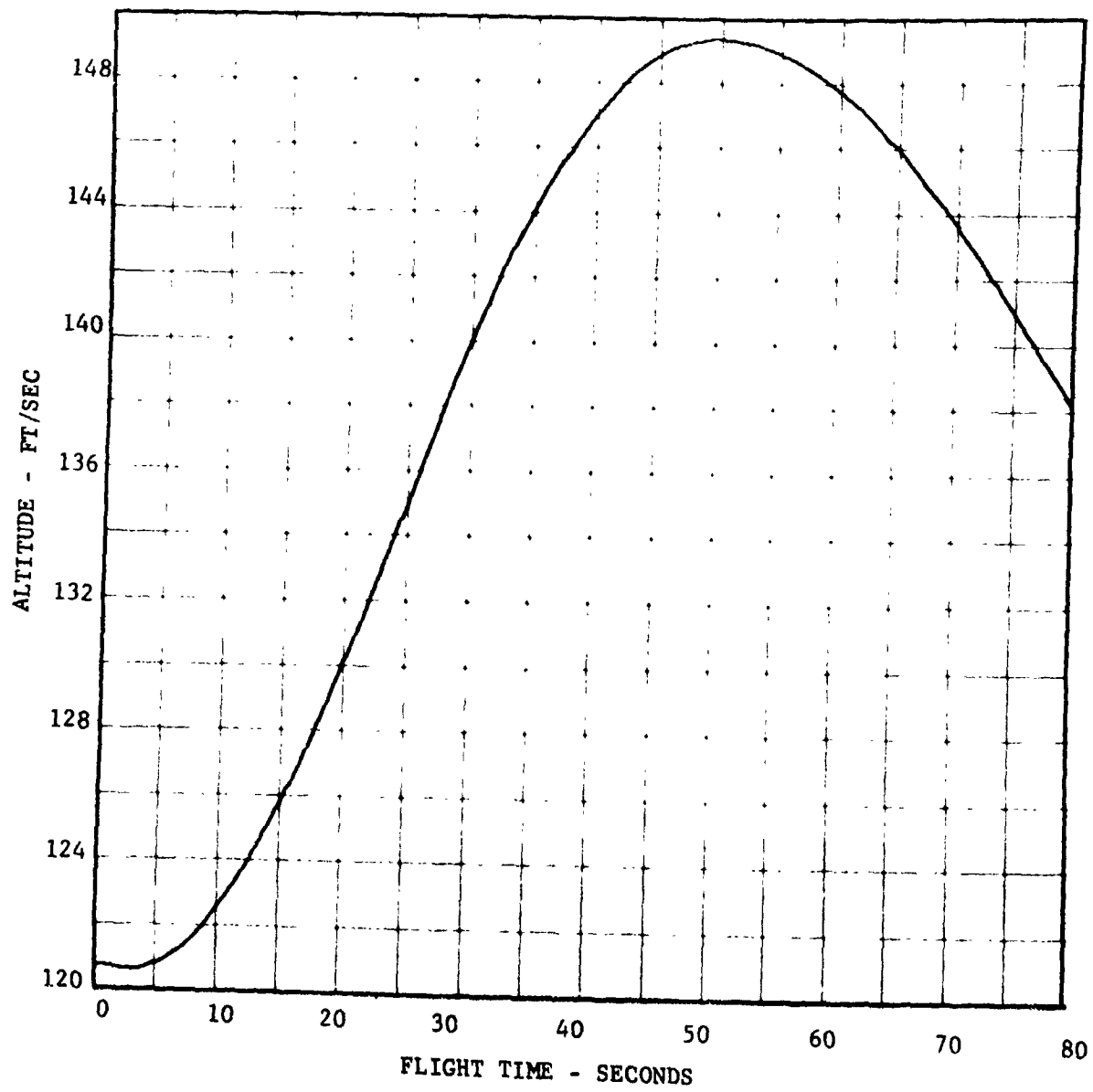


FIGURE VI-12 RADAR (R123) ALTITUDE (MSL) VS. FLIGHT TIME

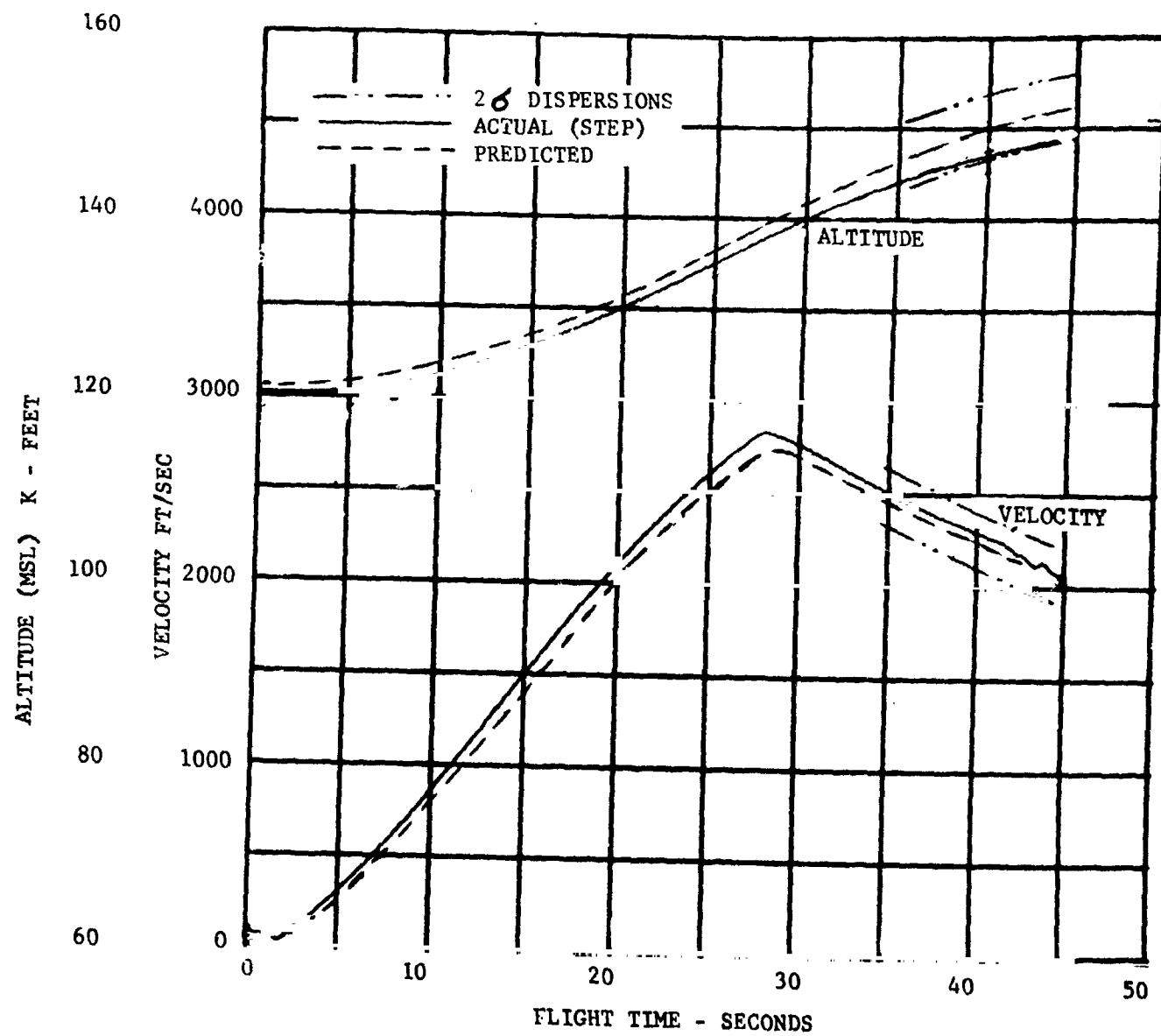


FIGURE VI-13 STEP TRAJECTORY RECONSTRUCTION OF ALTITUDE AND VELOCITY

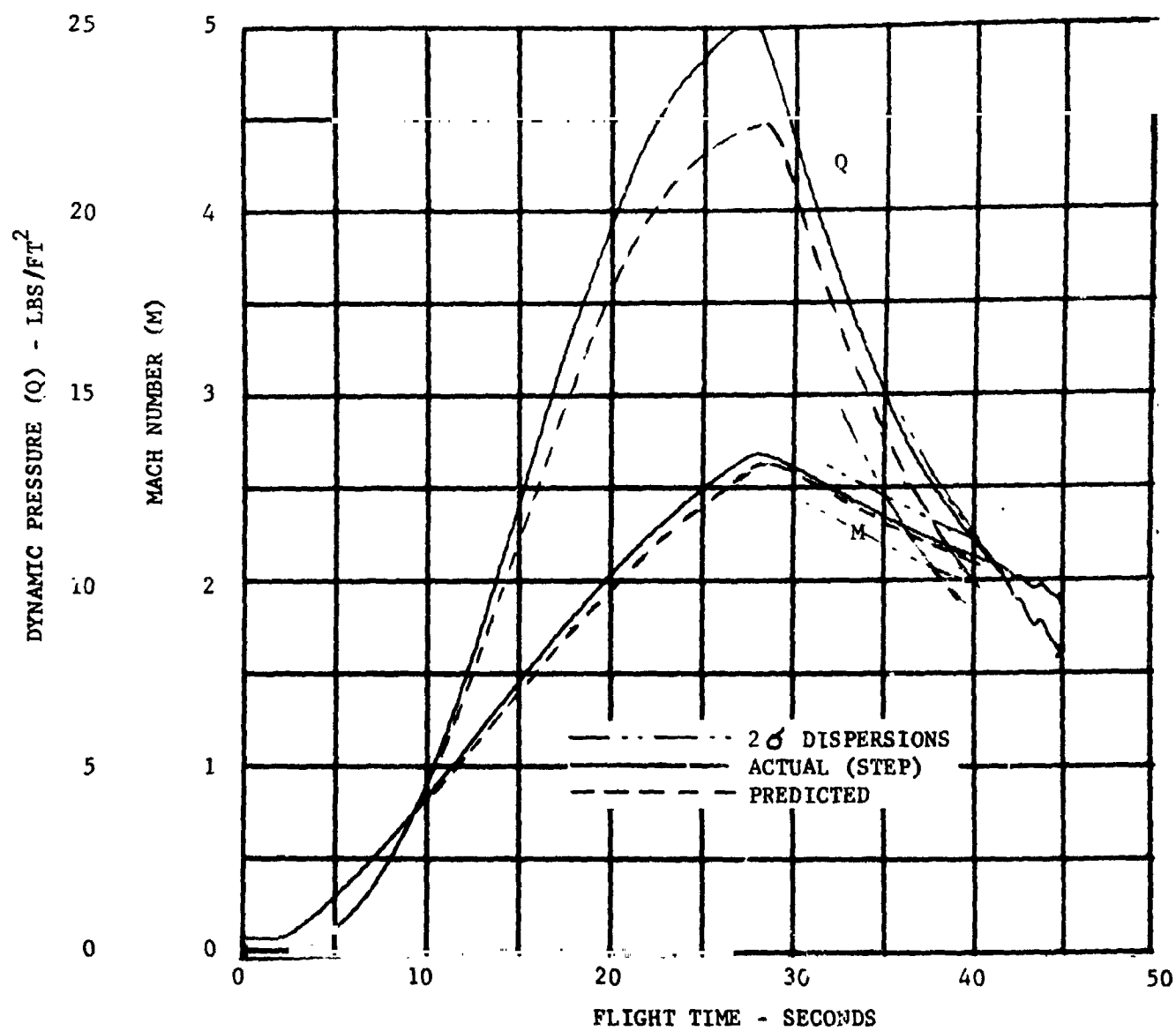


FIGURE VI-14 STEP TRAJECTORY RECONSTRUCTION OF MACH NUMBER AND DYNAMIC PRESSURE

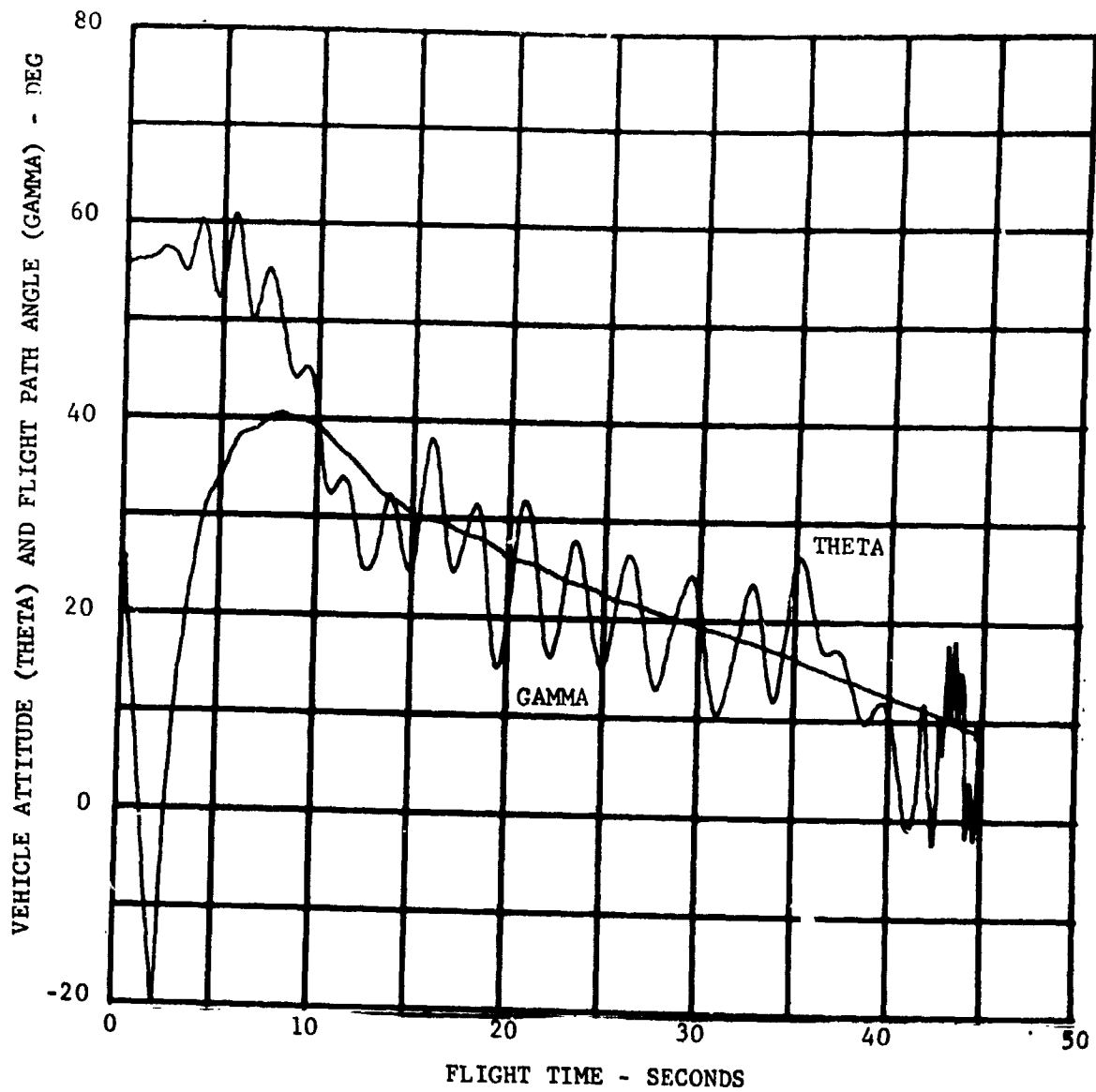


FIGURE VI-15 STEP TRAJECTORY RECONSTRUCTION OF VEHICLE ATTITUDE AND FLIGHT PATH ANGLE

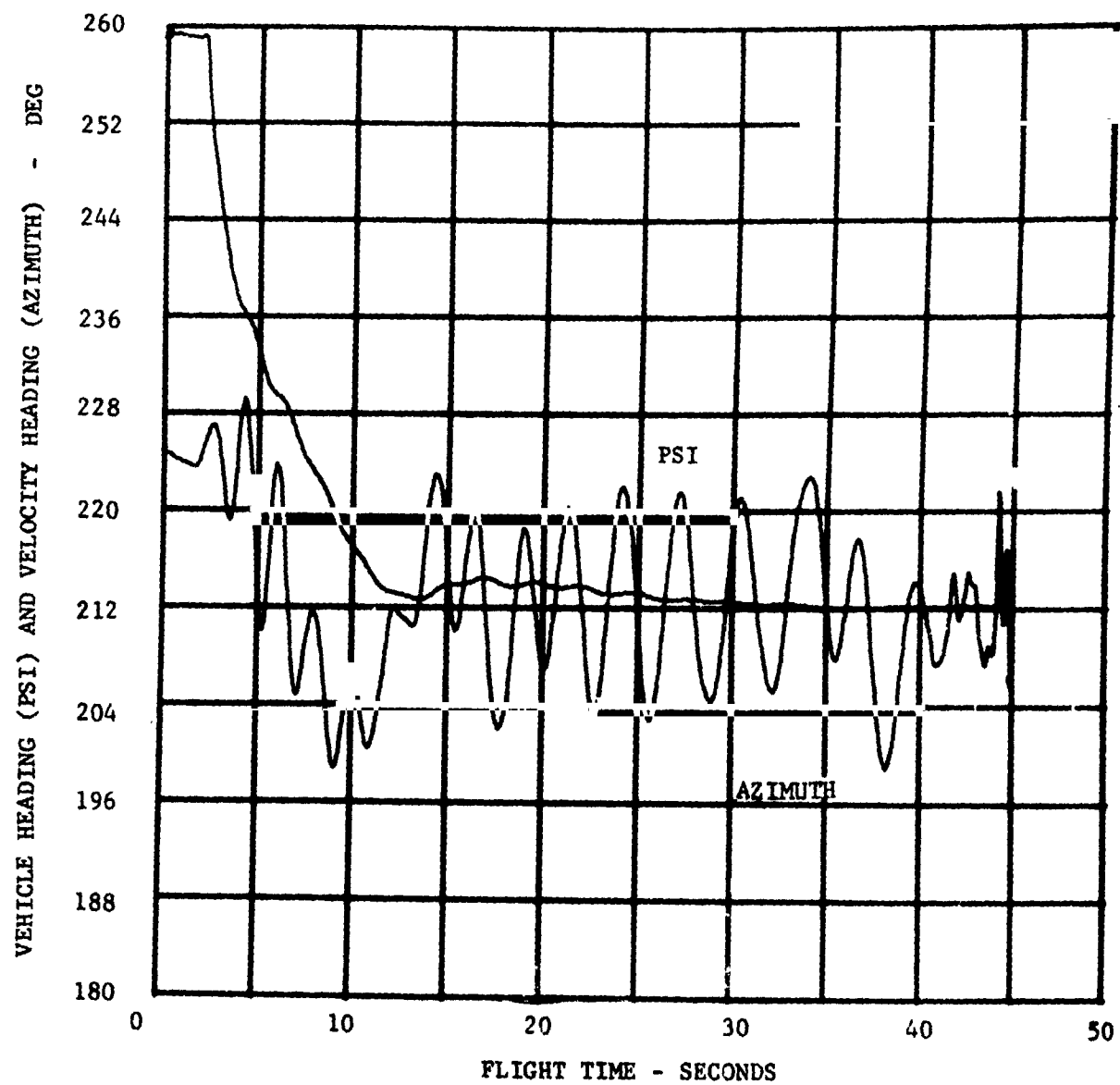


FIGURE VI-16 STEP TRAJECTORY RECONSTRUCTION OF THE BODY HEADING AND THE VELOCITY HEADING

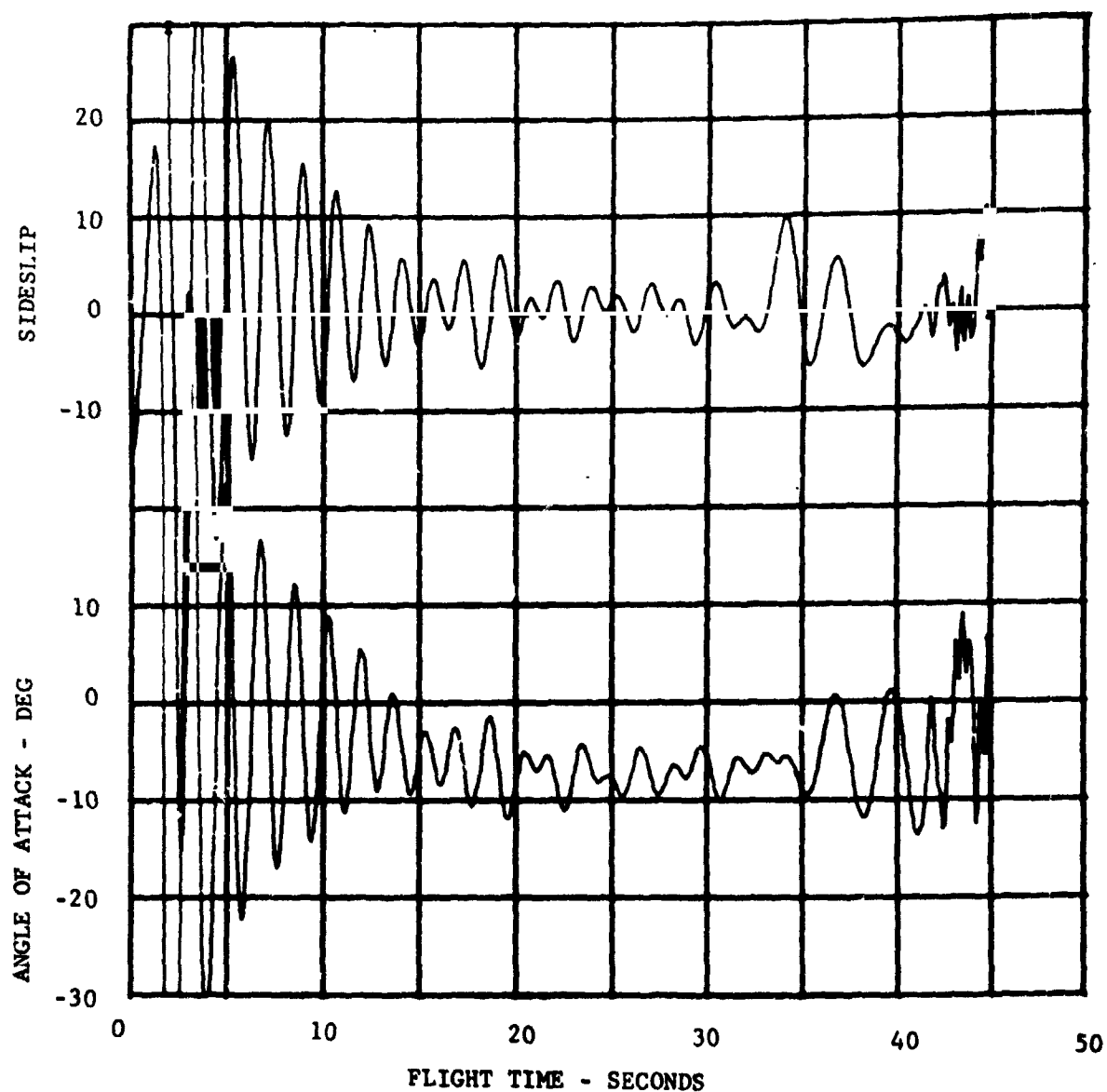


FIGURE VI-17 STEP TRAJECTORY RECONSTRUCTION OF ANGLE OF ATTACK AND SIDESLIP

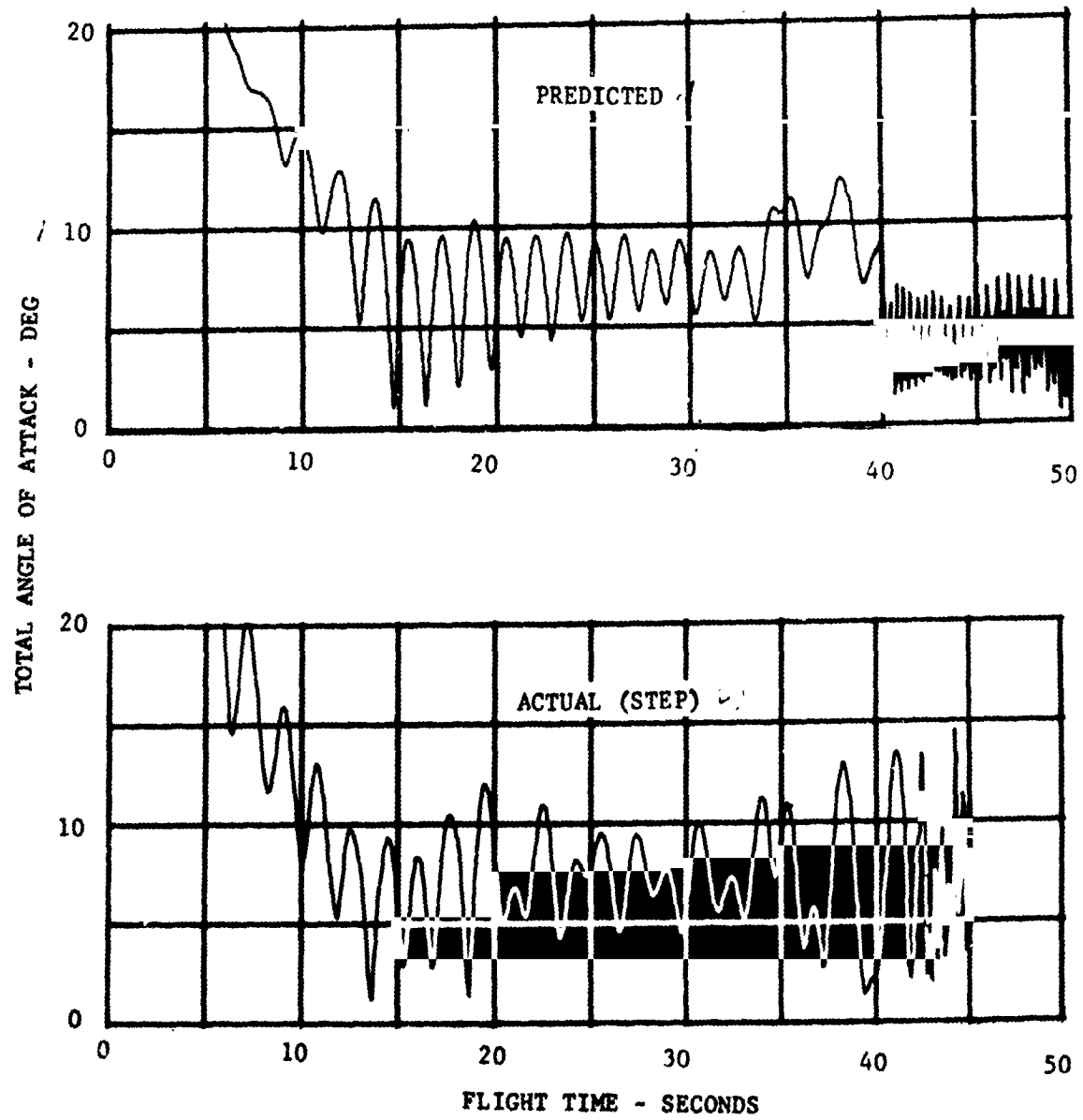


FIGURE VI-18 STEP TRAJECTORY RECONSTRUCTION OF TOTAL ANGLE OF ATTACK

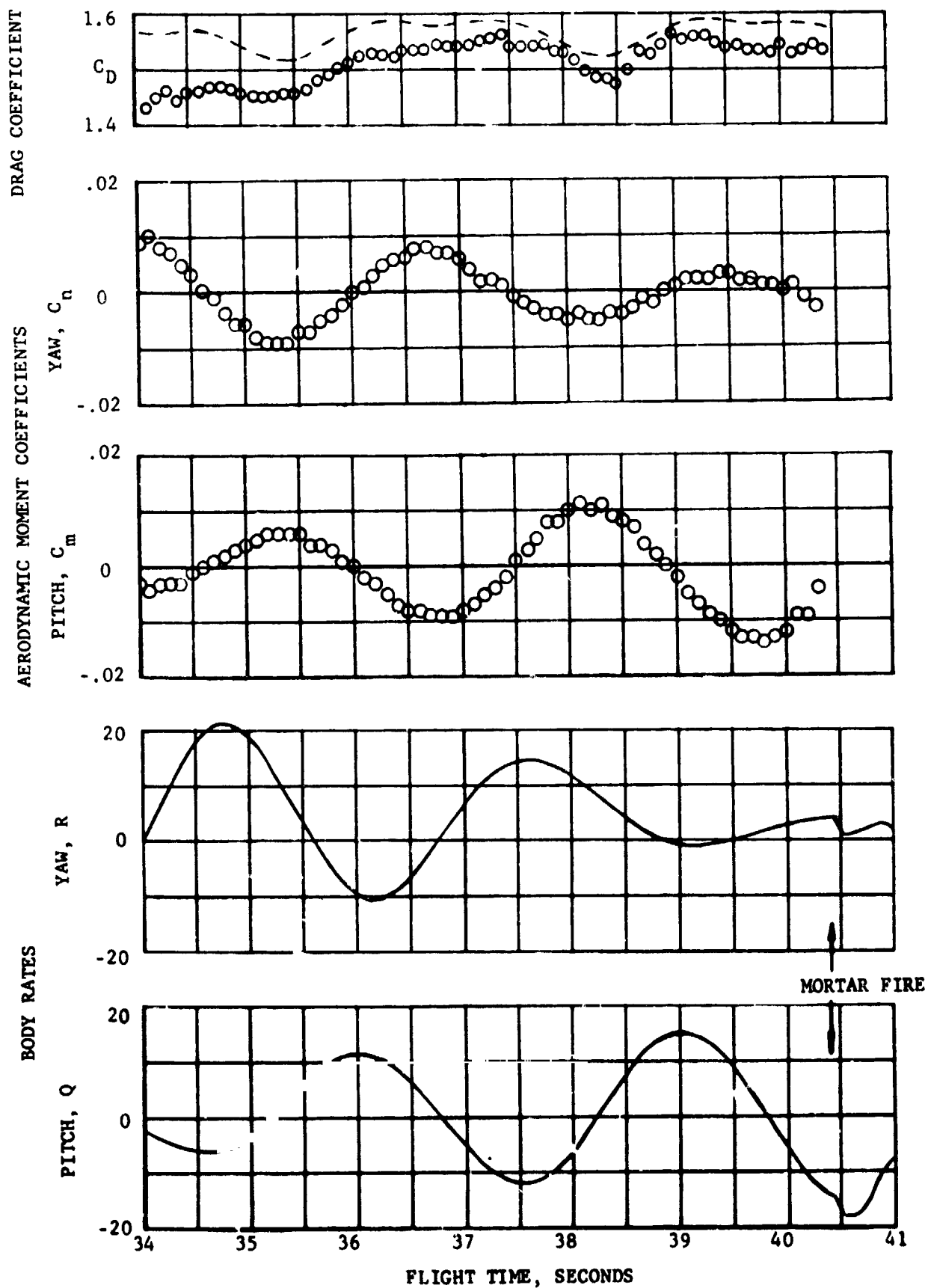


FIGURE VI-19 VEHICLE AERODYNAMIC CHARACTERISTICS

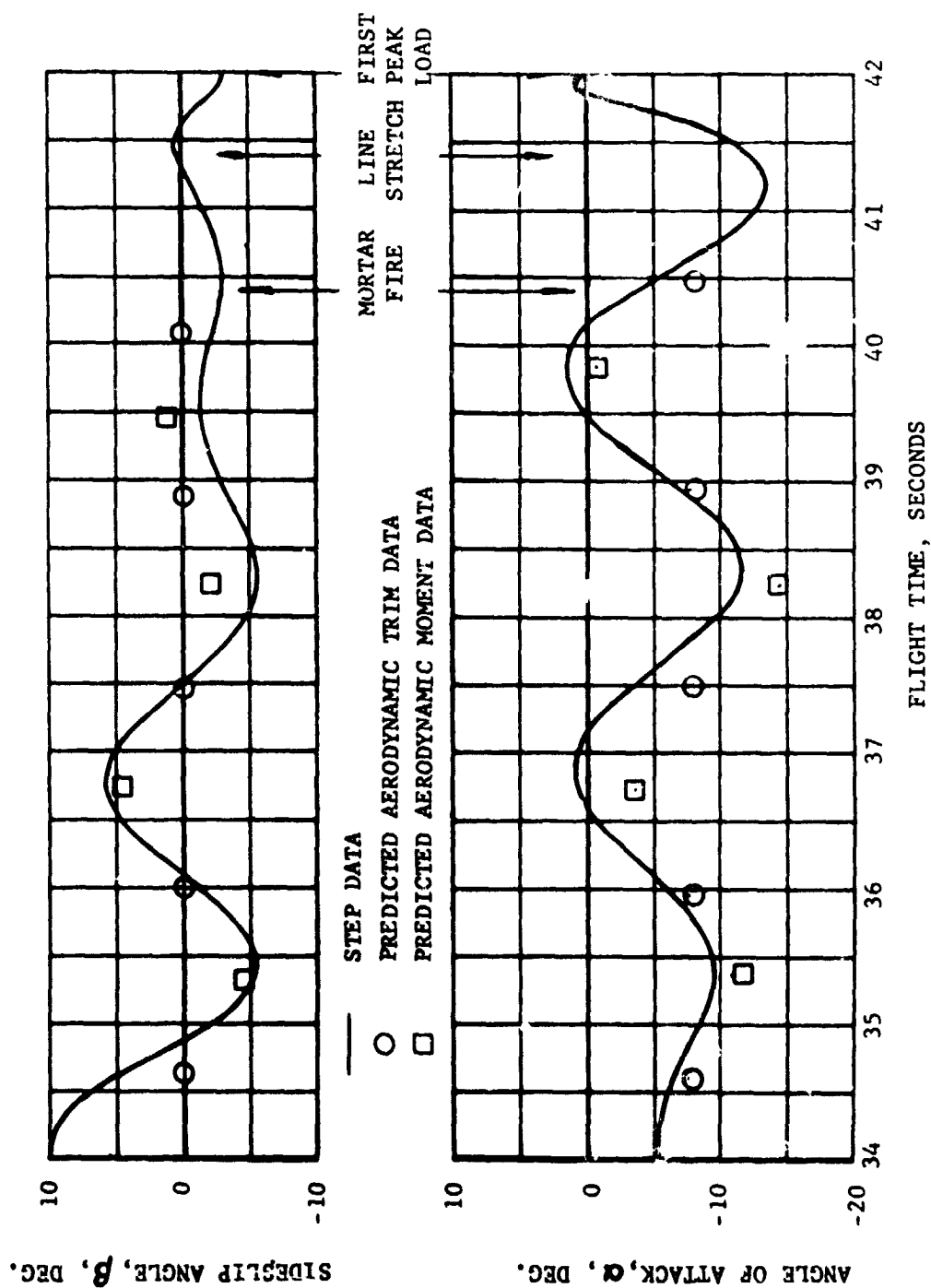
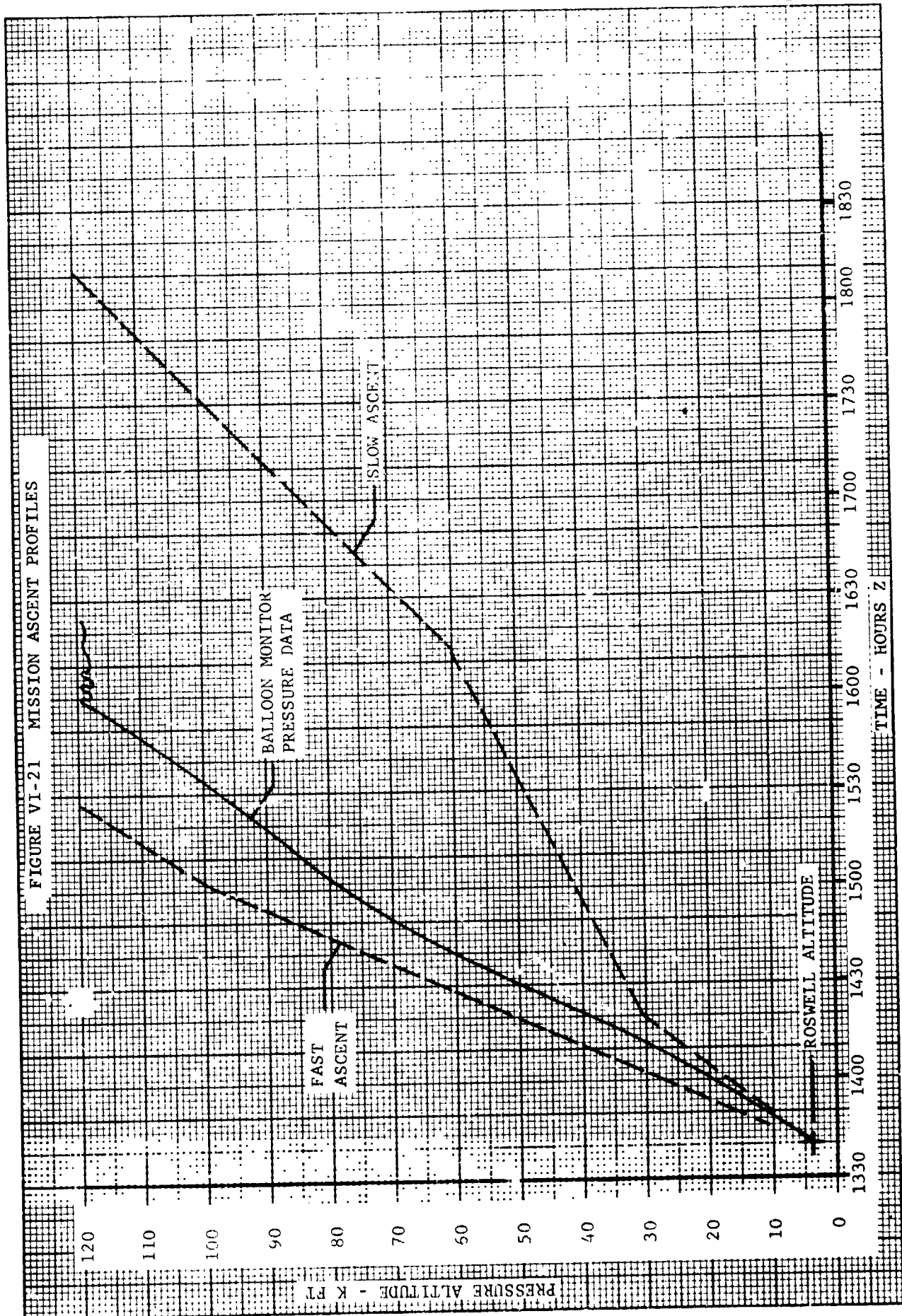


FIGURE VI-20 ANGLES OF ATTACK AND SIDESLIP AT PARACHUTE DEPLOYMENT

FIGURE VI-21 MISSION ASCENT PROFILES



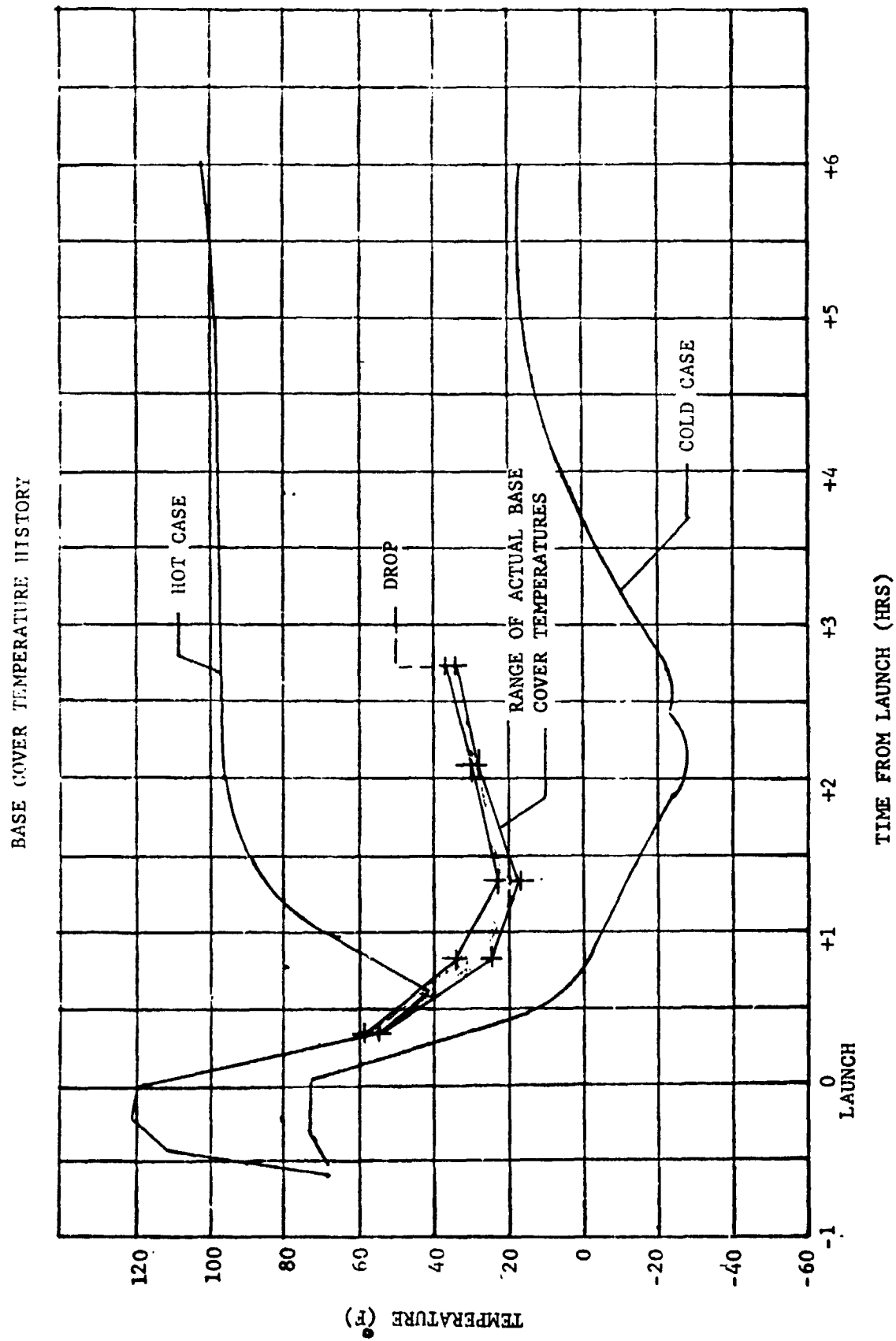
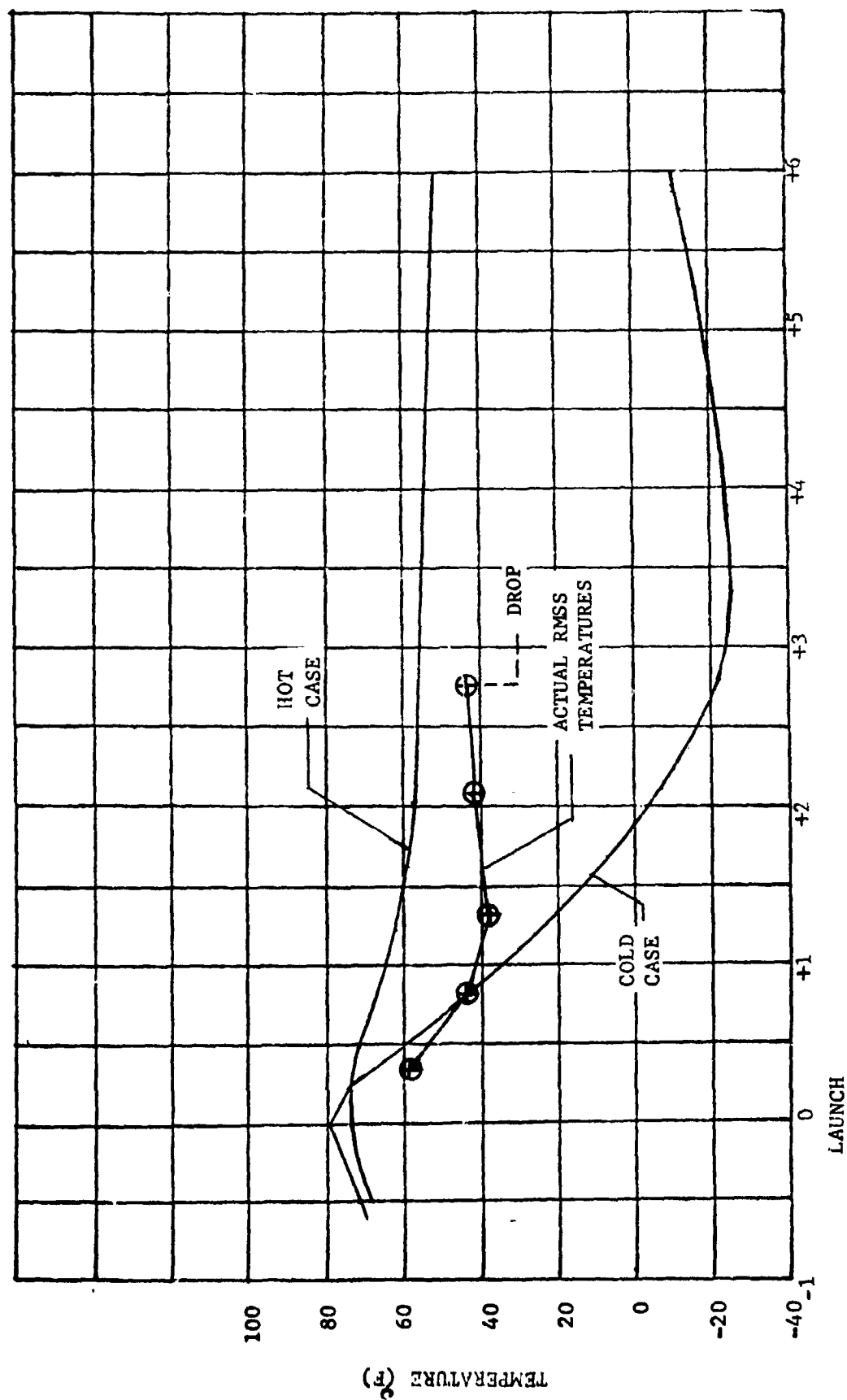


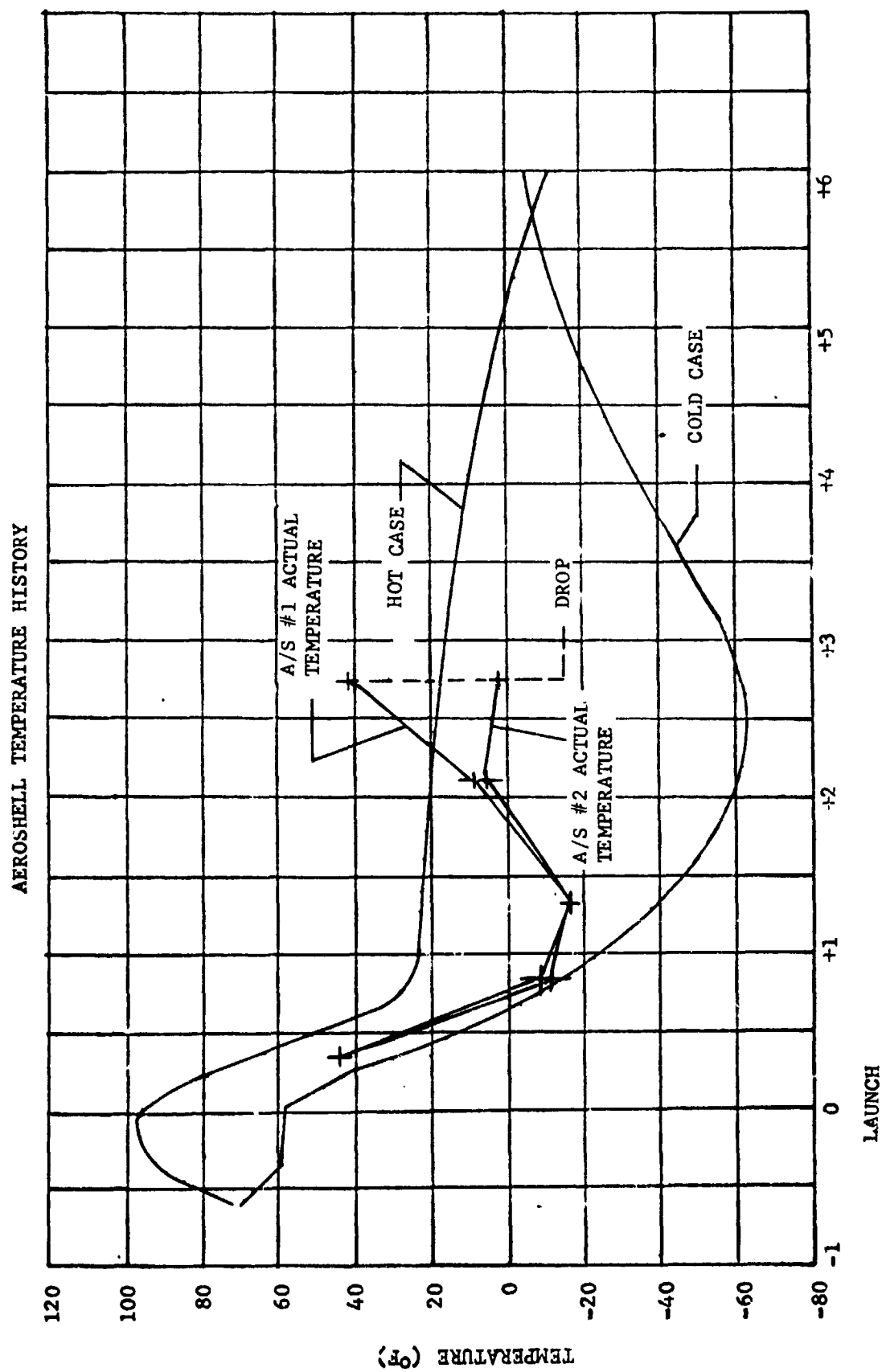
FIGURE VI-22

ROCKET MOTOR SUPPORT STRUCTURE TEMPERATURE HISTORY



TIME FROM LAUNCH (HRS)

FIGURE VI-23



TIME FROM LAUNCH (HRS)

FIGURE VI-24

S-BAND TRANSMITTER TEMPERATURE HISTORY

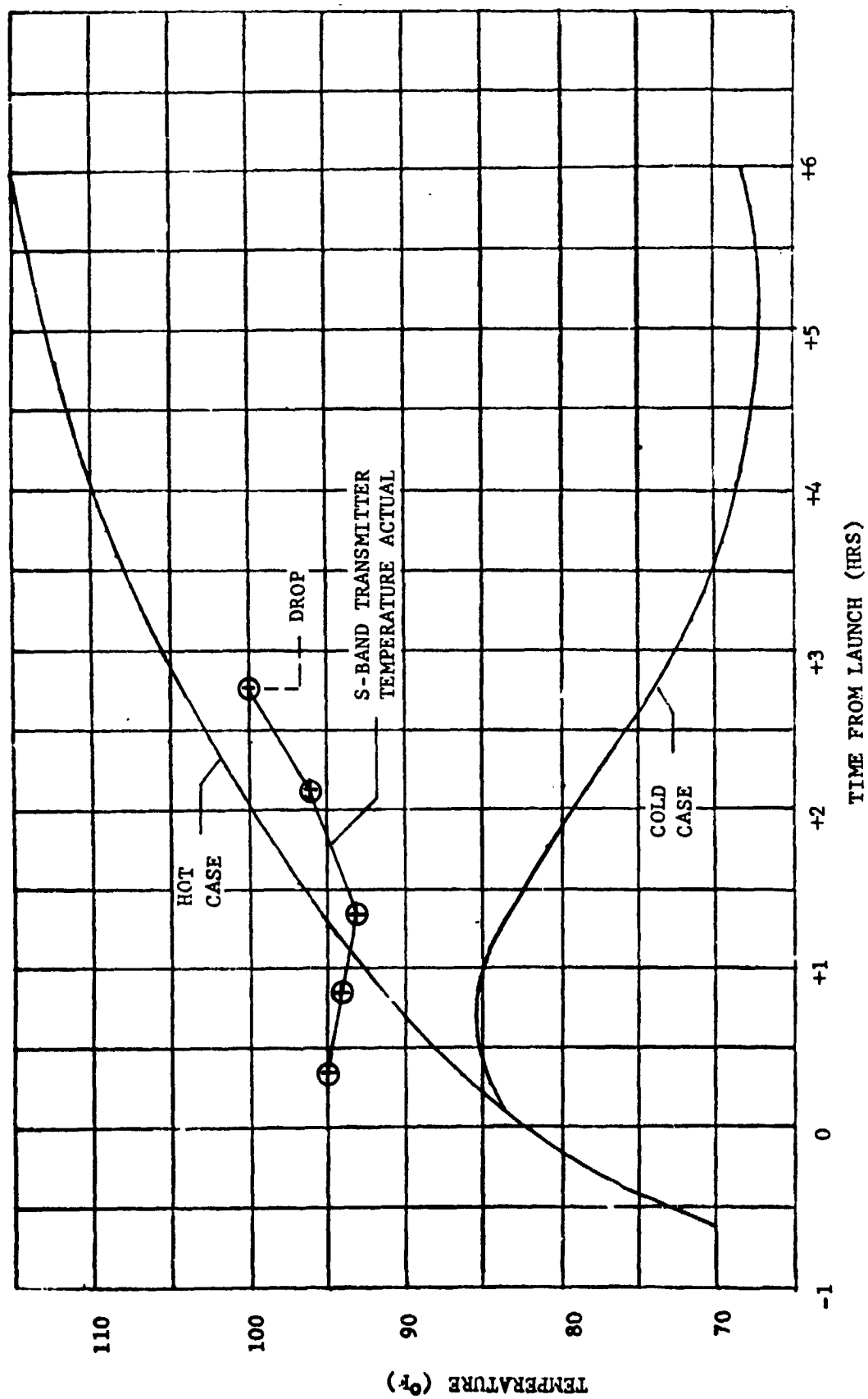


FIGURE VI-25

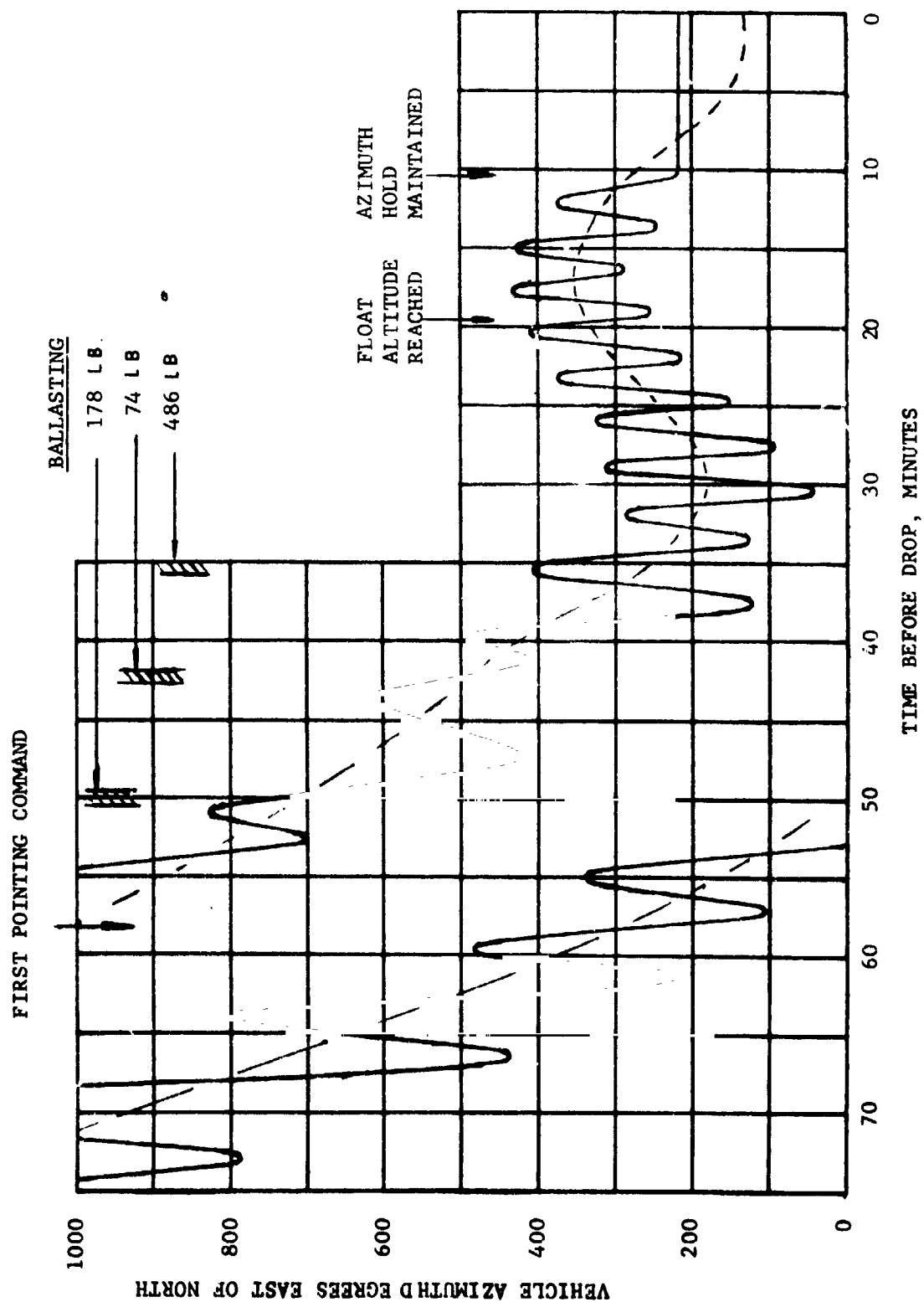


FIGURE VI-26 BLDT AV-4 VEHICLE AZIMUTH HEADING

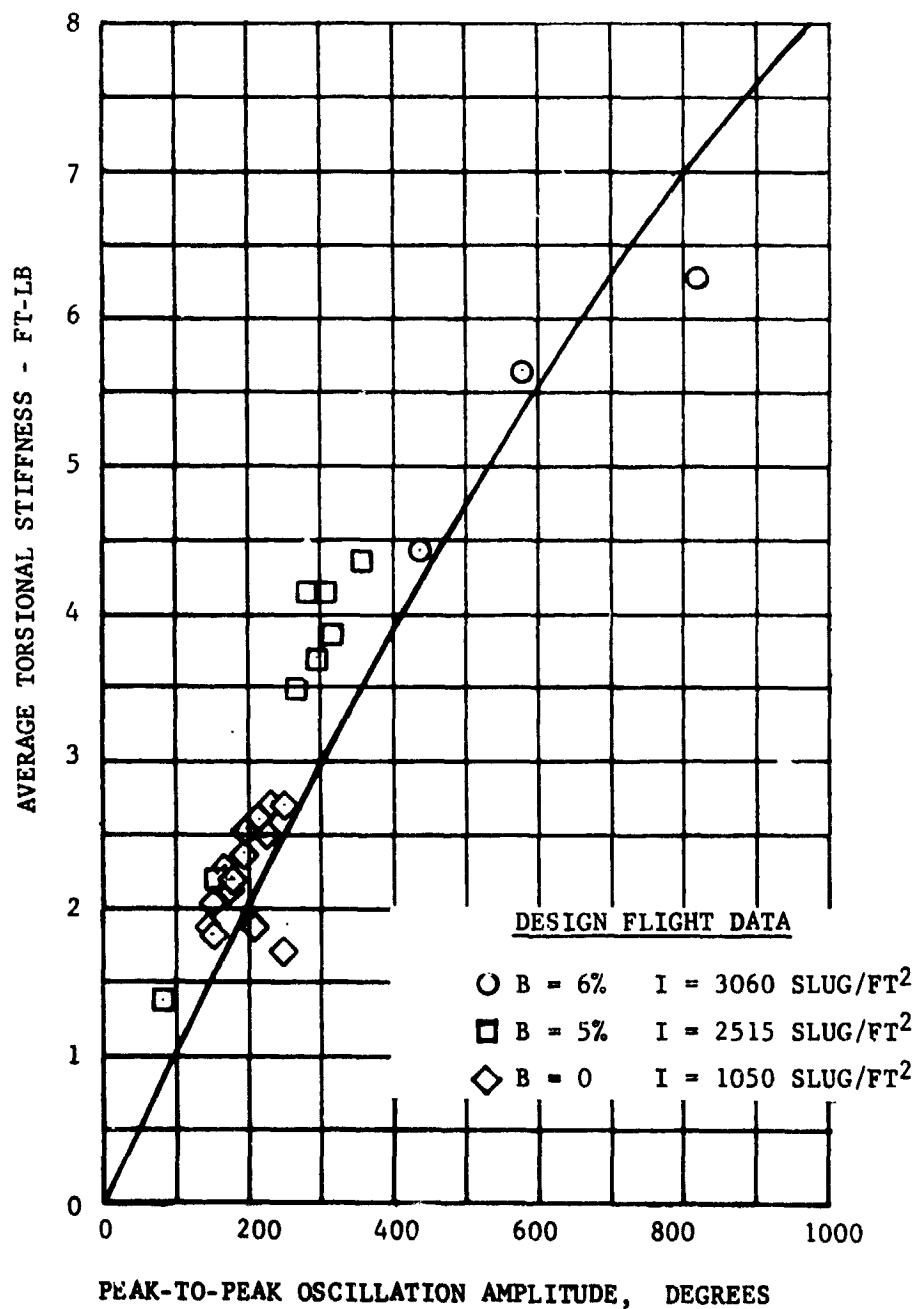


FIGURE VI-27 BLDT AV-4 TORSIONAL STIFFNESS

VII. CONCLUSIONS

The conclusions reached from the in-depth analysis of the AV-4 mission data and films are:

A. The flight of the vehicle was as programmed and within the predicted dispersions and tolerances.

B. The dynamic pressure conditions at mortar fire were slightly higher than predicted but within the tolerances required for the mortar fire command to have been issued by the ground computer based on dynamic pressure. The other BLDT requirements which were also met are:

Resultant Angle of Attack (DEG)	≤ 17
Residual Spin Rate (DEG/SEC)	≤ 100
Decelerator Temperature ($^{\circ}$ F)	≤ 80

C. The decelerator peak load occurred within the required Mach number/dynamic pressure performance box (See Figure II-1).

D. The mortar fire and decelerator peak load test conditions were within the bounds required for an acceptable case 2 supersonic qualification test.

E. The decelerator performed as predicted with no unusual damage. This constitutes successful qualification of the decelerator at the case 2 supersonic conditions.

F. The aeroshell separation function more than adequately met the requirement for 50 feet of separation distance in 3 seconds.

VIII. REFERENCES AND OTHER DATA SOURCESA. References

1. MMC RD-3720247, Parachute Test Objectives and Requirements for BLDT Program, Dated March 29, 1972.
2. MMC TR-3720052, Viking Vehicle Dynamics Data Book, Rev. F, July 6, 1972.
3. MMC TR-3720074, Volume I, Transonic Aerodynamic Characteristics and Pressure Distributions on 8 Percent Scale Models of the Viking Lander Capsule, Aeroshell and Lander plus Base Cover, February 1971.
4. MMC TR-37209014, Viking Aerodynamics Data Book, Rev. C, June 1972.
5. GAC GER 15215, Rev. A, Viking Decelerator Design Analysis Report, March 20, 1972.
6. NASA TND-5296, Inflation and Performance of Three Parachute Configurations from Supersonic Flight Tests in a low Density Environment, July 1969.
7. MMC TR-3720181, Scale Model Test Results of the Viking Parachute System at Mach Numbers from 1 through 2.6, November 1971.
8. MMC Memorandum 8943-72-116, Viking Parachute Swivel Loads and Pull-Off Angles from Dynamic Simulation, R. D. Moog, 10 May 1972.
9. NASA CR-1482, Statistical Trajectory Estimation Programs (STEP), Volumes I and II.
10. Users Guide No. 837L7041032, BLDT Six Degrees of Freedom Trajectory Program, dated February 1972.
11. TN-3770115, Aerothermodynamics Analysis of the BLDT Vehicle (CDR Configuration) dated July 1971.

B. Abbreviations

A/B	Airborne
AGC	Automatic Gain Control
A/S	Aeroshell
AV	BLDT Flight Vehicle Designator
BLDT	Balloon Launched Decelerator Test
B/U	Backup
Cg	Center of Gravity
CST	Combined System Test
CW	Clockwise
CCW	Counter Clockwise
DGB	Disk-Gap-Band
DEG	Degree
Deg/Sec	Degree/Second
fps	Feet per second
FRT	Flight Readiness Test
FT	Feet
GAC	Goodyear Aerospace Corporation
g's	Gravitational acceleration = 32.2 FPS^2
IRIG	Inter Range Instrumentation Group
K	1000
KHz	Kilohertz
LADT	Low Altitude Drop Test
MMC	Martin Marietta Corporation
NASA	National Aeronautics and Space Administration
NOP	North Oscura Peak
P	Roll Rate

PSF	Pounds per Square Foot
PSI	Pounds per Square Inch
PEPP	Planetary Entry Parachute Program
q	Dynamic Pressure
Q	Pitch Rate
R	Yaw Rate
RAOB	Radiosonde Observation Balloon
RF	Radio Frequency
RMSS	Rocket Motor Support Structure
RTDS	Real Time Data System
s	Aerodynamic Reference Area
SCO	Subcarrier Oscillation
S/N	Serial Number
STEP	Statistical Trajectory Estimation Program
T	Time
TDC	Telemetry Data Center
TM	Telemetry
VLC	Viking Lander Capsule
V	Time Rate of Change of Velocity
WSMR	White Sands Missile Range
Z,Zulu	Greenwich Mean Time

APPENDIX A

DESCRIPTION OF

BALLOON LAUNCHED DECELERATOR

TEST VEHICLE

APPENDIX A

DESCRIPTION OF BALLOON LAUNCHED DECELERATOR TEST VEHICLE

The BLDT Vehicle utilized for the high altitude qualification tests of the Viking Mars Lander Decelerator consisted of six (6) major subsystems which were:

- o Structural Subsystem
- o Electrical Subsystem
- o Instrumentation Subsystem
- o R. F. Subsystem
- o Propulsion/Pyrotechnic Subsystem
- o Thermal Control Subsystem

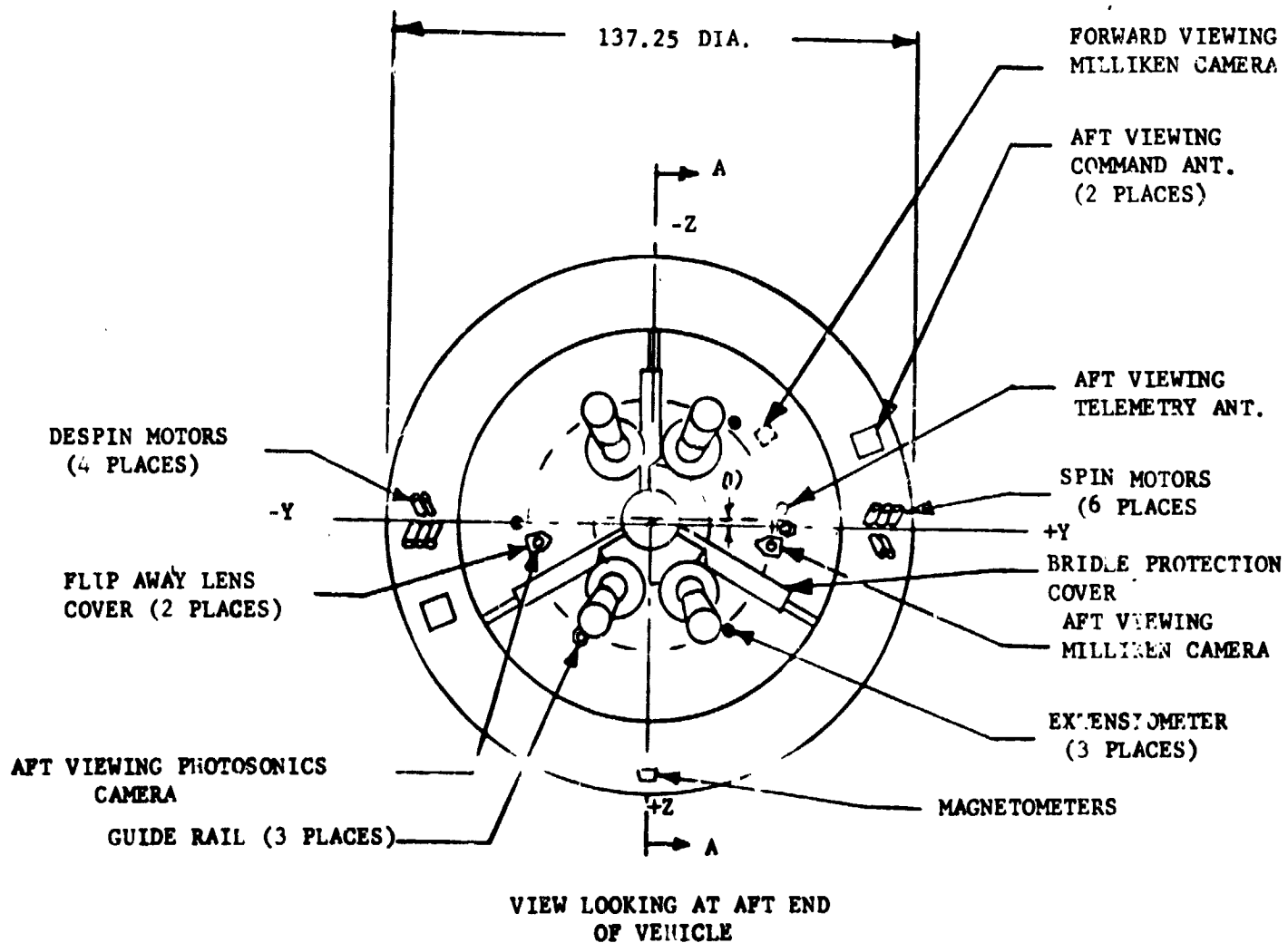
The BLDT vehicles are designed to be flown as supersonic, transonic and free fall vehicles in order to simulate the various anticipated Mars entry conditions for decelerator deployment.

A. Structural Subsystem

The vehicle structural configuration provides an external envelope which simulates the Viking Lander Capsule in order to qualify the Decelerator in the wake of a blunt body similar to the actual Mars VLC. The general configuration of the BLDT vehicle is shown in Figures A-1 through A-7.

At the initiation of the BLDT vehicle design, the test bed was to match the Mars VLC Cg and mass properties at decelerator deploy command. insofar as practical. The requirement was for the BLDT vehicle to have a weight of 1888 pounds with a Cg offset of 1.41 inches in the -Z direction at the time of decelerator mortar fire command. The final mass properties

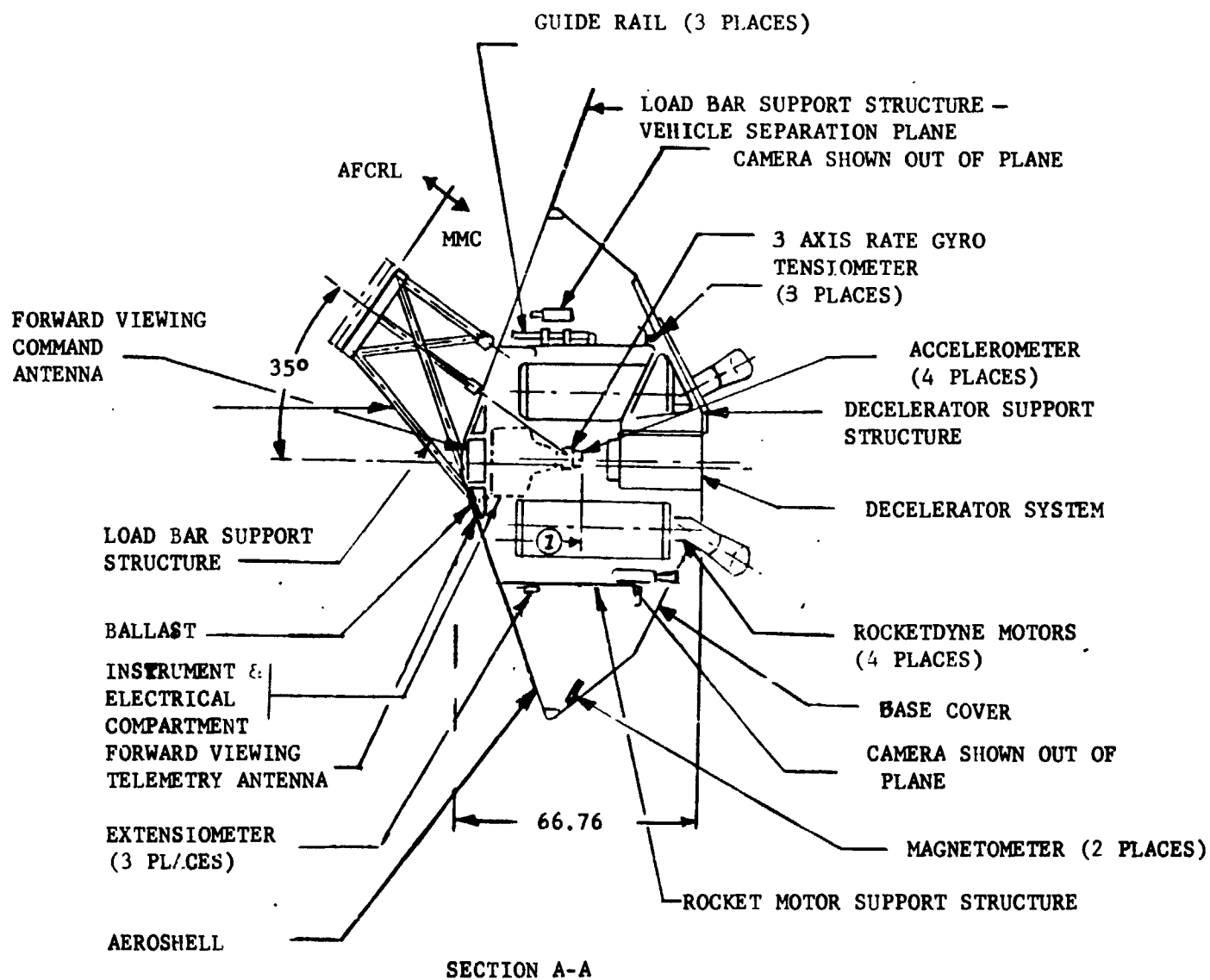
(1) -Z AXIS Cg OFFSET = $1.41'' \pm 0.030''$



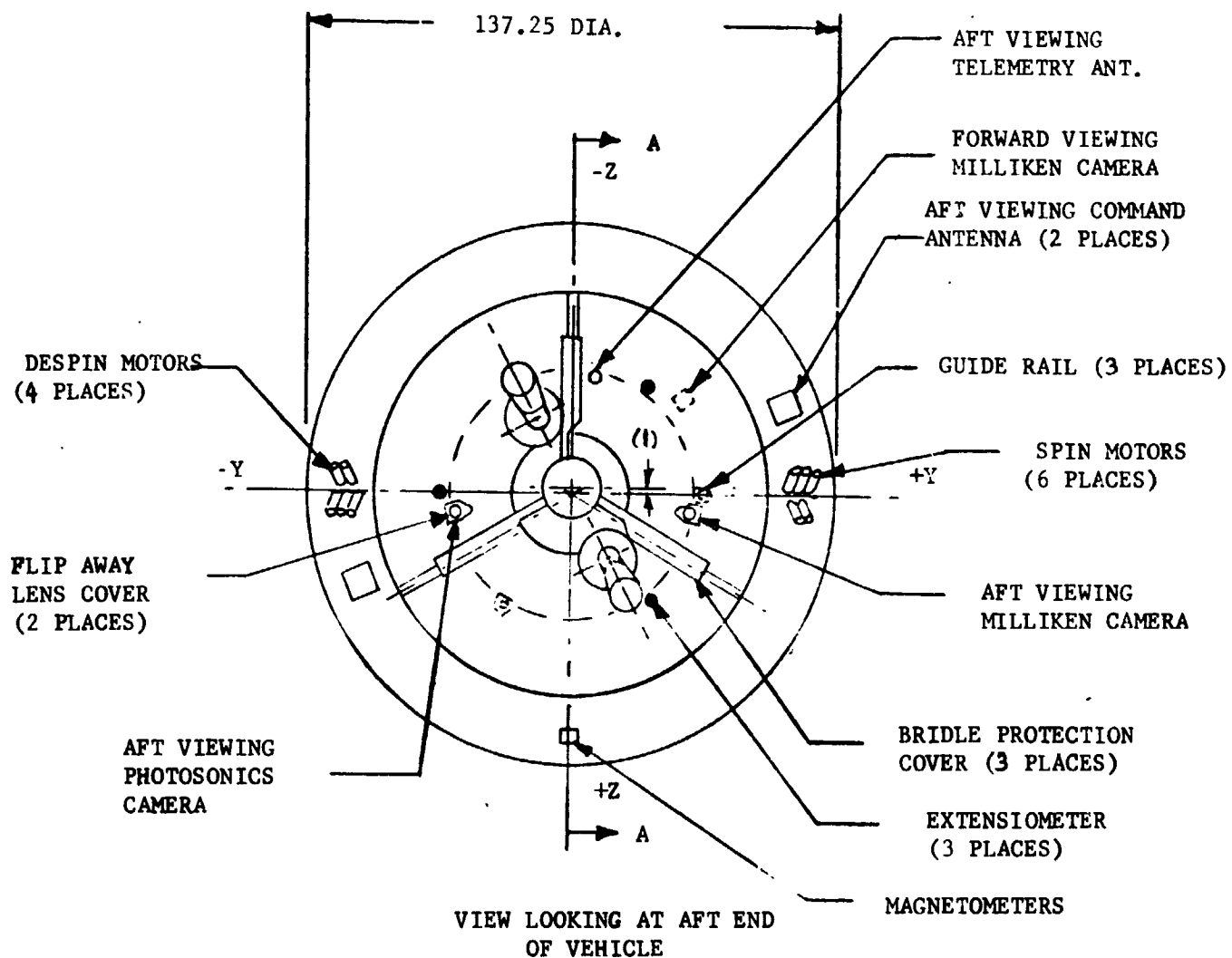
BLDT SUPERSONIC VEHICLE CONFIGURATION

FIGURE A-1

(1) X AXIS C_g AT MORTAR FIRE = 31.7" to 33.7"



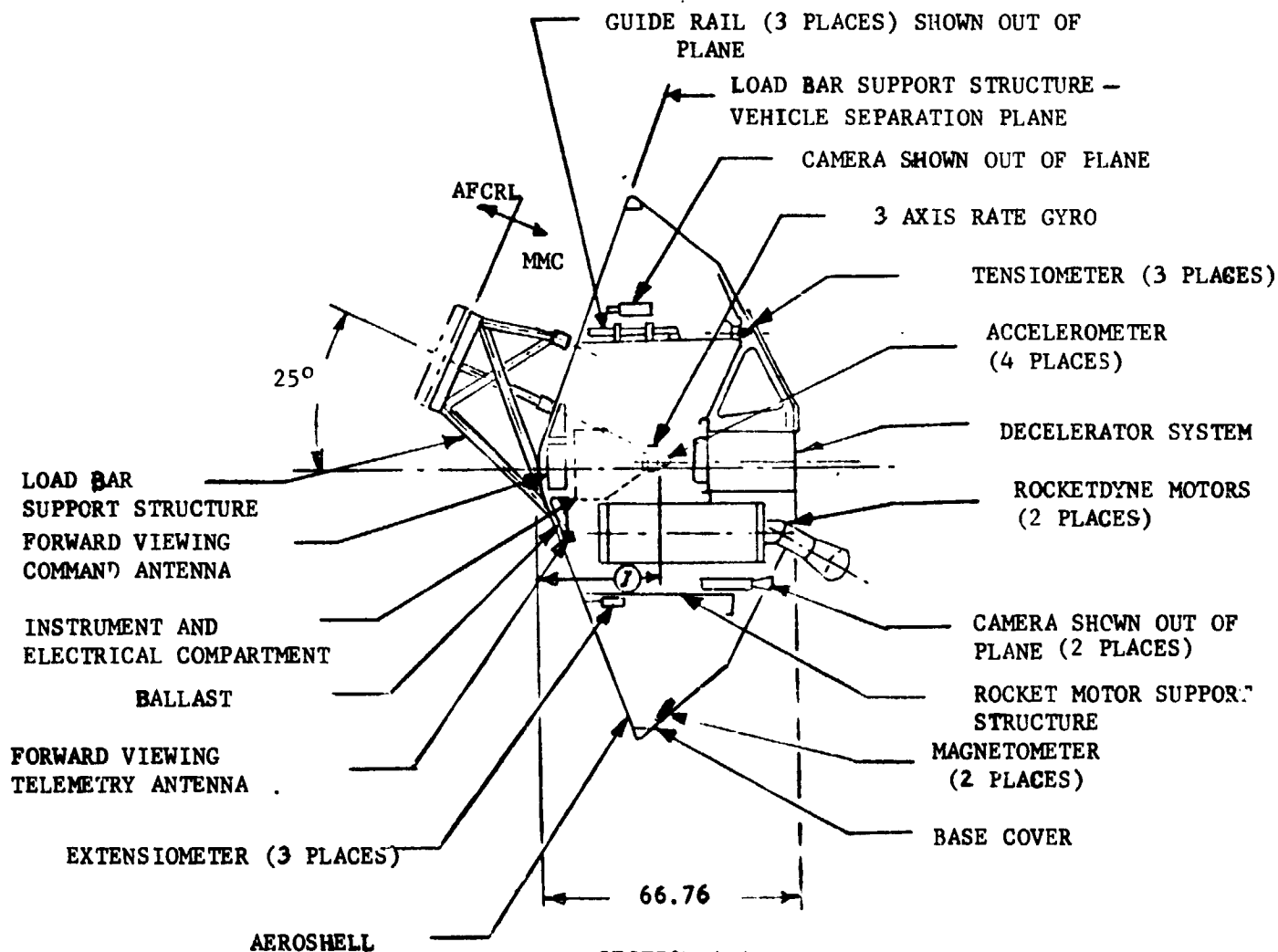
(1) -Z AXIS Cg OFFSET = 1.41" \pm C.030"



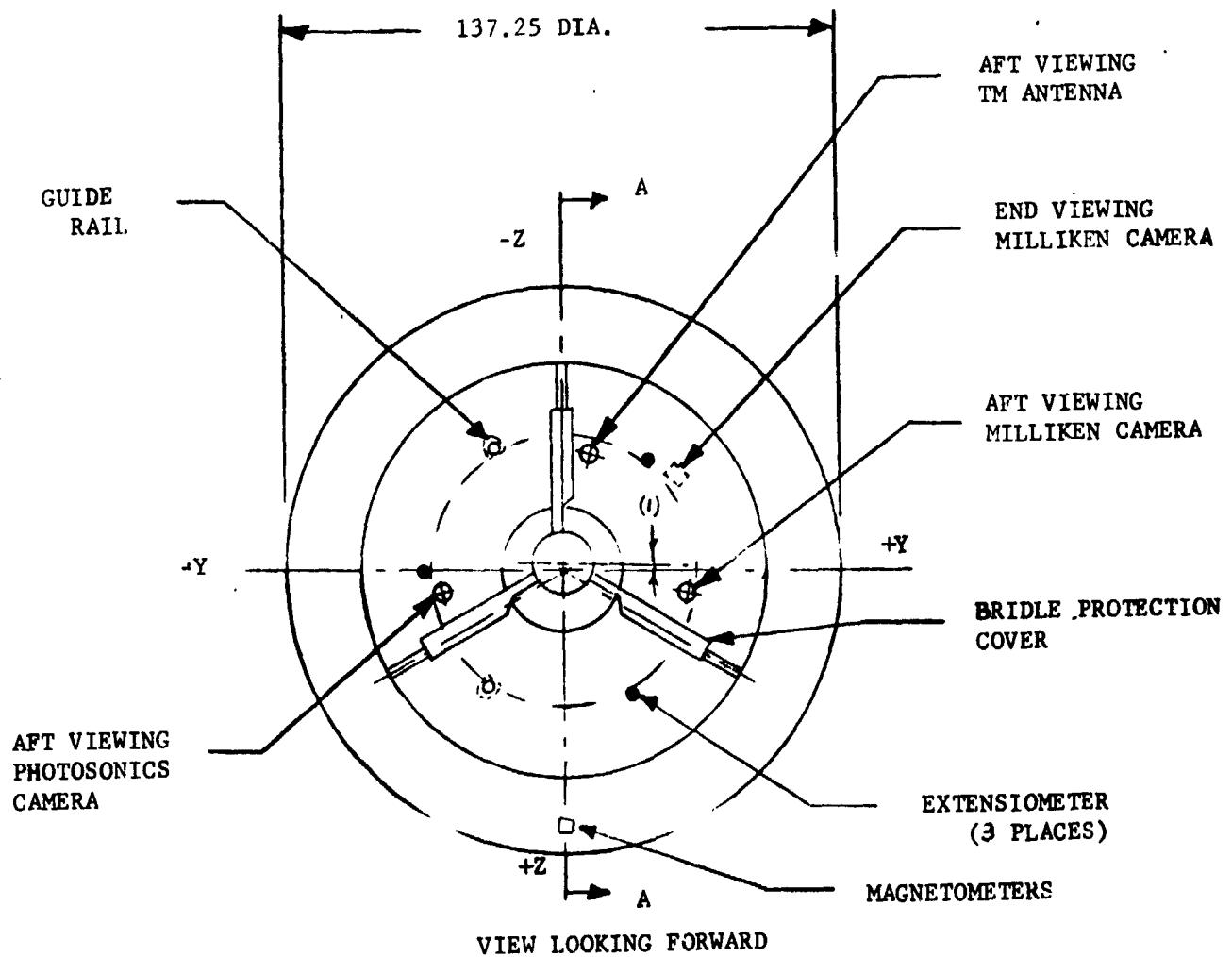
BLDT TRANSONIC VEHICLE CONFIGURATION

FIGURE A-3

(1) X AXIS C_g AT MORTAR FIRE = 31.7" to 33.7"



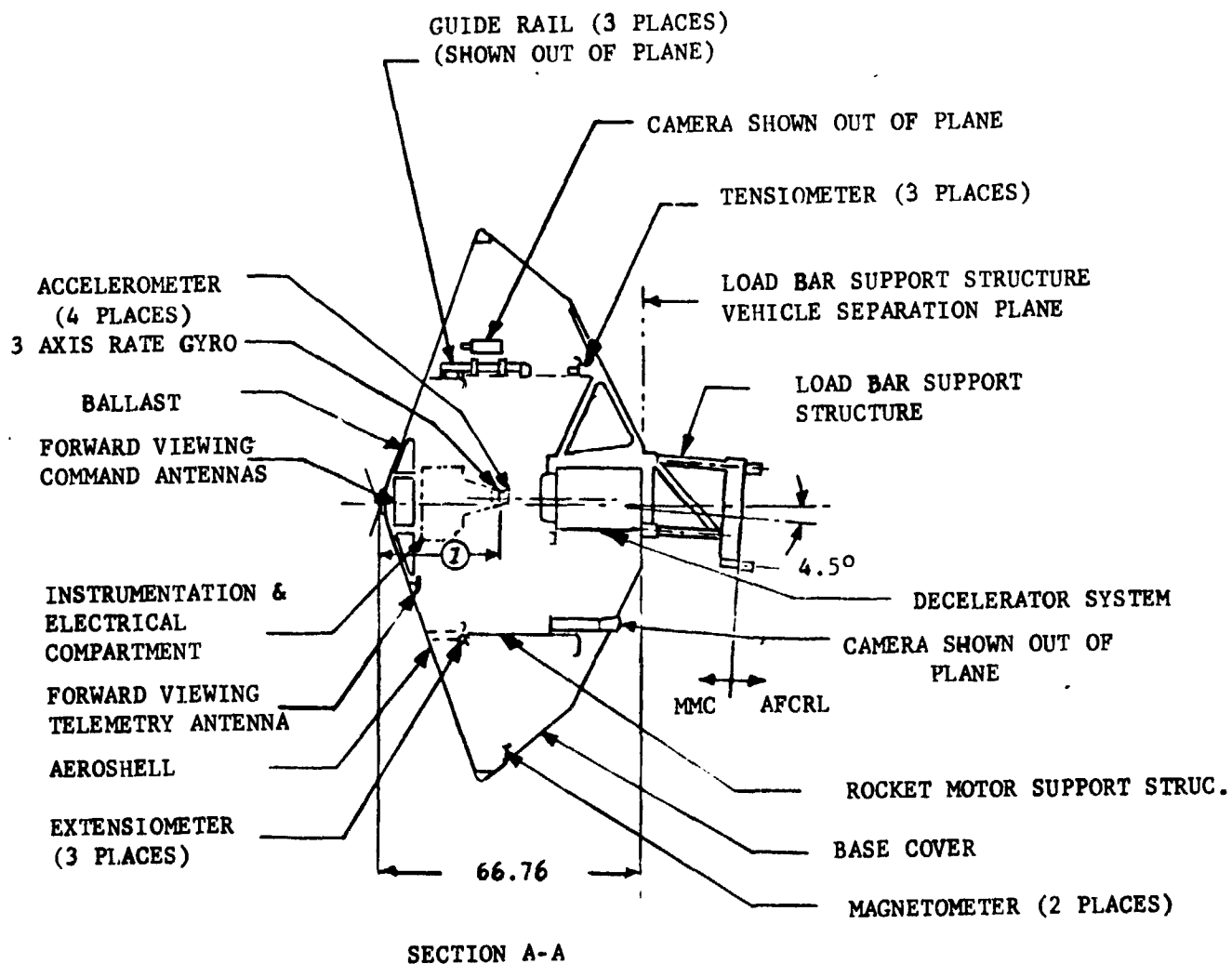
(1) -Z AXIS C_G OFFSET = 1.41" \pm 0.030"



BLDT SUBSONIC VEHICLE CONFIGURATION

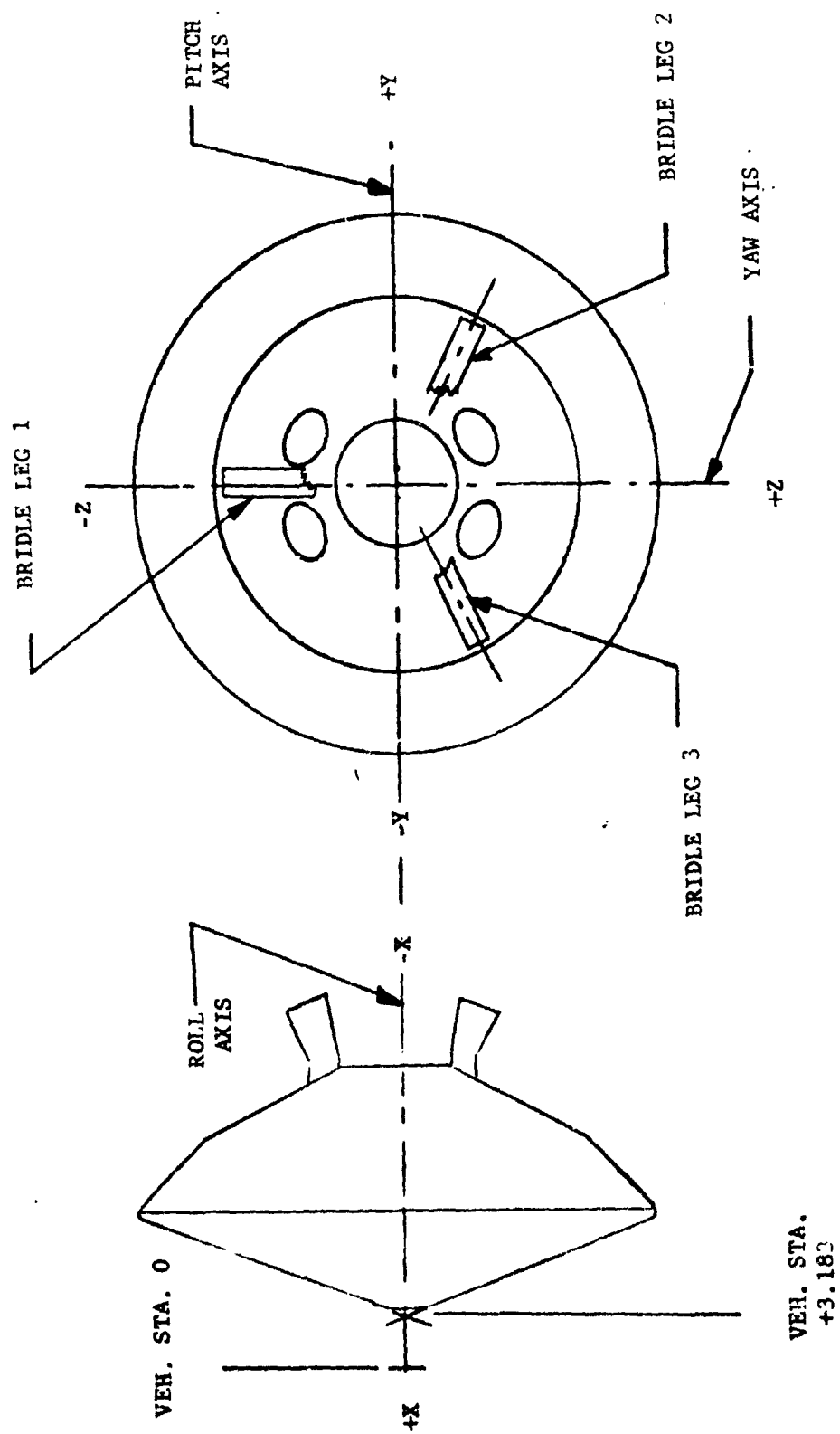
FIGURE A-5

(1) X AXIS C_g AT MORTAR FIRE = 31.7" to 33.7"



BLDT SUBSONIC VEHICLE CONFIGURATION

FIGURE A-6



A-9

BLDT COORDINATE SYSTEM
FIGURE A-7

for each vehicle, included in the individual reports, indicates the revisions which were made to the mass properties subsequent to the BLDT vehicle design.

The structural subsystem consisted of six (6) major components as follows:

1. Rocket Motor Support Structure

The rocket motor support structure is a cylindrical component, approximately 64 inches in diameter, which provides the major vehicle internal longitudinal support structure as well as providing the motor mounts for the supersonic and transonic vehicles.

2. Instrument Beam

The instrument beam is a structural beam which was tied to the forward surface of the RMSS and ran symmetrically along the Y, -Y axis. It also contained an aft facing pylon to mount the accelerometers and rate gyros at or near the vehicle longitudinal Cg.

3. Base Cover

The base cover is a lightweight external shell providing an aft configuration similar to the Mars VLC.

4. Decelerator Support Structure

The decelerator support structure is a three leg structure, similar to the Mars VLC decelerator support structure, with a cylindrical center section for mounting of the decelerator cannister parallel to the BLDT longitudinal centerline. The decelerator support structure assembled into the base cover to provide an intermediate assembly.

5. Aeroshell

The Aeroshell which is the forward surface of the vehicle provides a conical blunt aerodynamic surface approximately 11.5 feet in diameter with a 140° included angle. The aeroshell provides a forward configuration similar to the Mars VLC.

6. Load Bar Support Structure

The load bar support structure is a tubular structural member which provides the interface with the Air Force Cambridge Research Laboratory (balloon) load bar as well as providing the correct hanging pitch attitude.

B. Electrical Subsystem

The electrical subsystem provides the flight power, cabling and switching/sequencing devices required to properly sequence and activate the various functions. The electrical subsystem is shown schematically in Figure A-8.

The vehicle is powered by five (5) silver zinc batteries as follows:

1. Main Battery - 60 AH - MMC P/W PD94S0026

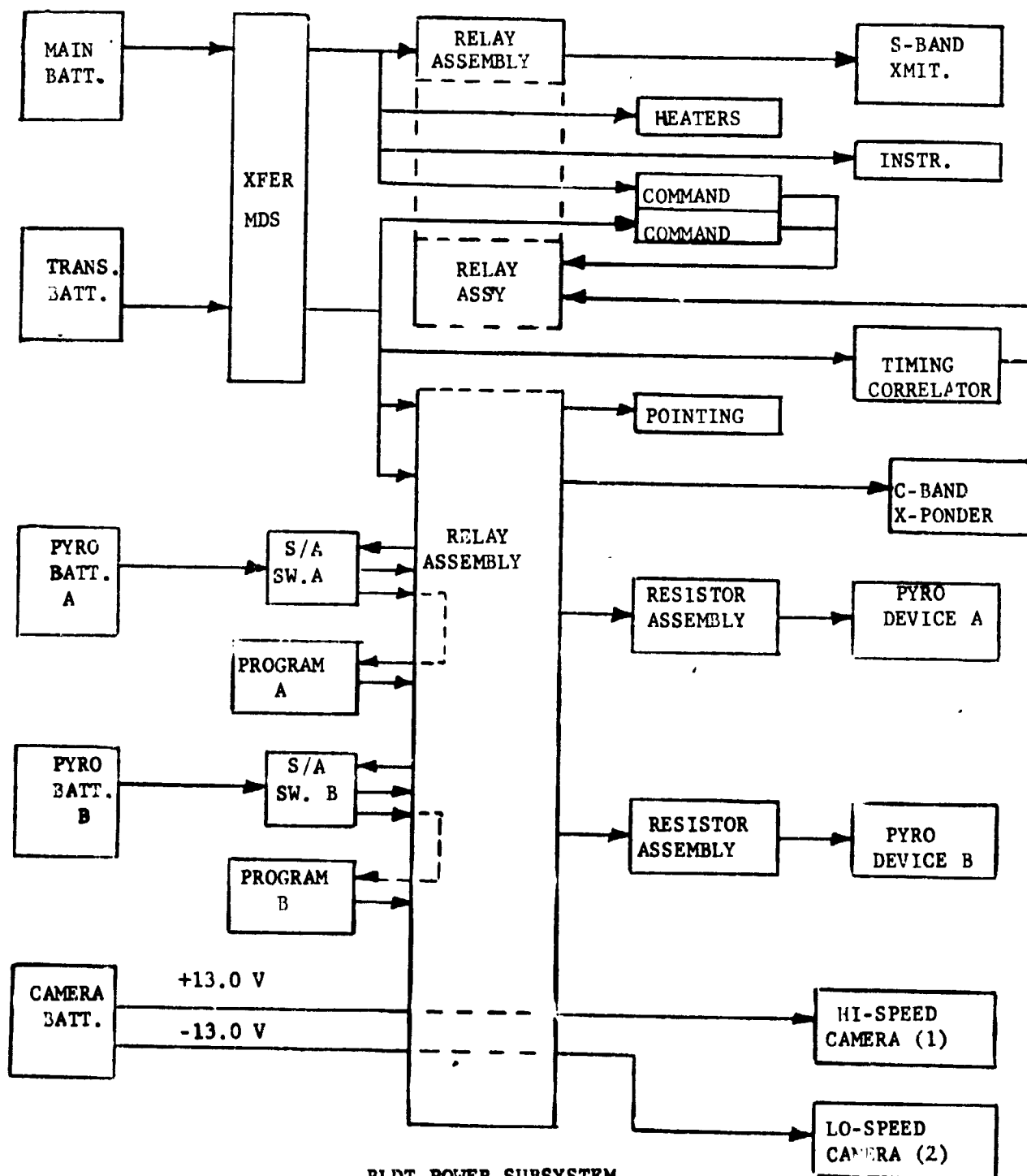
Provides power for telemetry, command system A and A/B heaters.

2. Transient Battery - 16 AH Engle Pitcher Model 4332

Provides power for timing correlator, C-band transponder and command system B.

3. Pyro Battery A - 1.0 AH - ESB Model 392

Provides power to all pyro A circuit ordnance devices and airborne programmer A.



BLDT POWER SUBSYSTEM

BLOCK DIAGRAM

FIGURE A-8

4. Pyro Battery B - 1.0 AH - ESB Model 392

Provides power to all Pyro B circuit ordnance devices and airborne programmer B.

5. Camera Battery - 1.0 AH - ESB Model 393 (Similar to model 392 except tapped at 9 cells and 18 cells).

Provide +13 volts power to onboard high speed cameras.

The electrical subsystem provides completely redundant airborne sequencing programmers and completely redundant pyrotechnic circuits.

In addition, the electrical subsystem provides all power switching relays, motor driven switches, power limiting resistors and airborne heaters.

C. Instrumentation Subsystem

The BLDT Instrumentation subsystem provides for the real time measurement and conditioning of the parameters listed in Table A-1 and provides timing correlation for the real time measurements and airborne camera. The instrumentation subsystem utilizes a PAM/FM/FM configuration as shown schematically in Figure A-9.

Additionally, the instrumentation subsystem provides the following photographic coverage:

1. Aft Looking Photosonics

Approximately 450 frames/second to record the decelerator deployment sequence.

2. Aft Looking Milliken

Sixty-four frames/second to record the decelerator deployment sequence.

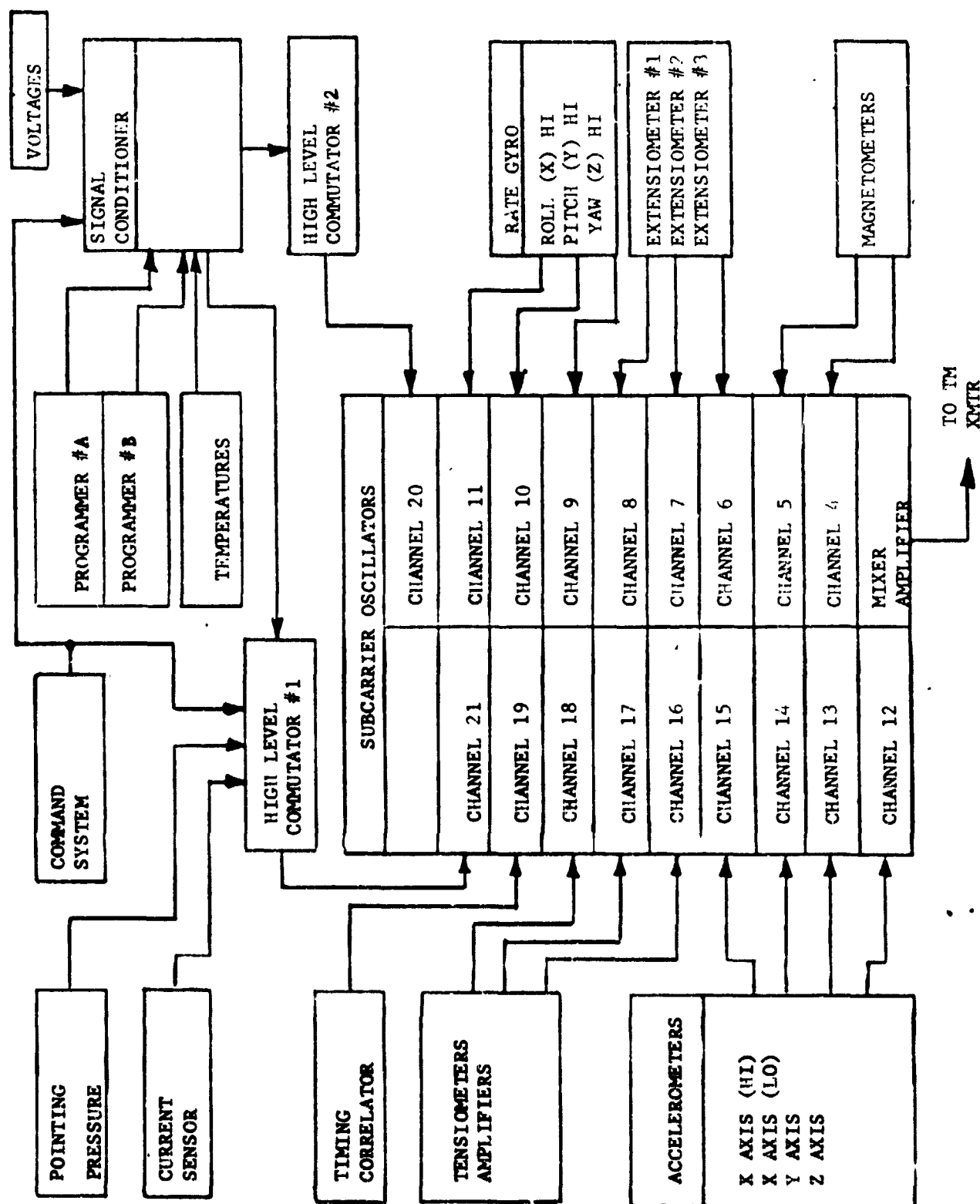


FIGURE A-9 BLDT INSTRUMENTATION SYSTEM

3. Forward Looking Milliken

Thirty-two frames/second to record the Aeroshell separation sequence and obtain a time/distance history.

D. R. F. Subsystem

The R. F. Subsystem consists of the TM transmitter, the C-Band transponder and the redundant command receiver/decoders with all of the required antenna systems.

1. TM Transmitter

The telemetry transmitter provides for the FM transmission of the composite FM data from the Instrumentation Subsystem mixer amplifier. The transmitter provides 5 watts power output in the S-Band (2285.5 MHz) range. The TM transmitter and antenna system is shown schematically in Figure A-10.

2. C-Band Tracking Transponder

The GFE tracking transponder was provided by White Sands Missile Range and is compatible with tracking radar AN/FPS-16 utilized at WSMR. The transponder and antenna system is shown schematically in Figure A-10.

3. Command Receiver/Decoder

The vehicle command system, including antenna, multicoupler, receivers and decoders, is shown schematically in Figure A-11.

The redundant receiver/decoders operate on an assigned frequency of 541 MHz and provide a 28 volt nominal decoder output for command inputs with seven command tones selected from IRIG-103-61 channels 1 through 20.

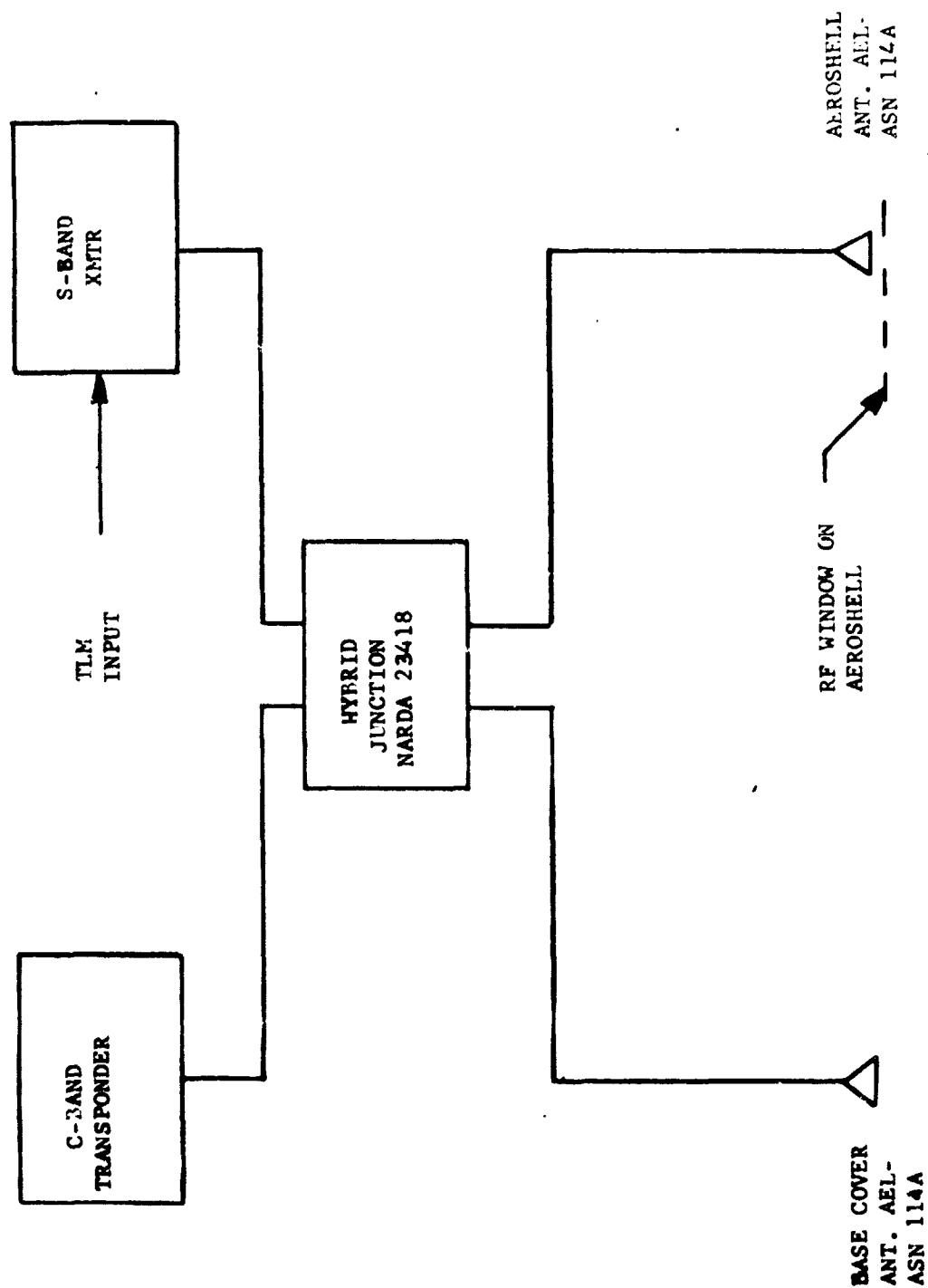
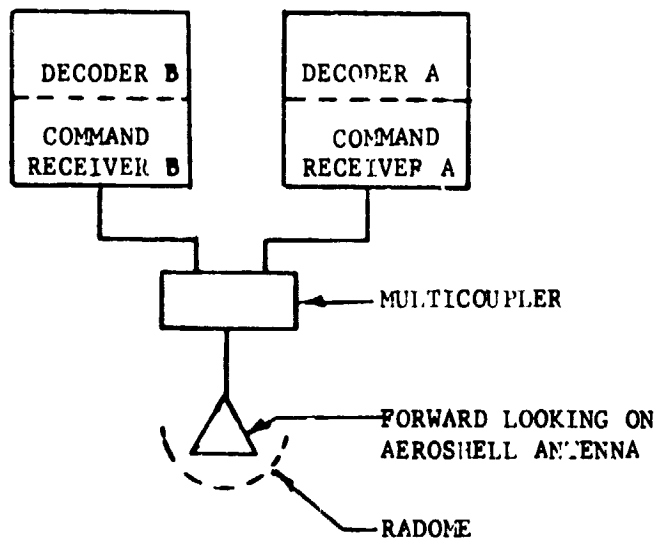
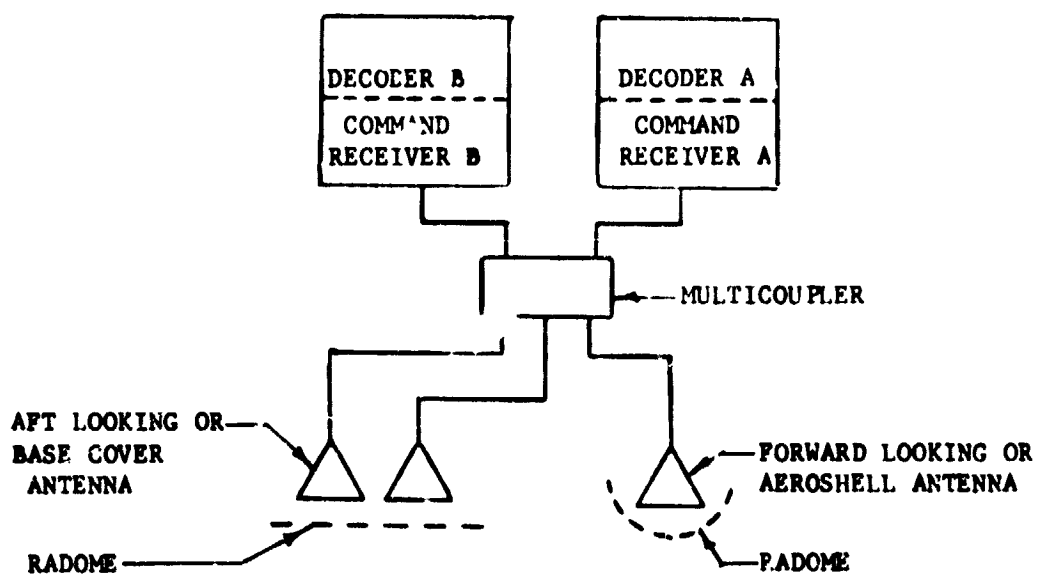


FIGURE A-10 TRACKING & TELEMETRY ANTENNA SYSTEM



SUBSONIC CONFIGURATION



SUPERSONIC AND TRANSONIC CONFIGURATION

FIGURE A-11

The system coding is such that triple tone ground commands result in the following airborne functions:

<u>Function</u>	<u>Commands</u>		
	<u>Primary</u>	<u>Backup</u>	<u>Redundant</u>
Release from load bar	X		X
Mortar Fire	X		X
Arm Ordnance Bus	X		X
Safe Ordnance Bus	X	X	
Turn RF on	X		
Turn RF off	X		
Pointing, Clockwise	X	X	
Pointing, Counterclockwise	X	X	

E. Propulsion/Pyrotechnic Subsystem

The propulsion/pyrotechnic subsystem consists of the solid rocket motors required on the supersonic and transonic vehicles, the azimuth pointing system required on the supersonic and transonic vehicles and the pyrotechnic devices required on all three configurations.

The main propulsion assembly consists of a set of Rocketdyne RS-B-535 solid propellant rocket motors each having the following characteristics:

	<u>Nominal</u>	<u>3 σ Variation</u>
Total Impulse, lbf-sec	Classified	0.6%
Burn Time Avg. Thrust, lbf	Classified	1.9%
Nozzle Cant Angle, deg	35	0.1
Thrust Vector Alignment, deg**		0.2
Ignition Interval, msec	49	+27, -17
Burn Time, sec	Classified	1.8%
Loaded Weight, lbm	461.2	0.25***
Burnout Weight, lbm	91.7	3.7****

The supersonic configuration vehicles are provided with 4 of the above motors with the transonic vehicle containing 2.

The spin/despin system is required to reduce trajectory dispersions during booster burn and despin after burnout. Spin Motors having the following characteristics are used:

	<u>Nominal*</u>	<u>3 σ Variation</u>
Total Impulse, lbf-sec	76.5	3.0%
Burn Time Avg. Thrust, lbf	86.2	8.0%
Ignition Interval, msec	10.0	+10.0, -5.0
Burn Time, sec	0.8/	+11.0%
Loaded Weight, lbm	1.2	0.1
Burnout Weight, lbm	0.9	0.1

- * Vacuum Conditions, 70°F
- ** Alignment with respect to nozzle geometric centerline.
- *** Actual weighing tolerance.
- **** Variation from predicted value.

The supersonic and transonic vehicles utilized 6 each of the above motors for spin-up and 4 each of the above for despin.

Other pyromechanical and pyrotechnic functions included in the vehicle are:

<u>Function</u>	<u>Supersonic</u>	<u>Transonic</u>	<u>Subsonic</u>
Aeroshell Sep. Nuts	3	3	3
Load Bar Release Nuts	0	0	3
Tension Rod Separator	1	1	0
Cable Cutters	2	2	0
Decelerator Mortar*	1	1	1

* Part of Decelerator System

Also included in the propulsion subsystem is an azimuth pointing system which is used to orient the supersonic and transonic vehicle azimuth at drop in order to assure impact within the White Sands Missile Range in the event of a complete decelerator failure.

The pointing system is comprised of a gaseous nitrogen thruster system located on the balloon load bar. The system provides paired clockwise or counterclockwise rotational moments in response to ground commands. The azimuth pointing system is shown schematically in Figure A-12.

F. Thermal Control Subsystem

The thermal control subsystem consists of those passive and active components required to maintain vehicle components within the required temperature levels. These components were generally:

1. Internal and external blankets,
2. Active heaters,
3. Base cover ablative material.

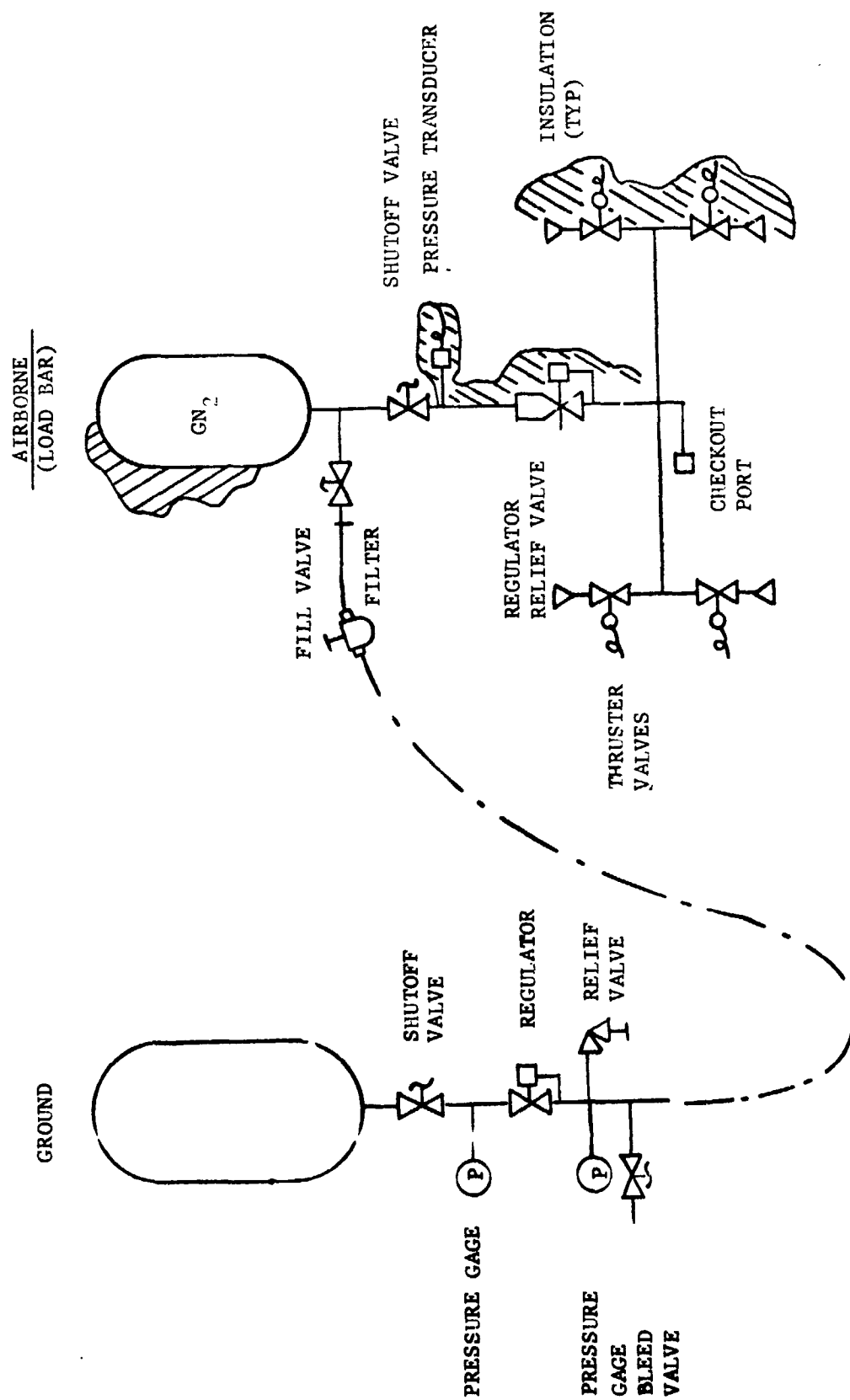


FIGURE A-12 BLDT POINTING SYSTEM

TABLE A-1

BLDT Telemetry Measurement List

No.	Measurement	Range	Accuracy End-to-End	Resolution	Response	Remarks
1	Accel. X Axis	-2, +5g * -2, +3g **	5%	0.07g 0.05g	100 Hz	Low Range
2	Accel. X Axis	-15, 1g * -7, +1g **	5%	0.16g 0.08g	100 Hz	High Range
3	Accel. Y Axis	+1.0g	5%	0.01g	100 Hz	
4	Accel. Z Axis	+1.0g	5%	0.01g	100 Hz	
5	Heading	360 deg.	±5 deg.	1 deg.	5 Hz	Magnetometer No. 1
6	Heading	360 deg.	±5 deg.	1 deg.	5 Hz	Magnetometer No. 2
7	Rate Gyro, X Axis	±300°/sec.	5%	3.0°/sec	20 Hz	
8	Rate Gyro, Y Axis	±300°/sec.	5%	3.0°/sec	20 Hz	
9	Rate Gyro, Z Axis	±300°/sec.	5%	3.0°/sec	20 Hz	
10	Strain Link	0 to 12,000 lbs. ***	5%	120 lbs.	100 Hz	Parachute Linkage No. 1

* Supersonic Flight

** Transonic and Subsonic Flight

*** Amplifier will be adjusted to read 18,000 pounds full scale for supersonic flight only.

TABLE A-1 (CONTINUED)
BLDT Telemetry Measurement List

No.	Measurement	Range	Accuracy End-to-End	Resolution	Response	Remarks
11	Strain Link	0 to 12,000 lbs. *	5%	120 lbs.	100 Hz	Parachute Linkage No. 2
12	Strain Link	0 to 12,000 lbs. *	5%	120 lbs.	100 Hz	Parachute Linkage No. 3
13	Timing Pulse	25 PPS, 0 to 1.25 VDC	1%	ON/OFF	125 Hz	Camera Correlation
14	Temperature	+25 to +150°F	5%	1.5F	10 Hz	Mortar Breech, Temp. Commuted at 30 SPS
15	Voltage	5 VDC	5%	0.05 VDC	10 Hz	Commutator #1 Full Scale Calibration at 30 SPS
16	Voltage	0 VDC	5%	0.05 VDC	10 Hz	Commutator #1 Zero Scale Calibration at 30 SPS
17	Voltage	0 to 36 VDC	5%	0.36 VDC	10 Hz	Main Battery, Commuted at 30 SPS
18	Current	0 to 16A	5%	0.16 A	10 Hz	Main Battery, Commuted at 30 SPS
19	Voltage	0 to 37 VDC	5%	0.37 VDC	10 Hz	Pyro Battery A Commuted at 30 SPS
20	Event, Cont.	0 to 14 VDC Step Change	± 50ms	(HI/LO)	10 Hz	Prog. A Reset Commuted at 30 SPS

* Amplifier will be adjusted to read 18,000 pounds full scale for supersonic flight only.

TABLE A-1 (CONTINUED)
BLDT Telemetry Measurement List

No.	Measurement	Range	Accuracy End-to-End	Resolution	Response	Remarks
21	Event, Pulse	0 to 14 VDC 0.1 sec Duration	+ 50 ms	(ON/OFF)	10 Hz	Prog. A TM Chan. Commuted at 30 SPS
22	Event, Pulse	0 to 14 VDC 0.1 sec Duration	+ 50 ms	(ON/OFF)	10 Hz	Prog. B TM Chan. Commuted at 30 SPS
23	Event, Cont.	0 to 4 VDC Step Change	+ 50 ms	(HI/LO)	10 Hz	CW Point. Valve Signal Commuted at 30 SPS
24	Event, Cont.	0 to 4 VDC Step Change	+ 50 ms	(HI/LO)	10 Hz	CCW Point. Valve Signal Commuted at 30 SPS
25	Event, Cont.	0 to 4 VDC Step Change	+ 50 ms	(HI/LO)	10 Hz	Safe/Arm Sw. A Arm Position Comm. at 30 SPS
26	Event, Cont.	0 to 4 VDC Step Change	+ 50 ms	(HI/LO)	10 Hz	Safe/Arm Sw. A Safe Position Comm. at 30 SPS
27	Pressure	0-2500 psia	5%	25 psi	10 Hz	Pointing system, Pressure Commuted at 30 SPS
28	Extensometer	0 to 12"	5%	0.12"	5 Hz	#1 Aeroshell Sep. Dist.
29	Extensometer	0 to 12"	5%	0.12"	5 Hz	#2 Aeroshell Sep. Dist.
30	Extensometer	0 to 12"	5%	0.12"	5 Hz	#3 Aeroshell Sep. Dist.
31	Voltage	0 to 37 VDC	5%	0.37 VDC	10 Hz	Pyro Battery B Commuted at 30 SPS
32	Voltage	0 to 33.5 VDC	5%	0.33	10 Hz	Transient Battery Commuted at 30 SPS

TABLE A-1 (CONTINUED)

BLDT Telemetry Measurement List

No.	Measurement	Range	Accuracy End-to-End	Resolution	Response	Remarks
33	Event, Cont.	0 to 4 VDC Step Change	± 50 ms	(HI/LO)	10 Hz	Safe/Arm Sw. B. Arm Position Comm. at 30 SPS
34	Event, Cont.	0 to 4 VDC Step Change	± 50 ms	(HI/LO)	10 Hz	Safe/Arm Sw. B Safe Position Comm. at 30 SPS
35	Event, Cont.	0 to 14 VDC Step Change	± 50 ms	(HI/LO)	10 Hz	Programmer B Reset Commu- tated at 30 SPS
36	Deleted					
37	Temperature	-90 to +210°F	5%	3.0°F	10 Hz	Bridle Temp. #1 Commutated at 30 SPS
38	Temperature	-90 to +210°F	5%	3.0°F	10 Hz	Bridle Temp. #2 Commutated at 30 SPS
39	Temperature	-90 to +210°F	5%	3.0°F	10 Hz	Bridle Temp. #3 Commutated at 30 SPS
40	Temperature	-90 to +210°F	5%	3.0°F	10 Hz	Cannister Temp. #1 Commu- tated at 30 SPS
41	Temperature	-90 to +210°F	5%	3.0°F	10 Hz	Cannister Temp. #2 Commu- tated at 30 SPS
42	Temperature	0 to +125°F	5%	1.5°F	10 Hz	Instr. Beam Temp. #1 Commutated at 30 SPS
43	Temperature	0 to +175°F	5%	2.0°F	10 Hz	Main Battery Temp. Commutated at 30 SPS

TABLE A-1 (CONTINUED)
BLDT Telemetry Measurement List

No.	Measurement	Range	Accuracy End-to-End	Resolution	Response	Remarks
44	Temperature	-100 to +150°F	5%	2.5°F	10 Hz	Rocket Mtr. Supp. Strt. Temp. Commutated at 30 SPS
45	Event	0 or 5 VDC	± 50 ms	HI/LO	10 Hz	Command Tone #1 Commu- tated at 30 SPS
46	Event	0 or 5 VDC	± 50 ms	HI/LO	10 Hz	Command Tone #2 Commu- tated at 30 SPS
47	Event	0 or 5 VDC	± 50 ms	HI/LO	10 Hz	Command Tone #3 Commu- tated at 30 SPS
48	Event	0 or 5 VDC	± 50 ms	HI/LO	10 Hz	Command Tone #4 Commu- tated at 30 SPS
49	Event	0 or 5 VDC	± 50 ms	HI/LO	10 Hz	Command Tone #5 Commu- tated at 30 SPS
50	Event	0 or 5 VDC	± 50 ms	HI/LO	10 Hz	Command Tone #6 Commu- tated at 30 SPS
51	Event	0 or 5 VDC	± 50 ms	HI/LO	10 Hz	Command Tone #7 Commu- tated at 30 SPS
52	Voltage	0 to 4 VDC	5%	0.04 VDC	10 Hz	Command Receiver A Signal Level Commutated at 30 SPS
53	Event	0 or 28 VDC 0.1 sec duration	± 50 ms	ON/OFF	10 Hz	Mortar Fire Commutated at 30 SPS
54	Temperature	+25 to 150°F	5%	1.5°F	10 Hz	Mortar Breech Flange Temp. Commutated at 30 SPS

TABLE A-1 (CONTINUED)
BLDT Telemetry Measurement List

No.	Measurement	Range	Accuracy End-to-End	Resolution	Response	Remarks
55	Temperature	0 to +175°F	5%	2.0°F	10 Hz	S-Band Transmitter Temp. Commuted at 30 SPS
56	Temperature	-100 to +150°F	5%	2.5°F	10 Hz	Aeroshell Temp. #1 Commuted at 30 SPS
57	Temperature	-100 to +150°F	5%	2.5°F	10 Hz	Aeroshell Temp. #2 Commuted at 30 SPS
58	Temperature	0 to +175°F	5%	2.0°F	10 Hz	Equipment Ballast Temp. Commuted at 30 SPS
59	Temperature	0 to +125°F	5%	1.5°F	10 Hz	Instrument Ream (#2) Temp. Commuted at 30 SPS
60	Temperature	0 to +125°F	5%	1.5°F	10 Hz	Gyro Temp. Commuted at 30 SPS
61	Temperature	-100 to +150°F	5%	2.5°F	10 Hz	Boost Motor #1 Temp. Commuted at 30 SPS
62	Temperature	-100 to +150°F	5%	2.5°F	10 Hz	Boost Motor #2 Temp. Commuted at 30 SPS
63	Voltage	0 to 4 VDC	5%	0.04 VDC	10 Hz	Command RCVR B Signal Level Commuted at 30 SPS
64	Voltage	5 VDC	5%	0.05 VDC	10 Hz	Commutator #2 Full Scale Calibration at 30 SPS
65	Voltage	0 VDC	5%	0.05 VDC	10 Hz	Commutator #2 Zero Scale Calibration at 30 SPS

APPENDIX B

DESCRIPTION OF BLDT

SYSTEM MISSION

APPENDIX B

A. Description of BLDT System Mission1. Purpose of the System

The BLDT System is designed to subject the Viking Decelerator System to Qualification Test Requirements at simulated Mars Entry atmospheric conditions.

2. System Requirements

The Viking Decelerator System earth atmospheric test conditions which result from consideration of the variation in probable Mars atmospheres are:

	<u>Supersonic Case 1</u>	<u>Supersonic Case 2</u>	<u>Transonic Case</u>	<u>Subsonic Case</u>
Peak Load Mach No.	2.17 ± 0.17	2.06 ± 0.16	1.15 ± 0.10	0.46 ± 0.03
Peak Load Dyn. Press. (PSF)	10.09 ± 0.57	9.39 ± 0.55	4.52 ± 0.30	6.46 ± 0.80
Angle of Attack at M/F (Degrees)	≤ 17	≤ 17	≤ 20	≤ 17

The design of the BLDT test bed is constrained by the Viking Lander Capsule design to the following:

- o Vehicle weight at mortar fire - 1888 pounds.
- o Cg offset in minus Z direction - 1.41 inches.
- o Vehicle external envelope similar to VLC (See Appendix A)
- o Decelerator Temperature at mortar fire - 80°F

3. System Description

The BLDT System design which evolved from the above test requirements provides for a large volume, high lift balloon system capable of floating the BLDT Vehicles at altitudes from which the test conditions can be achieved with reduced or no propulsion capability. The predicted test altitudes and balloon lift capability involved in the system design are:

	<u>Supersonic Case 1</u>	<u>Supersonic Case 2</u>	<u>Transonic Case</u>	<u>Subsonic Case</u>
* Balloon Float Altitude (FT)	119,000	119,000	120,500	92,000
* Decelerator Mortar Fire Alt. (FT)	147,800	148,600	137,500	89,300
BLDT Vehicle Launch Weight (LBS)	3,550	3,550	2,800	2,050

The system concept provides for the launch of the balloon/flight vehicle system from the Roswell Industrial Air Center, Roswell, New Mexico with the system ascending to float altitude during the approximately 100 mile westward flight to the White Sands Missile Range. Once over the range, the flight vehicle is released from the balloon load bar to complete its flight sequence.

For the powered flight tests, the vehicle concept provides for spin rotation of the vehicle prior to solid rocket motor boost to minimize thrust dispersion effects. Following the boost phase, the vehicle is despun and allowed to coast to the correct dynamic pressure condition. For the subsonic case, the vehicle is released from the load bar and allowed to free fall until the correct velocity is attained.

* USS62 Pressure Altitude

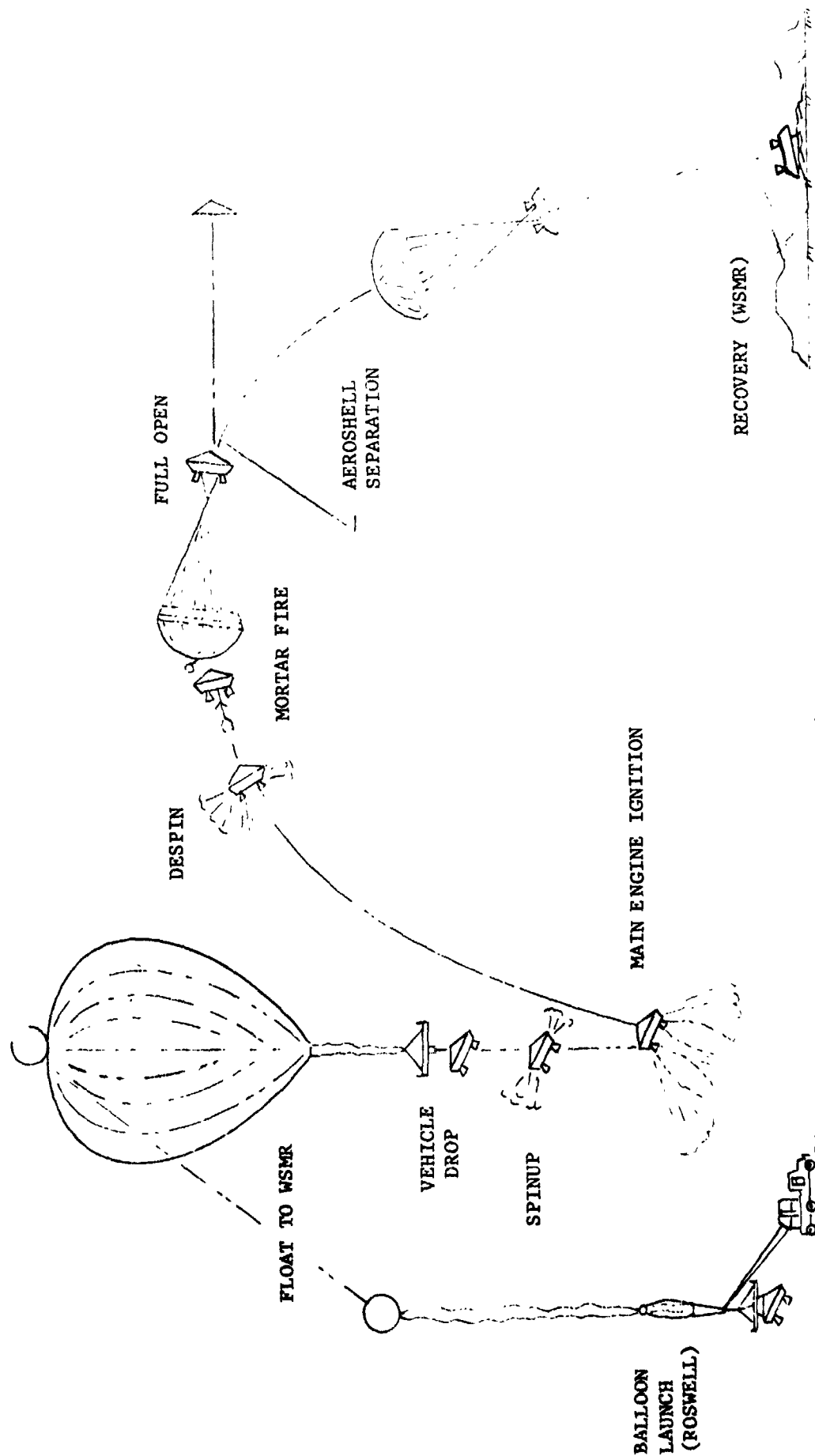
At the White Sands Missile Range, a ground computer system is programmed to receive tracking data which when integrated with predicted meteorological parameters provides the intelligence for the computer to issue a mortar fire command at the required test dynamic pressure for the powered flights. For the non-powered flight, the computer issues a timed mortar fire command following a delay for the correct velocity test conditions to be attained. In both powered and non-powered flights the vehicle incorporates an on-board programmer which provides a backup mortar fire command. Figure B-1 and B-2 depicted a typical powered and non-powered flight.

The system design includes all of the handling, checkout and control equipment necessary for prelaunch checkout, flight control and recovery of the system components.

4. Operations Description

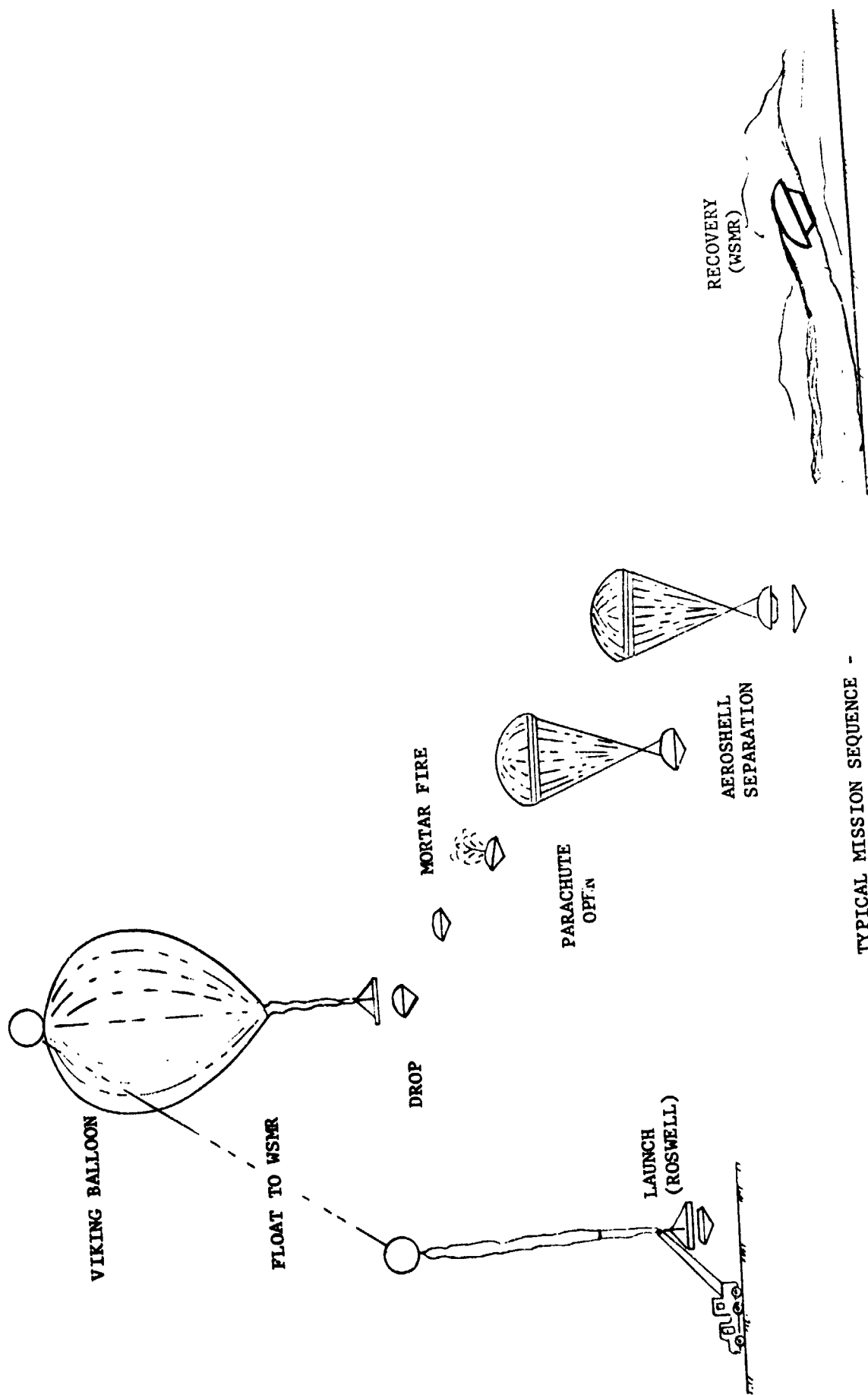
A typical sequence flow of the mission operations from assembly and checkout at Roswell, New Mexico through vehicle flight and recovery at WSMR, is shown in Figure B-3. Each of the sequence events is described below:

a. BLDT Vehicle Assembly and Checkout - This phase of the mission operation encompasses the assembly and checkout of the various system components. The BLDT vehicle, while connected to ground electrical power and in partially assembled condition, is subjected to subsystem and combined system testing in a close loop and open loop mode. The vehicle is then assembled including airborne batteries and subjected to a full flight readiness test on airborne power and in an open loop mode.



TYPICAL MISSION SEQUENCE -
POWERED FLIGHT

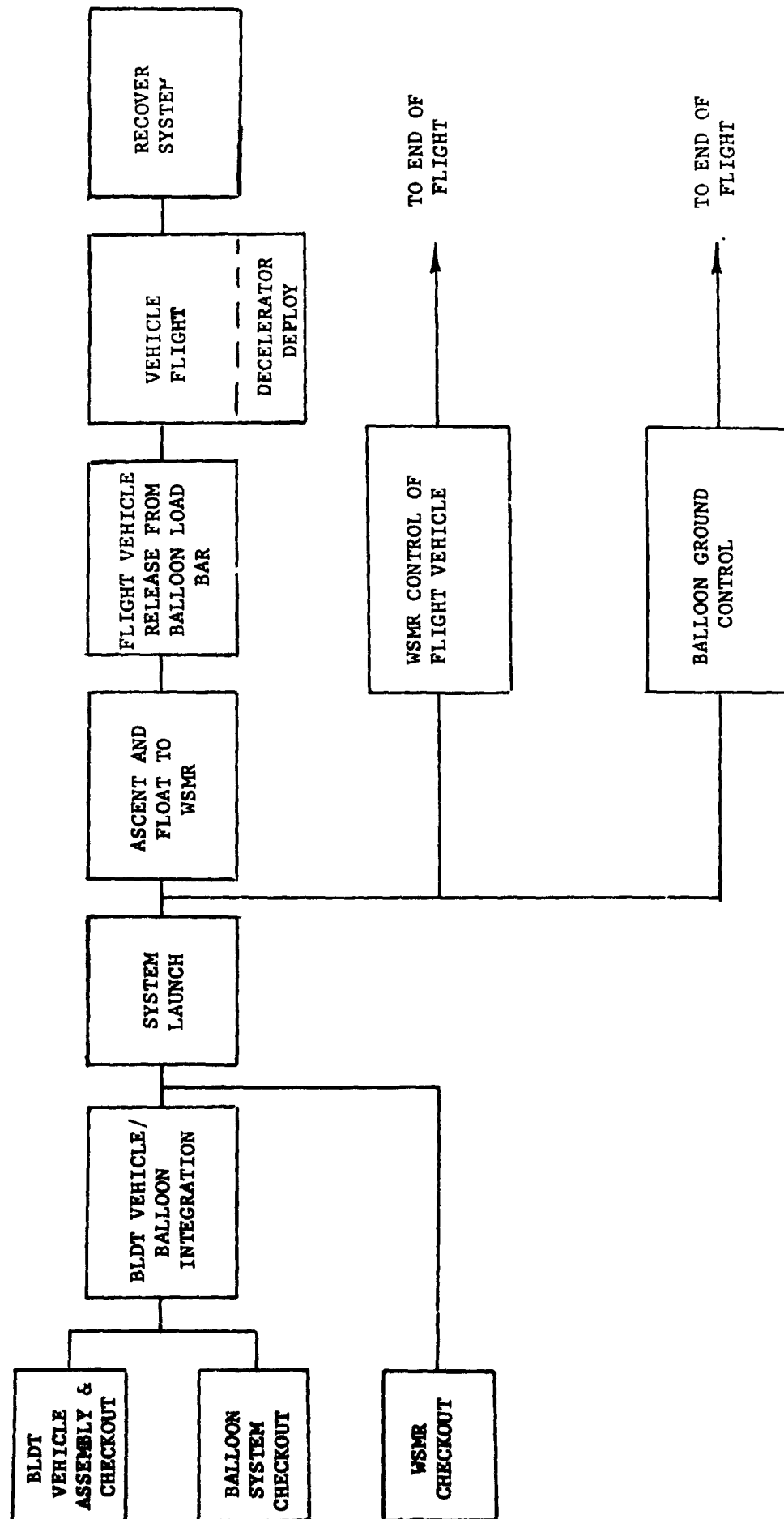
FIGURE B-1



B-6

TYPICAL MISSION SEQUENCE -
UNPOWERED FLIGHT

FIGURE B-2



TYPICAL OPERATIONS SEQUENCE

FIGURE B-3

While the flight vehicle is undergoing checkout and assembly, the balloon system is also being partially assembled and subjected to flight readiness testing. These checkout and assembly events were performed at the Roswell Industrial Air Center.

Coincident with the checkout of the flight system, the ground control system at the White Sands Missile Range is readied for the mission by assuring that:

- 1) The flight TM data is routed to the correct terminal data stations.
- 2) The ground command system is capable of transmitting acceptable commands.
- 3) The communications links are correctly activated.
- 4) The command station personnel are prepared to accept vehicle control.

b. BLDT Vehicle/Balloon Integration - When the prerequisite flight vehicle balloon system and WSMR Control Center checkout are completed and the meteorological constraints at the launch site and MR (launch winds, float winds, local weather, etc.) are satisfactory, the flight vehicle and balloon systems are moved from the checkout hanger to the launch runway where system integration and final checkout is made.

The flight vehicle is connected to ground power and final subsystem testing is completed to assure all subsystems are functioning. The vehicle ordnance is electrically connected and the vehicle access panels are installed. In this time period the launch balloon and float balloon are layed-out and integrated with the flight vehicle, the abort recovery cargo chutes, the balloon winch and the launch crane.

When the system integration is completed, the launch stand is removed from the flight vehicle leaving the flight vehicle suspended from the balloon load bar which in turn is suspended from the launch crane. Also, the launch balloon is filled with a precisely metered quantity of helium.

c. System Launch - Following the integration of the flight vehicle and balloon into the BLDT system, the system is ready for launch.

The launch process begins with a ground winching operation in which the launch balloon is permitted to rise and which upon rising takes the float balloon (uninflated) and the cargo abort chutes from a horizontal attitude to a vertical attitude above the launch crane. Once the system is in the vertical attitude, the winch cable is separated from the balloon system through the use of an ordnance device. At this point, the two balloons with the abort cargo chutes are floating above and tethered to the launch crane with the balloon load bar and flight vehicle suspended from the crane beneath the tethered balloon. At this point, the total system for a powered flight extend from ground level to approximately 1000 feet above ground level (800 feet for a non-powered flight).

With all of the preceeding operations complete, it only remains to release the flight system from the launch crane. To do this, the launch crane is driven down wind at a velocity necessary to position the crane approximately under the balloon at which point the crane release device is actuated and the balloon floats free of the ground system taking with it the balloon load bar and flight vehicle.

d. Ascent and Float Phase - During the ascent and float phase, the balloon system, floating freely, responds to the wind directions and velocities encountered as it ascends to the design float altitude. Generally, once clear of low altitude wind influence, the balloons float in a westerly direction intersecting the WSMR at about mid-range.

As the system ascends, the helium which was loaded in the launch balloon is forced down into the float balloon which slowly inflates the float balloon and causes the system to ascend. This process continues until the float balloon becomes fully inflated at which point no further lift can be obtained. The balloon ascent to float altitude is rapid enough to arrive at the float altitude prior to intersecting the WSMR.

The balloon ascent and direction is somewhat controllable through the use of ballast dumping operations to control floating altitude and rise rates in order to take advantage of winds at the upper levels. The control of the balloon during the ascent and float phase is from the Air Force Cambridge Research Laboratory control center at Holloman Air Force Base, Alamogordo, New Mexico.

When the ascending system passes through approximately 30 K feet, the WSMR tracking radar, command networks and TM receiving stations are able to acquire the flight vehicle and start checkout. Part of the float checkout assures operation of the command nets by sending commands which do not change vehicle configuration (i.e. safe ordnance circuits, turn R.F. on, etc.) and verifying receipt of the commands through flight vehicle TM data being received at the control center.

e. Vehicle Release from Load Bar - Once the BLDT system reaches the proper float altitude and intersects the range, the vehicle ordnance circuits are armed, the vehicle flight azimuth is attained using a cold gas pointing system and the vehicle release from the load bar is commanded. All of these functions occur as a result of ground commands issued by the flight vehicle control crew at WSMR.

f. Vehicle Flight - The vehicle flight events are a function of the type of mission being flown. Table B-1 presents a sequence of

events and event times for the Supersonic, Transonic and Subsonic missions. All of the event times in Table B-1 are times from release of the flight vehicle from the balloon load bar with the exception of the ground mortar fire command for the powered flights. This command is time variable and is issued by the ground computer during the vehicle coast following despin when the vehicle achieves the correct dynamic pressure.

For the powered flights following release of the vehicle from the load bar, the vehicle is under control of the redundant airborne programmers with the exception of the issuance of the decelerator mortar fire. The vehicle functions provide a flight profile as shown in Figures B-1 and B-2.

During the vehicle powered flights, the vehicle is tracked by the WSMR tracking devices to provide the ground computer with the intelligence for issuing the mortar fire command. For all flights, tracking devices provide data for post flight analysis and to support vehicle recovery operations.

For the non-powered, free fall mission, the vehicle functions are commanded by the on-board redundant programmers except for the mortar fire which is issued as a timed output from the ground computer.

g. Recovery Operations - During this phase of the mission, all of the system components are located and moved to WSMR facilities for post flight inspection. Also during this phase the various system cameras are recovered and the film processed for post flight analysis.

TABLE B-1

VEHICLE FLIGHT SEQUENCE OF EVENTS

<u>SUPERSONIC</u>		<u>TRANSONIC</u>		<u>SUBSONIC</u>		<u>FUNCTION</u>	<u>SOURCE</u>
<u>CASE 1</u>	<u>CASE 2</u>						
$T_D - 30$ min.	$T_D - 30$ min.	$T_D - 30$ min.	Drop - 30 min.	Drop - 30 min.	--	Attain Float Altitude	--
$T_D - 10$ min.	$T_D - 10$ min.	$T_D - 10$ min.	$T_D - 10$ min.	$T_D - 10$ min.	--	Start Azimuth Pointing	Ground Command
$T_D - 5$ min.	$T_D - 5$ min.	$T_D - 5$ min.	$T_D - 5$ min.	$T_D - 5$ min.	--	Arm Ordnance Bus	Ground Command
$T_D - 10$ sec.	$T_D - 10$ sec.	$T_D - 10$ sec.	$T_D - 10$ sec.	$T_D - 10$ sec.	--	Confirm Drop Azimuth	A/B T/M
T_D	T_D	T_D	T_D	T_D	--	Drop from Load Bar.	Ground Command
					--	Initiate A/B Programmer.	
					--	Ignite Spin Motors/Enable Boost Motor	A/B Programmer
$T_D + 1$ sec.	$T_D + 1$ sec.	$T_D + 1$ sec.	$T_D + 1$ sec.	$T_D + 1$ sec.	--	Ignite Boost Motors	A/B Programmer
$T_D + 2$ sec.	$T_D + 2$ sec.	$T_D + 2$ sec.	$T_D + 2$ sec.	$T_D + 12$ sec.	--	Start AFT Looking Camera, Enable Mortar	A/B Programmer
--	--	--	--	$T_D + 16$ sec.	--	Initiate Mortar Fire/Start AFT Hi-Speed Camera	Ground Command
--	--	--	--	$T_D + 18$ sec.	--	Initiate M/F Backup	A/B Programmer
--	--	--	--	$T_D + 30$ sec.	--	Separate Aeroshell	A/B Programmer
$T_D + 33$ sec.	$T_D + 33$ sec.	$T_D + 33$ sec.	$T_D + 33$ sec.	--	--	Ignite Despin Motors/Release Camera Lens Covers/Start AFT Camera Enable Mortar	A/B Programmer
T_D (q cond. correct)	T_D (q cond. correct)	T_D (q cond. correct)	T_D (q cond. correct)	--	--	Initiate Decelerator Mortar Fire/Start AFT Hi-Speed Camera	Ground Command
$T_D + 37$ sec.	$T_D + 38$ sec.	$T_D + 39$ sec.	$T_D + 39$ sec.	--	--	Initiate M/F Backup	A/B Programmer
$T_D + 47.6$ sec.	$T_D + 47.6$ sec.	$T_D + 47.6$ sec.	$T_D + 47.6$ sec.	--	--	Separate Aeroshell	A/B Programmer

APPENDIX C
GAC POST-TEST INSPECTION

Excerpts from GAC Report No. RSE-20926-18

GAC POST-TEST INSPECTION

Viking decelerator system S/N 16 was flown as BLDT 3 (AV-4). This system incorporated S/N 17 parachute. The following constitutes the post-flight inspection report.

Chute Canopy

The damage chart is presented in Figure C-1. As noted on the chart, several small black smudges are in evidence on various gores in the band. The smudges are in the mid-gore region. There is no evidence of excessive heat associated with the smudges.

Gore 9, panel D of the disk has eight small holes (See Figure C-2). The edges of the holes are hardened as if excessive heat were encountered. In two cases, there is cloth fused to itself near the holes.

Gore 33, panel E of the band, exhibits two holes (See Figure C-3). The larger hole is approximately 2-1/2" by 1". There appears to be some cloth missing from this hole. Also, there is a smearable, black residue on the edge of the hole.

Gore 48, panel E of the band, has four small holes similar in nature to gore 9.

Suspension Lines - No damage.

Deployment Bag

There is one small cut, about 1/4 inch, located approximately 7 inches from the bottom edge of the bag. The cut is near an imprint of the swivel bolt.

The bag is blackened on the outside surface.

Buffer

The quartz facing of the buffet is torn at each of the tie locations. One of the tears is completely through the buffer and extends approximately 3 inches.

The facing in the center of the buffer is torn at the points where the filler block is attached.

Filler Block - The filler block is missing.

Bridle Legs

The bridle legs are undamaged. Most of the basting stitches are broken. The bridle legs are blackened.

Cover Thermal Protection

Several random ruptures of the Min-K are in evidence. The Min-K is blackened near the mortar opening.

Bridle Thermal Protection

Several random ruptures of the Min-K are in evidence. The Min-K is blackened near the mortar opening.

Mortar

The inside of the mortar tube is blackened. The straps at the top of the mortar are all intact. The choker cord is fused to one of the straps. There is no apparent damage to the mortar.

Sabot

The sabot is blackened on the outer surface. The Teflon and stainless steel discs are still attached. The sabot retention are blackened but intact.

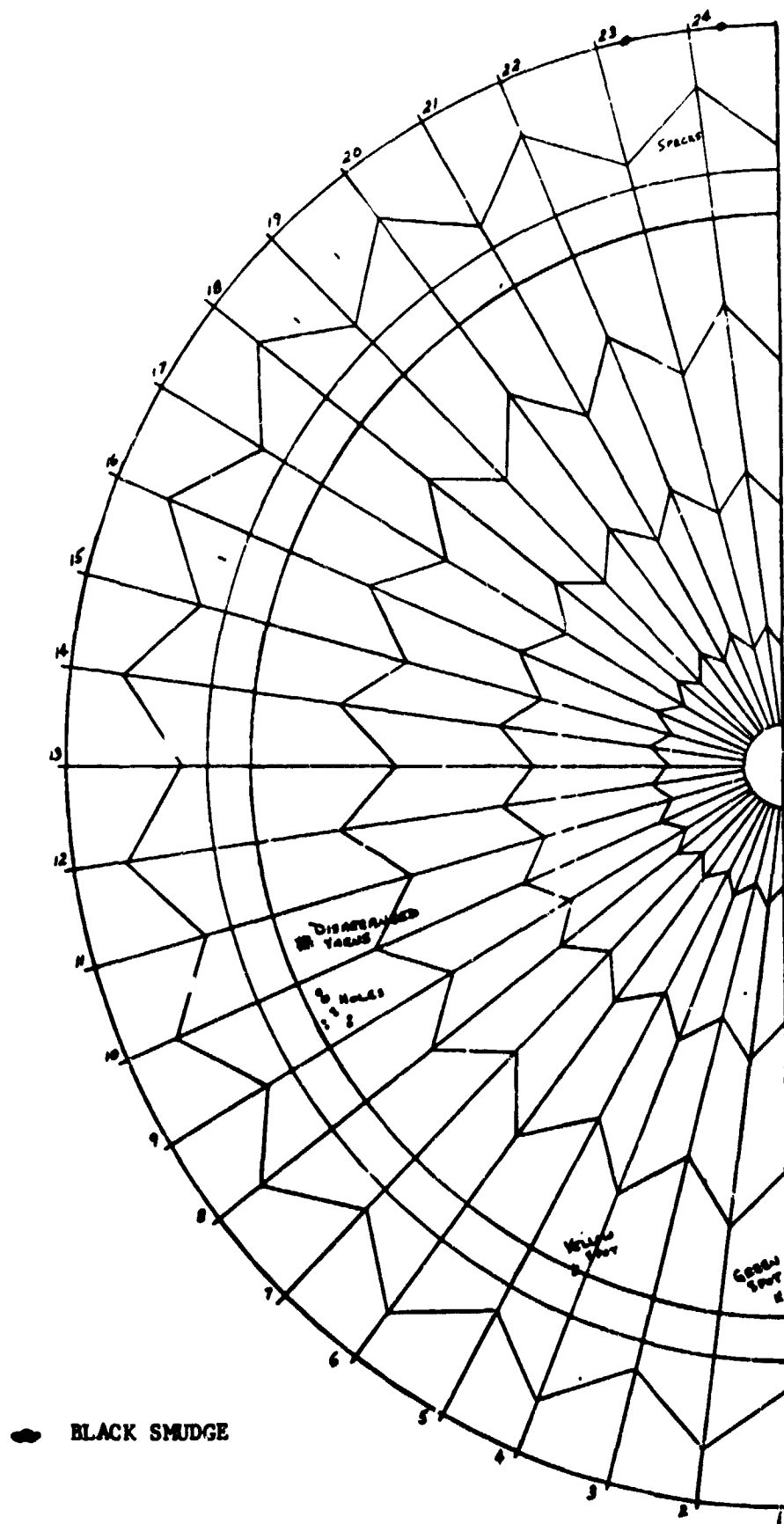


FIGURE C-1 PARACHUTE DAMAGE CHART

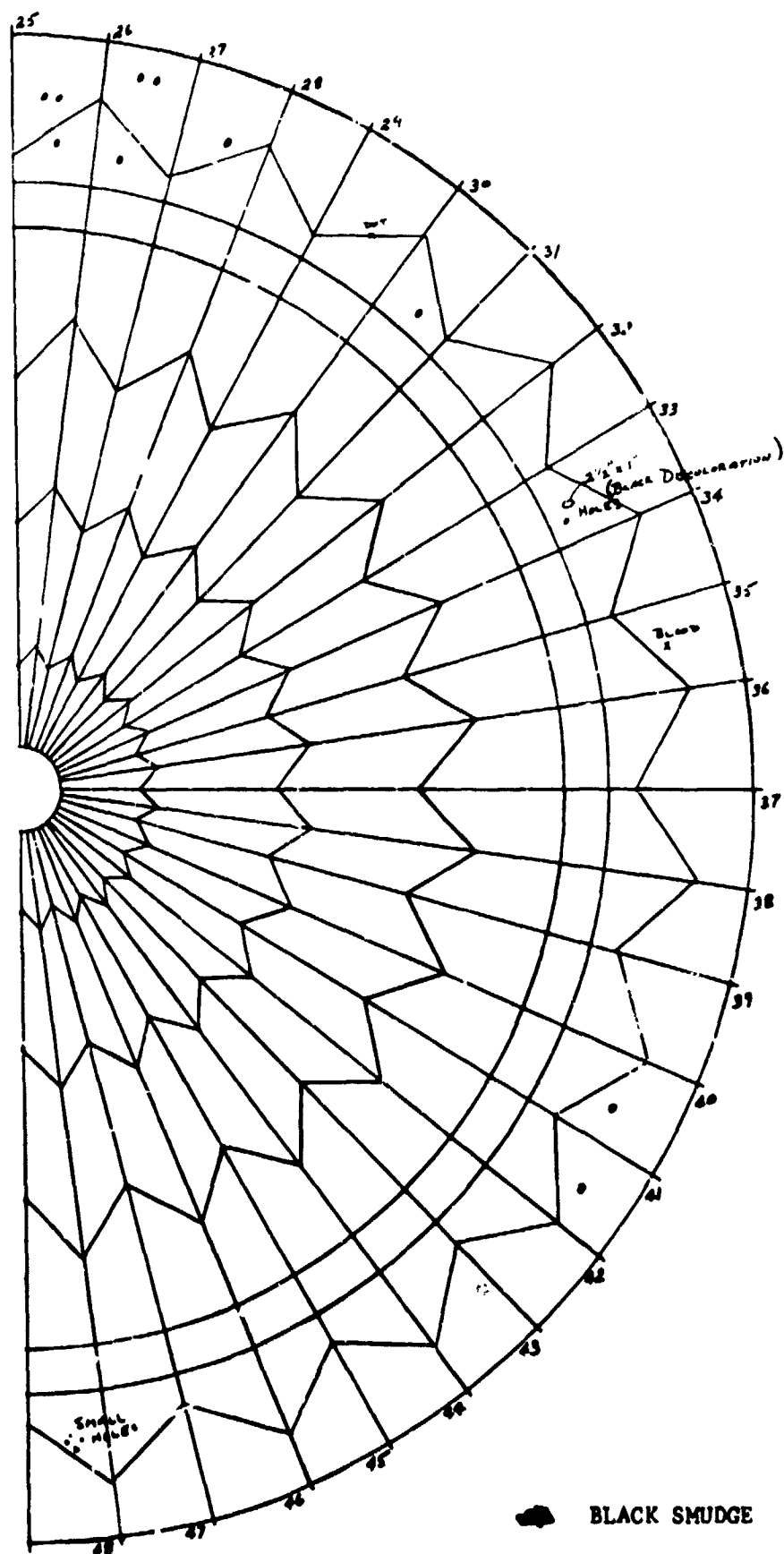


FIGURE C-1 PARACHUTE DAMAGE CHART (CONTINUED)

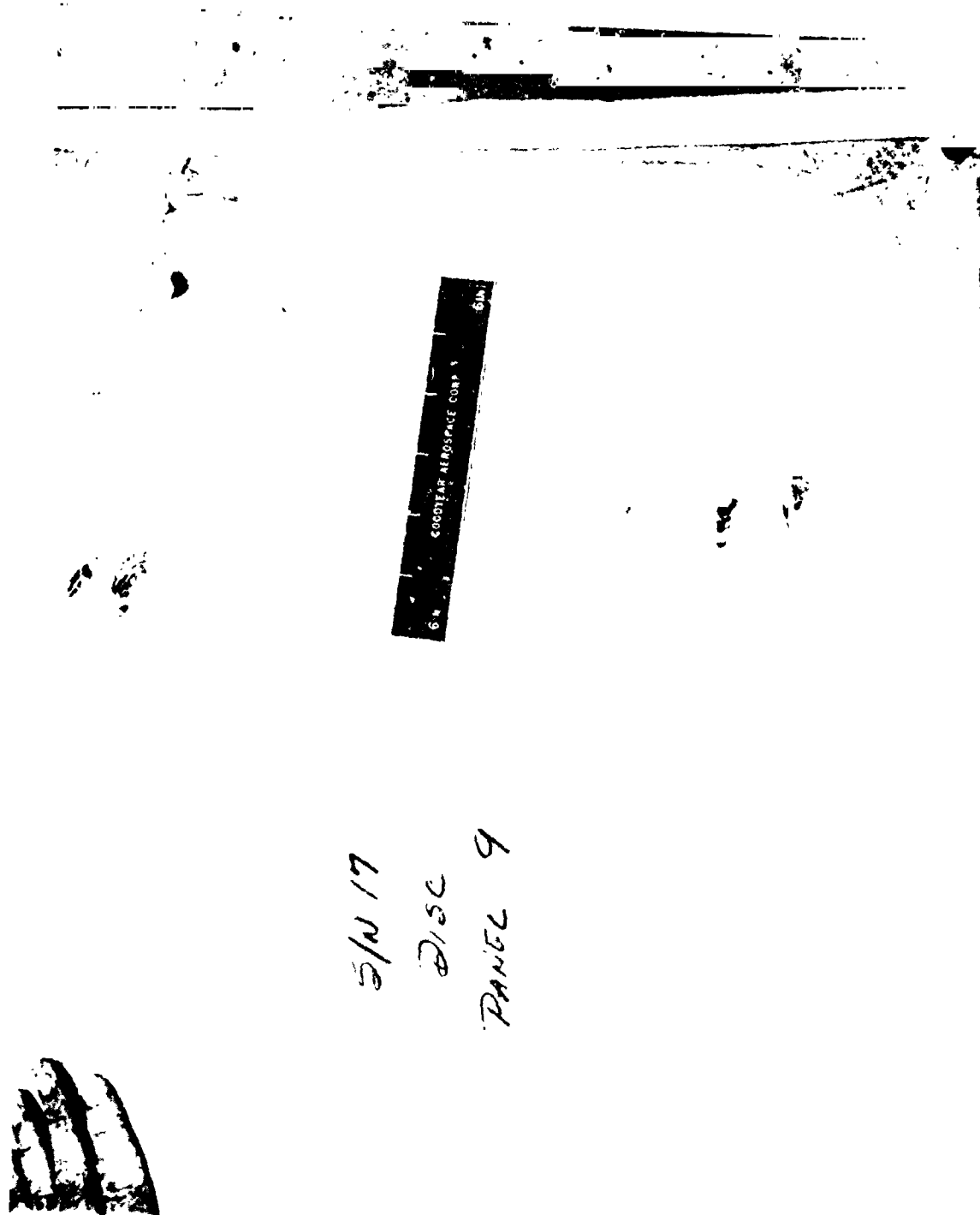


FIGURE C-2 CLOTH DAMAGE ON CHUTE S/N 17, GORE 9

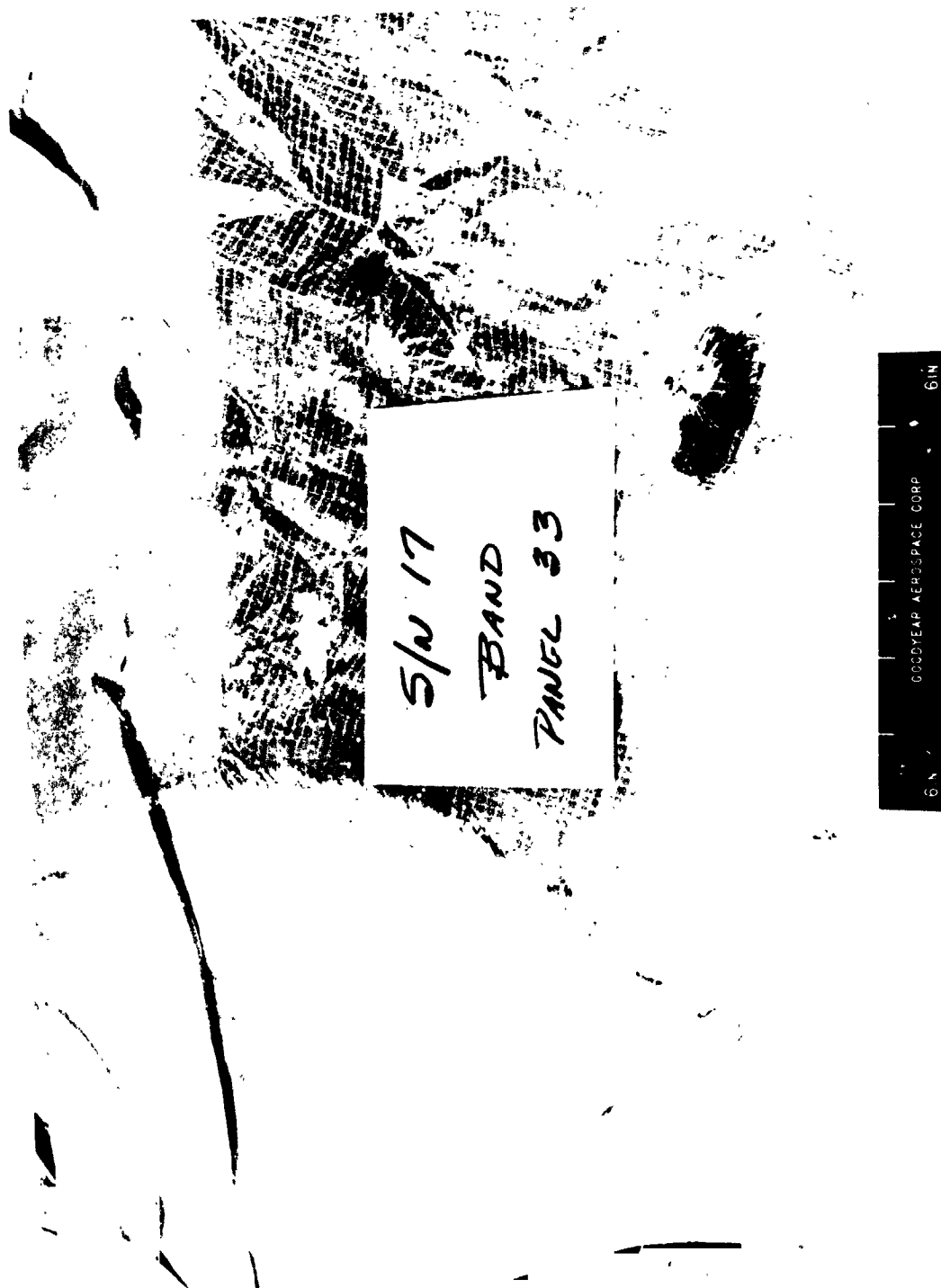
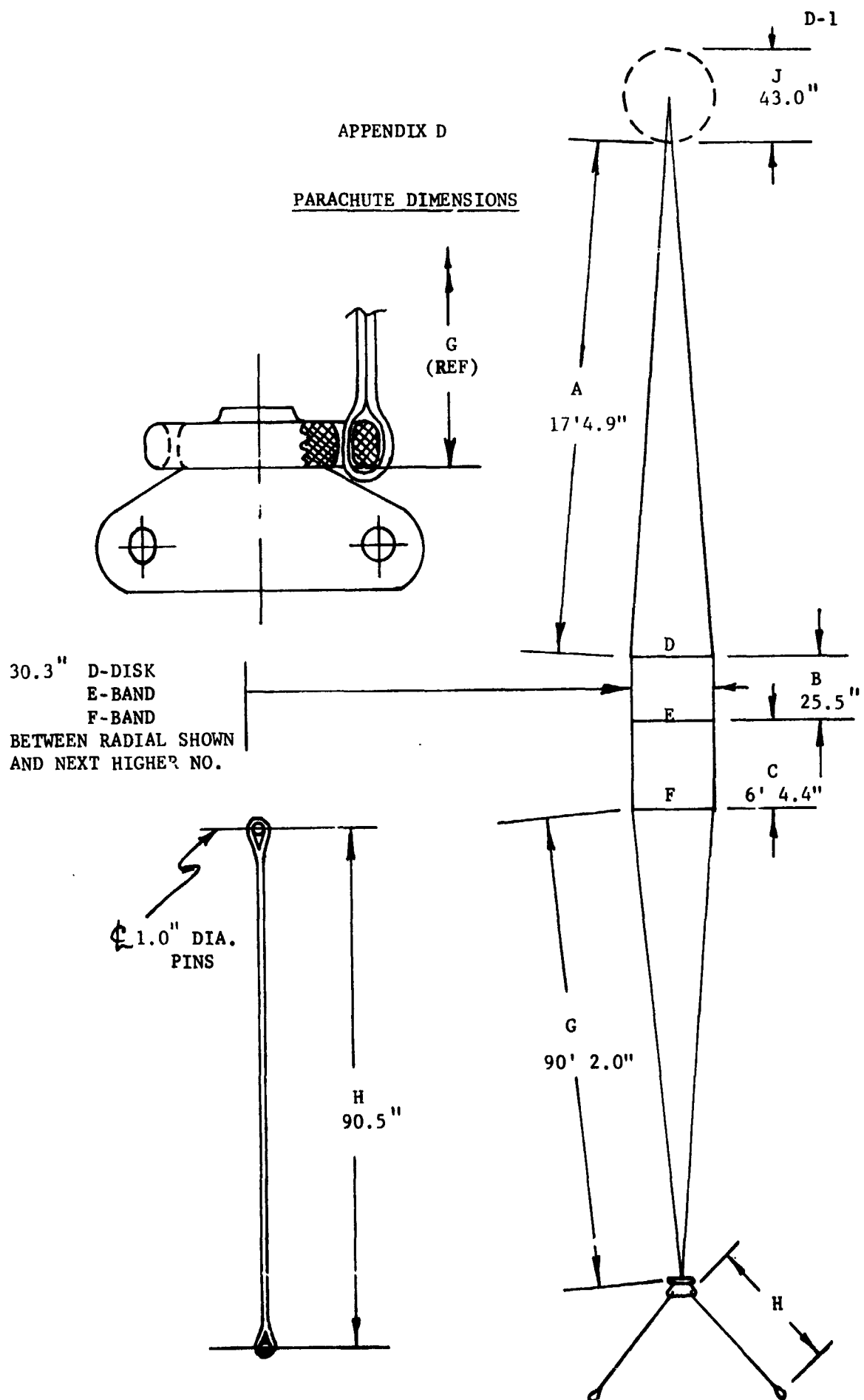


FIGURE C-3 CLOTH DAMAGE ON CHUTE S/N 17, GORE 33

APPENDIX D

PARACHUTE DIMENSIONS



PRE-FLIGHT AV-4

<u>RADIAL NO</u>	<u>A(DISC) FT-INCHES</u>	<u>B(GAP) INCHES</u>	<u>C(BAND) INCHES</u>	<u>D(DISC) INCHES</u>	<u>E(BAND) INCHES</u>	<u>F(BAND) INCHES</u>	<u>G(SUSP) FT-INCHES</u>
1	17-3 ³ / ₄	25 ⁵ / ₁₆	75 ⁵ / ₈	30 ¹ / ₈	30 ¹ / ₈	29 ⁷ / ₈	90-1
2	3 ¹ / ₂	5/ ₁₆	9/ ₁₆	3/ ₈	5/ ₁₆	30 ³ / ₈	1/ ₄
3	3 ³ / ₈	5/ ₁₆	3/ ₈	3/ ₁₆	1/ ₂	3/ ₈	3/ ₄
4	3 ¹ / ₄	5/ ₁₆	1/ ₄	5/ ₁₆	1/ ₈	5/ ₁₆	7/ ₈
5	3 ¹ / ₂	1/ ₄	5/ ₁₆	1/ ₈	5/ ₁₆	3/ ₈	3/ ₄
6	3 ¹ / ₂	1/ ₄	3/ ₈	7/ ₁₆	1/ ₄	5/ ₁₆	3/ ₄
7	3 ¹ / ₄	1/ ₄	3/ ₈	1/ ₄	3/ ₈	1/ ₄	3/ ₄
8	3 ¹ / ₈	1/ ₄	1/ ₄	3/ ₈	1/ ₂	9/ ₁₆	1 ¹ / ₄
9	3 ¹ / ₈	5/ ₁₆	5/ ₁₆	1/ ₈	3/ ₁₆	1/ ₄	1/ ₂
10	3 ¹ / ₈	5/ ₁₆	3/ ₈	3/ ₁₆	3/ ₈	7/ ₁₆	1 ¹ / ₂
11	3 ³ / ₁₆	1/ ₄	1/ ₄	7/ ₁₆	1/ ₄	7/ ₈	1/ ₂
12	3 ³ / ₈	5/ ₁₆	1/ ₂	3/ ₁₆	9/ ₁₆	1/ ₈	1
13	3 ¹⁵ / ₁₆	1/ ₄	3/ ₄	3/ ₁₆	1/ ₈	5/ ₁₆	1 ¹ / ₄
14	3 ³ / ₈	3/ ₈	5/ ₈	1/ ₈	5/ ₁₆	9/ ₁₆	1
15	3 ⁵ / ₈	5/ ₁₆	7/ ₁₆	7/ ₁₆	3/ ₈	3/ ₁₆	3/ ₄
16	3 ⁵ / ₈	5/ ₁₆	7/ ₁₆	5/ ₁₆	3/ ₈	9/ ₁₆	3/ ₄
17	3 ⁷ / ₈	5/ ₁₆	7/ ₁₆	1/ ₄	5/ ₁₆	1/ ₄	7/ ₈
18	3 ³ / ₄	5/ ₁₆	5/ ₈	0	3/ ₈	3/ ₁₆	1 ¹ / ₈
19	3 ⁷ / ₈	5/ ₁₆	7/ ₁₆	3/ ₈	1/ ₄	1/ ₂	1 ¹ / ₈
20	3 ¹ / ₈	1/ ₄	5/ ₁₆	3/ ₈	7/ ₁₆	1/ ₄	1
21	3 ¹ / ₂	5/ ₁₆	3/ ₈	1/ ₄	5/ ₁₆	9/ ₁₆	1
22	3 ⁹ / ₁₆	1/ ₄	1/ ₄	3/ ₁₆	1/ ₄	29 ⁷ / ₈	1 ¹ / ₄
23	3 ⁷ / ₈	5/ ₁₆	1/ ₄	3/ ₁₆	5/ ₁₆	1/ ₂	1 ¹ / ₄
24	3 ³ / ₄	5/ ₁₆	3/ ₈	1/ ₄	1/ ₂	1/ ₈	7/ ₈

PRE-FLIGHT AV-4 (CONTINUED)

<u>RADIAL NO</u>	<u>A(DISC) FT- INCHES</u>	<u>B(GAP) INCHES</u>	<u>C(BAND) INCHES</u>	<u>D(DISC) INCHES</u>	<u>E(BAND) INCHES</u>	<u>F(BAND) INCHES</u>	<u>G(SUSP) FT- INCHES</u>
25	17-4	25 ¹ / ₄	75 ⁵ / ₁₆	30 ¹ / ₄	30 ⁵ / ₈	30 ⁵ / ₈	90-3/ ₄
26	3 ⁵ / ₈	1/ ₄	3/ ₈	9/ ₁₆	5/ ₁₆	5/ ₁₆	1 ¹ / ₈
27	3 ³ / ₄	1/ ₄	3/ ₈	1/ ₄	1/ ₄	1/ ₄	3/ ₄
28	3 ¹ / ₂	3/ ₈	5/ ₁₆	3/ ₁₆	5/ ₁₆	5/ ₁₆	11/ ₂
29	3 ³ / ₄	1/ ₄	7/ ₁₆	1/ ₄	9/ ₁₆	3/ ₈	1
30	3 ¹ / ₂	1/ ₄	3/ ₈	5/ ₁₆	1/ ₁₆	5/ ₁₆	1 ¹ / ₄
31	3 ¹ / ₂	5/ ₁₆	5/ ₁₆	3/ ₈	3/ ₄	1/ ₄	11/ ₄
32	3 ¹ / ₄	3/ ₈	3/ ₈	5/ ₁₆	1/ ₈	3/ ₈	1 ¹ / ₄
33	3 ⁵ / ₁₆	1/ ₄	5/ ₁₆	3/ ₁₆	3/ ₈	3/ ₈	1 ¹ / ₄
34	3 ³ / ₈	3/ ₈	1/ ₂	3/ ₁₆	5/ ₁₆	1/ ₈	1 ¹ / ₄
35	3 ¹ / ₂	5/ ₁₆	3/ ₁₆	5/ ₈	3/ ₈	5/ ₈	11/ ₈
36	3 ¹ / ₄	5/ ₁₆	1/ ₄	1/ ₁₆	5/ ₁₆	1/ ₄	1
37	3 ³ / ₈	5/ ₁₆	3/ ₈	3/ ₈	3/ ₄	1/ ₂	11/ ₄
38	3 ⁵ / ₈	5/ ₁₆	3/ ₈	0	3/ ₈	1/ ₄	1 ³ / ₈
39	3 ³ / ₄	5/ ₁₆	3/ ₈	9/ ₁₆	7/ ₁₆	1/ ₈	11/ ₄
40	3 ¹ / ₂	3/ ₈	3/ ₁₆	1/ ₄	5/ ₁₆	3/ ₈	1
41	3 ⁵ / ₈	5/ ₁₆	5/ ₁₆	5/ ₁₆	1/ ₈	1/ ₂	11/ ₈
42	3 ⁵ / ₈	5/ ₁₆	3/ ₈	5/ ₁₆	7/ ₁₆	3/ ₁₆	1 ¹ / ₄
43	3 ¹ / ₄	1/ ₄	5/ ₁₆	1/ ₈	1/ ₄	3/ ₈	1 ¹ / ₄
44	3 ¹ / ₂	1/ ₄	1/ ₄	5/ ₁₆	9/ ₁₆	1/ ₄	1 ¹ / ₄
45	3 ¹ / ₄	1/ ₄	3/ ₈	1/ ₁₆	1/ ₄	1/ ₂	1 ¹ / ₈
46	3	1/ ₄	3/ ₈	3/ ₈	3/ ₈	1/ ₄	1 ¹ / ₄
47	3 ¹ / ₈	1/ ₄	1/ ₈	3/ ₈	7/ ₁₆	5/ ₁₆	1 ¹ / ₈
48	3	1/ ₄	1/ ₄	1/ ₁₆	1/ ₂	5/ ₈	1 ¹ / ₂

PRE-FLIGHT AV-4 (CONCLUDED)

BRIDLE LEG		H - INCHES
S/N	52	$90\frac{1}{2}$
S/N	53	$90\frac{3}{4}$
S/N	54	$90\frac{5}{8}$

VENT DIAMETER	
RADIAL	J - INCHES
1/25	$42\frac{1}{2}$
7/31	$42\frac{1}{2}$
13/37	42
19/43	$42\frac{1}{4}$

POST-TEST AV-4

<u>RADIAL NO</u>	<u>A(DISC) FT-INCHES</u>	<u>B(GAP) INCHES</u>	<u>C(BAND) INCHES</u>	<u>D(DISC) INCHES</u>	<u>E(BAND) INCHES</u>	<u>F(BAND) INCHES</u>	<u>G(SUSP) FT-INCHES</u>
1	17-5	25 ¹ / ₄	76 ¹ / ₂	30-0	30-0	30 ¹ / ₈	91-9 ³ / ₄
2	17-5 ¹ / ₂	25 ³ / ₈	76 ³ / ₄	1/ ₄	1/ ₄	1/ ₂	10 ³ / ₄
3	17-5 ¹ / ₄	25 ¹ / ₄	76 ³ / ₄	3/ ₁₆	3/ ₈	5/ ₈	92-0
4	17-5	25 ¹ / ₄	76 ¹ / ₂	1/ ₄	1/ ₁₆	1/ ₂	2 ¹ / ₂
5	17-5 ¹ / ₄	25 ¹ / ₄	76 ¹ / ₄	1/ ₁₆	3/ ₈	1/ ₂	5 ¹ / ₄
6	17-5 ¹ / ₂	25 ¹ / ₄	76 ¹ / ₂	3/ ₈	3/ ₁₆	1/ ₂	7 ³ / ₈
7	17-5 ¹ / ₂	25 ³ / ₈	76 ¹ / ₂	1/ ₄	1/ ₄	3/ ₈	5
8	17-5 ¹ / ₂	25 ¹ / ₄	76 ¹ / ₂	5/ ₁₆	7/ ₁₆	1/ ₂	4 ¹ / ₄
9	17-4 ¹ / ₂	25 ¹ / ₄	76 ³ / ₈	1/ ₈	1/ ₈	1/ ₄	1 ¹ / ₄
10	17-4 ³ / ₄	25 ¹ / ₄	76 ¹ / ₄	1/ ₈	5/ ₁₆	3/ ₈	1 ¹ / ₄
11	17-5	25 ³ / ₈	76 ¹ / ₄	3/ ₈	1/ ₄	1/ ₂	92-0
12	17-5 ¹ / ₄	25 ¹ / ₄	76 ¹ / ₂	1/ ₈	9/ ₁₆	0	1
13	17-5 ¹ / ₂	25 ³ / ₈	76 ¹ / ₂	1/ ₈	1/ ₁₆	3/ ₁₆	91-10 ¹ / ₄
14	17-5	25 ¹ / ₄	76 ¹ / ₂	1/ ₈	5/ ₁₆	7/ ₁₆	10
15	17-5 ¹ / ₄	25 ¹ / ₄	76 ¹ / ₂	1/ ₄	1/ ₄	1/ ₈	9 ³ / ₄
16	17-4 ¹ / ₂	25 ¹ / ₄	76 ¹ / ₄	1/ ₄	7/ ₁₆	3/ ₈	9 ¹ / ₄
17	17-5 ³ / ₄	25 ³ / ₈	76 ¹ / ₂	1/ ₄	5/ ₁₆	3/ ₁₆	7 ³ / ₄
18	17-5 ¹ / ₂	25 ¹ / ₄	76 ³ / ₄	297/ ₈	5/ ₁₆	1/ ₁₆	7 ¹ / ₂
19	17-5	25 ¹ / ₄	76 ³ / ₈	305/ ₁₆	3/ ₁₆	3/ ₈	6 ¹ / ₄
20	17-4 ¹ / ₂	25 ¹ / ₄	76 ¹ / ₄	1/ ₄	3/ ₈	1/ ₈	6 ¹ / ₂
21	17-4 ¹ / ₂	25 ³ / ₈	76 ¹ / ₈	1/ ₄	1/ ₄	7/ ₁₆	5 ³ / ₄
22	17-4 ¹ / ₂	25 ¹ / ₄	76-0	1/ ₈	1/ ₄	293/ ₄	5 ³ / ₄
23	17-5	25 ¹ / ₄	76-0	3/ ₁₆	5/ ₁₆	303/ ₈	5 ³ / ₄
24	17-5	25 ¹ / ₄	76-0	1/ ₄	1/ ₂	1/ ₁₆	5

POST-TEST AV-4 (CONTINUED)

<u>RADIAL NO</u>	<u>A(DISC) FT-INCHES</u>	<u>B(GAP) INCHES</u>	<u>C(BAND) INCHES</u>	<u>D(DISC) INCHES</u>	<u>E(BAND) INCHES</u>	<u>F(BAND) INCHES</u>	<u>G(SUSP) FT-INCHES</u>
25	17-5	25 ¹ / ₄	76-0	30- ³ / ₁₆	30 ¹ / ₂	30 ¹ / ₂	91-3
26	17-5 ¹ / ₄	25 ¹ / ₄	76 ¹ / ₂	⁵ / ₈	⁵ / ₁₆	¹ / ₄	3 ³ / ₄
27	17-4 ¹ / ₂	25 ¹ / ₄	76 ¹ / ₄	³ / ₁₆	¹ / ₄	³ / ₁₆	5
28	17-4 ³ / ₈	25 ³ / ₈	76-0	³ / ₁₆	⁵ / ₁₆	¹ / ₄	8 ¹ / ₂
29	17-5 ¹ / ₄	25 ¹ / ₈	76 ³ / ₈	⁷ / ₈	⁹ / ₁₆	³ / ₈	7
30	17-5 ¹ / ₂	25 ¹ / ₄	76 ¹ / ₂	¹ / ₄	¹ / ₈	¹ / ₄	6
31	17-4 ¹ / ₂	25 ¹ / ₄	76 ¹ / ₄	⁷ / ₁₆	⁵ / ₈	³ / ₁₆	5
32	17-5 ¹ / ₄	25 ³ / ₈	76 ¹ / ₂	¹ / ₄	¹ / ₈	³ / ₈	3 ¹ / ₂
33	17-4 ¹ / ₄	25 ¹ / ₄	76 ¹ / ₄	³ / ₁₆	³ / ₈	³ / ₈	2 ¹ / ₄
34	17-3 ¹ / ₂	25 ¹ / ₄	76-0	¹ / ₈	¹ / ₄	¹ / ₈	1
35	17-4 ³ / ₄	25 ¹ / ₄	76 ¹ / ₄	¹ / ₂	³ / ₈	⁵ / ₈	90-11 ³ / ₄
36	17-4 ³ / ₄	25 ³ / ₈	76 ¹ / ₄	0	³ / ₈	³ / ₁₆	91- ¹ / ₂
37	17-5	25 ¹ / ₄	76 ¹ / ₄	³ / ₈	⁵ / ₈	¹ / ₂	1 ¹ / ₄
38	17-5	25 ¹ / ₄	76 ¹ / ₄	0	³ / ₈	¹ / ₄	3 ¹ / ₄
39	17-5	25 ³ / ₈	76 ¹ / ₄	¹ / ₂	³ / ₈	¹ / ₈	4
40	17-4 ¹ / ₂	25 ¹ / ₄	76 ¹ / ₈	¹ / ₈	¹ / ₈	³ / ₈	5 ³ / ₄
41	17-5 ¹ / ₄	25 ³ / ₈	76 ³ / ₈	¹ / ₄	¹ / ₈	⁷ / ₁₆	5 ³ / ₄
42	17-5 ³ / ₈	25 ¹ / ₄	76 ³ / ₈	¹ / ₄	³ / ₈	¹ / ₈	7
43	17-4 ⁵ / ₈	25 ¹ / ₄	76 ¹ / ₄	¹ / ₄	¹ / ₈	³ / ₈	7
44	17-4 ³ / ₄	25 ¹ / ₄	76 ¹ / ₄	¹ / ₄	¹ / ₂	¹ / ₄	7 ¹ / ₂
45	17-4 ¹ / ₂	25 ¹ / ₄	76 ¹ / ₂	¹ / ₈	³ / ₁₆	¹ / ₂	8 ¹ / ₄
46	17-4 ¹ / ₂	25 ¹ / ₄	76 ¹ / ₂	³ / ₈	¹ / ₄	¹ / ₄	8
47	17-4 ¹ / ₂	25 ¹ / ₄	76 ¹ / ₄	³ / ₈	⁷ / ₁₆	¹ / ₂	6
48	17-4 ³ / ₄	25 ¹ / ₄	76 ¹ / ₄	¹ / ₁₆	⁷ / ₁₆	⁵ / ₈	7 ¹ / ₂

POST-TEST AV-4 (CONCLUDED)

BRIDLE LEG	H - INCHES
S/N 46	91
S/N 47	91 $\frac{1}{3}$
S/N 48	91

VENT DIAMETER	
RADIAL	J - INCHES
1/25	42 $\frac{1}{2}$
7/31	42 $\frac{1}{2}$
13/37	42 $\frac{1}{2}$
19/43	42 $\frac{1}{2}$

APPENDIX E

BLDT COMPUTER SOFTWARE

I. PURPOSE

The control of the Balloon Launch Decelerator Test Flights at WSMR was aided through computer predictions and operations. It was the responsibility of WSMR (RTDS) personnel to develop computer software necessary to fulfill operational requirements imposed by MMC and constraints imposed by Range Safety. The purpose of this appendix is to discuss the real time computer software needed at WSMR for the BLDT mission and, in particular, describe the software furnished by MMC. The major software functions were to:

- Predict impact of flight/payload components
- Issue a precision, real time decelerator mortar fire command
- Generate real time flight information

In support of the above requirements, the following computer programs were developed by MMC for WSMR implementation:

- Vehicle Flight Azimuth Program
- Vehicle Impact Prediction Program
- Decelerator Mortar Fire Command Program

II. VEHICLE FLIGHT AZIMUTH PROGRAM

A. Program Requirements

For the BLDT powered flights, it was a Range Safety requirement that the vehicle drop azimuth be such that the vehicle, or any separated components, impact within prescribed areas of the range under all flight and failure modes including failure of the qualification decelerator to deploy. Since the failure of the decelerator to deploy results in trajectories which are greater than the width of the White Sands Missile Range, it was necessary to control vehicle flight azimuth for a period of time prior to and at release from the balloon load bar in order to assure range impact for system components and provide Range Safety with real time vehicle and separated component impact predictions.

In order to comply with the above azimuth control requirement, the Vehicle Flight Azimuth Program was generated. This program processed airborne telemetry data from a set of on-board magnetometers to provide continuous control center displays of the vehicle heading and rotational rates as well as to provide input to the Vehicle Impact Prediction Program. The real time displays of the vehicle heading and rotational rates, coupled with an airborne gas thruster impulse system, provided the necessary means for vehicle azimuth control.

Program Implementation

The azimuth program utilizes the telemetry output of an airborne magnetic sensing system consisting of two magnetic field sensors oriented 90° apart and mounted so as to sense only the horizontal component of the

earth's magnetic field. When the vehicle, while still connected to the balloon load bar, is rotated through a 360° arc, the output from the magnetometers provides sinusoidal curves with a 90° phase shift as shown on Figure E-1. These data are sufficient to establish the vehicle heading.

The equations for computing the vehicle heading (θ) from the TM magnetometer data is:

$$(1) \quad \theta = \tan^{-1} \left(\frac{B_2 - Y}{X - B_1} \right) + \theta_I \text{ where:}$$

θ is the heading from true north

X is the voltage from Probe 1

Y is the voltage from Probe 2

B_1 is the voltage reading of Probe 1 when perpendicular to the magnetic field.

B_2 is the voltage reading of Probe 2 when perpendicular to the magnetic field.

θ_I is a constant which combines the corrections for installation alignment and the difference between true and magnetic north.

The above equation was derived from the following relationship:

$$(2) \quad X = R \cos (\theta + \theta_I) + B_1$$

$$(3) \quad Y = R \sin (\theta + \theta_I) + B_2 \text{ where}$$

R represents the horizontal component of magnetic field strength which varies slightly with altitude

Each vehicle was rotated over a compass rose where the magnetometer data were recorded at incremental headings from true north to provide calibration data for B_1 , B_2 and θ_I . The actual calibration values were obtained by a least square fitting of equation (2) and (3) above.

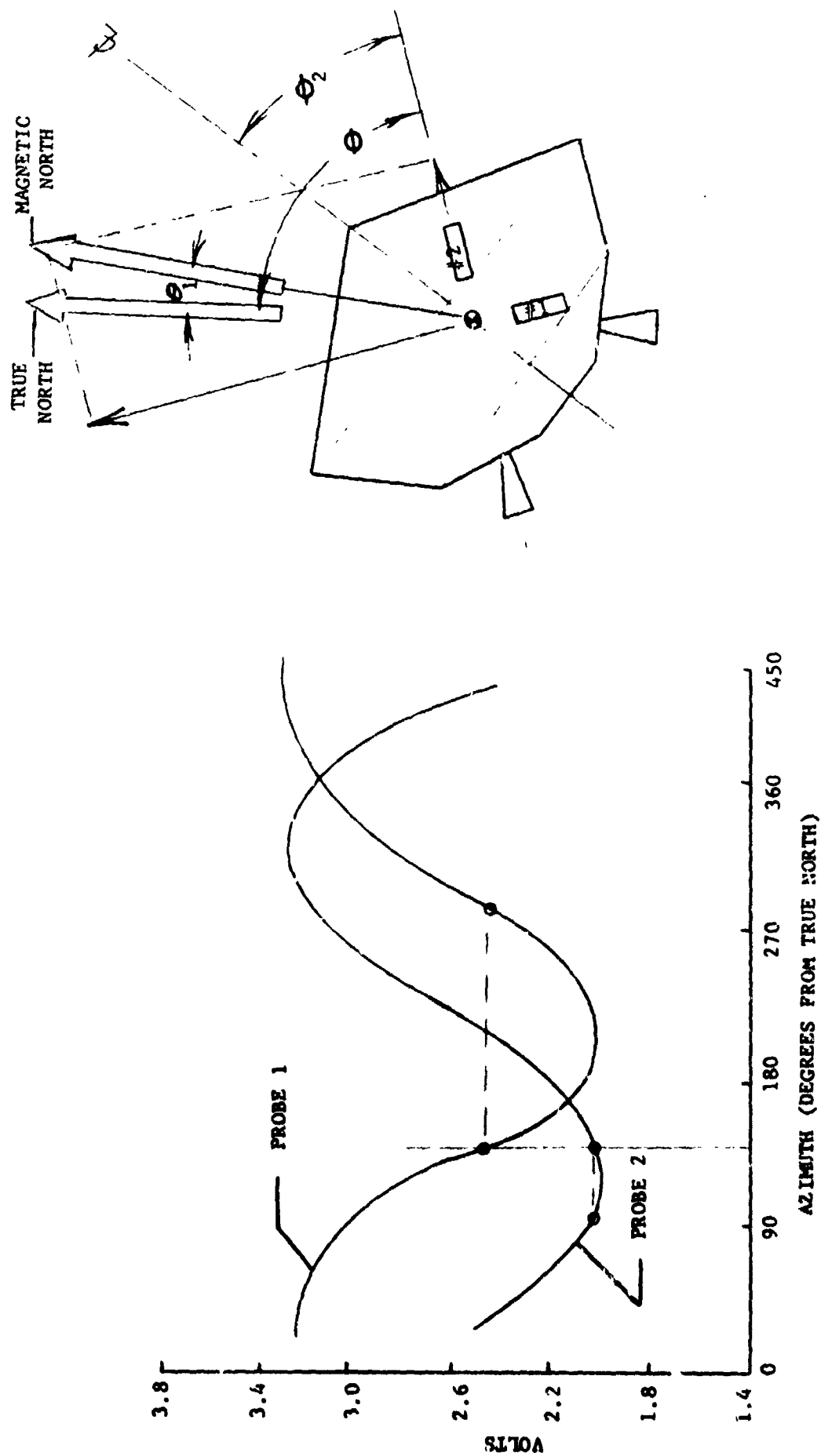


FIGURE E-1 MAGNETOMETER OUTPUT

Using the above calibration values and the TM values for X and Y, the vehicle heading can be computed using equations (1), (2), and (3). Equation (1) which uses input from both probes was normally used but in the event of a probe failure, the computer would switch to a mode which derived heading from a single probe using equations (2) or (3) depending upon which probe failed. Tests were included in the program to continuously validate each probe output by establishing acceptable minimum and maximum voltage limits. The field strength (R) was continuously calibrated to reflect its change with altitude using a gain filter to suppress noise.

To suppress inherent data noise and provide azimuth rate information, the TM data were edited and filtered with a standard, sliding 19 point, cubic polynomial, leading edge, least squares filter. The azimuth rate was obtained from the polynomial slope at the 15th point which lags real time by approximately 0.5 second. The azimuth rate data was then additionally smoothed by a 30 point summer filter which increased the lag to approximately 2 seconds.

In the event of a single probe failure, equations (2) and (3) encounter difficulty in deriving the azimuth quadrant. To circumvent this difficulty, the polynomial filter continuously extrapolates to the 20th point to predict the subsequent value of azimuth. This predicted value is used to determine the quadrant while the remaining probe data are used to compute the heading. For a condition of temporary TM drop-out, the azimuth is obtained directly from the filtered prediction.

The program listing is included in Table E-1. This computer program provided the intelligence to drive two (2) XY plotters (vehicle heading and vehicle azimuth rate) plus vehicle heading and azimuth rate digital

displays. It was these displays which were monitored while manually sending clockwise and/or counter clockwise commands to change or control the vehicle heading during the drop operations.

SUBROUTINE AZCOMP
C THIS ROUTINE COMPUTES AZIMUTH AND AZIMUTH RATE FROM TELEMETRY DATA.

```

COMMON /STATUS/ IRN,ITG,IPG,IRBC,LOC TAB(M.),LIGHTW(4),IDNAME,
1 IDDATE,NUNRDR(6),IPRISC(6,2),LDEH,IBDEH,LURECT,BURECT,TENPER,
2 IDEINP,IUEQ,MSLTGT(6,2),RDFLAG,IYERNO,ISPELL,IONEQ,IORUNG,
3 IPRINT(7),ITOUT,IVUG(6),FRECH(2),FRECT,GPDATA(32),DFSET
4 ,NVPAS,NSTAT
EQUIVALENCE (TLUREC,LURECT)
END

INCLUDE AZCHN,LIST
COMMON /AZCHN/ AZC,AZRATE,ICK,P,AZ

END

EQUIVALENCE (V1,GPDATA(5)),(V2,GPDATA(2)),(AZ0,AZRATE),(AZC,AZ)
DIMENSION Y(20),Z(15)
DATA INT,61,62,RMAX,RMIN,RC,RAD,GR/
1 0,2.5498,2.3551,3.97,1.03,1.0193,57.295779,.0001/
DATA S1,S2,S3,S4,S5,S6,0/865/5020.,-17739540.,750100.,
1 4539754.,-216600.,10830.,146919780./
DATA AZ1,RCH1,RCH2,IN/-32.55,1.25,0.00,0/
1,5A70,A,0,C/4*0.0/
C *** V1 = R * COS (AZ+AZ1) + B1
C V2 = R * SIN (AZ+AZ1) + B2
C
C *** CHECK MAG READINGS
CA=(V1-B1)/RC
SA=(B2-V2)/RC
IF (RMAX-V1) 6,0,1
1 IF (RMIN-V1) 2,0,6
2 IF (RMAX-V2) 9,9,3
3 IF (RMIN-V2) 1,9,9
C *** BOTH MAGS ARE GOOD
4 ICK=0
R=SQRT(CA*CA+SA*SA)*RC
IF (R.GT.RCH2.DR.R.LT.PCHN) GO TO 10
RC=RC+GR*(R-RC)
5 AZ = RAD*ATAN2(SA,CA)+AZ1
GO TO 11
C *** MAG 1 IS BAD
6 IF (RMAX-V2) 10,10,7
7 IF (RMIN-V2) 8,10,10
8 ICK=1
AP=(A+20.*R+25.*C)/D-AZ1
CA=COS(AP/RAD)
CK=1.-SA*SA
IF (CK.LE.0.) CK=1.E-20
CA=SIGN(SQRT(CK),CA)
GO TO 5
C *** MAG 2 IS BAD
9 ICK=2
AP=(A+20.*R+25.*C)/D-AZ1
SA=SIN(AP/RAD)
CK=1.-CA*CA
IF (CK.LE.0.) CK=1.E-20
SA=SIGN(SQRT(CK),SA)
GO TO 5

```

```

C *** BOTH MAGS ARE 9A)
10  ICK=3
    AZ=(A+20.*B+225.*C)/D
11  INIT = INIT+1

    Y(INIT) = AZ
    IF (INIT.NE.20) GO TO 16
    INIT=19

C * * * QUADRANT CHECK
    DEL=A7-AZ2
    ADEL=ABS(DEL)
    IF (ADEL.LT.180.) GO TO 21
    SD=SIGN(1.,DEL)
    DO 12 I=2,19
12  Y(I)=Y(I)+360.*SD
    AZZ=AZ+360.*SD
    DEL=AZ-AZZ
    ADEL=ABS(DEL)
21  IF (ADEL.LT.6.) GO TO 13
    Y(20)=AZZ+3.*SIGN(1.,DEL)
C * * * LEAST SQUARES FIT
13  SUM1=0.0
    SUM2=0.0
    SUM3=0.0
    DO 14 I=1,19
    Y(I) = Y(I+1)
    SUM1=SUM1+Y(I)
    SUM2=SUM2+1.*Y(I)
14  SUM3=SUM3+1.*Y(I)
    A = SUM1*S1+SUM2*S2+SUM3*S3
    B = SUM1*S2+SUM2*S4+SUM3*S5
    C = SUM1*S3+SUM2*S5+SUM3*S6
    AZZ=(A+19.*B+361.*C)/D
    AZ=AZZ
    IF (AZ.LT.0.) AZ=A7+360.
    AZD=17.*(A+30.*C)/D
    IN=MOD(14,150)
    IN=IN+1
    SAZD=SAZD-Z(I)+AZD
    Z(IN)=AZD
    AZD=SAZD/157.
    RETURN
16  AZZ = AZ
    A=AZ
    RETURN
END

```

III. IMPACT PREDICTION PROGRAM

A. Program Requirement

As previously discussed in IIA, it is a requirement to provide impact information to Range Safety in order to select a drop point and corresponding flight azimuth. Additionally, the impact data are used to select the best impact area to expedite recovery of the spent hardware and to direct the recovery crew to the predicted impact area.

The program is required to operate in two modes as follows:

1. A static mode in which drop parameters are selected and impact analysis are performed using range intersect predictions.
2. A dynamic mode in which real time drop parameters are used and real time impact predictions are derived.

The mode of operation is manually selected and requires only a change in the source of input data.

B. Program Implementation

The Impact Prediction Program is based upon a nominal trajectory (perturbed by current wind conditions), latitude and longitude of drop and vehicle heading at drop.

The software reflects two modes of flight; accelerated flight (powered flight and decelerator transients); and equilibrium descent, where the aerodynamic drag is nearly equal to the system weight and the rate of descent is a direct function of the atmospheric density. The point of impact is obtained by first computing the wind effect to the nominal, zero wind, accelerated flight trajectory and then adding the wind drift effect of the equilibrium descent.

1. Accelerated Flight Mode

The vehicle position, at the completion of accelerated flight, is computed by adding wind corrections to a nominal zero wind trajectory which is represented by a nominal range (R) for each vehicle configuration and a nominal azimuth shift (ΔA_Z) which occurs because of vehicle spin. The time equivalents of the nominal trajectory and wind velocities are tabulated as functions of altitude at intervals of 5000 feet. The position corrections due to wind are computed by multiplying the wind velocity (W_i) by the time (t_i) required to transverse each of the 5000 feet intervals of altitude.

The position (X_a, Y_a) at the completion of accelerated flight is given by the equations:

$$(4) \quad X_a = X_D + R \sin (A_Z + \Delta A_Z) + \sum_{i=1}^N t_i (W_{x_i})$$

$$(5) \quad Y_a = Y_D + R \cos (A_Z + \Delta A_Z) + \sum_{i=1}^N t_i (W_{y_i})$$

where: A_Z is the drop heading
 X_D, Y_D is the range drop position.

The position location (X_a, Y_a) is the starting location for the equilibrium descent portion of the computation which follows.

2. Equilibrium Descent

During equilibrium descent, the vehicle weight counterbalances aerodynamic drag as shown in the relationship:

(6) Weight = Drag

$$\begin{aligned} wt &= q C_D A \\ &= 1/2 \rho \left(\frac{dh}{dt} \right)^2 \end{aligned}$$

where: q is dynamic pressure

C_D is aerodynamic drag coefficient

ρ is atmospheric density

$\frac{dh}{dt}$ is rate of descent

It is noted that the atmospheric density (ρ) is considered constant over each altitude interval.

Rearranging equation (6), the time spent during any altitude interval can be computed as:

$$(7) \Delta t_i = \left(\frac{\rho C_D A}{2 wt} \right)^{1/2} \cdot 5000$$

The summation of the displacements obtained by multiplying the Δt by the corresponding wind velocity for each 5000 feet altitude interval gives the increment of vehicle displacement (X_b, Y_b) for the equilibrium descent portion of the impact prediction. This summation is represented by:

$$(8) X_b = \sum_{i=1}^N \Delta t_i (W_{x_i})$$

$$(9) Y_b = \sum_{i=1}^N \Delta t_i (W_{y_i})$$

The displacements given by equations (8) and (9) are added to the position computed by the accelerated flight operations to obtain the impact position (X_p, Y_p). The equations for this operation are:

$$(10) X_p = X_a + X_b$$

$$(11) Y_p = Y_a + Y_b$$

The impact prediction is computed separately for each of the possible flight conditions which are:

- o Powered flight followed by payload decelerated descent to impact.
- o Powered flight followed by aeroshell descent to impact.
- o Powered flight without decelerator deployment (abort mode).

The impact prediction program drove an XY plotted which displayed impact locations of the above flight articles superimposed on a map of the White Sands Missile Range. During the dynamic mode of operation, where the heading angle was fed directly to the impact prediction program from the azimuth program, the impact prediction was displayed continuously for the abort mode which was the most critical case due to its extended trajectory. This continuous impact display provided assurance to Range Safety that the overall azimuth control operation was adequate and stable and since the display was for the worst case (abort), Range Safety was assured that all flight articles would impact within an acceptable area.

IV. DECELERATOR MORTAR FIRE COMMAND PROGRAM

A. Program Requirement

The airborne command receiver was used to allow the ground computer to fire the decelerator mortar at the proper flight conditions. This real time command system minimized the effect of vehicle dispersions on the parachute qualification dynamic pressure test condition. The vehicle programmers were set to open a time window for this signal to prevent inadvertent mortar fire prior to despin and also to backup the ground command in the event this command link failed.

The ground computer compared real time information from all available radar sites and automatically selected the best radar tracking information. The velocity and altitude data were then used with the current atmospheric density and winds to compute the dynamic pressure. The dynamic pressure data were then compared to the nominal predictions and the flight deviation converted to an effective time shift in the mortar fire time for the powered flights. The subsonic flight mission used a fixed time from initiation of drop, due to the predictable nature of the gravitational acceleration.

B. Program Implementation

The generation of the ground mortar fire command is based on flight deviations from a reference trajectory. The radar data subsequent to drop is used in conjunction with current atmospheric density and wind velocity data to compute the dynamic pressure and ascent rate. The deviations from the reference trajectory are used with sensitivity coefficients to predict the time increment from nominal when the desired dynamic pressure will

probably occur. The predicted mortar fire time was continuously calculated after drop and filtered such that the latest information was weighted most heavily. The equation for predicting the mortar fire time is:

$$(12) \quad T = T_N + S_Q \left(\frac{Q - Q_N}{Q + DQ} \right) + S_H (H - H_N) + \Delta t$$

where: S_Q , S_H , Q_N , H_N are time varying functions.

The various elements are individually discussed below.

1. Nominal Trajectory Parameters (Q_N , H_N)

The reference trajectory was determined from the best estimate of the "as built" vehicle performance and the US Standard 1962 atmosphere.

2. Sensitivity Coefficients (S_Q , S_H)

The correlation between the deviations of randomly dispersed trajectories from the nominal trajectory and the deviation in the time from nominal at which these trajectories attain the desired dynamic pressure was used to generate the sensitivity coefficients. The two parameters, dynamic pressure and ascent rate, were evaluated separately. The dynamic pressure sensitivity coefficient (S_Q) is expressed as a percent variation and to avoid possible division by zero, early in flight when Q is small, it was incremented by a constant DQ .

3. Radar Track Data (Q, \dot{H})

The radar track furnished the position and rate of change of position data which when coupled with current atmospheric data defined dynamic pressure (Q). Ascent rate (\dot{H}) was obtained directly from the radar data.

4. Filter Constants

A dual filter was used to suppress the effect of random noises on the radar tracking data.

Variation in mortar fire time comes primarily from erratic velocity derived from radar position data, however, systematic variations in velocity are averaged and used to bias the mortar fire time such that a lower dynamic pressure is obtained. The primary filter was given a shorter time constant to respond to the latest data on dynamic pressure and still give a margin based on the overall variability in the data. This filter used a 5 second time constant on the variability of the mortar fire time with a 2 second time constant when the predicted mortar fire is shifting earlier and a 1 second time constant when shifting late. This filter is initialized by setting the initial value of mortar fire time equal to T MAX (dispersed backup programmer setting). This bias is reduced by a .5 second time constant as soon as valid data becomes available.

5. Nominal Mortar Fire Time (T_N)

Although a 6.0% (2σ) dispersion on mortar fire dynamic pressure was assumed, this value represents in part radar data uncertainties which are to some degree detected by the mortar fire program and used to bias the mortar fire time late. The nominal time is therefore selected based on the expected meteorological data uncertainty only. It is made up of two parts, density and winds. The density uncertainty is expected to be $\pm 3.5\%$ (3σ) and the winds 1.53% (3σ). The resultant 2σ dynamic pressure bias below the 30% overload dynamic pressure is 2.5%.

5. Time Delay (ΔT)

The transmission time delay from ground to air affects the mortar fire program in two ways. First, the mortar fire program uses a reference drop time which would be earlier than actual drop time due to the combined transmission and pyro delay. The second is the time delay between the commanding of mortar fire on the ground and the flight occurrence of mortar fire. To some degree, these delays are compensatory except that the radar data does not have this delay and therefore the actual trajectory and the reference nominal trajectory will not be time correlated. For this reason, care was taken to make the mortar fire program insensitive to time delays. A mortar fire transmission time delay of .03 seconds was included.

In the event the predicted mortar fire time is outside an acceptable mortar fire window, the data is assumed to be bad and the current mortar fire time estimate is slowly moved later. This rate of change was evaluated such that if acceptable data is never obtained, the mortar fire time would revert to the airborne backup programmer time.

The Fortran source programs for computing mortar fire command time are given in Table E-2.

```

FUNCTION FIRE(T,G,HD)
*****
C      *
C      *      MORTAR FIRE REAL TIME CALCULATION PROGRAM      *
C      *
C      *****
C      T = TIME FROM DROP - SECONDS
C      Q = DYNAMIC PRESSURE ,PSF
C      HD= VERTICAL VELOCITY,FPS (POSITIVE UPWARD)
C      TDEL=SYSTEM TIME DELAY
C      SIGT=INITIAL VALUE OF NCISE
C      SIGQ=Q BIAS TO PREVENT DIVISION BY 0.0
C      TMIN=EARLIEST MORTAR FIRE TIME
C      TMAX=LATEST MORTAR FIRE TIME
C      TNOM=TIME NOMINAL TRAJECTORY ACHIEVES DESIRED MORTAR FIRE Q
C      DTBD=OUT OF RANGE DATA BIAS ON TIME
COMMON /DATA/D(170)
EQUIVALENCE (D(161),G1 ),(D(162),G2 ),(D(163),G3 )
1,(D(164),DTBD),(D(165),TDEL),(D(166),SIGT),(D(167),SIGQ)
2,(D(168),TMIN),(D(169),TMAX),(D(170),TNOM)
DATA G1 ,G2 ,G3 ,DTBD ,TDEL,SIGT,SIGQ,TMIN,TMAX,TNOM/
. 0.02,2.0,0.05,0.012,0.00,2.00,2.00,33.5,38.5,36.5/
IF(T.GT.1.0) GO TO 2
SDT=SIGT
TMFL=TNOM+SDT
TMFC=TMFL
1 FIRE=TMFC-TDEL
RETURN
2 IF(T.GT.40.) GO TO 1
CALL TABNOM(T,HN,QN,HS,JS)
TMF=TNOM+HS*(HD-HN)+QS*(Q-QN)/(Q+SIGQ)
IF(TMFC.GT.TMAX) GO TO 3
IF(TMFC.GT.TMIN) GO TO 4
3 TMF=TMFC+DTBD
GO TO 5
4 DT=ABS(TMFC-TMFL)-SDT
SDT=SDT+G1*DT
TMFL=TMF
TMF=TMF+SDT
5 IF(TMFC.GT.TMAX) TMF=TMAX
DT=TMF-TMFC
IF(DT.GT.0.0) DT=G2*DT
TMFC=TMFC+G3*DT
GO TO 1
END

```

TABLE E-2 MORTAR FIRE COMMAND LISTING

SUBROUTINE TABNOM(T,HN,QN,HS,OS)

 *
 * NOMINAL FREIGHT VERTICAL VELOCITY (HN),DT/DV (HS),
 * DYNAMIC PRESSURE (QN),DT/DQ (QS) TABLE INTERPOLATION
 *

COMMON /DATA/D(170)

DIMENSION HN1(40),QN1(40),HS1(40),OS1(40)

1, HN2(39),QN2(39),HS2(39),OS2(39)

EQUIVALENCE (D(2),QN1(2),QN2(1)),(D(42),HN1(2),HN2(1))

1, (D(82),OS1(2),OS2(1)),(D(122),HS1(2),HS2(1))

IT=1

DT=0.0

IF(T.LT.1.0) GO TO 1

IT=39

DT=1.0

IF(T.GE.40.) GO TO 1 ;

IT=T

DT=IT

DT=T-DT

1 HN=HN1(IT)+DT*(HN2(IT)-HN1(IT))

QN=QN1(IT)+DT*(QN2(IT)-QN1(IT))

HS=HS1(IT)+DT*(HS2(IT)-HS1(IT))

QS=QS1(IT)+DT*(QS2(IT)-QS1(IT))

RETURN

END

TABLE E-2 (CONTINUED)